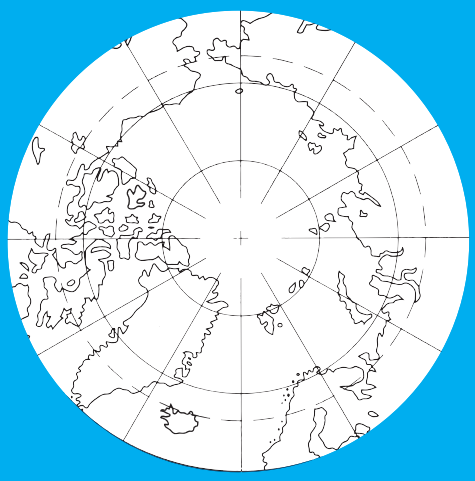

Polarforschung

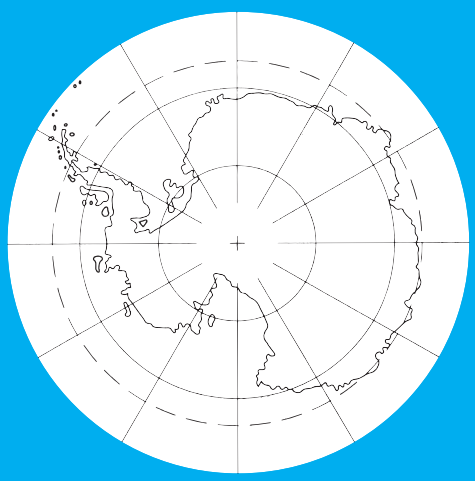

85. Jahrgang • Nr. 2 • 2015 (erschienen 2016)

ISSN (print) 0032-2490
ISSN (online) 2190-1090

POLARFORSCHUNG

herausgegeben vom
Alfred-Wegener-Institut Helmholtz-Zentrum
für Polar- und Meeresforschung
und der
Deutschen Gesellschaft für Polarforschung e. V.

published by the
Alfred Wegener Institute Helmholtz Centre
for Polar Polar and Marine Research
and the
German Society of Polar Research

POLARFORSCHUNG – published by the Deutsche Gesellschaft für Polarforschung (DGP) and the Alfred Wegener Institute Helmholtz Centre for Polar Polar and Marine Research (AWI) – is a peer-reviewed, multidisciplinary research journal that publishes the results of scientific research related to the Arctic and Antarctic realm, as well as to mountain regions associated with polar climate. The POLARFORSCHUNG editors welcome original papers and scientific review articles from all disciplines of natural as well as from social and historical sciences dealing with polar and subpolar regions. Manuscripts may be submitted in English (preferred) or German. In addition POLARFORSCHUNG publishes Notes (mostly in German), which include book reviews, general commentaries, reports as well as communications broadly associated with DGP issues.

Contents / Inhalt

Cover illustration: Installation of Snow Depth Buoy 2013S7, an autonomous platform, on drifting Antarctic sea ice of the Weddell Sea, deployed on 9 July, 2013, during the RV "Polarstern" Antarctic Winter Expedition (cruise ANT-XXIX/6, PS81). Snow depth buoys represent a simplified form of mass balance buoys and have only an acoustic sensor unit to measure the height of the snow surface and thus the accumulation of snow on sea ice, representing the area around the buoy. The snow depth buoy is equipped with four independent ultrasonic sensors, compensating for possible measurement failures and measurement inaccuracies. The buoy was installed on first year ice. In addition to snow height, geographic position, barometric pressure, air temperature, and ice surface temperature are measured. All data of the buoy can be accessed through "meereisportal.de" on daily basis (Photo: S. Hendricks, AWI).

Umschlagbild: Installation einer Schneebilanzboje (2013S7) auf dem antarktischen Meereis am 9. Juli 2013 während der Winter-Expedition ANT-XXIX/6 (PS81) des FS „Polarstern" ins Weddelmeer. Schneebilanzbojen stellen eine vereinfachte Form der Massenbilanzboje dar und besitzen im Gegensatz zu diesen nur eine akustische Sensoreinheit, um die Höhe der Schneeoberfläche und damit den Schneezutrag auf dem Meereis im Bereich der Boje zu messen. Dabei ist die Schneeboje mit vier Ultraschallsensoren ausgestattet, wodurch mögliche Messausfälle und Messungenauigkeiten ausgeglichen werden können. Die Boje wurde auf einjährigem Meereis aufgebaut. Zusätzlich zur Schneehöhe werden geographische Position, Luftdruck, Lufttemperatur und Temperatur der Schneeoberfläche gemessen. Die Daten der Schneebilanzbojen können täglich über die Wissensplattform „meereisportal.de" abgerufen werden, (Foto: S. Hendricks, AWI).

Polarforschung • 85. Jahrgang • Nr. 2 • 2015

(erschienen 2016)

ISSN (print) 0032-2490 / ISSN (online) 2190-1090

Polarforschung 85 (2), 65–68, 2015 (erschienen 2016)

The Helmholtz Regional Climate Initiative REKLIM from a Polar Perspective – a Preface –

by Klaus Grosfeld[1*], Peter Lemke[1], Peter Braesicke[2], Achim Brauer[3], Klaus Dethloff[1], Michael Kunz[2], Mojib Latif[4], Beate Ratter[5], Torsten Sachs[3], Hans Peter Schmid[6], Renate Treffeisen[1] and Reimund Schwarze[7]

One of the great challenges of humankind is global climate change, the mitigation of CO_2 emissions at the lowest possible level and, at the same time, the adaptation to its current and future impacts. The Working Group 1 (WG1) contribution to the Fifth Assessment Report (AR5) of the Intergovernmental Panel on Climate Change (IPCC 2013) presented clear conclusions that warming of the climate system is unequivocal, owing to increasing atmospheric greenhouse gas concentrations, decreasing Arctic sea ice cover and diminishing amounts of snow and land ice, sea level rise and many more consequences. It is extremely likely (95 percent certainty), that human influence has been the dominant cause of the observed warming since the mid-20th century (IPCC 2013).

Although the ability to project climate change on the global scale and its potential impacts under different representative concentration pathways (equivalent to future anthropogenic greenhouse gas emission scenarios) has significantly increased in recent years, one of the remaining great challenges is to understand and project the regional and local patterns of global climate change, and especially to assess societal impacts and consequences. This is what the Helmholtz Climate Initiative REKLIM (Regional Climate Change) focuses on.

Since October 2009 experts of nine German Centres of the Helmholtz Association, most of them in the research field "Earth and Environment", have been working together on eight interdisciplinary research topics. In cooperation with nine university partners, the Helmholtz Centres combine their expertise in regional climate change research. Regional observations and process studies coupled with model simulations aim at improving regional and global climate models, providing a more solid basis for climate-related decision support. Hence, REKLIM is contributing to the strengthening of multidisciplinary regional climate research in Germany and internationally.

doi:10.2312/polfor.2016.001

[1] Alfred Wegener Institute Helmholtz Centre for Polar and Marine Research, Bremerhaven, Germany.
[2] Institute of Meteorology and Climate Research, Karlsruher Institute of Technology, Karlsruhe, Germany.
[3] GFZ German Research Centre for Geosciences, Potsdam, Germany.
[4] GEOMAR Helmholtz Centre for Ocean Research Kiel, Germany.
[5] University of Hamburg and Helmholtz Centre Geesthacht, Germany.
[6] Institute of Meteorology and Climate Research - Atmospheric Environmental Research, Karlsruher Institute of Technology, Garmisch-Partenkirchen, Germany.
[7] Helmholtz Centre for Environmental Research, Leipzig, Germany.
[*] Corresponding: <Klaus.Grosfeld@awi.de>, <Peter.Lemke@awi.de>

REKLIM addresses the following research topics:
Topic 1: Coupled modelling of the regional Earth systems.
Topic 2: Sea level changes, from global, regional to local scales.
Topic 3: Regional climate changes in the Arctic: Forcing and long-term effects at the land-ocean interface.
Topic 4: The land surface in the climate system.
Topic 5: Chemistry-climate interactions on global to regional scales.
Topic 6: Modelling and understanding extreme meteorological events.
Topic 7: Risk analysis and risk management for integrated climate strategies.
Topic 8: Abrupt climate change derived from proxy data.

The Helmholtz Climate Initiative REKLIM also puts a focus on knowledge transfer processes as well as on dialogue processes between science and society, which is an increasingly important aspect of modern science. To achieve this goal a range of activities was established that are adapted to the needs and requirements of the various target groups as well as to the according scientific basis involved. Particular emphasis is placed on the joint development and implementation of ideas between science and society.

Via the Helmholtz Regional Climate Offices and the Climate Service Centre Germany (GERICS) policymakers and other decision makers are supported in assessing risks and opportunities and designing mitigation and adaptation strategies based on results obtained from the REKLIM research network.

In conclusion of the first five year funding period and in order to foster the international collaboration on regional climate change research, the Helmholtz Climate Initiative REKLIM organised the international symposium "Our climate – Our Future, regional perspectives on a global challenge", which took place in Berlin, Germany, 6–9 October 2014 (Fig. 1). The conference served as a forum for scientists from all over the world to present and discuss new results from regional climate research in the context of the REKLIM research topics.

The conference was divided into two parts:
The first part was a three-day international scientific conference held during 6–8 October, 2014. The scientific programme offered a broad and interdisciplinary range of current national and international research activities in the field of regional climate change research and addressed the eight topics of REKLIM in eight sessions (REKLIM Conference).

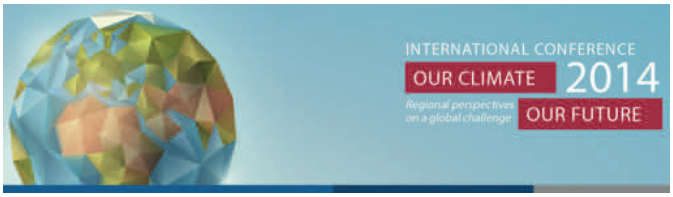

Fig. 1: Banner of the REKLIM international conference "Our Climate - Our Future: Regional Perspectives on a Global Challenge", which took place from 6–9 October 2014 in Berlin, Germany.

Abb. 1: Banner der internationalen REKLIM-Konferenz "Our Climate – Our Future: Regional Perspectives on a Global Challenge", die vom 6.–9. Oktober 2014 in Berlin, Deutschland, veranstaltet wurde.

The second part consisted of a public outreach event on "Regional climate change – causes and effects" on 9 October, 2014, which focused on the dialogue between scientists and decision makers from the fields of politics, administration, economics and associations.

More than 320 participants from 28 countries attended the REKLIM international conference (Fig. 2). During the scientific conference, 135 oral presentations and 99 posters were presented. An overview of the conference programme and the corresponding abstracts is given in Lemke et al. (2014). Eight internationally renowned keynote speakers presented overview talks related to the different REKLIM research topics:

Topic 1: René Laprise (Université du Qúebec à Montréal) *Limited area domain atmospheric energetics*.

Topic 2: Jason Box (Geological Survey of Denmark and Greenland) *Darkening Greenland ice: integrating a spectrum of climate change processes*.

Topic 3: Larry Hinzman (International Arctic research Centre, University of Alaska Fairbanks) NGEE: *The Study of the Interaction of Atmospheric, Hydrologic, Geomorphic and Ecosystem Processes on the Alaskan Arctic Coastal Plain*.

Topic 4: Martyn Chipperfield (University of Leeds, School of Earth and Environment) *Composition Climate Interactions from Global to Local Scales*.

Topic 5: Mark Pelling (Department of Geography, King's College London) *Transformative adaptation*.

Topic 6: Stefan Brönnimann (Oeschger Center, University of Bern) *Extreme Events: Reenacting past winter storms*.

Topic 7: Edouard Davin (Institute for Atmospheric and Climate Science, ETH Zürich) *Role of land surface processes and land use change at the regional scale*.

Topic 8: Helge Arz (Leibniz Institute for Baltic Sea Research Warnemünde) *Environmental changes in the Black Sea region during the last ~140 kyrs*.

The German Society of Polar Research and the Alfred Wegener Institute Helmholtz Centre for Polar and Marine Research (AWI) offered to publish a conference volume of all papers related to the Arctic and Antarctic realms, as well as to all aspects on polar climate. The POLARFORSCHUNG (Polar Research) editors and the scientific steering committee (see authors of this contribution) of the conference welcomed original papers, scientific review articles and extended abstracts from natural as well as societal and

Fig. 2: Group picture of the participants of the REKLIM international conference 2014, Berlin, Germany (photo: AWI).

Abb. 2: Gruppenfoto der Teilnehmer an der internationalen REKLIM-Konferenz 2014 in Berlin, Deutschland (Foto: AWI).

historical sciences, dealing with polar and subpolar regions in the context of the REKLIM conference. All submitted articles were peer-reviewed and are published in digital and printed version.

More than 70 authors in 14 papers contributed to this special issue, providing a wide range of current understanding and knowledge about the different aspects of regional climate change, its causes, impacts and challenges. Mainly themes from topics 1, 2, 3 and 8 were covered by papers, ranging from modelling of the regional climate system (Nikiéma et al., Niederdrenk and Mikolajewicz, Madsen et al. a,b), to general process understanding (Bogorodski et al., Konrad et al., Lohmann et al., Stepanek et al.), from data analysis (Müller, Lüdecke et al.) to the development of databases and associated web-based infrastructures, making scientific knowledge and data available for research and the wider public (Dvornikov et al., Elger et al., Haas et al., Grosfeld et al.). The order of the papers is organized according to their contextual contribution to the conference topics.

Herewith we thank all contributors to this conference volume. Their abiding patience is most appreciated. Twenty-three reviewers from eight countries contributed substantially to the quality of this special issue. Their efforts have been invaluable to improving the scientific content and integrity of the papers. Several agencies and governments supported the data acquisition and analysis, including the arrangement of the conference. Here, especially the Helmholtz Association needs to be mentioned, which fostered the initiation and funding of the Helmholtz Climate Initiative REKLIM.

REKLIM *media project*

In addition to the exchange and discussion of the scientific community during the conference, REKLIM aimed at opening the international REKLIM conference to the German general public. Special attention was given to raise awareness for the discussion of regional climate change's causes and effects among those being most affected in future: the "Young Generation". For them it is important to recognize that their participation in the public discussion of climate change and its consequences is crucial because the embracing needs for measures of climate protection and adaptation will constitute an important component for their own future. Therefore, the REKLIM coordination office and the Climate Office for Polar Regions and Sea Level Rise at the Alfred Wegener Institute initiated for this REKLIM conference in particular an accompanying interdisciplinary media project together with the DEKRA Hochschule für Medien Berlin (University of Applied Science, Media). Target group of this media project was the adolescent generation at the age of 16–30 years.

REKLIM scientists and DEKRA students from three different units (television and film, journalism, and media management) created a multimedia and Interactive Internet Media Platform to convey the topic of "Regional Climate Change" into everyday life and to make results of climate change research available to the broader public. One of the objectives of the platform is to stress the need for adaption and mitigation measures to be taken, urgently. More than 80 students were involved before and at the REKLIM conference and transposed scientific contents cinematically and journalistically into cross-media approaches for the young audience. In their own design and production the students worked on different aspects of regional climate change research in the context of REKLIM and came up with a variety of media products (e.g., a blog, five documentary films, three viral videos and daily reports from the conference). For example, the documentary film "Vernagt" addresses the fact of melting and retreating alpine glaciers, using the example of the Vernagtferner Glacier in the Oetztal Alps, Austria, which is under investigation for more than 400 years. Since more than 50 years the Commission for Glaciology of the Bavarian Academy of Science and Humanity, Munich, Germany, investigates the mass balance of this glacier with increasing temporal resolution, revealing a consistent pattern of the mass loss of the Vernagtferner over more than 30 years. The research on the glacier and its connection to climate change impacts is documented in this film in a personal perspective of the scientific head of the commission (Fig. 3). The students played two important roles in the media project: transforming the scientific content into artistic films, journalistic and young language with their impartial perspective on climate research issues and at the same time involving the scientists with their exact science and precise description into their work. Therefore, an important dialogue and learning process between the various disciplines arose with the REKLIM Media Project, contributing to the increasingly important need for knowledge transfer processes between science and society.

The success of the project cannot be described in just one dimension. Looking at the general perception, more than 16,400 views of around 7,000 visitors of the website (as of 13 December 2014) document a clear success. For evaluating the quantitative success of these numbers it has to be considered that the project webpage was built from scratch and went online shortly before the conference on 1 October 2014. Moreover, the produced viral videos were viewed more than 2,000 times and the documentaries about 1,600 times. Meanwhile, requests for the re-use of documentary films by environmental organizations and research institutions have been received. The interdisciplinary REKLIM Media Project

Fig. 3: Scene at the filming of the documentary "Vernagt", describing long-term observation and scientific work on the Vernagtferner Glacier, Oetztal Alps, Austria (photo: DEKRA).

Abb. 3: Szene während der Dreharbeiten zum Dokumentarfilm „Vernagt", der die Langzeitbeobachtungen und wissenschaftlichen Arbeiten auf dem Vernagtferner in den Ötztaler Alpen beschreibt (Foto: DEKRA).

as a best practice example was already adopted once for a national conference (IPCC AR5 Pre-Briefing "Konferenz des Deutschen Klimakonsortiums im Auswärtigen Amt" on 12 November, 2015) and for an international conference (International Conference on Permafrost (ICOP) in Potsdam, Germany, 20–24 June, 2016) as accompanying social media coverage. A new dimension of publically relevant knowledge transfer and dialogue between science and society was thus generated within REKLIM.

Further information on the conference, the REKLIM climate initiative and the current research activities can be found in English at <www.reklim.de/en.html> or German at <www.reklim.de>.

References

Alfred Wegener Institute Helmholtz Centre for Polar and Marine Research (AWI): <www.awi.de> (accessed 18 April 2016)

Climate Office for Polar Regions and Sea Level Rise: <www.awi.de/forschung/besondere-gruppen/klimabuero.html> (accessed on 18 April 2016)

Climate Service Centre Germany GERICS: <www.climate-service-centre.de> (accessed 18 April 2016)

Commission for Glaciology of the Bavarian Academy of Science and Humanity: <www.glaziologie.de> (accessed 18 April 2016)

DEKRA Hochschule für Medien, Berlin: <www.dekra-hochschule.de> (accessed 18 April 2016)

German Society of Polar Research: <*www.dgp-ev.de*> (accessed 18 April 2016)

Helmholtz Association: <www.helmholtz.de> (accessed 18 April 2016)

Helmholtz Climate Initiative REKLIM: <www.reklim.de> (accessed 18 April 2016)

Helmholtz Regional Climate Offices: <www.klimabuero.de> (accessed 18 April 2016)

Interactive Internet Media Platform: <www.reklim-medienprojekt.de> (accessed 18 April 2016)

POLARFORSCHUNG: <html://www.polarforschung.de> (accessed 18 April 2016)

REKLIM Conference: <https://reklim-confernce-2014.de/> (accessed 18 April 2016)

REKLIM Media Project: <https://doi.pangaea.de/10.1594/PANGAEA.854792> (accessed 18 April 2016)

Vernagt: https://doi.pangaea.de/10.1594/PANGAEA.854710 (accessed 18 April 2016)

IPCC (2013): Climate Change 2013: The Physical Science Basis. Contribution of Working Group I to the Fifth Assessment Report of the Intergovernmental Panel on Climate Change.- T.F. Stocker, D. Qin, G.-K. Plattner, M. Tignor, S.K. Allen, J. Boschung, A. Nauels, Y. Xia, V. Bex & P.M. Midgley (eds), Cambridge University Press, Cambridge, United Kingdom and New York, NY, USA, 1-1535.

Lemke, P., Grosfeld, K., Treffeisen, R. & Weigelt, M. (eds) (2014): Our Climate – Our Future; Regional perspectives on a global challenge: International REKLIM Conference, 6–9 October 2014, Umweltforum Auferstehungskirche, Berlin, Germany, Programme and abstracts, Terra Nostra 2014/1: 1-125, ISBN: 0946-8978.

Polarforschung 85 (2), 69–80, 2015 (erschienen 2016)

Chaotic Behaviour of the Regional Climate Models, CRCM5 and HIRHAM5, in Ensemble Simulations over an Arctic Domain

by Oumarou Nikiéma[1*], Anja Sommerfeld[2], René Laprise[1], Annette Rinke[2] and Klaus Dethloff[2]

Abstract: In a chaotic system such as the Earth's atmosphere, the differences between the members in an ensemble of global climate model simulations launched from different initial conditions initially grow in time until they reach the level of natural variability, indicating that member simulations become uncorrelated. In nested Regional Climate Models (RCMs), however, the growth of inter-member differences is quenched due to the control exerted by the lateral boundary conditions (LBCs), but it nevertheless exhibits episodes of large fluctuations. Earlier work has speculated that this puzzling behaviour may simply reflect remaining chaos allowed by the incomplete control exerted by LBC.
In this work, two large ensembles of twenty simulations were performed over an Arctic domain with two different RCMs: the Canadian RCM (CRCM5) and the High-Resolution Limited-Area Model (HIRHAM5). The inter-member variability (IV) of each ensemble was methodically analysed in the framework of the potential temperature IV budget. The study reveals that, despite being simulated by models with entirely different formulation, the two ensembles exhibit nearly identical IV patterns and time evolution, and in both cases baroclinic processes trigger fluctuations of IV. These results confirm earlier speculations that IV in RCMs is not an artefact of specific model nesting technique, but rather a natural phenomenon arising from the chaotic nature of the atmosphere.

Zusammenfassung: Wird mit einem globalen Klimamodell ein Ensemble mit unterschiedlichen Anfangsbedingungen generiert, dann führt dies aufgrund des chaotischen Verhaltens der Atmosphäre dazu, dass die Differenzen zwischen den Ensemblemitgliedern mit der Zeit anwachsen, bis ein Zustand entsprechend der natürlichen Variabilität erreicht ist. Dies führt zu Simulationen, die sich zueinander unkorreliert verhalten. In genesteten regionalen Klimamodellen (RCM) ist das Anwachsen der Variabilität zwischen den Ensemblemitgliedern aufgrund der äußeren Randbedingungen (LBC) gedämpft. Dennoch können Episoden mit starken Schwankungen der Variabilität zwischen den Ensemblemitgliedern auftreten. In früheren Studien wird die Vermutung geäußert, dass dieses rätselhafte Verhalten durch mangelhafte LBC und das damit zusammenhängende verbleibende Chaos initiiert wird.
In dieser Arbeit werden zwei große Ensemble mit je 20 Ensemblemitgliedern über der Arktis mit zwei verschiedenen RCMs erzeugt: dem kanadischen RCM (CRCM5) und dem „High-Resolution Limited-Area Model" (HIRHAM5). Für diese Ensemble wird die Variabilität zwischen den Ensemblemitgliedern (inter-member Variability; IV) mit Hilfe einer IV Budgetstudie für die potentielle Temperatur analysiert. Die Studie ergab, dass trotz der sehr unterschiedlichen Modellformulierungen die räumlichen Muster und die zeitliche Entwicklung der IV in beiden RCM Ensembles sehr ähnlich sind. Außerdem werden in beiden Fällen die Schwankungen der IV durch barokline Prozesse ausgelöst. Diese Ergebnisse bestätigen die früheren Vermutungen, dass die IV in RCMs nicht durch die Nestingmethode bedingt, sondern eher ein natürliches Phänomen ist, dessen Ursache in der chaotischen Natur der Atmosphäre liegt.

doi:10.2312/polfor.2016.002

[1] Université du Québec à Montréal (UQAM), ESCER Centre, Département des Sciences de la Terre et de l'Atmosphère, UQAM, P.O. 8888, Stn Downtown, Montréal (QC) Canada H3C 3P8;
[*] Corresponding author: <oumarou.nikiema@uqam.ca>
[2] Alfred Wegener Institute, Helmholtz Centre for Polar and Marine Research, Telegrafenberg A 43, D-14473 Potsdam, Germany.
This paper was presented as an oral presentation at the International Conference "Our Climate – Our Future: Regional perspectives on a global challenge", 6–9 October 2014 in Berlin, Germany.
Manuscript received 01 May 2015; revised version 05 November 2015; accepted in revised form 03 December 2015.

INTRODUCTION

Regional Climate Models (RCMs) are very powerful tools used to make retrospective climate simulations and future climate projections due to their capacity of representing the physical processes with high resolution. RCMs are integrated on a limited domain from initial conditions (ICs) and lateral boundary conditions (LBCs) provided either by an archived simulation of a driving Global Climate Model (GCM) or by a gridded analysis of observations. Starting from alternative initial conditions leads to an ensemble of simulations that can be used to quantify uncertainties in response of inter-member (or internal) variability (IV) effects. The question then arises as to the causes underlying IV and resulting simulation uncertainties: Do they arise from approximations or errors in the discretisation of the model's equations, in the parameterisation of subgrid-scale processes, or as an artefact of the nesting procedure?

Several studies, such as those of Weisse et al. (2000), Giorgi & Bi (2000), Rinke & Dethloff (2000), Christensen et al. (2001), Caya & Biner (2004), Lucas-Picher et al. (2004, 2008), Rinke et al. (2004), Alexandru et al. (2007), have shown that nested RCM simulations exhibit some level of IV. The IV is defined as the difference between members in an ensemble of simulations that differ only in their IC, while the LBC are the same and thus exert a constraint that limits the freedom of the nested simulations, at least at large scales. However, the physical processes responsible for the presence of IV in RCM's simulations have remained a scientific issue till recently.

Nikiéma & Laprise (2011a, 2011b, hereafter referred to as NL11a and NL11b, respectively) have performed a budget diagnostics of the Canadian RCM's simulations IV that shed some light on the physical processes responsible for the development of IV and its fluctuations in time. But, these studies, however, were limited because they have been done using a specific RCM, and the simulations were performed over a domain located in mid-latitudes covering North America and bordering Atlantic Ocean. Sommerfeld et al. (2015) conducted the same budget analysis with another RCM over a circum-Arctic domain. They calculated significantly higher IV and emphasise differences in the relative importance of the individual processes compared to NL11a and NL11b. The present study is based on two different RCMs: the 5th-generation Canadian RCM (CRCM5) and the version 5 of the High-Resolution Limited-Area Model (HIRHAM5). A set of twenty simulations were performed over an Arctic domain with both RCMs for the same period and using the same

LBC from Era-interim data (Dee et al. 2011). The different members of the ensembles were generated by launching the simulations at different initial times.

This paper compares results of two RCMs ensembles and analyses the processes responsible for IV. We use the methodology described in NL11a and NL11b for potential temperature in order to perform a quantitative diagnostic calculation of the various diabatic and dynamic contributions to the temporal variation and spatial distribution of IV. The paper is organised as follows. The following section "Data and Evaluation Methods" describes the two RCMs and the simulations design, and the IV budget equation is reminded. Thereafter, results are presented where the time evolution and vertical structure of IV from the two RCMs are compared and analysed. Then, we discuss the time evolution and time-average of various contributions to the IV tendency. Finally, the conclusion will be summarised.

DATA AND EVALUATION METHODS

Overview of the CRCM5 and HIRHAM5 models

A complete description of the 5th-generation Canadian RCM (CRCM5) is given in Hernandez-Diaz et al. (2013). To summarise, CRCM5 is based on the limited-area model (LAM) version of the Canadian Global Environment Multiscale (GEM) model (Zadra et al. 2008). It was developed through a collaboration established between RPN/MSC (2016), ESCER/UQAM (2016), and OURANOS (2016). GEM uses an implicit semi-Lagrangian two-time-level marching scheme (Côté et al. 1998), with slight off-centring to reduce the spurious response to orographic forcing (Tanguay et al. 1992). In the horizontal the discretisation uses an Arakawa staggered C-grid and in the vertical a hybrid terrain-following hydrostatic-pressure coordinate (σ-p-coordinates; Laprise 1992). The parameterisations of the ensemble effect of subgrid-scale physical processes include the Kain & Fritsch (1990) deep-convection, the Kuo-transient (Kuo 1965, Bélair et al. 2005) shallow-convection schemes, the Sundqvist (Sundqvist et al. 1989) relative humidity based large-scale condensation scheme, and the correlated-K radiation scheme (Li & Barker 2005). The vertical diffusion is computed following approaches described in Benoit et al. (1989), Delage & Girard (1992), and Delage (1997). The model uses a weak lateral diffusion.

The version 5 of the High-Resolution Limited-Area Model (HIRHAM5) is based on the dynamics of the High-Resolution Limited-Area Model (HIRLAM7; Undén et al. 2002) and the parameterisations of subgrid-scale physical processes from the global atmospheric model ECHAM5 (Roeckner et al. 2003) developed at the Max-Planck Institute (MPI) for Meteorology. HIRHAM5 is described in detail in Christensen et al. (2007); it was developed in collaboration between the Danish Climate Centre at Danish Meteorological Institute (DMI) and the Potsdam Research Unit of the Alfred Wegener Institute Helmholtz Centre for Polar and Marine Research (AWI). The model's dynamics uses a semi-implicit leapfrog scheme. In the horizontal, the discretisation uses also an Arakawa staggered C-grid and σ-p-coordinates in the vertical. The parameterisations include convection mass-flux scheme of Tiedtke (1989), condensation using the prognostic statistical cloud scheme of Tompkins (2002), solar and terrestrial radiation schemes based on Fouquart & Bonnel (1980) and Mlawer et al. (1997), and vertical diffusion of Roeckner et al. (2003). The model also uses a weak lateral diffusion.

Experiment design and simulations

Two sets of 20-member simulations were performed with CRCM5 and HIRHAM5 over the Arctic region with its complex topography, including the Greenland Ice Sheet exceeds 3 km of height (Fig. 1). The study domain is rectangular, centred on the North Pole (Fig. 1). For each RCM, integrations were launched starting on July 1st, 2012 at 0000 UTC (1st simulation), and followed on each 6 hours up to July 5th, 2012 at 1800 UTC (20th simulation). All integrations share exactly the same LBC for atmospheric fields and lower boundary conditions with prescribed sea-surface temperature (SST) and sea-ice cover (SIC) for the ocean surface from the ERA-Interim data. For other surface ICs, such as land-surface temperature and volumetric water contents of soil, sea ice temperature and snow depth and density, the two models use different sources of data since these were not available in ERA-Interim. The CRCM5 applies data from an earlier simulation run from November 2008 to July 2012, while the HIRHAM5 uses the archived climate data for the month of July (Hagemann 2002). Another detail is that the sea ice thickness is computed in CRCM5 following Semtner (1976) for the model thermodynamic of sea ice growth and following Ebert & Curry (1993) and Flato & Brown (1996) for the parameterisation of albedo, conductivity and heat, whereas it is set constant at 2 m in HIRHAM5. In CRCM5, the growth of sea ice can reach a thickness more or less than the 2 m in different sectors of the Arctic region (result not shown).

The simulations were integrated over a horizontal grid mesh of 0.25° of rotated longitude and latitude, with a 12-minute

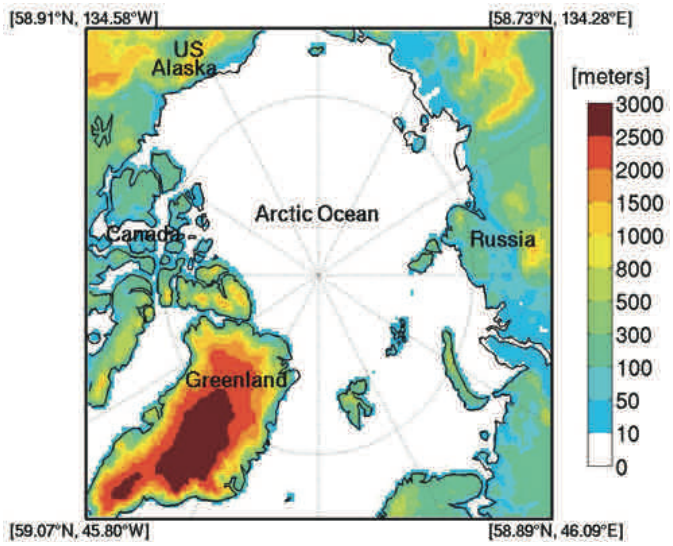

Fig. 1: The common analysis domain for the two RCMs (CRCM5 and HIRHAM5) over the Arctic area and topography (m). The longitude and latitude coordinates of the corners are indicated.

Abb. 1: Das Gebiet der Arktis inklusive der Orographie (m) für das die beiden RCMs (CRCM5 und HIRHAM5) angewendet werden. In den Ecken sind die Längen- und Breitengrade angegeben.

time step and 2-minute time step for CRCM5 and HIRHAM5, respectively. For technical reasons related to the model's computational, the CRCM5 has 236 × 220 grid points including a 10-grid-point wide semi-Lagrangian halo and a 10-grid-point wide sponge zone around the perimeter, resulting in a 196 × 180 free computational domain. The HIRHAM5 has 218 × 200 grid cells, with 10-grid-point wide sponge zone around the perimeter, resulting in a 198 × 180 free computational domain. Hence the two models use nearly identical free domains. The analysis domain will comprise a common subset region of 188 × 170 grid points (Fig. 1) in order to facilitate comparison. In the vertical, 56 and 40 terrain-following levels were used for CRCM5 and HIRHAM5, respectively, with the top level near 10 hPa. The simulated fields of both models were interpolated on the following 19 pressure levels: 1000, 975, 950, 925, 900, 850, 800, 700, 600, 500, 400, 300, 250, 200, 100, 70, 50, 30 and 10 hPa. The simulations were archived at 3 and 6 hours intervals for CRCM5 and HIRHAM5, respectively, from July 6th, 2012 at 0000 UTC to September 30th, 2012 at 1800 UTC.

Inter-member variability budget equation for potential temperature

The potential temperature $\left(\theta = T\left(p_0/p\right)^{R/C_p}\right)$ is the temperature that a parcel of dry air at pressure p and temperature T would have if it were expanded or compressed adiabatically to a standard pressure p_0. This atmospheric variable is important because every air parcel has a unique value, which is conserved for dry adiabatic motion (e.g., HOLTON 2004). This variable gives a simple mathematic expression of the first law of thermodynamic expressed as follows

$$d\theta/dt = J \tag{1}$$

where $J = Q\left(p_o/p\right)^{R/C_p}/C_p$ and Q is the sum of heat sources/sinks in the atmosphere. Starting from this equation, NL11a established budget equation for the potential temperature IV. In the following, we briefly summarise the methodology and we refer the reader to NL11a for more details on the algebraic details. Noting by n the simulation index in an ensemble of N members, each atmospheric variable $\varphi_n \in \{\theta_n, U_n, V_n, \omega_n, J_n\}$ can be split in two parts: an ensemble-mean part $\langle\varphi\rangle$ and the member deviations there of φ'_n:

$$\varphi_n = \langle\varphi\rangle + \varphi'_n \tag{2}$$

with the ensemble-mean calculated as

$$\langle\varphi\rangle = \frac{1}{N}\sum_{n=1}^{N}\varphi_n \tag{3}$$

The inter-member variability is calculated as the inter-member variance σ_φ^2 of the variable φ_n approximated as the ensemble-mean of the deviation square:

$$\sigma_\varphi^2(i,j,k,t) \approx \frac{1}{N}\sum_{n=1}^{N}\varphi'^2_n(i,j,k,t) \equiv \left\langle\varphi'^2_n\right\rangle(i,j,k,t) \tag{4}$$

Starting from (1), the budget equation for the potential temperature IV (σ_θ^2) is written as follows:

$$L_\theta = R_\theta = A_h + A_v + B_h + B_v + C + E \tag{5}$$

where terms are given by:

$$L_\theta = \frac{\partial\sigma_\theta^2}{\partial t};$$

$$A_h = -\vec{\nabla}\bullet\left(\left\langle\vec{V}\right\rangle\sigma_\theta^2\right); \quad A_v = -\frac{\partial\left(\left\langle\omega\right\rangle\sigma_\theta^2\right)}{\partial p}$$

$$B_h = -2\left\langle\theta'_n\vec{V'_n}\right\rangle\bullet\vec{\nabla}\left\langle\theta\right\rangle; \quad B_v = -2\left\langle\theta'_n\omega'_n\right\rangle\frac{\partial\left\langle\theta\right\rangle}{\partial p}$$

$$C = 2\left\langle\theta'_n J'_n\right\rangle;$$

$$E = -2\left\langle\theta'_n\vec{\nabla}\bullet\left(\theta'_n\vec{V'_n}\right)\right\rangle - 2\left\langle\theta'_n\frac{\partial}{\partial p}\left(\theta'_n\omega'_n\right)\right\rangle$$

The local change of the potential temperature variance (L_θ, referred to as the "left-hand side" term) is calculated from the time evolution of the inter-member variance of the ensemble. The "right-hand side" term (R_θ) results from the sum of six contributions:

- The horizontal (A_h) and vertical (A_v) transport terms that describe the convergence of the potential temperature IV by the ensemble-mean flow;
- The horizontal (B_h) and vertical (B_v) conversion terms that represent the covariances of potential temperature and horizontal and vertical flow fluctuations in the direction of the ensemble-mean potential temperature gradient;
- The term C represents a diabatic generation (source/sink) term resulting from the covariance of fluctuations of potential temperature and diabatic heating rate (J'_n), which includes contributions from latent heat release (C_{cond}), convective heating (C_{conv}), radiation heating (C_{rad}), vertical diffusion (C_{VDif}) and lateral diffusion (C_{HDif});
- The third-order term (E) is the covariance of the potential temperature fluctuations and divergence of potential temperature flux due to fluctuations.

RESULTS AND ANALYSIS

Inter-member variability (IV) in CRCM5 and HIRHAM5 simulations

Figure 2a displays the time evolution of the potential temperature IV for CRCM5 (solid lines) and HIRHAM5 (dashed lines) at 500 hPa (red lines), at 925 hPa (blue lines), and integrated over the troposphere between 300 hPa and the surface (black lines). The potential temperature IV is displayed as the square root of the horizontal domain average of σ_θ^2. The inter-member variability of the ensemble simulations of both models show remarkable similarity: the IV grows during a "spin-up" period of around 5 days and then reaches a quasi-equilibrium due to the control exerted by the LBC (GIORGI & BI 2000), with fluctuations in time and occasional episodes of larger IV. Although the CRCM5's IV is slightly larger than HIRHAM5's IV most the time, the time evolution of the two RCM's IV are highly synchronous, with correlation coefficients of 0.90, 0.91 and 0.93 for 500 hPa, 925 hPa and tropospheric average, respectively.

Figure 2b shows the vertical profile of the domain-averaged potential temperature IV, averaged in time over 82 days (from July 11th to September 30th 2012, thus excluding the spin-up period). Although the CRCM5's IV is larger than HIRHAM5's IV at all pressure levels, the two models exhibit very similar

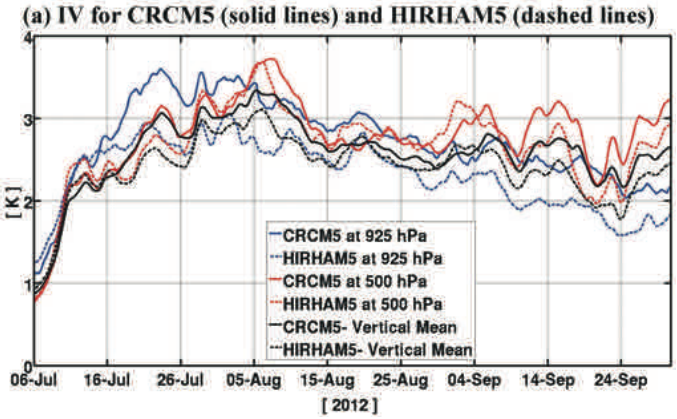

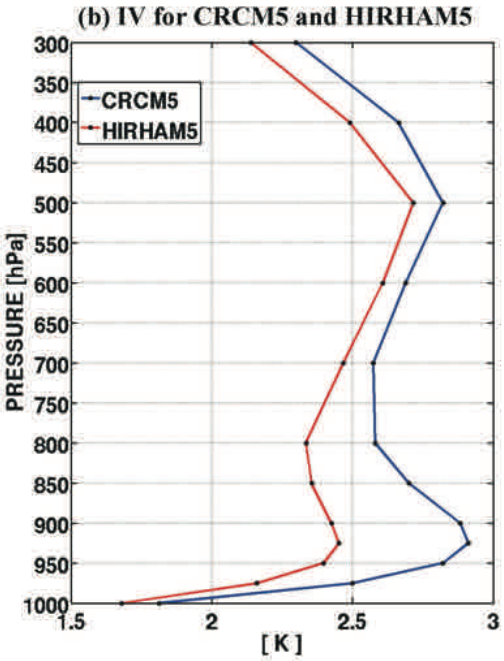

Fig. 2: (a): Time evolutions of the domain-averaged IV (inter-member variability) in K and (b): vertical profiles of time- and horizontal-averaged IV for potential temperature.

Abb. 2: (a): Zeitreihen der gebietsgemittelten IV (inter-member variability/ Variabilität zwischen den Ensemblemitgliedern) (in K) und (b): Vertikalprofile der zeitlich und räumlich gemittelten IV für die potentielle Temperatur.

vertical profiles of IV, with minimum values of about 1.8 K and 1.7 K at 1000 hPa, and maximum values of 2.8 K and 2.4 K at 925 hPa, and 2.8 K and 2.7 K at 500 hPa for CRCM5 and HIRHAM5, respectively. By comparison with mid-latitude regional domains, NL11a found that the maximum values of IV are located at around 200 hPa, close to the tropopause level.

Figure 3 presents the maps of the 82-day time-averaged potential temperature IV for CRCM5 at 500 hPa (a), 925 hPa (b), and the vertical integral between 300 hPa and the surface (c). The intense IV is found in the middle of the study domain and it decreases toward the boundaries because all simulations share the same LBC and, hence perforce $\sigma_\theta^2 = 0$, HIRHAM5 IV patterns were found to be very similar to those of CRCM5 and, for this reason, panels on the right-hand side in Figure 3 rather show the differences between the two models IV (CRCM5 minus HIRHAM5). Figure 3e shows that the maximum difference in IV occurs in the low levels near the Severnaya Zemlya Archipelago; we speculate that this could be the result of the use of different parameterisations for boundary-layer, land-surface and sea-ice schemes in the two models.

Contributions to potential temperature IV (Inter-member variability) budget

Figure 4a presents the time evolution of the various contributions to the tendency of potential temperature IV, averaged over the domain, for the two models (CRCM5 in solid lines and HIRHAM5 in dashed lines). There is a remarkable similarity of the various contributions between the two models, both in terms of amplitude of contributions and synchronicity of their fluctuations, confirming that the same physical processes are acting in both models to contribute to the IV tendency. It is clearly seen that B_h and C are systematically positive contributions, while the terms B_v and A_h are negative contributions for both RCMs, with the dominant positive and negative contributions to the IV tendency being B_h and B_v, respectively. In both models, the vertical IV transport term (A_v) and the third-order term (E) do not contribute much to IV tendency on average, although the term E is occasionally non-negligible when the IV is large.

Figure 4b shows the vertical profiles of the time-mean and horizontal average of each contribution to σ_θ^2 tendency. Again the vertical structure indicates four dominant terms, A_h, B_h, B_v, and C, with similar vertical structure in the two models. The largest difference between the two models occurs in the term C, which will be commented upon later in the following section. At all pressure levels, B_h contributes positively to the IV tendency, while A_h and B_v act as negative contributions. Contrary to what is seen in Figure 4a where the term C contributes positively in a vertically averaged sense, we note that it exhibits a negative contribution near the surface in both models. In the mid-troposphere, the positive contributions of B_h and C counterbalance the negative contributions of B_v and A_h, resulting in a vanishing IV tendency on long time scales. Indeed, the two RCM's results reveal that the tendency term (L_θ) is nearly zero at all pressure levels (not shown); this means that there is no trend in IV although it greatly fluctuates in time. Below 900 hPa, the only positive contribution comes from the horizontal baroclinic conversion term B_h, which is offset by the negative contributions of (B_v + C). The terms A_v and E are much smaller compared to the other terms at all levels, and they will not be discussed further in the following.

Figure 5 shows the spatial patterns of the time-averaged contributions to the 500-hPa potential temperature IV tendency for CRCM5 (panels on the left-hand side), for the four dominant terms (A_h, B_h, B_v, and C). Again given that the HIRHAM5 results are very similar to those of CRCM5, we chose to show the differences between the two models (CRCM5 minus HIRHAM5) on the right-hand side panels in Fig. 5). It is clearly seen that B_h and C contribute to generate IV while B_v contributes to destroy IV, at 500 hPa. The two models exhibit very similar patterns overall, but with locally some larger differences, especially for A_h and to some extent also for B_h.

Figure 6 presents similar maps, but this time for the vertical integral of the contributions. Again the results of both models

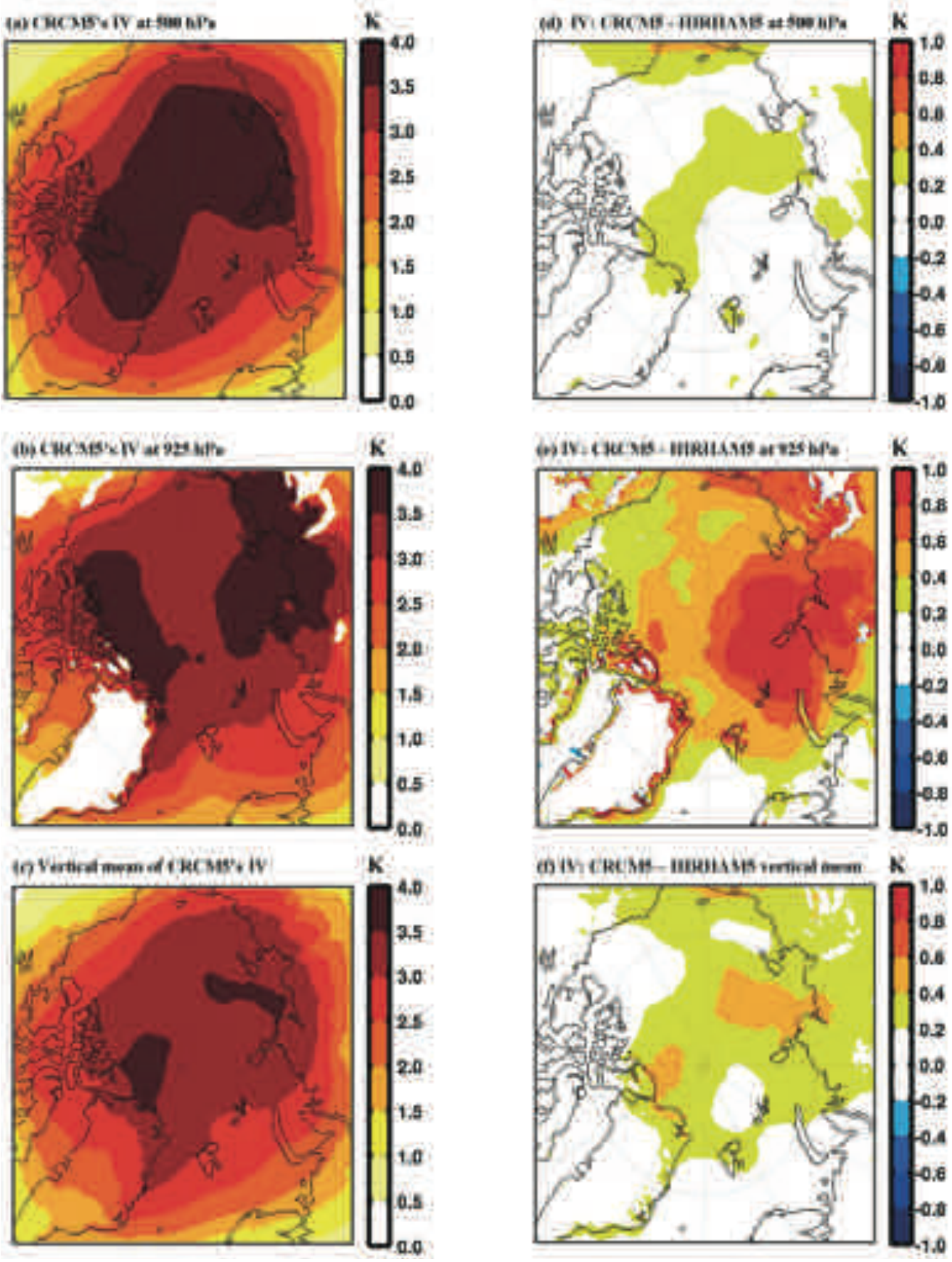

Fig. 3: Time average of potential temperature IV for CRCM5 at 500 hPa (a), 925 hPa (b) and vertical average from 300 hPa to the surface (c). The right-hand side panels (d, e, f) show the corresponding differences between CRCM5 and HIRHAM5.

Abb. 3: Zeitlich gemittelte IV der potentiellen Temperatur für das CRCM5 in 500 hPa (a), 925 hPa (b) und vertikal von 300 hPa bis zum Boden gemittelt (c). Die rechten Abbildungen zeigen die entsprechenden Differenzen zwischen CRCM5 und HIRHAM5.

are very similar. The largest systematic difference is found in the term C, mostly near the coasts and adjacent land, and high mountains (e.g., East-Siberian and Ural mountains). Investigation has revealed that this difference is due to the neglect of the lateral diffusion contribution in the HIRHAM5 IV budget. This also explains the difference of results between the two models seen in Figure 4b for the vertical profile of *C*, as the lateral diffusion contributes negatively to IV tendency (NL11a). The term *C* in Figure 6 also shows that largest difference in IV tendency between the two RCMs occurs around the perimeter of the Arctic Ocean. We speculate that this could be connected with the differing soil and land-surface schemes in the two models.

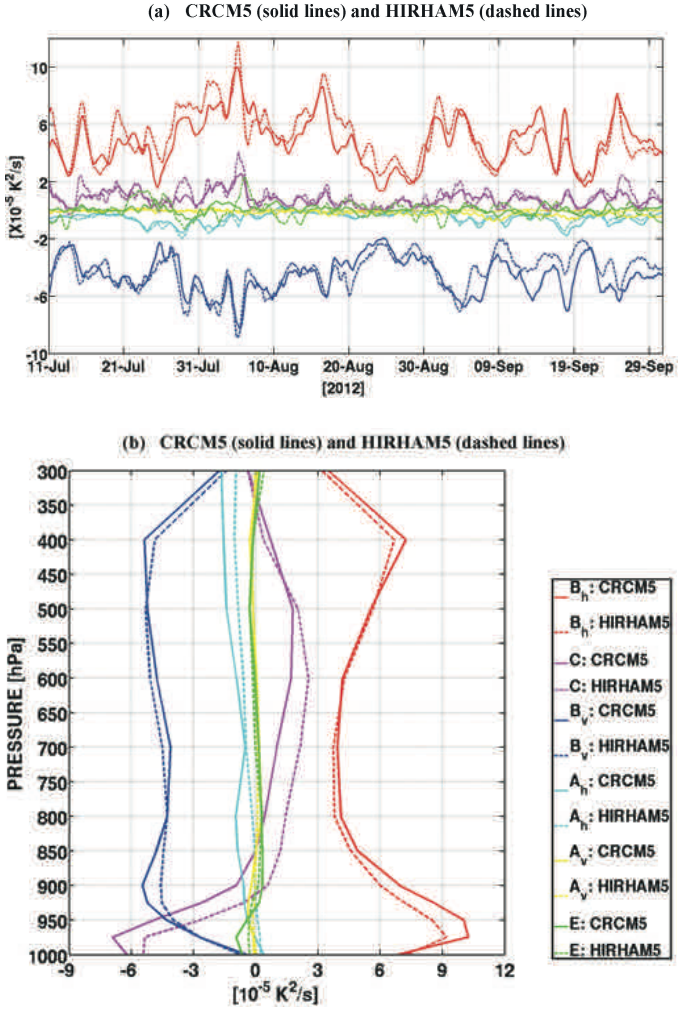

Fig. 4: (a) Time evolution of the domain average and (b) vertical profiles of the time- and horizontal-average of different terms in the budget equation of potential temperature IV (inter-member variability) for CRCM5 (solid lines) and HIRHAM5 (dashed lines). The legend on the bottom right-hand side identifies the various terms in the two panels (a) and (b).

Abb. 4: (a) Zeitreihen der räumlich gemittelten und (b) Vertikalprofile der zeitlich und räumlich gemittelten Terme der IV (Variabilität zwischen den Ensemblemitgliedern) Budgetgleichung für die potentielle Temperatur für CRCM5 (durchgezogene Linien) und HIRHAM5 (gestrichelte Linie). Die Legende rechts unten zeigt die verschiedenen Terme in den beiden Abbildungen (a) und (b).

Physical interpretation of potential temperature IV (Inter-member variability) budget

The analysis of various contributions to the term *C* for CRCM5 (Fig. 7a) indicates that its positive contribution to IV tendency in mid-troposphere is mainly due to effect of the condensation process (C_{cond}). The radiation process (C_{rad}) also contributes positively to IV tendency in mid-troposphere, but with less intensity. At the vicinity of 925 hPa, we note that C_{cond} and C_{rad} processes have compensating contributions to C in a horizontal average sense (Fig. 7a). This compensation even holds to a large extent in the spatial distribution of these fields at 925 hPa (Fig. 7b, 7c). These results indicate that the radiative heating and temperature perturbations are positively correlated throughout the atmosphere, whereas condensational heating and temperature perturbations are positively correlated in the middle troposphere (probably due to preferential condensation in warmer and more humid air) and negatively correlated in the low troposphere (apparently due to preferential condensation in colder air or evaporation of precipitation in warmer air). Finally, the lateral (horizontal) diffusion (C_{HDif}) contributes negatively to IV tendency throughout the atmosphere, while the vertical diffusion (C_{VDif}) contributes negatively to IV tendency near the surface and positively aloft. For both RCMs, the dominant positive and negative contributions to the IV tendency are the baroclinic terms B_h and B_v, respectively, with rather small differences between the two models.

The positive contribution of the term B_h (Fig. 6) indicates that the horizontal heat flux due to perturbation wind and temperature covariance is "down the gradient" of the ensemble-mean potential temperature, as noted by NL11a and NL11b. This reflects the fact that positive covariance of horizontal wind and potential temperature fluctuations ($\langle \overline{V}'_n \theta'_n \rangle$) occurs where there is negative horizontal gradient of the ensemble-mean potential temperature ($\overline{\nabla} \langle \theta \rangle$). This means that warm air flux moves heat towards cold regions, and cold air flux moves heat away from warm regions.

On the other hand, the intense negative contribution of B_v (Fig. 6) indicates a negative covariance of vertical motion ω and potential temperature fluctuations ($\langle \omega'_n \theta'_n \rangle < 0$) given the general presence of a negative presence of a negative vertical (pressure) gradient of ensemble-mean ($\partial \langle \theta \rangle / \partial p < 0$), potential temperature in stable atmosphere (Fig. 8). This means that warm air rises and cold air sinks in perturbations from the ensemble-mean conditions, which tends to suppress the potential temperature IV, as noted by NL11a and NL11b.

On a horizontal-mean and time-average basis, the term A_h acts as a sink to IV (Fig. 4). This means that IV is lost by its transport outside the study domain by the ensemble-mean horizontal flow (NL11a and NL11b). On the other hand, the spatial distribution of A_h (Fig. 6) shows locally positive and negative contributions; the dipoles of signs indicate the direction of IV's transport within the study domain by the ensemble-mean horizontal flow.

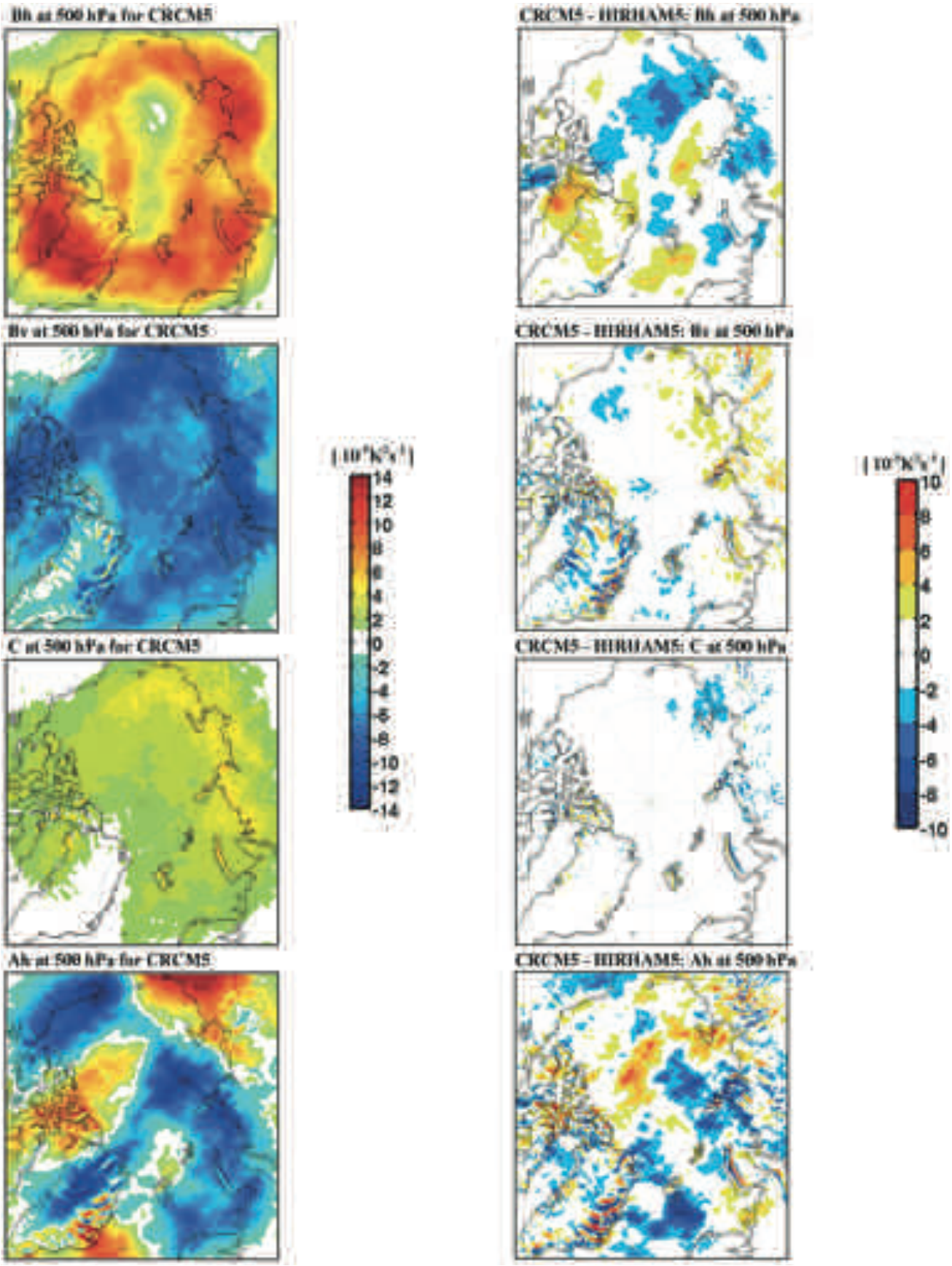

Fig. 5: On the left-hand side: Time-average maps of the four main terms in the budget equation of potential temperature IV (see Equation 5) at 500 hPa for CRCM5. On the right-hand side: Difference time-average between the two models (CRCM5 minus HIRHAM5).

Abb. 5: Links: Zeitlich gemittelte vier Hauptterme der IV-Budgetgleichung für die potentielle Temperatur (Gleichung 5) in 500 hPa für das CRCM5. Rechts: Zeitlich gemittelte Differenzen zwischen beiden Modellen (CRCM5 und HIRHAM5).

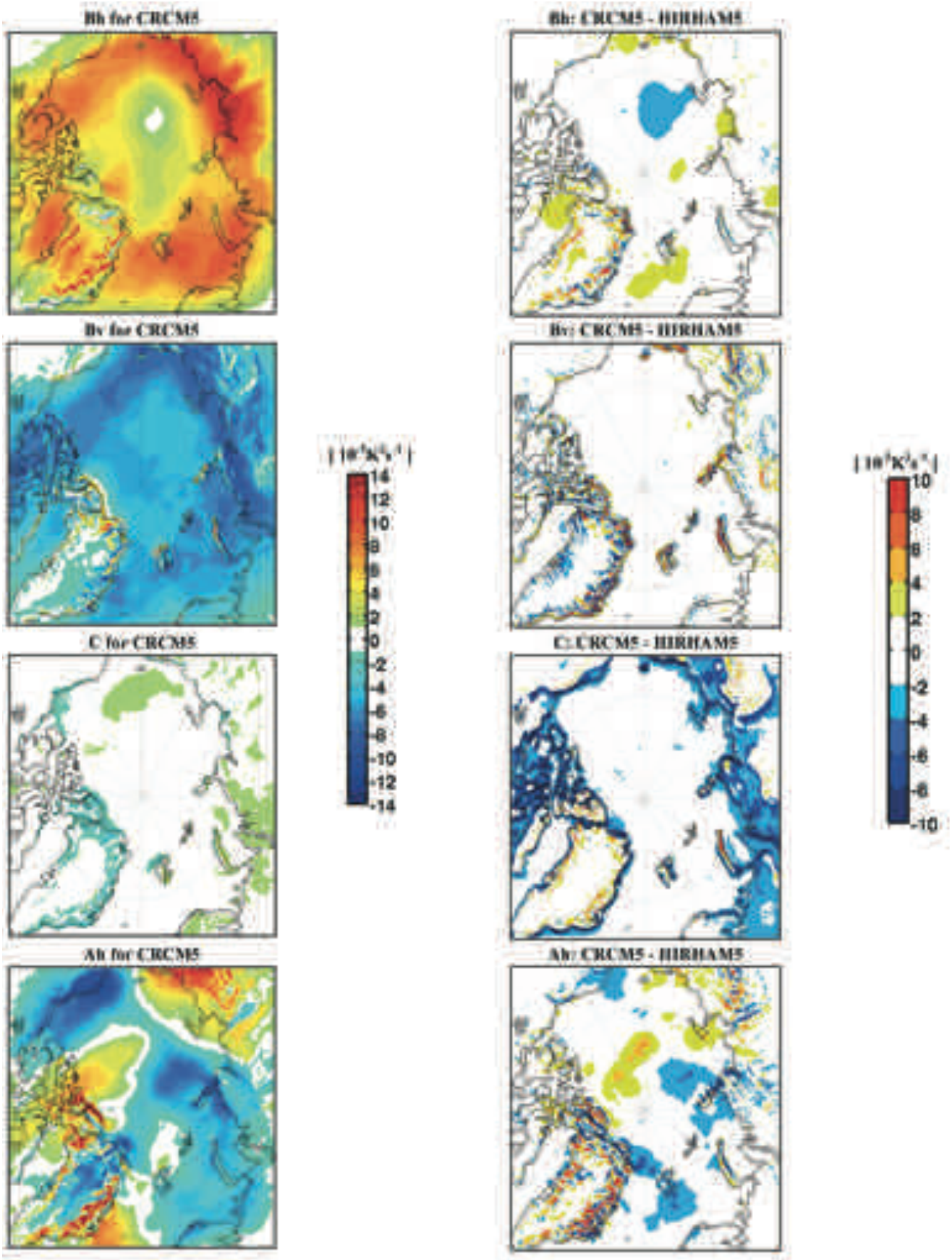

Fig. 6: Time- and vertical-average for CRCM5 (left panels) and differences of the time- and vertical-average (right panels) between the two models (CRCM5 minus HIRHAM5) of the main four terms in the budget equation of potential temperature IV (Equation 5).

Abb. 6: Zeitlich und vertikal gemittelte vier Hauptterme der IV-Budgetgleichung für die potentielle Temperatur (Gleichung 5) für das CRCM5 (links) und die Differenz zwischen beiden Modellen (CRCM5 minus HIRHAM5) (rechts).

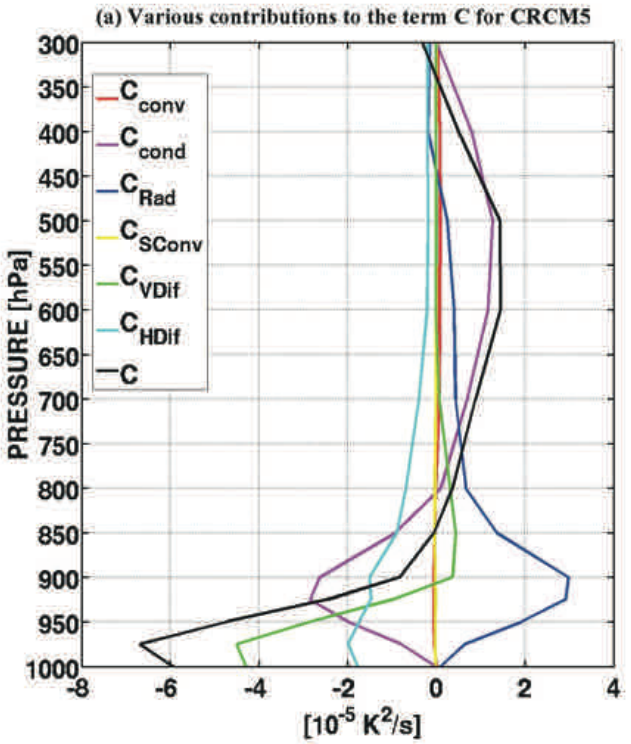

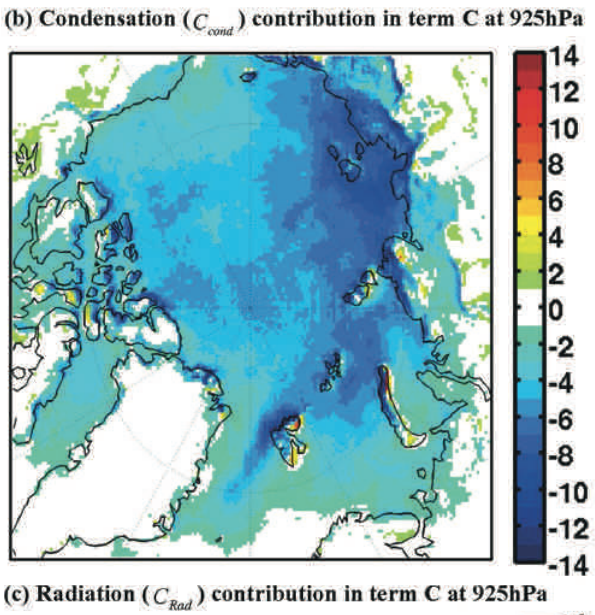

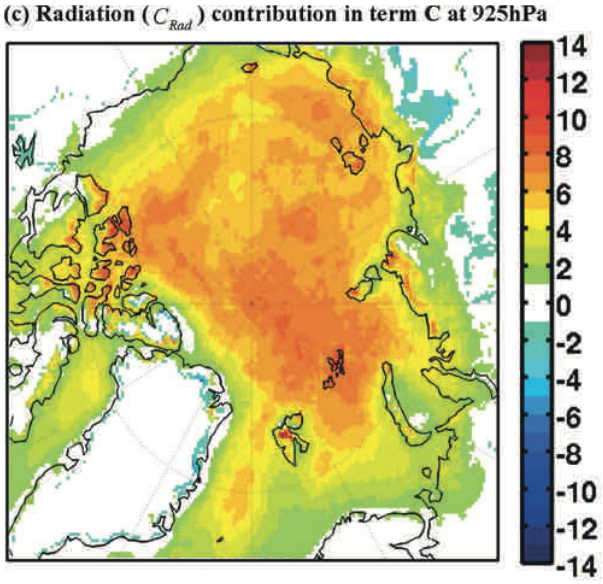

Fig. 7: (a): Vertical profiles of time- and domain-average of various physical processes in J_n of the term C which contributes to the potential temperature IV (inter-member variability) tendency in CRCM5. (b): The patterns of condensation and (c): radiation processes contributions are shown at 925 hPa. The unity of the colour bar in (b) and (c) is 10^{-5} K^2s^{-1}.

Abb. 7: (a): Vertikalprofile der zeitlich und räumlich gemittelten individuellen physikalischen Prozesse in J_n des Terms C der zur IV (Variabilität zwischen den Ensemblemitgliedern) Tendenz der potentiellen Temperatur im CRCM5 beiträgt. Die räumlichen Muster zeigen die Beiträge der Kondensations- (b) und Strahlungsprozesse (c) in 925 hPa. Die Einheit der Farbskala in (b) und (c) ist 10^{-5} K^2s^{-1}.

Fig. 8: Time- and vertical-average of (a) the covariance of fluctuations and (b) the vertical gradient of the ensemble-mean potential temperature in the term $\boldsymbol{B}_v$ for the CRCM5.

Abb. 8: Zeitlich und vertikal gemittelte (a) Kovarianz der Abweichungen und (b) vertikale Gradient des Ensemblemittels der potentiellen Temperatur des Terms $\boldsymbol{B}_v$ für das CRCM5.

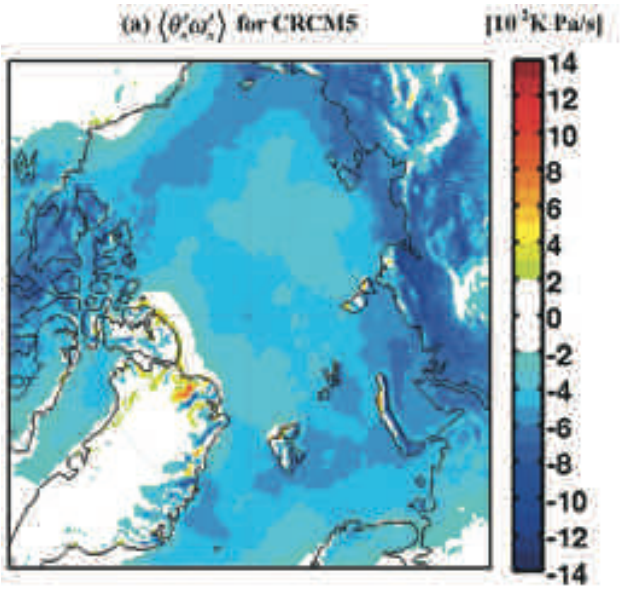

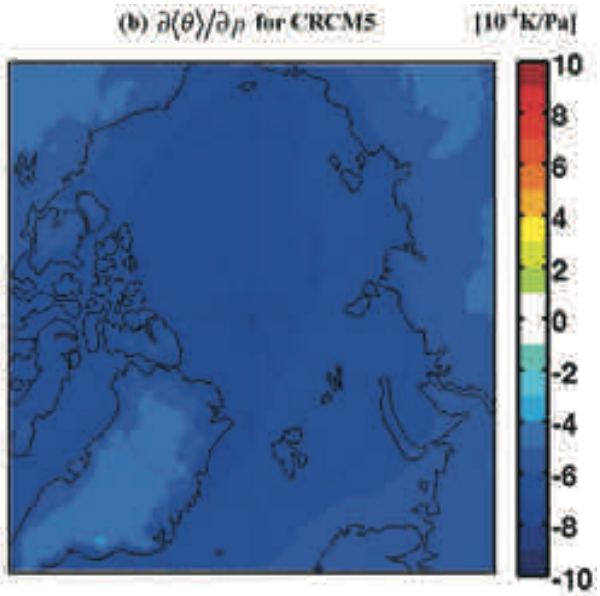

SUMMARY AND CONCLUSION

In ensembles of nested RCM simulations driven by identical lateral boundary conditions (LBC), inter-member variability (IV, defined as the spread amongst members around the ensemble-mean) greatly varies depending on atmospheric weather regimes, season, domain size and the regional domain of interest, as other studies have shown. Previous studies of budget diagnostics of IV have shed some light on physical processes responsible for the maintenance of IV and its variations in time (NL11a, NL11b, SOMMERFELD et al. 2015), but these studies were performed with only a single RCM. This study explored processes related to IV using two sets of twenty simulations performed with two different RCMs, CRCM5 and HIRHAM5, over the same study domain, the circum-Arctic, for the months of July, August and September 2012.

Despite the very different model formulations, the time evolution of domain-averaged IV, the vertical profile of horizontal- and time-averaged IV, and horizontal maps of the time- and vertical-averaged IV were found to be very similar in both models, although the IV was somewhat larger in CRCM5 than in HIRHAM5. The good time correlations between IV fluctuations is indicative that the IV is closely tied to synoptic events during the simulations, as noted by previous studies (e.g., ALEXANDRU et al. 2007, NL11a, NL11b, SOMMERFELD et al. 2015).

The budget study of IV in the two ensembles revealed that two terms ($B_h = -2\left\langle \vec{V}_n' \theta_n' \right\rangle \cdot \vec{\nabla}\langle\theta\rangle$ and $B_v = -2\langle \omega_n' \theta_n' \rangle \frac{\partial\langle\theta\rangle}{\partial p}$) are the most important contributions, contributing systematically positively and negatively at all pressure levels, respectively, to the potential temperature IV tendency. The contribution B_h acts positively because the heat transport by covariance of fluctuations is down-the-gradient in the ensemble-mean state. On the other hand, the term B_v acts negatively, which implies that warm fluctuations rise and cold fluctuations sink on average. There appears to exist a close analogy between this IV budget, with perturbation growth due to the term B_h and decay due the term B_v, and the baroclinic conversion from transient-eddy perturbations available potential enthalpy to perturbation kinetic energy (e.g., LORENZ 1955, 1967, NL11a, NL11b).

The term $C\ (=2\langle \theta_n' J_n' \rangle)$ also exhibits positive contributions to IV tendency in mid-troposphere due mainly to the condensation process that is positively correlated with temperature. Near the surface, this term C acts negatively to IV tendency due to diffusion (horizontal and vertical) processes. The contribution $A_h = -\vec{\nabla} \cdot (\langle \vec{V} \rangle \sigma_\theta^2)$ reflects the transport of IV by the ensemble-mean flow. On average, this term acts as a sink because it contributes to reduce IV by transport outside the study domain. But, the term A_h shows patterns of positive and negative values, indicating the IV transport within the study domain.

This budget study of the potential temperature IV performed with two models over an Arctic domain revealed rather different underlying processes to the existence and fluctuations of IV from the study of NL11a and N11b over a mid-latitude domain for a summer season. They found that the term B_v has similar magnitude as C throughout the troposphere, but with opposite sign. Their study also showed that the term C is the most important contribution to IV growth associated with local and intermittent physical processes linked with convection and condensation. Over the Arctic domain the term B_h is the most important contribution to IV growth, confirming that the baroclinic processes are more important over the Arctic region (RINKE & DETHLOFF 2000, SOMMERFELD et al. 2015) compared to North America domain where convection and condensation processes (in term C) are important in summer (NL11a, NL11b). The present study and those of NL11a, NL 11b and SOMMERFELD et al. (2015) reveal that the term B_v is the most important contribution that suppresses the potential temperature IV. Contrary to what is seen for Arctic region, the term A_h contributed only negatively over North American domain (NL11b) because of the actions of horizontal ensemble-mean flow that transports large pockets of IV outside the regional domain. Over the mid-latitude region, the episode of rapid decrease of IV is due to westerly flow that contributes to sweep away the IV. This result is different compared to what is seen over Arctic region where IV moves and mostly remains within the regional domain.

Despite the very different model formulations, the IV features of the two RCMs ensembles were found to be very similar, lending confidence in the earlier speculation that RCMs IV reflects a physical behaviour of numerical simulations of the chaotic climate system, subject to the partial control exerted by LBC of nested models, and not a numerical artefact associated, for example, to the nesting technique. How IV connected with baroclinic instability processes could feed back with planetary atmospheric circulation structures and influence climate variability from seasonal to inter-annual and decadal time scales is a matter of ongoing discussion with respect to Arctic-mid-latitude linkages as, e.g., discussed by COHEN et al. (2014).

IV, rather than being seen as an evil in RCM simulations, might even be exploited to facilitate accessing the full range of physiccally plausible solutions corresponding to a set of imposed LBC. When, however, an RCM experiment is carried out for which synchronicity is required between the RCM-simulated weather and the large-scale driving fields provided at the LBC – such as for case studies or seasonal prediction – then techniques to suppress IV such as large-scale spectral nudging (e.g., von STORCH et al. 2000, ALEXANDRU et al. 2009, ŠEPAROVIĆ et al. 2009, LUCAS-PICHER et al. 2015) may be applied.

ACKNOWLEDGMENTS:

This research was done in collaboration between the UQAM's ESCER Centre in Montréal (Québec, Canada) and the Alfred Wegener Institute Helmholtz Centre for Polar and Marine Research (AWI) in Potsdam (Germany). This study was founded in Canada by the Climate Change and Atmospheric Research (CCAR) programme of the Natural Sciences and Engineering Research Council of Canada (NSERC) through a grant to the Canadian Network for Regional Climate and Weather Processes (CNRCWP), and in Germany by the Helmholtz Climate Initiative (REKLIM). The simulations were made possible through Compute Canada – Calcul Québec supercomputers for CRCM5, and the German Climate

Computing Centre (DKRZ, Hamburg) for HIRHAM5. The authors thank Mrs. Katja Winger, Mrs. Ines Hebestadt, Mrs. Nadjet Labassi and Mr. Georges Huard for the technical support and maintaining efficient and user-friendly local computing facilities.The authors wish to thank Jens Hesselbjerg Christensen and Emilia Sanchez-Gomez for their thorough reviews and helpful comments on the Manuscript.

References

CNRCWP <http://www.cnrcwp.uqam.ca>: Canadian Network for Regional Climate and Weather Processes; function tested on 15.03.2016.
ESCER/UQAM <http://www.escer.uqam.ca>: Centre pour l'etude et la simulation á l'echelle régionale (ESCER); function tested on 15.03.2016.
OURANOS <http://www.ouranos.ca/>: Consortium on regional climatology and adaptation to climate change; function tested on 15.03.2016.
REKLIM <http://www.reklim.de/en/>: Helmholtz Climate Initiative RE-KLIM (Regionale Klimaänderungen/Regional Climate Change); function tested on 15.03.2016.
RPN/MSC <http://collaboration.cmc.ec.gc.ca/science/rpn/>: Environment and climate change Canada; function tested on 15.03.2016.

Alexandru, A., de Elia, R. & Laprise, R. (2007): Internal Variability in regional c1imate downscaling at the seasonal scale.- Mon. Weather. Rev. 135: 3221-3238.
Alexandru, A., de Elía, R., Laprise, R., Šeparović, L. & Biner, S. (2009): Sensitivity study of regional climate model simulations to large-scale nudging parameters.- Mon. Weather Rev. 137: 1666-1686, doi: 10.1175/2008MWR2620.1,
Bélair, S., Mailhot, J., Girard, C. & Vaillancourt, P. (2005): Boundary-layer and shallow cumulus clouds in a medium-range forecast of a large-scale weather system.- Mon. Weather. Rev. 133: 1938-1960.
Benoit, R., Côté, J. & Mailhot, J. (1989): Inclusion of a TKE boundary layer parameterization in the Canadian regional finite-element model.- Mon. Weather Rev. 117:1726-1750.
Caya, D. & Biner, S. (2004): Internal variability of RCM simulations over an annual cycle.- Clim. Dyn. 22: 33-46.
Cohen, J., Screen, J.A., Furtado, J.C., Barlow, M., Whittleston, D., Coumou, D., Francis, J.A., Dethloff, K., Entekhabi, D., Overland, J.E., & Jones, J. (2014): Recent Arctic amplification and extreme mid-latitude weather.- Nature Geosci. 7: 627-637, doi: 10.1038/ngeo2234.
Côté, J., Gravel, S., Méthot, A., Patoine, A., Roch, M. & Staniforth, A. (1998): The operational CMC-MRB Global Environmental Multiscale (GEM) model: Part I. Design considerations and formulation.- Mon. Weather Rev. 126: 1373-1395.
Christensen, O.B., Gaertner, M.A., Prego, J.A. & Polcher, J. (2001): Internal variability of regional climate models.- Clim. Dyn. 17: 875-887.
Christensen, O.B., Drews, M., Christensen, J.H., Dethloff, K., Ketelsen, K., Hebestadt, I., & Rinke, A. (2007): Technical Report 06-17, The HIRHAM Regional Climate Model Version 5 (β).
Dee, D.P., Uppala, S.M., Simmons, A.J., Berrisford, P., Poli, P., Kobayashi, S., Andrae, U., Balmaseda, M.A., Balsamo, G. & Bauer, P. (2011): The ERA-Interim reanalysis: Configuration and performance of the data assimilation system.- Quart. J. Royal Meteorol. Soc. 137: 553-597, doi: 10.1002/qj.828.
Delage, Y. (1997): Parameterising sub-grid scale vertical transport in atmospheric models under statically stable conditions.- Bound Layer Meteorol. 82: 23-48.
Delage, Y. & Girard, C. (1992): Stability functions correct at the free convection limit and consistent for both the surface and Ekman layers.- Bound Layer Meteorol. 58: 19-31.
Ebert, E.E. & Curry, J.A. (1993): An intermediate one-dimensional thermodynamic sea ice model for investigating ice-atmosphere interactions.- J. Geophys. Res. 98: 10085-10109.
Flato, G.M. & Brown, R.D. (1996): Variability and climate sensitivity of landfast Arctic sea ice.- J. Geophys. Res. 101: 25,767-25,777.
Fouquart, Y. & Bonnel, B. (1980): Computation of solar heating of the Earth's atmosphere: a new parameterization.- Beitr. Phys. Atmos. 53: 35-62.
Giorgi, F. & Bi, X. (2000): A study of internal variability of regional climate model.- J. Geophys. Res. 105: 29503-29521.
Hagemann, S. (2002): An improved land surface parameter dataset for global and regional climate models.- Report 336, Max Planck-Institute for Meteorology, Hamburg.
Hernández-Díaz, L., Laprise, R., Sushama, L., Martynov, A., Winger, K. & Dugas, B. (2013): Climate simulation over CORDEX Africa domain using the fifth-generation Canadian Regional Climate Model (CRCM5).- Clim. Dyn. 40: 1415-1433, doi: 10.1007/s00382-012-1387-z.
Holton, J.R. (2004): An introduction to dynamic meteorology.- Academic Press, 1-535.
Kain, J.S. & Fritsch, J.M. (1990): A one-dimensional entraining/detraining plume model and application in convective parameterization.- J. Atmos. Sci. 47: 2784-2802.
Kuo, H.L. (1965): On formation and intensification of tropical cyclones through latent heat release by cumulus convection.- J. Atmos. Sci. 22: 40-63.
Laprise, R. (1992): The Euler equation of motion with hydrostatic pressure as independent variable.- Mon. Weather Rev. 120: 197-207.
Li, J. & Barker, H.W. (2005): A radiation algorithm with correlated-k distribution. Part I: local thermal equilibrium.- J. Atmos. Sci. 62: 286-309.
Lorenz, E.N. (1955): Available potential energy and the maintenance of the general circulation.- Tellus 7: 157-167.
Lorenz, E.N. (1967): The nature and theory of the general circulation of the atmosphere.- World Meteorol. Organ 218 TP 115, 1-161.
Lucas-Picher, P., Caya, D. & Biner, S. (2004): RCM's internal variability as function of domain size.- In: J. CÔTÉ (ed), Research activities in atmospheric and oceanic modelling, WMO/TD, 1220, 34: 7.27-7.28.
Lucas-Picher, P., Caya, D., de Elía, R. & Laprise, R. (2008): Investigation of regional climate models' internal variability with a ten-member ensemble of 10-year simulations over a large domain.- Clim Dyn 31: 927-940, doi: 10.1007/s00382-008-0384-8.
Lucas-Picher, P., Cattiaux, J., Bougie, A. & Laprise R. (2015): How does large-scale nudging in a regional climate model contribute to improving the simulation of weather regimes and seasonal extremes over North America?- Clim. Dyn. doi: 10.1007/s00382-015-2623-0.
Mlawer, E.J., Taubman, S.J., Brown, P.D., Iacono, M.J. & Clough, S.A. (1997): RRTM, a validated correlated-k model for the longwave.- J. Geophys. Res. 102: 16663-16682.
Nikiéma, O. & Laprise, R. (2011a): Diagnostic budget study of the internal variability in ensemble simulations of the Canadian RCM.- Clim. Dyn. 36: 2313-2337, doi: 10.1007/s00382-010-0834-y,
Nikiéma, O. & Laprise, R. (2011b): Budget study of the internal variability in ensemble simulations of the Canadian RCM at the seasonal scale.- J Geophys. Res. Atmos. 116: doi: 10.1029/2011JD015841.
Nikiéma, O. & Laprise, R. (2013): An approximate energy cycle for inter-member variability in ensemble simulations of a regional climate model.- Clim. Dyn. 44: 831-852, doi: 10.1007/s00382-012-1575-x.
Nikiéma, O. & Laprise, R. (2015): Energy cycle associated with inter-member variability in a large ensemble of simulations with the Canadian RCM (CRCM5).- Clim. Dyn. doi: 10.1007/s00382-015-2604-3.
NL11a = Nikiéma, O. & Laprise, R. (2011a): Diagnostic budget study of the internal variability in ensemble simulations of the Canadian RCM.- Clim. Dyn. 36: 2313-2337, doi: 10.1007/s00382-010-0834-y.
NL11b = Nikiéma, O. & Laprise, R. (2011b): Budget study of the internal variability in ensemble simulations of the Canadian RCM at the seasonal scale.- J Geophys. Res. Atmos. 116: doi: 10.1029/2011JD015841.
Rinke, A. & Dethloff, K. (2000): On the sensitivity of a regional Arctic climate model to initial and boundary conditions.- Clim. Res. 14: 101-113.
Rinke, A., Marbaix, P., & Dethloff, K. (2004): Internal variability in Arctic regional climate simulations: case study for the SHEBA year.- Clim. Res. 27: 197-209.
Roeckner, E., Bäuml, G., Bonaventura, L., Brokopf, R., Esch, M., Giorgetta, M., Hagemann, S., Kirchner, I., Kornblueh, L., Manzini, E., Rhodin, A., Schlese, U., Schulzweida, U. & Tompkins, A. (2003): The Atmospheric General Circulation Model ECHAM5-Part 1: Model Description.- Technical Report 349, Max-Planck-Institute (MPI) for Meteorology: Hamburg.
Semtner, A.J. (1976): A model for the thermodynamic growth of sea ice in numerical investigations of climate.- J. Phys. Oceanogr. 6: 379-389.
Šeparović, L., de Elía, R. & Laprise, R. (2012): Impact of spectral nudging and domain size in studies of RCM response to parameter modification.- Clim. Dyn. 38: 1325-1343, doi: 10.1007/s00382-011-1072-7.
Sommerfeld, A., Nikiéma, O., Rinke, A., Dethloff, K. & Laprise, R. (2015): Arctic budget study of Inter-member variability using HIRHAM5 ensemble simulations.- J. Geophys. Res. Atmos. 120: 9390-9407. 10.1002/2015JD023153.
Sundqvist, H., Berge, E. & Kristjansson, J.E. (1989): Condensation and cloud parameterization studies with a mesoscale numerical weather prediction model.- Mon. Weather Rev. 117: 1641-1657.
Tanguay, M., Yakimiv, E., Ritchie, H. & Robert, A. (1992): Advantages of spatial averaging in semi-implicit semi-Lagrangian schemes.- Mon. Weather Rev. 120: 115-123.
Tiedtke, M. (1989): A comprehensive mass flux scheme for cumulus parameterization in large-scale models.- Mon. Weather Rev. 117: 1779-1800, doi:
http://dx.doi.org/10.1175/15200493(1989)117<1779:ACMFSF>2.0.C0j2.
Tompkins, A.M. (2002): A prognostic parameterization for the subgridscale variability of water vapor and clouds in large-scale models and its use to diagnose cloud cover.- J. Atmos. Sci. 59: 1917-1942.

Undén, P., Rontu, L., Järvinen, H., Lynch, P., Calvo, J., Cats, G., Cuxart, J., Eerola, K., Fortelius, C. & Garcia-Moya, J.A. (2002): HIRLAM-5 scientific documentation. In HIRHAM-5 Project, Swedish Meteorological and Hydrological Institute (SMHI): Norrköping, Sweden, http://www.hirlam.org/index.php/meeting-reports-and-presentations/doc_view/270-hirlam-scientific-documentation-december-2002.

von Storch, H., Langenberg, H. & Feser F. (2000): A spectral nudging technique for dynamical downscaling purposes.- Mon. Weather Rev. 128: 3664-3673.

Weisse, R., Heyen, H. & von Storch, H. (2000): Sensitivity of a regional atmospheric model to a sea state dependent roughness and the need of ensemble calculations.- Mon. Weather Rev. 128: 3631-3642.

Zadra, A., Caya, D., Côté, J., Dugas, B., Jones, C., Laprise, R., Winger, K. & Caron, L.-P. (2008): The next Canadian regional c1imate model.- Phys. Canada 64: 74-83.

Polarforschung 85 (2), 81–84, 2015 (erschienen 2016)

Variability of Winter Sea Ice in Greenland-Iceland-Norwegian Sea in a Regionally Coupled Climate Model

by Anne Laura Niederdrenk[1*] and Uwe Mikolajewicz[1]

Abstract: To investigate interaction and feedback mechanisms of different climate components in the Arctic, we use a regional atmosphere-ocean model setup, consisting of the global ocean – sea-ice model MPIOM with high resolution in the Arctic coupled to the regional atmosphere model REMO. We perform an experiment using reanalysis data from the European Center of Medium Range Weather Forecast (ERA-40) as external forcing to simulate the climate of the last decades (1958–2001). We analyze this experiment in order to improve our understanding of ocean – sea-ice – atmosphere processes at the marginal ice zone in the Greenland-Iceland-Norwegian (GIN) Sea. We present first results on the variability of the marginal ice zone in GIN Sea, where in the last century the commonly named Arctic Odden has been observed frequently, an ice tongue with large daily variability in size and shape. We are interested in the dynamics of the formation of such a sea-ice tongue and show that in our model advection of ice rather than new ice formation is the driving mechanism.

Zusammenfassung: Um das Zusammenspiel und Rückkopplungseffekte zwischen den arktischen Klimakomponenten zu analysieren, verwenden wir ein regional gekoppeltes Atmosphären – Ozean-Modell, bestehend aus dem globalen Ozean – Meereis-Modell MPIOM mit hoher regionaler Auflösung in der Arktis und dem regionalen Atmosphärenmodel REMO. Als Randdaten für dieses Modell verwenden wir Reanalyse-Daten (ERA-40) des europäischen Zentrums für mittelfristige Wettervorhersagen ECMWF und simulieren das Klima der letzten Dekaden (1958–2001). Wir präsentieren erste Ergebnisse über die Meereisvariabilität in der Grönland-Island-Norwegen-See, in der im letzten Jahrhundert regelmäßig der sogenannte arktische Odden, eine Zunge aus Meereis mit großer täglicher Variabilität in Größe und Form, beobachtet wurde. Diese Eiszunge hat direkten Einfluss auf den Wärme- und Salzhaushalt in dieser Region und dadurch auf die Dynamik der darunterliegenden Wassermassen und die Tiefenwasserproduktion. Wir sind daran interessiert, wie solche arktischen Odden entstehen und zeigen, dass in unserem Modell eher Advektion von Eis als Bildung von neuem Eis der zugrunde liegende Mechanismus ist.

INTRODUCTION

The Arctic climate shows large annual and interannual variability. This variability and the interplay of the atmosphere, ocean and sea ice are poorly understood. Furthermore, large changes have been observed in recent years, such as the summer sea ice minimum in 2012. Observational time series are short and the resolution of global general circulation models is too coarse to adequately resolve small-scale processes and complex topography such as the Canadian archipelago. Hence, we use a high-resolution regionally coupled climate model to simulate the Arctic climate. Here we present first results on the variability of the marginal ice zone in the Greenland-Iceland-Norwegian (GIN) Sea, where in the last century the commonly named Arctic Odden has been observed frequently, an ice tongue with large daily variability in size and shape. Affecting the heat and salinity budgets and thereby the dynamics of the underlying water masses, this ice tongue has a direct influence on the deep-ocean convection (Paluszkiewicz et al. 1994, Wadhams et al. 2002). We are interested in the dynamics of such a sea ice tongue and how it is formed within our model. Is it Polar surface water diverted eastward from the East Greenland Current, leading to new ice formation or is eastward advection of multi-year sea ice or sea ice advected from the main pack the driving mechanism?

MODEL SETUP

Our regionally coupled model consists of the global ocean – sea-ice model MPIOM (Marsland et al. 2003) with shifted grid poles over North America and Russia, leading to high resolution in the Arctic (approximately 15 km in the mean and up to 5 km horizontal resolution in the coupled domain). The ocean model is coupled to the regional atmosphere model REMO (Aldrian et al. 2005, Mikolajewicz et al. 2005, Sein et al. 2014). The horizontal resolution of the atmosphere model is about 55 km. The domain of the atmosphere model covers the full catchment area of the Arctic rivers and a discharge model, providing lateral terrestrial water flows, is included. The model domains are shown in Figure 1. As external forcing needed for the ocean model in the uncoupled domain as well as for the atmosphere model at the lateral boundaries, we use the ERA-40 reanalysis dataset (ECMWF, 2002) from the European Center for Medium-Range Weather Forecasts. Our experiment covers the time period 1958–2001. The simulation was started from a pre-existing present-day state from a similar setup and was spun up for 40 years, using the 1960–1999 ERA-40 forcing. The model simulation shows a realistic mean state of the Arctic climate of the second half of the 20th century. An earlier version of the model setup has been validated in Niederdrenk (2013). The sea-ice extent is well represented (Fig. 2), especially in winter.

However, the number of months with a mean sea-ice concentration larger than 0.15 is slightly underestimated (Fig. 2), due to an underestimation of September sea-ice volume (not shown). In contrast to most global climate models, this regional model is capable to simulate an ice tongue in the marginal sea-ice zone in GIN Sea, namely the Arctic Odden, with large daily variability in shape and size.

RESULTS

Similar to the Nordbukta index defined by Germe et al. (2011), we define an Odden index as the difference between

doi:10.2312/polfor.2016.003

[1] Max Planck Institute for Meteorology, Bundesstraße 53, 20146 Hamburg, Germany;
[*] corresponding author <laura.niederdrenk@mpimet.mpg.de>

This extended abstract was presented as an oral contribution at the Inter-national Conference "Our Climate – Our Future: Regional Perspectives on a Global Challenge", 6–9 October 2014 in Berlin, Germany.
Manuscript received 31 May 2015; revised version 15 September; accepted 09 November 2015.

sea-ice concentration exceeding 0.15 in the region of the ice tongue (4.5° - 3° W, 72.8° - 73.5° N), when apparent, and in the Nordbukta region (8° - 6.8° W, 74.3° - 75.1° N). Since we are mainly interested in the Arctic Odden in a tongue form rather than large ice accumulations in the Nordbukta region, only positive values of the daily Odden index are presented (Fig. 3). In our model and similar to observations, the appearance of such an Odden persists from few days to several months. The earliest appearance can be found in December, the latest in April, almost equally distributed within these months. Some of the events in Figure 3, however, do not show a typical ice tongue but large ice deformations (in 1967 and 1979), sometimes even reaching the northern coast of Iceland (in 1965). In addition, there are winters, when instead of a tongue a large island evolves or splits from the ice east of Greenland, wobbling in the Greenland Sea for a few days and then melting or reattaching to the ice edge (in 1983). Since we are using a regionally coupled climate model, simulating a considerable internal variability, we are not able to simulate specific observed Odden events. However, the above-mentioned Odden formations all have been observed in the last century (Comiso et al. 2001, Rogers & Hung 2008). A specific example of an Odden ice tongue in January 1962 is given in Figure 4.

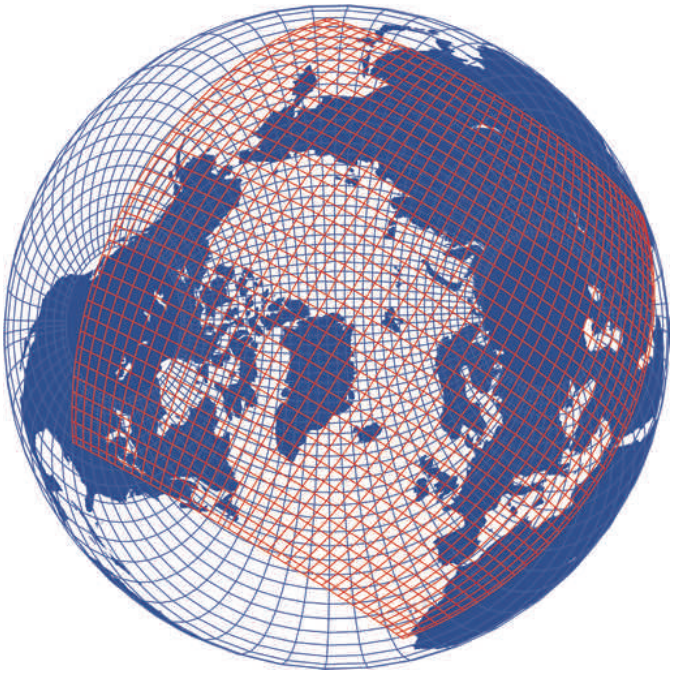

Fig. 1: Computational grids of the ocean – sea-ice model MPIOM (in blue) and the atmosphere model REMO (in red). Not every grid line is shown.

Abb. 1: Modellgitter des Ozean – Meereis-Modells MPIOM (in blau) und des Atmosphärenmodells REMO (in rot). Nicht jede Linie Gitterlinie wird gezeigt.

The formation of the Arctic Odden can be caused either by eastward advection of sea ice or due to freezing of cold polar water, which has been diverted eastward from the East Greenland current (Wadhams & Comiso 1999). Thus, the change of sea-ice thickness H is given by divergence of sea-ice transport Hv and freezing or melting due to oceanic and atmospheric fluxes ($F_{Oc} + F_{At}$):

$$\frac{\partial H}{\partial t} = -\nabla \cdot (Hv) + F_{Oc} + F_{At}$$

In contrast, previous studies state that especially in early winter, the Odden is a result of new ice formation associated with moderate westerly winds, bringing cold air from the Greenland Ice Sheets (Shuchman et al. 1998, Comiso et al. 2001, Rogers & Hung 2008). Wadhams & Comiso (1999), however, define a second Odden type and show that especially in late spring, when the thermodynamic conditions do not permit new ice growth in that region, also advection can be the driving mechanism for an Odden formation.

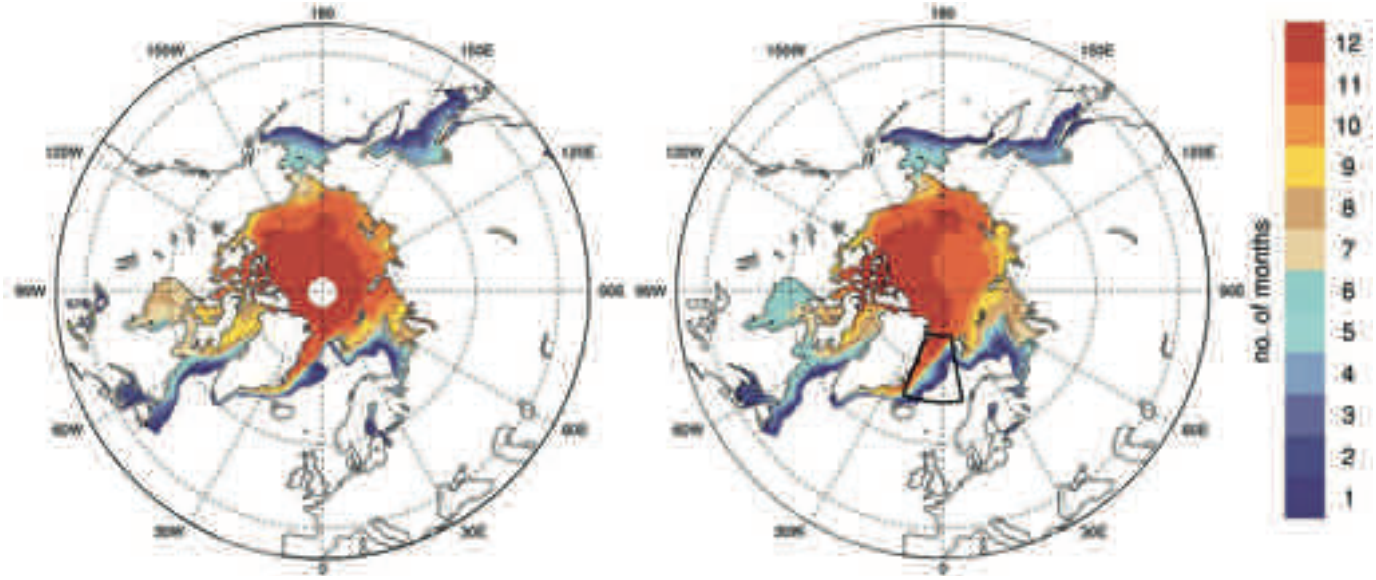

Fig. 2: Number of months with a sea-ice concentration larger than 0.15 for the years 1980–1999 of observations (SSM/I, left) and the model (right). The black box in the right panel is indicating the region shown in Fig. 4 and Fig. 5.

Abb. 2: Anzahl der Monate mit einer Meereiskonzentration größer als 0.15 für die Jahre 1980–1999 von Beobachtungen (SSM/I, links) und vom Modell (rechts). Die schwarze Box in der rechten Grafik zeigt die Ausschnittsregion, die in den Abbildungen 4 und 5 gezeigt ist.

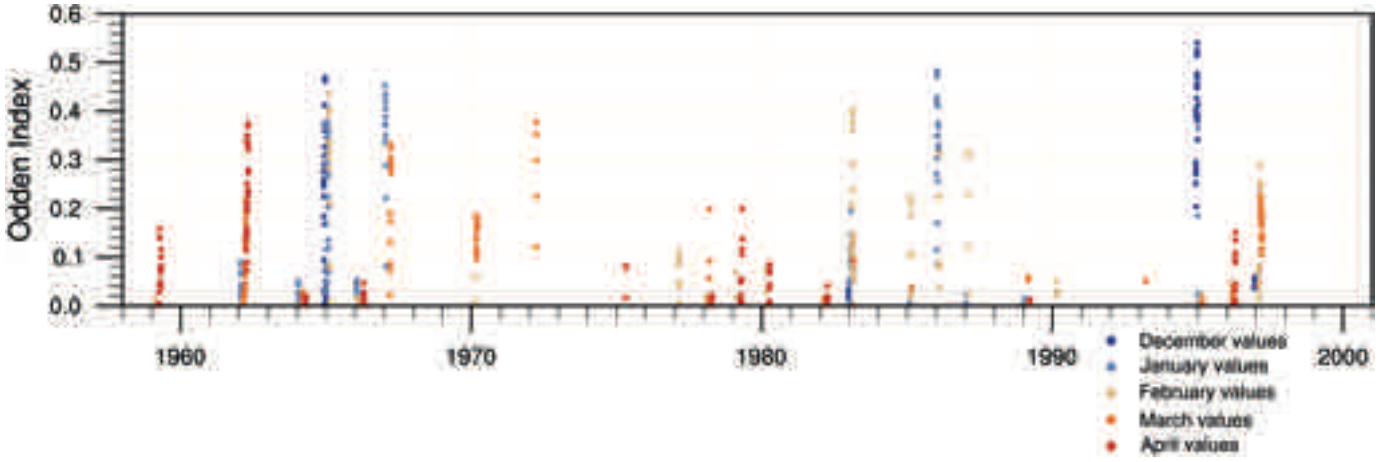

Fig. 3: Time series of an Odden Index calculated with daily data for the winter months (December to April) of the years 1958–2001. The index is defined as the difference of sea-ice concentration exceeding 0.15 in the region of the ice tongue (4.5° - 3° W, 72.8° - 73.5° N) and in the Nordbukta region (8° - 6.8° W, 74.3° - 75.1° N). Only positive values are shown.

Abb. 3: Zeitserie eines Odden Index von täglichen Daten der Wintermonate (Dezember bis April) der Jahre 1958–2001. Der Index ist als die Differenz der Meereiskonzentration größer als 0.15 der Region der Meereiszunge (4.5° - 3° W, 72.8° - 73.5° N) und in der Nordbukta Region (8° - 6.8° W, 74.3° - 75.1° N) definiert. Es sind nur positive Werte gezeigt.

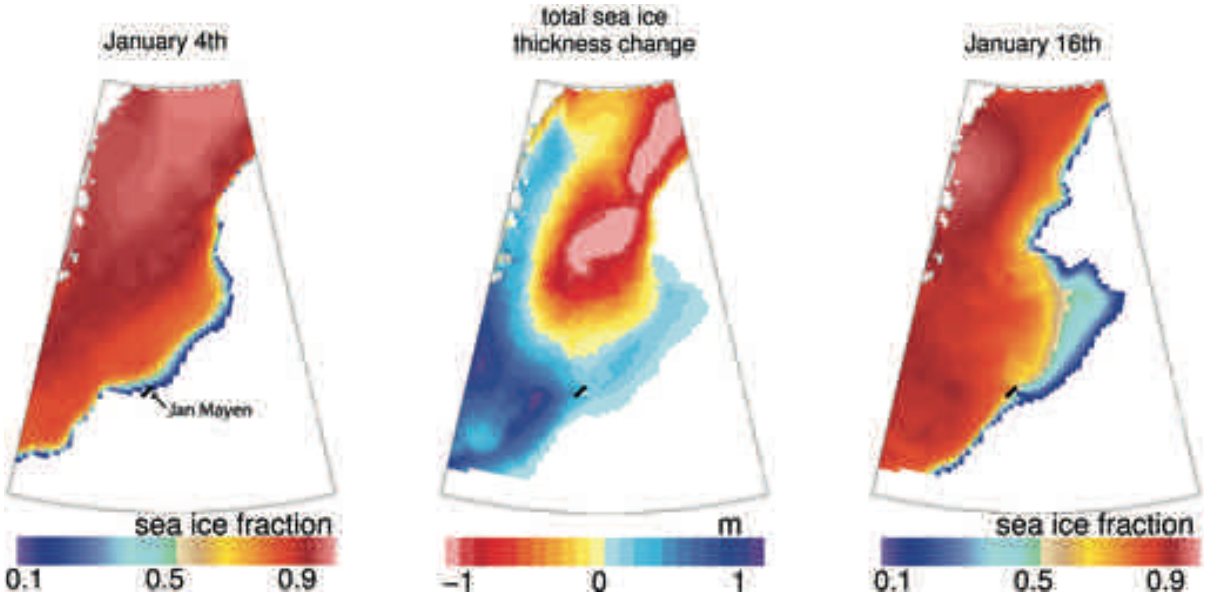

Fig. 4: Sea-ice concentration of one specific Arctic Odden event, at the beginning (left) and at the end (right). Change of sea-ice thickness (difference of end and beginning, in m) during this event (middle). The geographical domain covers the region from 67° to 81° N and from 20° W to 8° E.

Abb. 4: Meereiskonzentration für ein charakteristisches arktisches Odden-Ereignis, zu Beginn (links) und am Ende (rechts). Änderung der Meereisdicke (in m) während des Ereignisses (Mitte). Das dargestellte Gebiet reicht von 68° bis 81° N und von 20° W bis 8° E.

In our model we investigated several Odden events and find that in contrast to observations, Arctic Odden formation is mainly due to advection of sea ice from the Greenland coast and eastward advection from the main ice pack in GIN Sea irrespective of the time when it occurs. Again, to highlight the main mechanism behind the Odden formation within the model, the example of January 1962 is given in Figure 5. The behavior of this specific event is coherent with other investigated Odden events. While in the mean southward ice drift freezing is dominating, in the north-eastern marginal ice zone it is melting that supports the Arctic Odden formation (Fig. 5, right panel). This leads, in some events more than in others, to the tongue shape of the Odden. The Odden itself (the south-eastern part of the ice edge) shows only small changes due to melting and freezing. However, freezing seems to strengthen the center of the southern shape of the Odden (north of Jan Mayen) in most of the events. Within our coupled model, the Arctic Odden formation is coherent with a weak Icelandic low as well as with a strong gyre circulation of sea ice in the Central Arctic. This indicates a linkage to the large-scale Arctic sea-ice variability and the appearance of such Odden. As previously suggested by, e.g., GERME et al. (2011), the marginal ice-zone variability might be to some extent linked with large-scale processes which impact the whole Arctic, but the regional atmospheric and oceanic forcing is also responsible for the Odden formation. Consequently, the large-scale atmospheric conditions as well as the small-scale processes in the region of interest in both, the atmosphere and in the ocean should be taken into account when further analyzing the Odden formation.

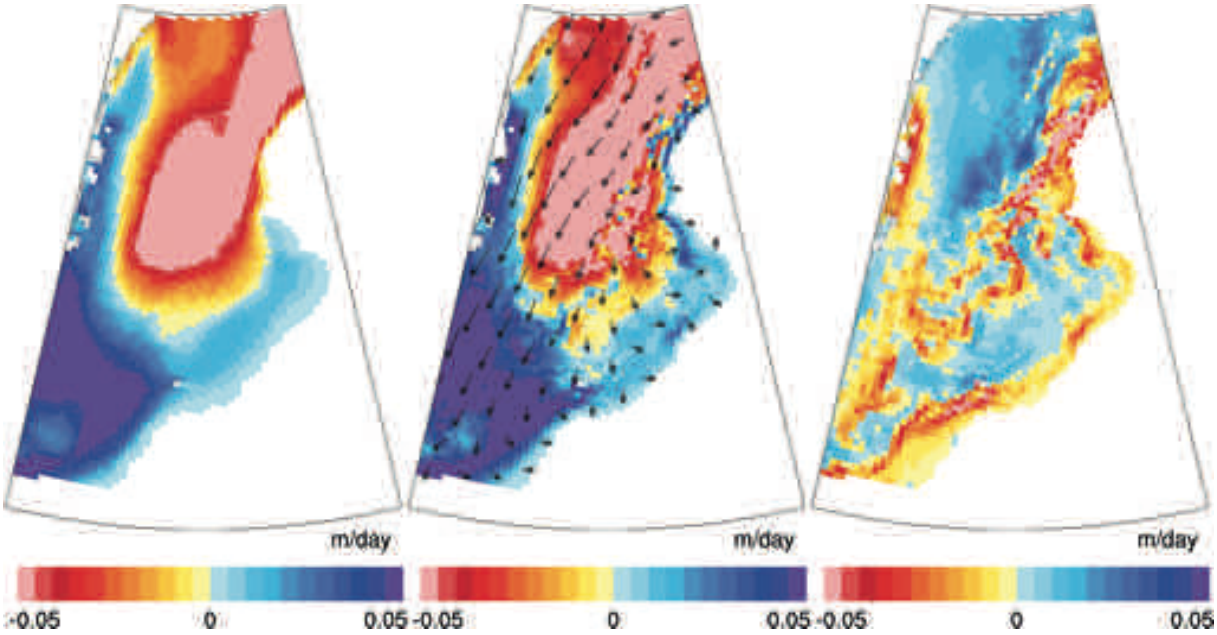

Fig. 5: Mean sea-ice thickness (*H*) change per day (left), divergence of sea-ice transport (*Hv*) and superimposed sea-ice transport (middle). The residual term (right) includes oceanic and atmospheric fluxes ($F_{Oc} + F_{At}$) that cause melting (negative values) and freezing (positive values). The geographical domain covers the region from 67° to 81° N and from 20° W to 8° E.

Abb. 5: Änderung der Meereisdicke (*H*) pro Tag (links), Divergenz des Meereistransports (*Hv*) und überlagert der Meereistransport (Mitte). Das Residuum (rechts) beinhaltet ozeanische und atmosphärische Flüsse ($F_{Oc} + F_{At}$), die zu Schmelzen (negative Werte) und Frieren (positive Werte) von Meereis führen. Das dargestellte Gebiet reicht von 68° bis 81° N und von 20° W bis 8° E.

ACKNOWLEDGMENTS

This work was supported through the Cluster of Excellence CliSAP, University of Hamburg, funded through the German Science Foundation (DFG) and the Max Planck Society for the Advancement of Science. The model integrations were performed at the German Climate Computing Centre (DKRZ) through support from the German Federal Ministry of Education and Research (BMBF). The authors wish to thank Marie-Noëlle Housais and an anonymous reviewer for helpful comments on this manuscript.

References

Aldrian, E., Sein, D.V., Jacob, D., Dümenil Gates, L. & Podzun, R. (2005): Modelling of Indonesian rainfall with a coupled regional model.- Clim. Dyn. 25: 1-17, doi: 10.1007/s00382-004-0483-0.

Comiso, J.C., Wadhams, P., Pedersen, L.T. & Gersten, R.A. (2001): Seasonal and interannual variability of the Odden ice tongue and a study of environmental effects.- *J. Geophy. Res.* 106: 9093-9116, doi: 10.1029/2000JC000204.

ECMWF (2002): ECMWF 40 Year Re-analysis (ERA-40) Data Archive URL http://www.ecmwf.int/products/data/archive/descriptions/e4/index.html

Germe, A., Houssais, M.-N., Herbaut, C. & Cassou, C. (2011): Greenland Sea sea-ice variability over 1979-2007 and its link to the surface atmosphere.- J. Geophy. Res. 116: C10034, doi:10.1029/2011JC006960.

Marsland, S.J., Haak, H., Jungclaus, J.H., Latif, M. & Röske, F. (2003): The Max-Planck-Institute global ocean/sea ice model with orthogonal curvilinear coordinates.- Ocean Mod. 5: 91-127. doi: 10.1016/S1463-5003(02)00015-X.

Mikolajewicz, U., Sein, D.V., Jacob, D., Königk, T., Podzun, R. & Semmler, T. (2005): Simulating Arctic sea ice variability with a coupled regional atmosphere-ocean-sea ice model.- Meteorol. Zeitschrift 14: 793-800.

Niederdrenk, A.L. (2013): The Arctic hydrologic cycle and its variability in a regional coupled climate model.- PhD Thesis, Universität Hamburg, 1-186.

Paluszkiewicz, T., Garwood, R.W. & Denbo, D.W. (1994): Deep convective plumes in the ocean.- Oceanogr. 7: 37-44.

Rogers, J.C. & Hung, M.-P. (2008): The Odden ice feature of the Greenland Sea and its association with atmospheric pressure, wind, and surface flux variability from reanalyses.- Geophy. Res. Lett. 35: L08504, doi: 10.1029/2007GL032938.

Sein, D.V., Koldunov, N.V., Pinto, J.G. & Cabos, W. (2014): Sensitivity of simulated regional Arctic climate to the choice of coupled model domain.- Tellus A 66: 23966. doi: 10.3402/tellusa.v66.23966.

Shuchman, R.A., Josberger, E.G., Russel, C.A., Fischer, K.W., Johannesen, O.M., Johannessen, J. & Gloersen, P. (1998): Greenland Sea Odden sea ice feature: Intra-annual and interannual variability.- J. Geophy. Res. C: Oceans 103: 12709-12724, doi:10.1029/98JC00375.

Wadhams, P. & Comiso, J.C. (1999): Two modes of appearance of the Odden ice tongue in the Greenland Sea.- Geophy. Res. Lett. 26: 2497-2500, doi:10.1029/1999GL900502.

Wadhams, P., Holfort, J., Hansen, E., & Wilkinson, J.P. (2002): A deep convective chimney in the winter Greenland Sea.- Geophy. Res. Lett. 26: 76-1–76-4, doi:10.1029/2001GL014306.

Polarforschung 85 (2), 85–88, 2015 (erschienen 2016)

Evaluation of a Regional Coupled Ocean – Atmosphere – Sea-Ice Model System over Greenland and the Arctic

by Kristine Skovgaard Madsen[1*], Ruth Mottram[1], Till Andreas Soya Rasmussen[1], and Mads Hvid Ribergaard[1]

Abstract: Rapid changes in key climatic indicators such as sea ice, seasonal snow cover, and glacier and ice sheet surface mass balance show that the Arctic is a region in transition. Understanding the feedbacks and processes requires a wide range of data, observations and model studies. Here we introduce a high-resolution coupled regional model system that describes ocean, atmosphere, ice sheet and sea ice processes in the Arctic Ocean and North Atlantic, with special focus on the area around Greenland. The system has been developed using the regional climate model HIRHAM5 and a fully coupled version of the ocean model HYCOM and the sea ice model CICE. We use the models in offline and coupled mode for a two-year experiment to examine the relative importance of ocean and atmospheric forcing and internal dynamics, as a first step towards investigating the recent rapid decline of Arctic sea ice and low surface mass balance of the Greenland Ice Sheet. The model setup can successfully reproduce the seasonal variability in sea-ice extent and highlights the bounds of internal variability in the system, while Greenland Ice Sheet surface mass processes are well represented.

Zusammenfassung: Schnelle Änderungen klimatischer Kenngrößen, wie Meereis, saisonale Schneebedeckung sowie die Massenbilanz von Gletschern und Inlandeis zeigen, dass die Arktis eine Region im Wandel ist. Um die Rückkopplungen und Prozesse besser zu verstehen, benötigt es einer Vielzahl an Daten, Beobachtungen und Modellstudien. Im Folgenden wird ein hoch aufgelöstes, gekoppeltes, regionales Modellsystem beschrieben, dass die Prozesse in Ozean, Atmosphäre, Inlandeis und Meereis im Arktischen Ozean und im Nordatlantik vereint, mit besonderem Fokus auf die Region um Grönland. Das Modellsystem wurde mit dem regionalen Klimamodell HIRHAM5 und einer vollständig gekoppelten Version des Ozeanmodells HYCOM und des Meereismodells CICE entwickelt. Die Modelle werden im offline und gekoppelten Modus für einen Zeitraum von zwei Jahren betrieben, um die relative Bedeutung der ozean- und atmosphärengetriebenen Antriebsprozesse und der internen Dynamik als einen ersten Schritt in Richtung der Erforschung der jüngsten, schnellen Abnahmen des arktischen Meereises und niedrigen Massenbilanzen des grönländischen Eisschildes zu untersuchen. Die Modellkonfiguration kann die saisonale Variabilität der Meereisausdehnung erfolgreich simulieren und macht die Grenzen der internen Variabilität des Systems deutlich, während die Massenbilanz des Inlandeises auf Grönland gut dargestellt wird.

INTRODUCTION

The Arctic is undergoing rapid climate change due to several feedback mechanisms that amplify global change at high latitudes. The albedo feedback for sea ice and seasonally snow-free land is relatively well understood, and can explain much of the amplification. Other feedbacks are less well mapped, especially when it comes to the interplay between the Greenland Ice Sheet, ocean dynamics and sea ice (e.g., HALL 2004, CROOK et al. 2011). To model these feedbacks, and especially the forcing of the Greenland Ice Sheet, high resolution is preferred, raising the need for regional models (e.g., LANGEN et al. 2015, LUCAS-PICHER et al. 2012). In this paper, we apply a regional coupled ocean – sea ice – atmosphere model to the entire Arctic domain, to make a first evaluation of how well the climate of Greenland is represented.

MODEL SETUP AND EXPERIMENTS

The model system consists of a stand-alone atmosphere model, a fully coupled ocean and sea-ice model, and a script level two-way coupling procedure. The model domain covers the entire Arctic domain and the Atlantic sub-polar gyre (Fig. 1), whereas the atmospheric domain is about 100 km larger in each direction to avoid forcing the ocean surface with atmospheric data from the boundary zone.

The atmospheric regional climate model

The HIRHAM5 regional climate model (CHRISTENSEN et al. 2006) is derived from the physical schemes of the ECHAM5 global climate model (ROECKNER et al. 2003) and the dynamical scheme of the HIRLAM numerical weatherprediction model (EEROLA 2006). In these experiments we use a domain covering the Arctic at 0.25° (~27 km) resolution on a rotated polar grid with a dynamical time step of 300 seconds and 31 vertical levels (Fig. 1). The regional model is forced at the boundaries with the ERA-Interim reanalysis dataset, but allowed to evolve entirely freely inside the domain in a set-up similar to that of LUCAS-PICHER et al. (2012). Sea ice and snow thicknesses on the lower boundaries are fixed at 2 m and 2 cm, respectively, in all areas with sea ice.

The ocean and sea-ice models

For modelling the ocean and sea ice, we use a fully coupled and slightly modified version of the HYbrid Coordinate Ocean Model (HYCOM) v2.2.55 (e.g., CHASSIGNET et al. 2007) and the Community Ice COde (CICE) v4.0 (e.g., HUNKE 2001). The horizontal resolution is roughly 20 km (Fig. 1) and the model has three fixed surface layers in the top ten metres and additional 34 flexible vertical layers. All ocean experiments were made with climatological temperature and salinity (STEELE et al. 2001, CONKRIGHT et al. 2002) on the open lateral boundaries in the Atlantic Ocean and the Bering Strait, and with a 30-day relaxation of surface salinity. No other assimilation was used in this study. Further details on the ocean and

doi:10.2312/polfor.2016.004

[1] Danish Meteorological Institute, Lyngbyvej 100, 2100 Copenhagen OE, Denmark;
[*] corresponding author <kma@dmi.dk>.

This extended abstract was presented as an oral contribution at the Inter-national Conference "Our Climate – Our Future: Regional Perspectives on a Global Challenge", 6–9 October 2014 in Berlin, Germany.
Manuscript received 02 June 2015; accepted in revised form 16 October 2015.

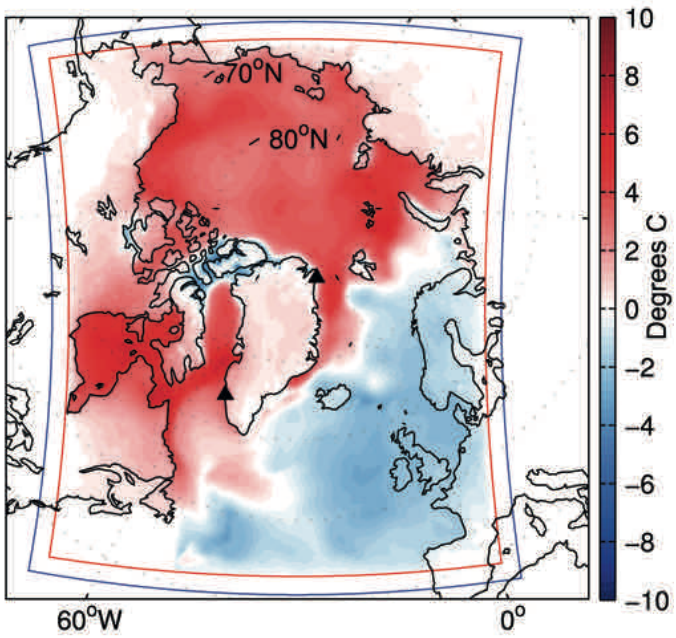

Fig. 1: The model domain of the atmospheric model (blue line) and the ocean and sea-ice models (red line), the 2006–2007 annual mean 2-m air temperature difference between coupled and atmosphere reference runs (colours), and positions of validation stations on Greenland (black triangles: south = Nuuk, north = Henrik Krøyer Holme).

Abb. 1: Modellgebiet des Atmosphärenmodells (blaue Linie) und des Ozean- und Meereismodells (rote Linie), die mittlere 2 m Lufttemperaturdifferenz zwischen Modelsimulation des gekoppelten Modells und Atmosphärenreferenz-Läufen für das Simulationsjahr 2006–2007 (farbig) und die Lage der Validationsstationen in Grönland (schwarze Dreiecke: im Süden = Nuuk, im Norden = Henrik Krøyer Holme).

sea-ice model system and setup can be found in MADSEN et al. (2016).

Coupling method

We apply the 24 hour script-level coupling method of TIAN et al. (2013) which gives us a high level of flexibility to investigate the interplay of the model components without being required to make alterations to the stand-alone models. In this setup of the coupled run, the atmospheric model is first run for 24 hours (0–24h) with 3-hourly output. The ocean and sea-ice models are then run for the same 24 hours (0–24h), forced with the 3-hourly output atmospheric data. Finally, sea-surface temperature and sea-ice concentration at 24h are fed back to the atmospheric model to be used for the next day's run. Though, the models cover the same area, their horizontal resolutions are different, and bi-linear interpolation has been used between them. No flux corrections have been applied.

Experiments

Since both, the atmospheric and the oceanic model setups were new, different experiments have been made to analyse the properties of the models and provide control simulations. We studied the two-year period 2006–2007 and used the Era Interim reanalysis (DEE et al. 2011) as a reference, as suggested by LINDSAY et al. (2014).

The experiments include:

1) Ocean reference run: The ocean – sea-ice model was forced by Era Interim. Initialized by more than nine years spin up (Sep 1996–Dec 2005).
2) Atmosphere reference run: The atmospheric model was forced with the same ocean and sea-ice conditions as used for Era Interim. One year spin up (2005).
3) Uncoupled run: The ocean – sea-ice model was forced by the atmosphere reference run. One year spin up (2005), initialized from the ocean reference run.
4) Coupled run: The atmosphere and ocean – sea-ice models were run coupled. One year spin up (2005), ocean and sea ice initialized from the ocean reference run.

RESULTS

The two years of simulation from the different experiments allow us to examine the importance of the coupling to improve model performance in the Arctic domain. We focus on three key variables sea-ice concentration, air temperature and Greenland Ice Sheet surface mass balance.

Sea ice extent and concentration

All model experiments show that the model system is capable of reproducing the seasonal cycle and magnitude of sea-ice concentration in the Arctic. In the ocean reference run, the timing of the minima, maxima, freeze-up and break-up seasons closely replicates observations (EASTWOOD et al. 2011), while the amplitude of the seasonal cycle of total sea-ice extent is about 10 % too large (Fig. 2). The use of HIRHAM5 as driver for the ocean – ice model (uncoupled run) shows an improvement in the minimum extent, with a value very close to the observed one in 2006 and 0.2 million km^2 too high in 2007. In the coupled simulation, the maximum ice extent and the timing of the break up is close to the observed, whereas a delay in the freeze up of about one month is seen. The minimum sea-ice extent is very similar for the two years and very close to the observed value for 2007, while the model underestimates the extent in 2006.

Atmospheric 2-meter temperatures

Validating a climate model in data-poor regions such as the Arctic is always challenging (LINDSAY et al. 2014). We therefore compare the experiments to ERA-Interim reanalysis data, though note that it also has important biases compared with observations (DEE et al. 2011).

The air temperature time series shown in Figure 3a show that in general the model can reproduce the seasonal cycle in the high Arctic, but there is a delay in cooling in the coupled run, corresponding to the delayed freeze-up. This is seen as a temperature bias of more than 5 °C from end August 2006 to January 2007, and again from mid-October to November 2007. The bias is seen in most sea ice affected areas (Fig. 1). An exception is the Canadian Archipelago, where the increased resolution in the sea-ice product of the coupled model gives significant improvements.

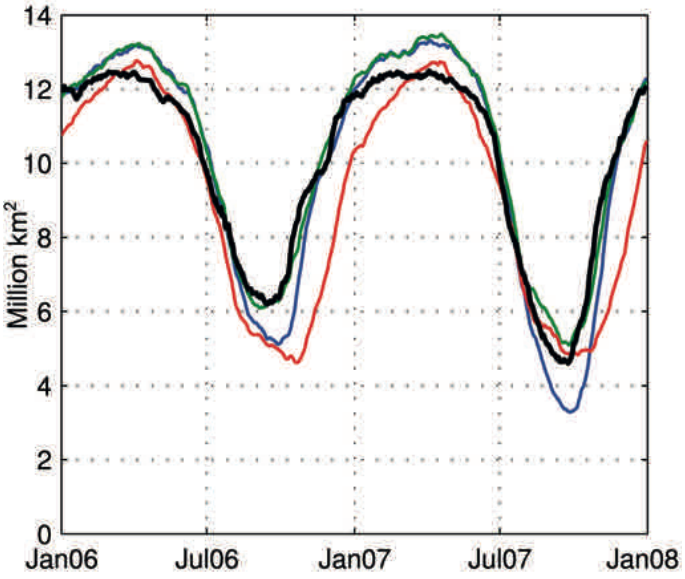

Fig. 2: Daily total Arctic sea ice extent (at least 15 % ice cover, million km²) in the ocean – sea ice reference simulation (blue line), the uncoupled simulation (green line), the coupled simulation (red line) and as observed by satellite (EASTWOOD et al. 2011) (black line). The model system shows full ice cover in the Arctic in winter, but summer sea ice concentrations are too low with values 30–50 % lower than observed values in the central Arctic Ocean.

Abb. 2: Tägliche arktische Meereisausdehnung (mindestens 15 % Eisbedeckung, in Mio. km²) der Ozean – Meereis Referenzsimulation (blaue Linie), der ungekoppelten Simulation (grüne Linie), der gekoppelten Simulation (rote Linie) und der Beobachtung durch Satelliten (EASTWOOD et al. 2011) (schwarze Linie). Das Modell zeigt vollständige Eisbedeckung der Arktis im Winter. Im Sommer sind die Meereiskonzentrationen mit 30–50 % unterhalb der beobachteten Werte für den zentralen Arktischen Ozean zu niedrig.

Comparison with observations on Greenland (CAPPELEN 2014) also reveals the interplay with the ocean and sea ice (Fig. 3b). Temperatures are highly steered by differences in sea-ice extent, particularly at locations such as Henrik Krøyer Holme. This observation point is on a flat island surrounded by ocean. Temperatures observed here mostly reflect the prevailing sea ice and SST conditions. Nuuk, on a narrow, rocky spit of land with fjords on both sides, is rather poorly resolved in the model, giving a warm bias in January 2007 and cool bias in summer in both HIRHAM5 runs. However, compared to the coarser ERA-Interim, the bias is much reduced.

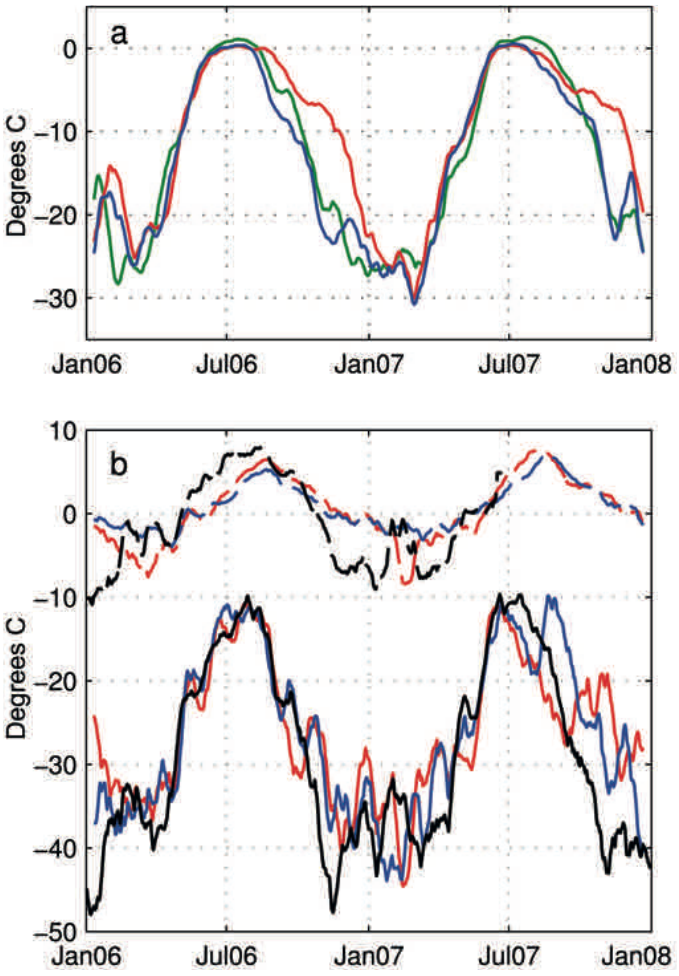

Fig. 3: 21 day running mean 2-meter air temperature a) averaged north of 80°N, b) point data from Greenland (location, see Fig. 1): Nuuk (dashed) and Henrik Krøyer Holme (solid, no observations in July–December 2007); for the reference simulation (blue), the coupled simulation (red), Era Interim reanalysis (green, only a) and observations from validation stations (CAPPELEN 2014) (black, only b).

Abb. 3: 21-tägige mittlere 2 m Lufttemperatur für a) nördlich 80°N gemittelt, b) Punktdaten von Grönland (Stationen siehe Abb. 1): Nuuk (gestrichelt) und Henrik Krøyer Holme (durchgezogen, keine Beobachtung von Juli bis Dezember 2007); für die Referenzsimulation (blau), die gekoppelte Simulation (rot), ERA Interim Reanalyse (grün, nur a) und Beobachtungen an Validationstationen (CAPPELEN 2014) (schwarz, nur b).

Surface mass balance of the Greenland Ice Sheet

Surface mass balance (SMB) is the sum of snowfall and melt induced runoff from land ice. The SMB scheme in these runs is rather simple and does not include a parameterisation for retention and refreezing of liquid water (LANGEN et al. 2015). It is therefore steered by both, precipitation, temperature and radiative forcing in the surface energy budget and indicates the future direction of land ice mass change. Both reference and coupled simulations show a representative distribution of SMB as compared with other models (e.g., FETTWEIS et al. 2011, HANNA et al. 2014) over the Greenland Ice Sheet, with high values in the South-East and North-West, where most of the precipitation falls, and lower values in South, North-East and West, where there is more melt and run-off during the ablation season (Fig. 4). The coupled model has more precipitation falling further to the south on the east coast than the reference, likely reflecting different ocean forcing. The higher SMB overall in the coupled simulation likely reflects the warmer air temperatures in autumn and early winter, bringing more snowfall in the early part of the accumulation season.

SUMMARY AND DISCUSSION

A coupled model is applied to the Arctic and North Atlantic domain. In the Arctic region, it is common practice to tune the sea-ice model to fit observations, due to uncertainties in models and lack of observations. We have investigated the effects of switching between ERA-Interim and HIRHAM5 atmospheric forcing, and of coupling the ocean – sea-ice – system with the atmosphere, without the need for tuning.

The low 2007 sea-ice minimum is captured in the reference models, but not in the uncoupled model, which likely reflects the greater freedom for the weather to evolve freely

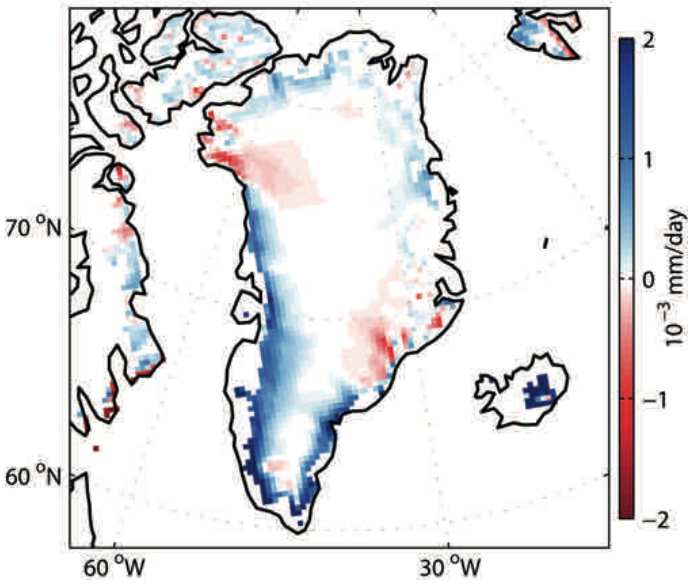

Fig. 4: Mean difference in surface mass balance (colours, 10–3 mm water equivalent per day), coupled minus reference run.

Abb. 4: Mittlere Differenz der Oberflächenmassenbilanz des Inlandeises (farbig, 10–3 mm Wasseräquivalent pro Tag) für den gekoppelten Lauf minus Referenzlauf.

in the large domain as with ice sheet SMB (Koenigk et al. 2015, Dorn et al. 2012). This indicates that regional coupled models, like our setup, have an important role in evaluating the importance of stochastic weather processes, and should preferably be used in ensemble-mode to span the range of internal variability.

Another important result is the role of ocean heat fluxes in modulating sea-ice formation. The low summer sea-ice concentration in the Arctic initiates a heating of the surface ocean in the coupled simulation. This heat needs to be released before freeze-up occurs, resulting in a delay of the atmospheric surface cooling and sea-ice freeze-up of about one month with knock-on effects on precipitation and SMB. In the uncoupled simulation, the feedback does not occur, since SST and sea-ice concentration are prescribed in the atmospheric model. This is a focus for future work on the coupled model system.

The limited simulation- and spin-up times of this study means that results should be used with care. Still, we have proof of concept of a coupled atmosphere – ocean – sea-ice model system for the Arctic, which may be used to further study climate processes in the Arctic and assist in attributing environmental changes in the future.

ACKNOWLEDGMENTS

This study has been financially supported by the Danish Agency for Science, Technology and Innovation and is a part of the Greenland Climate Research Centre. Helpful comments by Annette Rinke and one anonymous reviewer are gratefully acknowledged.

References

Cappelen, J. (2014): Weather observations from Greenland 1958-2013. Observation data with description.- Technical Report 14-08, Danish Meteorological Institute, Copenhagen, Denmark.

Chassignet, E.P., Hurlburt, H.E., Smedstad, O.M., Halliwell, G.R., Hogan, P.J., Wallcraft, A.W., Baraille, R. & Bleck, R. (2007): The HYCOM (HYbrid Coordinate Ocean Model) data assimilative system.- J. Marine Syst. 65: 60-83, doi:10.1016/j.jmarsys.2005.09.016.

Christensen, O.B., Drews, M., Christensen, J.H., Dethloff, K., Ketelsen, K., Hebestadt, I. & Rinke, A. (2006): The HIRHAM Regional Climate Model. Version 5.- Technical Report, 06-17, Danish Meteorological Institute, Copenhagen, Denmark.

Conkright, M.E., Locarnini, R.A., Garcia, H.E., O'Brien, T.D., Boyer, T.P., Stephens, C. & Antonov, J.I. (2002): World Ocean Atlas 2001: Objective analyses, data statistics, and figures, CD-ROM Documentation.- National Oceanographic Data Center, Silver Spring, MD, 1-17.

Crook, J.A., Forster, P.M. & Stuber, N. (2011): Spatial patterns of modeled climate feedback and contributions to temperature response and polar amplification.- J. Clim. 24: 3575-3592, doi:10.1175/2011JCLI3863.1.

Dee, D.P. et al.: 35 co-authors (2011): The ERA-Interim reanalysis: configuration and performance of the data assimilation system.- Quat J. Royal. Meteor. Soc. 137: 553-597, doi:10.1002/qj.828.

Dorn, W., Dethloff, K. & Rinke, A. (2012): Limitations of a coupled regional climate model in the reproduction of the observed Arctic sea-ice retreat.- The Cryosphere 6: 985-998, doi:10.5194/tc-6-985-2012.

Eastwood, S., Larsen, K.R., Lavergne, T., Nielsen, E. & Tonboe, R. (2011): Global sea ice concentration reprocessing.- Product User Manual. Product OSI-409. Document version: 1.3. Data set version: 1.1. <http://osisaf.met.no/docs/pum_seaicereproc_ss2_v1p3.pdf.>

Eerola, K. (2006): About the performance of HIRLAM version 7.0.- HIRLAM Newsl. 51: 93-102.

Fettweis, X., Tedesco, M., van den Broeke, M. & Ettema, J. (2011): Melting trends over the Greenland Ice Sheet (1958-2009) from spaceborne microwave data and regional climate models.- The Cryosphere 5: 359-375, doi:10.5194/tc-5-359-2011.

Hall, A. (2004): The role of surface albedo feedback in climate.- J. Clim. 17: 1550-1568,doi:10.1175/1520-0442(2004)017<1550:TROSAF>2.0.CO;2.

Hanna, E., Fettweis, X., Mernild, S.H., Cappelen, J., Ribergaard, M.H., Shuman, C.A., Steffen, K., Wood, L. & Mote, T.L. (2014): Atmospheric and oceanic climate forcing of the exceptional Greenland Ice Sheet surface melt in summer 2012.- Internat. J. Climatol. 34 1022-1037, doi:10.1002/joc.3743.

Hunke E.C. (2001): Viscous-plastic sea ice dynamics with the EVP model: linearization issues.- J. Comp. Phys. 170 (1): 18-38, doi:10.1006/jcph.2001.6710.

Koenigk, T., Berg, P. & Döscher, R. (2015): Arctic climate change in an ensemble of regional CORDEX simulations.- Polar Research 34: 24603, doi:10.3402/polar.v34.24603.

Langen, P.L., Mottram, R.H., Christensen, J.H., Boberg, F., Rodehacke, C.B., Stendel, M., van As, D., Ahlstrøm, A.P., Mortensen J., Rysgaard, S., Petersen, D., Svendsen, K.H., Adalgeirsdottir, G. & Cappelen, J. (2015): Quantifying energy and mass fluxes controlling Godthåbsfjord freshwater input in a 5-km simulation (1991-2012).- J. Clim. 28 (9), doi:10.1175/JCLI-D-14-00271.1.

Lindsay, R., Wensnahan, M., Schweiger, A. & Zhang, J. (2014): Evaluation of seven different atmospheric reanalysis products in the Arctic.- J. Clim. 27: 2588-2606.

Lucas-Picher, P., Wulff-Nielsen, M., Christensen, J.H., Aðalgeirsdóttir, G., Mottram, R., & Simonsen, S.B. (2012): Very high resolution regional climate model simulations over Greenland: Identifying added value.- J. Geophys. Res. 117: D02108, doi:10.1029/2011JD016267.

Madsen, K.S., Rasmussen, T.A. R., Ribergaard, M.H. & Ringgaard, I. (2016): High resolution sea-ice modelling and validation of the Arctic with focus on South Greenland Waters.- Polarforschung 85: 85–88.

Roeckner, E. & et al.: 13 co-authors (2003): The atmospheric general circulation model ECHAM5. PART I: Model description.- Report 349: 1-127, Max Planck Institute for Meteorology, Hamburg, Germany (available at mpimet.mpg.de).

Steele, M., Morley R. & Ermold W. (2001): PHC: A global ocean hydrography with a high quality Arctic Ocean.- J. Clim. 14: 2079-2087 (Updated to PHC 3.0 in 2005).

Tian, T., Boberg, F., Christensen, O.B., Christensen, J.H., She, J. & Vihma, T. (2013): Resolved complex coastlines and land – sea contrasts in a high-resolution regional climate model: a comparative study using prescribed and modelled SSTs.- Tellus A 65, 19951, doi: 10.3402/tellusa.v65i0.19951.

Polarforschung 85 (2), 89–99, 2015 (erschienen 2016)

Sensitivity of Grounding-Line Dynamics to Viscoelastic Deformation of the Solid-Earth in an Idealized Scenario

by Hannes Konrad[1*], Ingo Sasgen[1], Volker Klemann[1], Malte Thoma[2], Klaus Grosfeld[2] and Zdeněk Martinec[3, 4]

Abstract: We investigate the behaviour of the grounding line (GL) of an idealised ice sheet and ice shelf by coupling a thermomechanical ice-sheet model to a self-gravitating viscoelastic solid-Earth model (SGVEM) in which a gravitationally self-consistent sea-level evolution is considered. The steady-state ice-sheet – shelf configuration is subject to forcing by sea-level rise, or altered surface mass balance and basal conditions, resulting in a retreat of the GL. We confirm previous studies showing that GL retreat can be decelerated and stopped by viscoelastic deformation of the solid Earth. We focus on the influence of lithosphere thickness and the upper mantle viscosity on the GL retreat and find that the time scales of solid-Earth relaxation, which are parameterised by the upper mantle viscosity, are most important for GL stability. We compare these retreat characteristics with results from the simpler "elastic lithosphere – relaxing asthenosphere" (ELRA) approximation of solid-Earth deformation, which is common in ice-sheet modelling. We find that the inconsistent description of sea level and the simplified relaxation behaviour of the ELRA approximation introduce an artificial bias on GL migration. Finally, we discuss the implications of similar time scales, on which ice dynamics and solid-Earth adjustment proceed, for the long-term stability of the ice sheet.

Zusammenfassung: Wir untersuchen das Verhalten der Aufsetzlinie eines idealisierten Eisschildes mit angrenzendem Schelfeis, indem wir ein numerisches thermomechanisches Eisschildmodell mit einem selbstgravitativen, viskoelastischen Modell für die feste Erde koppeln. In letzterem werden Meeresspiegeländerungen gravitativ konsistent berücksichtigt. Das gegebene Gleichgewicht, in welchem sich das System aus Eisschild und -schelf befindet, wird durch Anstieg des Meeresspiegels, bzw. veränderte Oberflächenmassenbilanz und basale Randbedingungen gestört, wodurch sich die Aufsetzlinie zurückzieht. Wie bereits in früheren Studien beschrieben, kann die viskoelastische Deformation der festen Erde den Rückzug der Aufsetzlinie bremsen und stoppen. Ein besonderes Augenmerk wird darauf gerichtet, wie sich der Einfluss der Lithosphärenmächtigkeit sowie der Viskosität des oberen Mantels auf den Rückzug der Aufsetzlinie auswirkt. Dabei stellen sich die Relaxationszeiten der festen Erde, die durch die Viskosität des oberen Mantels gegeben sind, als wichtigste Parameter für die Stabilität der Aufsetzlinie heraus. Die damit einhergehenden Rückzugsmerkmale werden mit Ergebnissen verglichen, die durch Anwendung einer vereinfachten Berücksichtigung der festen Erde („elastische Lithosphäre – relaxierende Asthenosphäre", ELRA) erzielt werden, wie es in der Modellierung von Eisschilden üblich ist. Wir zeigen, dass die inkonsistente Beschreibung des Meeresspiegels, sowie das vereinfachte Relaxationsverhalten der festen Erde die Bewegung der Aufsetzlinie beeinflussen. Schließlich behandeln wir die Implikationen ähnlicher Zeitskalen von Eis- und Erddynamik auf die langfristige Stabilität eines Eisschildes.

doi:10.2312/polfor.2016.005

[1] Helmholtz Centre Potsdam, German Research Centre for Geosciences GFZ, Telegrafenberg, 14473 Potsdam, Germany;
[*] now at School of Earth and Environment, University of Leeds, Leeds LS2 9JT, United Kingdom, <h.h.konrad@leeds.ac.uk>
[2] Alfred Wegener Institute, Helmholtz Centre for Polar and Marine Research, Am Handelshafen 12, 27570 Bremerhaven, Germany.
[3] Dublin Institute of Advanced Studies, 5 Merrion Square, Dublin 2, Ireland.
[4] Department of Geophysics, Charles University, V Holešovičkách 2, 18000 Praha 8, Czech Republic.
This paper was presented as a poster contribution at the International Conference "Our Climate – Our Future: Regional Perspectives on a Global Challenge", 6–9 October 2014 in Berlin, Germany.
Manuscript received 27 May 2015; revised version 09 December 2015; accepted 28 December 2015.

INTRODUCTION

The advance and retreat of the large continental ice sheets during glacial cycles load and unload the solid-Earth and thereby force viscoelastic deformation in the Earth's interior (Peltier 1974). In the ice sheet's vicinity, the deformation leads to subsidence of the Earth's surface in response to ice advance (loading) and uplift in response to retreat (unloading). Both are delayed by decades to millennia through the viscous flow in the Earth's mantle (Haskell 1935). The redistribution of ice masses, ocean masses due to ice discharge into the oceans and mantle material also induce changes in the gravity field, which affects the sea level as this coincides with the geoid, an equipotential surface of the gravity field.

The ice sheet's dynamical evolution is influenced by the Earth's response, mainly via three feedback mechanisms. First, a vertically moving ice – bedrock interface implies respective vertical motion of the ice-sheet surface. The uplift or subsidence of the ice – atmosphere interface leads to less or more ice accumulation in the interior accumulation areas (Oerlemans 1980, Huybrechts 1993). Second, the slopes of the bedrock topography, which are important boundary conditions for the near-bed ice velocities, are tilted by the vertical motion of the Earth's surface. Third, the ocean depth (or relative sea level RSL (all acronyms and labels are listed in Tab. 1) at the grounding line (GL, the transition from the ice sheet to the adjacent ice shelves), and thereby the GL positioning itself, is determined by the solid-Earth gravitational response and vertical motion of the ocean bottom. Accounting for this feedback in numerical ice-sheet models is of great importance, as glacial/interglacial sea-level variations are a major driver of ice-sheet advance and retreat (e.g., Pollard & DeConto 2009).

In our study, we employ a coupled numerical model for ice and solid-Earth dynamics, the latter one featuring a gravitationally consistent description of sea level. With the first two feedbacks treated by Konrad et al. (2014), this study addresses the feedback between RSL and GL dynamics, particularly in the case of an ice sheet subject to the Marine Ice Sheet Instability (MISI). Such an ice sheet is characterized by marine-based portions on bedrock, which deepens inland from the GL, as it is the case for the West Antarctic Ice Sheet. As the GL retreats downslope, the outflow across the GL into the ice shelf increases as the RSL increases due to the deepening. This leads to on-going disintegration of the ice sheet (Thomas & Bentley 1978, Schoof 2007).

Gomez et al. (2012) found in idealised numerical simulations that such an ice sheet can be stabilised by viscoelastic uplift following the unloading of the solid Earth by GL retreat.

Acronym A	Label L	Meaning
ACCU	L	Forcing scenario based on SMB reduction
BASL	L	Forcing scenario based on SMB and basal friction reduction
ERLA	A	Elastic Lithosphere / Relaxing Asthenosphere
ESL	A	Equivalent Sea Level
GL	A	Grounding Line
GMT	A	Generic Mapping Tool
ISM	A	Ice Sheet Model
MISI	A	Marine Ice Sheet Instability
PREM	A	Preliminary Earth Reference Model
RIGID	L	Viscoelastic layering in VILMA
RIMBAY	A	Revised Ice Sheet Model Based on frAnk pattYn (employed ice sheet model)
RSL	A	Relative Sea Level
S120	L	Forcing scenario based on sea-level rise
S150	L	Forcing scenario based on sea-level rise
SGVEM	A	Self-Gravitating ViscoElastic Earth Model
SIA	A	Shallow Ice Approximation
SLE	A	Sea Level Equation
SMB	A	Surface Mass Balance
SSA	A	Shallow Shelf Approximation
VE_L035_M19	L	viscoelastic layering in VILMA
VE_L100_M19	L	viscoelastic layering in VILMA
VE_L035_M21	L	viscoelastic layering in VILMA
VE_L100_M21	L	viscoelastic layering in VILMA
VILMA	A	Viscoelastic Lithosphere and MAntle model (employed Earth model)

Tab. 1: List of all used acronyms (A) and labels (L).

Tab. 1: Liste aller verwendeten Akronyme (A) und Bezeichnungen (L).

Similar to this study, we extensively analyse the influence of the Earth-model parameters on the ice-sheet – shelf dynamics. In a geometrically simplified ice-sheet scenario, the sensitivity of the GL position to the viscoelastic structure of the underlying solid Earth is investigated, in particular to the thickness of the lithosphere and to upper-mantle viscosity. Starting from an ice-sheet and ice-shelf configuration in steady state, the coupled model system is subject to a forcing by sea-level rise from ice melting on a remote continent – similar to the Antarctic Ice Sheet under the influence of Northern Hemispheric melt-water pulses during the deglaciation after the Last Glacial Maximum – as well as to changes in the boundary conditions at the ice-sheet surface and at the ice-sheet – bedrock interface.

Additionally, we employ the common approximate approach to solid-Earth dynamics in ice-sheet modelling, the so-called "elastic lithosphere – relaxing asthenosphere" (ELRA) approximation (e.g., Le Meur & Huybrechts 1996). Here, the lithosphere is considered as a thin and horizontally infinitely extended plate, whereas the viscous mantle flow is approximated by one *a priori* relaxation time. Sea level cannot be treated gravitationally consistently in ELRA. Consequently, eustatic sea-level variations are prescribed in the ice-sheet model (ISM) domain.

MODELLING

Ice-sheet modelling

We employ the thermomechanical ISM RIMBAY (Thoma et al. 2014). In the applied configuration, it solves for ice thickness, ice temperature and ice velocity by applying the Shallow Ice Approximation (SIA) for the linear momentum balance for grounded ice and the Shallow Shelf Approximation (SSA) for floating ice. In a transition zone, the solutions from SIA and SSA are mixed (e.g., Thoma et al. (2014) for details). The ISM domain is resolved with a 10 × 10 km Cartesian grid.

A constant rate factor A as well as the common value of $n = 3$ for the flow law exponent in Glen's Flow law for the viscous deformation of polycrystalline ice (Cuffey & Paterson 2010) is applied. A power law for basal sliding (Weertman 1957) is employed, parameterised by the basal sliding coefficient C and the basal sliding exponent $m = 1/3$ (Thoma et al. 2014).

The applied parameterisation for basal melt rates in the floating areas ($\dot{b}_B^{shelf}$) follows Beckmann & Goosse (2003):

$$\dot{b}_B^{shelf} = A_{eff} \frac{\rho_{oc}\, c_{p,oc}}{\rho L_{Ice}} \gamma_T (T_{oc} - T_{fp}) \qquad (1)$$

where the freezing-point temperature at the ice-shelf base T_{fp} is computed as (Foldvik & Kvinge 1974)

$$T_{fp} = 0.0939°C - 0.057°C\,(PSU)^{-1}\, S_{oc} - 7.64 \bullet 10^{-4}°C\, m^{-1}\, z_{bsl} \qquad (2)$$

Here, z_{bsl} is the depth below sea level of the ice-shelf base. The tuning parameter A_{eff} in Equation 1 specifies the "effective melting area". The remaining quantities in equations 1 and 2 are the ocean water density $\varrho_{oc} = 1028$ kg m^{-3}, the specific heat of ocean water $c_{p,oc} = 3974$ J (kg °C)$^{-1}$, the latent heat of the ice – water transition $L_{Ice} = 333.5$ kJ kg^{-1}, the ocean temperature $T_{oc} = -1.7$ °C, the salinity $S_{oc} = 35$ PSU, and the exchange velocity $\gamma_T = 10^{-4}$ m/s.

In the applied configuration, the calving front, where the ice shelves do not only share a vertical boundary with the ocean, but also a horizontal one, can only retreat but not advance in the model. Retreat occurs if the ice thickness at the calving front goes down to zero. Advance is not modelled explicitly here. Instead, all ice that is flowing accross the front is assumed to have calved off and by that has gone into the ocean.

Solid-Earth and sea-level model

We employ the self-gravitating viscoelastic Earth model (SGVEM) developed by Martinec (2000) in the implementation VILMA. Under the assumption of a spherical and incompressible Earth in hydrostatic equilibrium at the initial time, the equations for mass continuity and linearised linear momentum balance, the Poisson equation for the incremental gravitational potential and the constitutive equation of a Maxwell viscoelastic solid are solved. The SGVEM is composed of a fluid core, a viscoelastically stratified mantle and an elastic lithosphere. With the angular dependencies treated by spherical harmonics and the radial dependencies by

finite-elements, the model approach is referred to as a spectral-finite-elements approach. The Legendre cut-off degree has been fixed to $j = 256$ (KONRAD et al. 2014) (~80 km spatial resolution).

The sea-level equation (SLE, FARRELL & CLARK 1976, MITROVICA & MILNE 2003) has been implemented by HAGEDOORN et al. (2007). Based on the surface load σ as the forcing quantity of viscoelastic deformation in the solid-Earth, it solves for changes of RSL Δs_{rsl} by ensuring (1) the coincidence of the ocean surface with an equipotential surface of the gravity field and (2) the conservation of the global water budget during the exchange of water masses between ice sheets and oceans. Changes in the rotational potential due to the redistribution of surface masses are also taken into account. The surface load σ is given by changes in the weight of the ice or ocean column, depending on whether a specific location is covered by grounded ice or flooded with ocean water. In the case of a migrating GL, the vanishing weight of the initial ice or ocean-water column at a location traversed by the GL is partially compensated by inflowing ocean water or an advancing ice sheet, respectively, which is corrected for in the surface load.

An important feature of the modelled sea-level variations in response to the redistribution of ice and ocean masses and mantle material is their non-uniformity (MITROVICA et al. 2001, SPADA et al. 2013). Especially in the vicinity of advancing or retreating ice sheets, the sea level deviates strongly from the global mean.

ELRA

In ice-sheet modelling, the ELRA approximation of solid-Earth relaxation is often applied (e.g., HUYBRECHTS et al. 2011, GREVE et al. 2011, POLLARD & DECONTO 2012, BINDSCHADLER et al. 2013, MARIS et al. 2014). It is based on two assumptions. First, the lithosphere is considered as a thin plate characterised by its flexural rigidity D (in N m). Following BROTCHIE & SILVESTER (1969) and LE MEUR & HUYBRECHTS (1996), its equilibrium deflectional response to a surface load σ as a function of horizontal coordinates x and y can be written as

$$U_{eq}(x,y,t) = \frac{gL_r^2}{2\pi D}\int \sigma(x',y',t) \bullet \chi\left(\sqrt{(x-x')^2+(y-y')^2}/\,L_r\right)dx'dy' \quad (3)$$

Here, $g = 9.81$ m s^{-2} is the gravitational acceleration at the Earth's surface, $L_r = (D/\varrho_a/g)^{0.25}$ is the radius of relative stiffness with $\varrho_a = 3300$ kg m^{-3} being the asthenosphere density, and χ is the Kelvin function of zeroth order (e.g., ABRAMOWITZ & STEGUN 1964).

Second, the viscous mantle flow is modelled by one *a priori* relaxation time τ_r, so that the actual lithospheric deflection U is given by

$$\frac{\partial U}{\partial t} = -\frac{U-U_{eq}}{\tau_r} \quad (4)$$

The gravitationally consistent non-uniform sea-level variations as described for the SGVEM in Section 2.2, cannot be solved for in the ELRA approximation. Instead, eustatic (i.e., global average) sea-level variations are applied here, by which the local sealevel is typically overestimated (e.g., GOMEZ et al. 2013).

Coupling

In contrast to other comparable model systems (LE MEUR & HUYBRECHTS 1996, VAN DEN BERG et al. 2008, GOMEZ et al. 2012, 2013, DE BOER et al. 2014), the coupling of the ISM and the SGVEM employed in this study is straightforward: The weak formulation of the solid-Earth dynamics (MARTINEC 2000) – in contrast to the normal-mode approach (PELTIER 1974) used by the Earth models employed in the above coupling studies – allows an explicit time stepping, so that the two models can run synchronously in time. The ISM runs from one coupling time step t_i to the next $t_{i+1} = t_i + \Delta t_c$ while linearly extrapolating the sea-level and the bedrock-deformation fields from the last two coupling time steps (t_i, t_{i-1}) in time. Then, ice thickness changes are handed to the SGVEM, which now also runs from t_i to t_{i+1} while linearly interpolating ice thickness in time. After handing sea level and bedrock deformation at t_{i+1} from the SGVEM to the ISM, the coupling procedure is finished for the interval from t_i to t_{i+1}. The explicit time stepping also allows a much shorter coupling interval (here, Δt_c = 50 yr) than most of the above studies.

The ISM operates on a regional equidistant Cartesian grid, whereas the SLE in the SGVEM is solved on a global Gauss-Legendre grid for geographical latitude (512 nodes) and longitude (1024 nodes). Hence, the exchanged fields need to be regridded. We opt for centering the ISM model domain at the equator, so that the Gauss-Legendre grid is almost equidistant in the x and y coordinates of the ISM grid (~39 km, four times the horizontal ISM resolution). This would not be the case if the ISM domain was centered at a pole. Our choice makes Delaunay triangulation as provided by the Generic Mapping Tool (GMT, WESSEL & SMITH 1991) a suitable choice for regridding the ice-thickness changes to the global grid. The sea-level and bedrock-deformation fields are regridded by bicubic interpolation to the regional Cartesian grid, again using GMT (e.g., KONRAD et al. 2014). Please note that this choice for an equatorial situation of the ice sheet is only due to the relation of the two numerical models' grids and has no implications for the climatic forcing of the ice sheet, as the latter is prescribed separately and independently from the location of the ice sheet, see below.

SCENARIO

Steady-state ice sheet

The steady-state set-up at the beginning of the perturbation experiments ($t = 0$) comprises an ice shelf which is confined at three sides by an ice sheet (Fig. 1A, B, C). This ice-sheet geometry is reached after 60 kyr of initialization (i.e., starting at t = -60 kyr) under a constant surface mass balance (SMB) of 0.2 m/yr, a surface temperature of -15 °C, and a basal sliding coefficient of $C = 10^7$ Pa (m/s)$^{1/3}$. The melting rates in the ice shelf areas are forced to be close to zero compared to the accumulation rate by setting the adjustment parameter in Equation 1 to $A_{eff} = 0.001$ m^2. The bedrock topography is designed

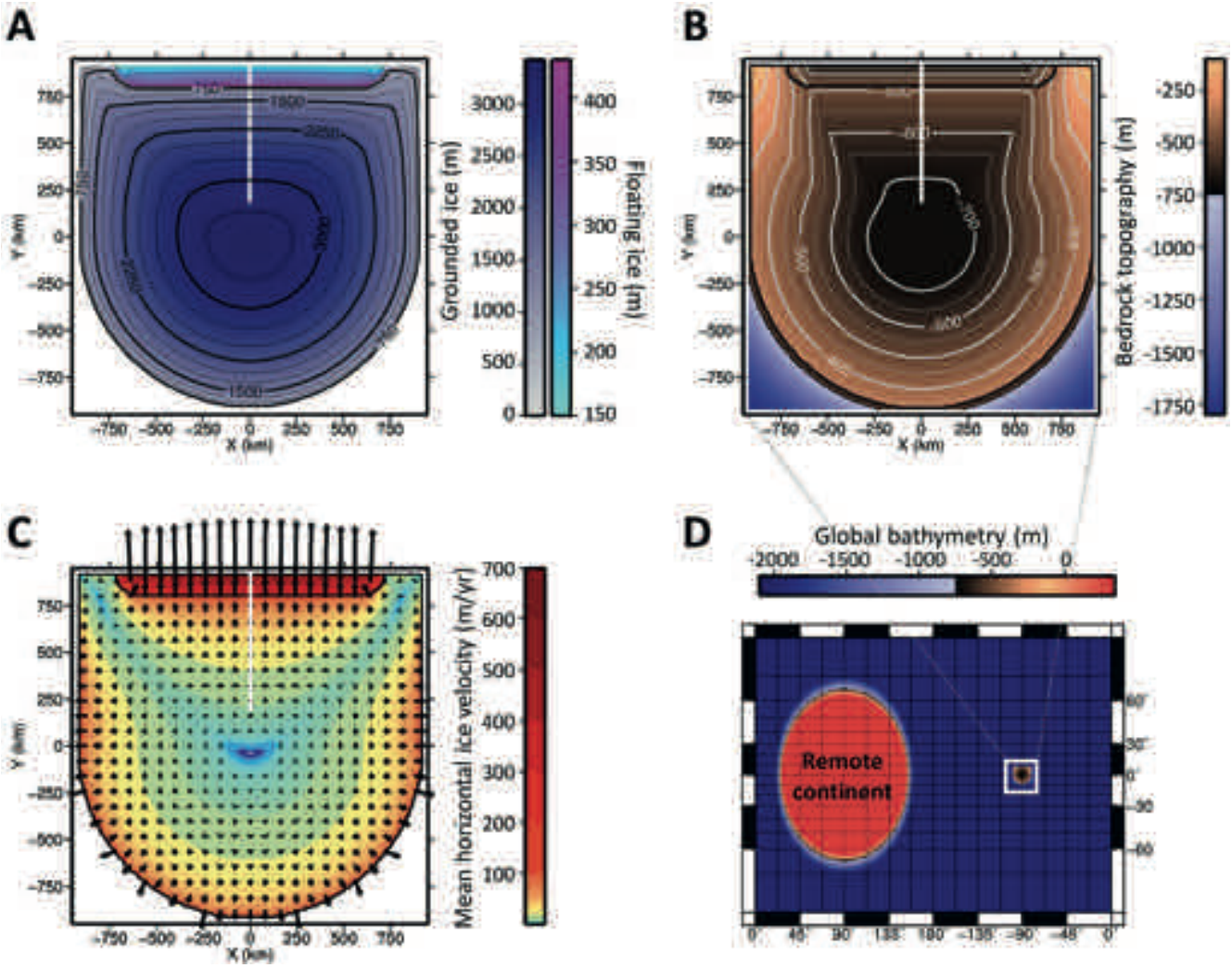

Fig. 1: Initial set-up of the considered model configuration. A: Ice thickness; note the different colour scales for grounded and floating ice. B: Bedrock topography; the topography is referenced to sea level at $t = 0$. C: Mean horizontal ice velocities; in B and C, the black lines mark the transition between grounded ice, floating ice, and ocean. The white line at $x = 0$ indicates the cross section along which the results are analysed. D: Global bathymetry featuring the ISM domain (-90° longitude), a remote circular continent (+90° longitude; in Mercator projection appearing as elliptical), and an ocean.

Abb. 1: Zustand des Modellsystems zu Beginn des Experiments. A: Eismächtigkeit; beachte die unterschiedlichen Farbskalen für aufsitzendes und aufschwimmendes Eis. B: Topographie des Felsbettes, bezogen auf den Meeresspiegel zum Zeitpunkt $t = 0$. C: Mittlere horizontale Geschwindigkeiten des Eises. Die schwarzen Linien in B und C stellen die Übergänge zwischen aufsitzendem und aufschwimmendem Eis, sowie dem Ozean dar. Die weiße Linie bei $x = 0$ zeigt den Querschnitt an, entlang dessen die Ergebnisse betrachtet werden. D: Globale Bathymetrie, bestehend aus dem Eismodellbereich (bei -90° geografischer Länge), einem entfernt davon liegenden kreisförmigen Kontinent (bei +90° geografischer Länge; erscheint in der Mercator-Projektion elliptisch) und einem Ozean.

symmetrically with respect to the y-axis and features an inland slope such that a GL perturbation will cause further retreat (MISI; see "Introduction"). The solid-Earth is in rest at $t = 0$ (hydrostatic equilibrium).

Global bathymetry

The SGVEM requires a global bathymetry ζ (Ω,$t = 0$) for initialization. The applied bathymetry (Fig. 1D) incorporates the ISM domain continent at the Equator with the y-axis of the ISM domain, coinciding with the meridian at ϕ = -90° (270°) longitude (positive y-axis points to the North Pole; positive x-axis points eastward). A remote continent (circular with radius r_{cont} = 7000 km and altitude ζ_{cont} = 300 m above sea-level) is equatorially centered as an antipode to this continent at ϕ = +90°. The remaining part of the planet is deep ocean (ζ_{ocean} = -2000 m) and distance-weighted interpolations between continental altitudes and deep ocean depth in transition zones around the two continents.

Solid-Earth representation

The Earth structure is given by radially symmetric (i.e., one-dimensional) distributions of viscosity and shear modulus. In this study, five different sets of solid-Earth parameters are applied (Tab. 2). Four of them are three-layered, obtained by combining a thin or a thick lithosphere (h_L = 35 km vs. 100 km) with a low-viscous or a high-viscous upper mantle (η_{UM} = 1×10^{19} Pa s *versus* 1×10^{21} Pa s). In these cases, the lower mantle has a viscosity of η_{LM} = 1×10^{22} Pa s. The boundary between upper and lower mantle is at 670 km depth. The core-mantle boundary is at 2891 km depth. The shear modulus in these settings is adopted from the Preliminary Earth Reference Model (PREM, Dziewonski & Anderson 1981).

Label	h_L (km)	η_{UM} (P as)	η_{LM} (P as)	μ
VE_L035_M19	35	1×10^{19}	(P as)	PREM
VE_L100_M19	100	1×10^{19}	1×10^{22}	PREM
VE_L035_M21	35	1×10^{21}	1×10^{22}	PREM
VE_L100_M21	100	1×10^{21}	1×10^{22}	PREM
RIGID	–	1×10^{30}	1×10^{30}	1×10^{20} Pa

Tab. 2: Solid-Earth rheologies used in this study. The controlling parameters are h_L: thickness of lithosphere; η_{UM}: upper mantle viscosity; η_{LM}: lower mantle viscosity and μ: the shear modulus. Note that the values for the RIGID Earth are practically infinite. PREM stands for Preliminary Earth Reference Model (DZIEWONSKI & ANDERSON 1981).

Tab. 2: Rheologien der festen Erde, wie sie in dieser Studie verwendet werden. Die variablen Parameter sind die Mächtigkeit der Lithosphäre h_L, die Viskosität des oberen Mantels η_{UM}, die des unteren Mantels η_{LM}, sowie das elastische Schermodul μ. Man beachte, dass die Werte im Falle der RIGID Erde praktisch unendlich sind. PREM steht für Preliminary Earth Reference Model (DZIEWONSKI & ANDERSON 1981).

Additionally, by applying practically infinite values for the viscosity (1×10^{30} Pa s) and the shear modulus (1×10^{20} Pa), the effects of a rigid (i.e., non-deforming) Earth (labelled as RIGID), which allows only for gravitational feedbacks, are investigated. The labels for viscoelastic rheologies (VE) are made up of sub-labels: L035 and L100 indicating the lithosphere thickness, and M19 and M21, indicating the logarithm of upper mantle viscosity.

The results from the coupled model are compared with simulations featuring the ELRA approximation for solid-Earth dynamics (see Section ELRA). With the elastic structure given by PREM, the flexural rigidity D can be related to the thickness of the lithosphere (LAMBECK & NAKIBOGLU 1980). However, since the viscoelastic layering in the SGVEM implies a full spectrum of relaxation times, the single ELRA relaxation time τ_r cannot be related to the SGVEM viscoelastic structures uniquely (VAN DEN BERG et al. 2008). The combinations of the considered ELRA parameters are listed in Table 3: The values $D = 1\times10^{23}$ N m and $D = 2.5\times10^{24}$ N m include the 35 km lithosphere, while $D = 1\times10^{25}$ N m and $D = 3\times10^{25}$ N m comprise the 100 km lithospheres. For the relaxation time, $\tau_r = 20$ yr and $\tau_r = 500$ yr are chosen for comparison with the low-viscous upper mantle and $\tau_r = 1000$ yr and $\tau_r = 5000$ yr for the high-viscous upper mantle.

ELRA run No	D (N m)		τ_r(yr)	Corresponding VE layering
1	1×10^{23}	(20 km)	20	VE_L035_M19
2	2.5×10^{24}	(54 km)	20	VE_L035_M19
3	1×10^{23}	(20 km)	500	VE_L035_M19
4	2.5×10^{24}	(54 km)	500	VE_L035_M19
5	1×10^{25}	(84 km)	1000	VE_L100_M21
6	3×10^{25}	(119 km)	1000	VE_L100_M21
7	1×10^{25}	(84 km)	5000	VE_L100_M21
8	3×10^{25}	(119 km)	5000	VE_L100_M21

Tab. 3: ELRA parameters: The viscoelastic layering, to which the respective ELRA run is compared, is indicated (Tab. 2). The bracketed values give the lithospheric thickness corresponding to D.

Tab. 3: Parameter des ELRA-Ansatzes: Die viskoelastische Schichtung, dem der entsprechende ELRA-Modelllauf zugeordnet wird, ist angegeben (vgl. Tab. 2).

Forcing

The steady-state ice-sheet and ice-shelf configuration is forced out of its equilibrium with a) rising sea level, b) decreased accumulation rate (in terms of changing SMB), or c) decreased accumulation rate and changed conditions at the base of both, the ice shelf and the grounded ice. The applied forcing scenarios are summarized in Table 4.

If the SGVEM is considered for solid-Earth dynamics, the sea-level forcing is applied by removing a uniform ice layer from the remote continent when handing the global ice thickness field from the ISM to the SGVEM: In the two scenarios S120 and S150, the ice is removed at a constant rate of 0.1 m yr^{-1} equivalent sea-level (ESL) from the remote continent starting at t = 100 yr until the maximum forcing of h^f = 120 m ESL or 150 m ESL, respectively, is reached, coinciding with a respective ice volume $\Delta V_{ice}^f = h^f A_{oc}\, \rho_{oc}/\rho$ (ocean area $A_{oc} = 3.68\times10^8$ km^2). For the ELRA-based simulations, these rates are directly applied as sea-level rise, together with the sea-level rise from the retreating modelled ice sheet (see Section ELRA).

The applied rate of global sea-level rise is approximately twice as large as the highest rates during the last deglaciation (meltwater pulse 1A: 20 m in ~500 yr; WEAVER et al. 2003). This high value, as well as the high amplitudes of more than 120 m ESL is due to the relatively low sensitivity of the ice-sheet model to sea-level rise (see Section DISCUSSION). This should, however, not affect the systematic effects found in the later results.

In the third scenario (labelled as ACCU), a linear decrease in the accumulation rate from 0.2 m/yr to 0.1 m/yr is realised between t = 100 yr and t = 600 yr. The fourth scenario (labelled as BASL) addresses the basal parameters in the ISM. It adopts the ACCU accumulation rate change together with an increased parameter A_{eff} in Equation 1 (sub-shelf melting increases to values of >0.18 m/yr) as well as reduced basal friction at $t = 0$.

Scenario	h^f (m)	ΔV^f_{ice} (km^3)	t_{start}/t_{end} (yr)	$\dot{b}_s$ (m WE/yr)	A_{eff} (m^2)	C (Pa (m/s)$^{1/3}$)
S120	120	-4.8×10^7	100/1300	0.2*	10^{-3}*	1.0×10^7*
S150	150	-5.9×10^7	100/1600	0.2*	10^{-3}*	1.0×10^7*
ACCU	0*	0*	100/600	0.1	10^{-3}*	1.0×10^7*
BASL	0*	0*	100/600	0.1	0.01	0.7×10^7*

Tab. 4: Applied forcing scenarios: The forced equivalent sea-level rise h^f corresponds to the ice volume removed from the remote continent ΔV^f_{ice}. Start and end time refer to the melting pulse from the remote continent (S120, S150) or to the interval for linear decrease of the SMB to the given value (ACCU, BASL). $\dot{b}_s$ is the model domain-wide SMB, A_{eff} is the tuning parameter for basal melting in the shelf regions (Equation 1), and C is the basal friction coefficient. Asterisk-indexed values are unchanged in the respective scenario.

Tab. 4: Verwendete Antriebsszenarien: Der äquivalente Meeresspiegelanstieg h^f entspricht dem Eisvolumen ΔV^f_{ice}, das vom entfernt liegenden Kontinent entnommen wird. Die Zeitpunkte t_{start} und t_{end} beschreiben das Intervall des Schmelzens auf dem entfernt liegenden Kontinent (S120, S150) oder der linearen Abnahme der Oberflächenmassenbilanz auf den angegeben Werten (ACCU, BASL). $\dot{b}_s$: Im gesamten Modellbereich angewandte Oberflächenmassenbilanz, A_{eff}: Kontrollparameter für basales Schmelzen im Schelfeis (Gleichung 1). C: Koeffizient für die basale Reibung. Werte mit Sternchen versehen sind in dem entsprechenden Szenario unverändert.

RESULTS

General findings

In all scenarios with non-rigid solid-Earth modelled by either ELRA or the SGVEM, the forced GL retreat decelerates and eventually ceases. Figure 2 shows the initial geometry and the final geometry for the VE_L035_M19 and VE_L100_M21 simulations under the S120 forcing along the cross section coinciding with the *y*-axis of the ISM domain (Fig. 1). Here, a first effect of the viscoelastic layering of the solid-Earth on the ice dynamics becomes visible: A more localised and faster uplift of the solid Earth (VE_L035_M19 – Fig. 2B) leads to less GL retreat than a long-wave and slower response (VE_L100_M21 – Fig. 2C). The backward slopes at the GL, however, at least partially remain. This is not surprising as GL retreat is treated in a three-dimensional set-up here. Consequently, GL stability is not only determined by the bedrock gradient, but also by the stress field in the ice body (GUDMUNDSSON et al. 2012, GUDMUNDSSON 2013).

Figure 3 shows the GL retreat along the central cross section over 15 or 20 kyr, respectively, for the four applied forcing scenarios and the five SGVEM Earth structures. The stepwise GL retreat, as it can be seen in the time series, is a feature of the numerical approach to the GL migration. The GL – and thus the whole ice sheet – on the RIGID Earth is not yet in steady state at the end of the illustrated time spans in all four forcing scenarios. On a viscoelastically adjusting Earth, the GL retreat has stopped before t = 7 kyr (S120, S150), or t = 10 kyr (ACCU) and t = 15 kyr (BASL). The exact time depends on the viscoelastic layering and the forcing strength. At this stage, only maximum GL retreat during each experiment is considered. The respective ice/Earth configuration is not necessarily in a steady state: Below, the possibilities of GL re-advance after reaching the maximum GL retreat distance will be discussed.

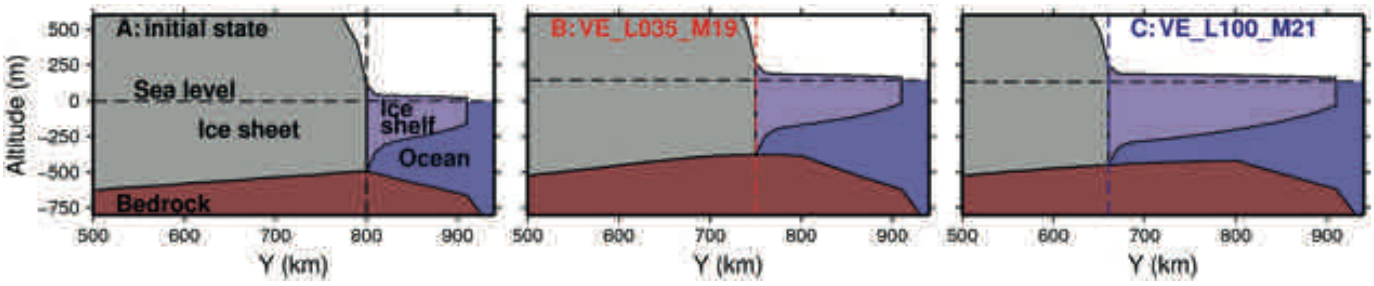

Fig. 2: Cross sections through the ice sheet. A: at time t = 0; B: after 8000 yr for VE_L035_M19 simulation; C: for VE_L100_M21 simulation at x = 0 for the S120 forcing. The grounding line (GL) positions correspond to the vertical dashed lines.

Abb. 2: Querschnitte (x = 0) durch den Eisschild zum Zeitpunkt t = 0 (A) und nach 8000 Jahren im Falle der VE_L035_M19-Simulation (B) und der VE_L100_M21-Simulation (C) und dem S120-Szenario. Die Positionen der Aufsetzlinie (GL) entsprechen den senkrechten, gestrichelten Linien.

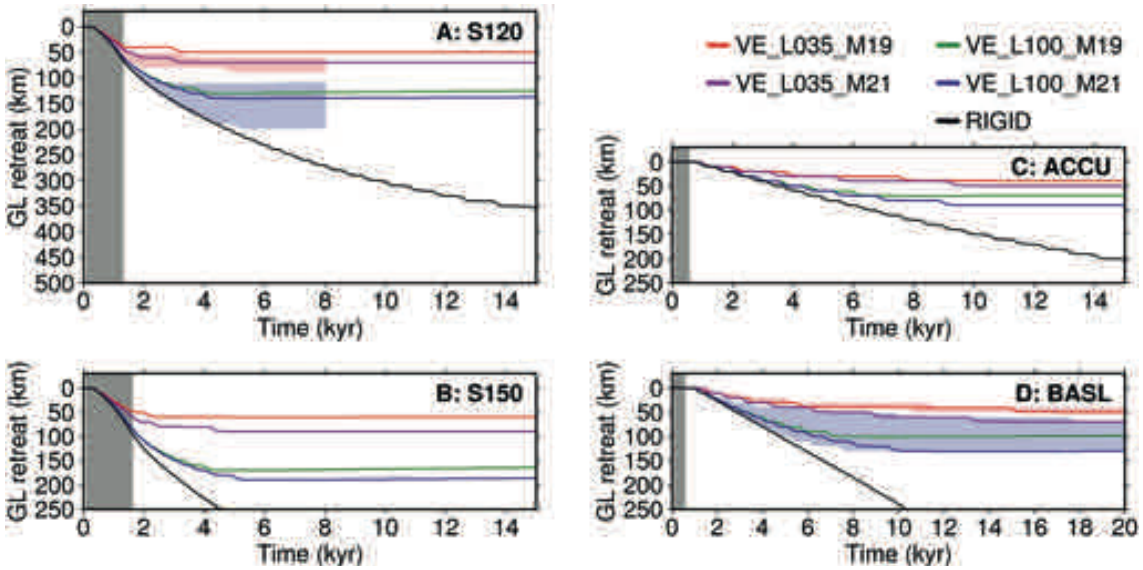

Fig. 3: Time series of GL retreat for the A: S120, B: S150, C: ACCU, and D: BASL forcing scenarios. The GL retreat refers to the x = 0 cross section (Fig. 1). The grey areas mark the periods of gradual melting on the remote continent and thus the forced sea-level rise (S120, S150), or the time interval of decreasing SMB (ACCU, BASL). The red shaded areas in A and D indicate the results spanned by the applied ELRA parameters corresponding to the VE_L035_M19 layering (Tab. 3). The blue shaded area shows the respective comparative ELRA results for the VE_L100_M21 layering. Note that the time series in D show data until t = 20 kyr, whereas it is only 15 kyr in A through C.

Abb. 3: Zeitreihen des Rückzugs der Aufsetzlinie im Falle der Antriebsszenarien A: S120, B: S150, C: ACCU und D: BASL. Der Rückzug bezieht sich auf den x = 0 Querschnitt (Abb. 1). Die grauen Bereiche bezeichnen die Intervalle des allmählichen Abschmelzens auf dem entfernt liegenden Kontinent (entspricht dem angetriebenen Meeresspiegelanstieg, S120, S150) oder das Intervall, in welchem die Oberflächenmassenbilanz abnimmt (ACCU, BASL). Die roten Bereiche in A und D umfassen die zu VE_L035_M19 gehörigen ELRA-Ergebnisse (Tab. 3). Die blauen Bereiche zeigen die entsprechenden zu VE_L100_M21 gehörigen ELRA-Ergebnisse. Man beachte, dass die Zeitreihen in D über 20.000 Jahre gehen, während es im Fall von A, B und C nur 15.000 Jahre sind.

There are notable systematic differences between the viscoelastic settings: The ice sheet in the case of a fast adjusting, low-viscous upper mantle (VE_L035_M19, VE_L100_M19) is less sensitive in terms of final GL position along the y-axis to the GL retreat forcing than in the case of the high-viscous upper mantle (VE_L035_M21, VE_L100_M21). Additionally, in both of these subgroups, the thinner lithosphere (L035) leads to less GL response to the forcing. The maximum retreat distances along the cross section are listed in Table 5. It is also visible that simulations with a low-viscous upper mantle are less sensitive to an increase in forcing: the maximum retreat positions under the S120 and S150 forcings differ only by 10 km and 20 km, while the higher upper mantle viscosity leads to respective differences of 40 km and 50 km.

Scenario	VE_L035_M19	VE_L100_M19	VE_L035_M21	VE_L100_M21
S120	50	70	130	140
S150	60	90	170	190
ACCU	40	50	70	90
BASL	50	70	100	130

Tab. 5: Maximum distances of grounding line (GL) retreat in km along the $x = 0$ cross section as inferred from Fig. 3. The possible re-advance as discussed in Fig. 6 is not considered here.

Tab. 5: Maximale Strecken des Aufsetzlinienrückzuges (GL) entlang des $x = 0$ Querschnittes (in km), wie sie aus Abb. 3 abgelesen werden können. Ein möglicher Wiedervorstoß, wie in Abb. 6 gezeigt, ist hier unberücksichtigt.

Comparison with ELRA under the S120 forcing

Figure 3A shows the results of the ELRA simulations under the S120 forcing with different choices for the flexural rigidity D and the relaxation time τ_r (red and blue shading). Overall, the ELRA simulations are similar to those with the real viscoelastic coupling in terms of the effect on the GL retreat: the faster and more local the solid-Earth can adjust to the unloading by a GL retreat, the less sensitive the ice sheet responds to the forcing.

Here, however, the ELRA approximation reveals shortcomings by a considerably higher sensitivity to the applied forcing: While the VE_L100_M21 results lie in the range of the respective ELRA results and consistency is hence given in terms of GL retreat, the comparison of VE_L035_M19 to the respective ELRA results indicates that the ice sheet with the ELRA response is more sensitive to the forcing even in the case of extremely low values for the relaxation time τ_r and flexural rigidity D. The ELRA results in this parameter range seem more appropriate for the VE_L100_M19 with its thicker lithosphere than for the VE_L035_M19 case. This is due to the higher sea level in the ELRA runs as a consequence of not considering the sea-level drop due to the ice-sheet retreat.

This higher sensitivity to sea-level rise in the ELRA approximation can be found more indirectly in the comparison of the "well-fitted" VE_L100_M21 results with those from ELRA: Figure 4 shows the RSL at the GL as it retreats for VE_L100_M21 and two respective ELRA simulations. The time markers along the graphs show that the RSL falls faster in the ELRA simulations in general and so should provide earlier stability. The coverage of the VE_L100_M21 results by the ELRA in the case of the S120 forcing results must then be due to the overestimation of sea-level rise.

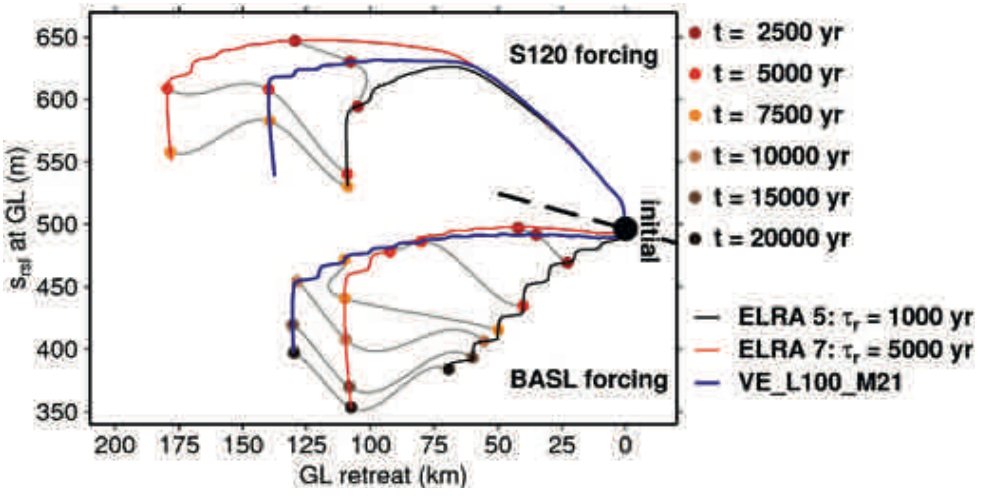

Fig. 4: Relation between RSL s_{rsl} at the GL and GL position along the central cross section in the S120 and BASL forcing scenarios for the VE_L 100_M21 Earth and two of the corresponding ELRA parameterisations (No. 5 and 7; Tab. 3). All simulations start from the same initial state; consequently, all graphs are to be read from the black marker at approximately (0 km, 500 m). At given times (colour-coded dots), the ELRA and SGVEM graphs are connected by grey lines. The black dashed line separates the S120 and the BASL results.

Abb. 4: Zusammenhang zwischen relativem Meeresspiegel s_{rsl} an der Aufsetzlinie (GL) und Position der Aufsetzlinie (GL) entlang des Querschnittes bei $x = 0$ im Falle der Antriebsszenarien S120 und BASL und der VE_L100_M21-Erdparametrisierung, sowie für zwei der zugehörigen ELRA-Parametrisierungen (Nr. 5 und 7, vgl. Tab. 3). Alle Simulationen beginnen bei demselben initialen Zustand; entsprechend sollten alle abgebildeten Graphen von dem schwarzen Marker bei ungefähr (0 km, 500 m) aus gelesen werden. Zu angegebenen Zeitpunkten, markiert durch die farbigen Punkte, sind die zu ELRA gehörigen Graphen und die zum vollwertigen Erdmodell gehörigen Graphen durch graue Linien verbunden. Die schwarze gestrichelte Linie trennt die S120 und die BASL Ergebnisse.

Comparison with ELRA under the BASL forcing

In the scenarios without externally forced sea-level rise, the BASL scenario shall be evaluated exemplarily in terms of ELRA and SGVEM differences. The main difference to the sea-level forced scenarios is that the forcing does not only affect the ice sheet directly at the GL, but that the whole ice sheet shrinks and, due to the changes in the basal parameters, changes its geometry. The ice flow is accelerated by the decrease in basal friction, such that more ice is transported towards the margins. The overall unloading of the continent due to the shrinkage leads to considerable uplift that stabilises the GL to some extent even before it starts to retreat.

The VE_L035_M19 und the respective ELRA simulations

(red shading) are consistent in this scenario (Fig. 3d) in terms of the inclusion of the VE_L035_M19 results by the ELRA results. Due to the small increase in sea level from melting of the ice sheet, which results in less than 4 m eustatic sea-level rise for the ELRA runs No 1-4 (see Tab. 3 for the numbering), the above drawback concerning non-consistent sea-level rise is of minor importance.

The same comparison for the VE_L100_M21 simulation and the respective ELRA runs (No 5-8), however, shows a clear preference towards τ_r = 5000 yr: While τ_r = 1000 yr to 5000 yr reproduce the VE_L100_M21 results under the S120 forcing, different τ_r parameters need to be chosen to encompass the combination of VE_L100_M21 layering and BASL forcing. As for the S120 forcing, the respective graphs in Figure 4 show a faster RSL fall at the GL in the ELRA simulations. In the BASL scenario, this relatively fast Earth response is not compensated by an overestimated sea-level rise as in S120 so that the slower relaxation of the solid-Earth effectively yields more GL retreat for the VE_L100_M21 simulation.

Relation between ice dynamical and solid-Earth time scales

A feature of the simulations with a low-viscous upper mantle is the significantly increasing time span between two discrete GL steps in the model. These are partially of the order of several thousand years in the presented scenarios, whereas the high-viscous upper mantle runs feature a modest increase of the time intervals before the next GL step. As already mentioned above, the stepwise character is a numerical feature, but the long time spans in the case of low upper mantle viscosity still contains a physical message, as will be discussed here.

The BASL scenario serves as a prominent example for comparing the time scales of solid-Earth relaxation and ice-flow adjustment to the changed conditions for the thin lithosphere runs VE_L035_M19 and VE_L035_M21 and for the RIGID Earth. Figure 5 shows the time series of RSL at the GL (again along the central cross section) and GL flux integrated along the whole GL, confining the ice shelf. In order to not focus on numerical aspects of GL migration, the smoothened time series (solid, thick lines; obtained as running mean) are considered. Three issues concerning the phenomena shown in Figure 5 can be highlighted:

(1) There is a GIA-induced fall of RSL at the GL in the viscoelastic runs: Following the GL retreat, there is unloading around the GL and thus bedrock uplift and sea-level fall. This is not the case for the RIGID Earth, where a steady increase of RSL occurs due to the backward sloping design of the bedrock geometry until flatter areas are reached ($t \approx$ 16 kyr).
(2) The time intervals between two GL steps are equal over the whole time span for the RIGID run (distance between neighbouring vertical black lines in Figure 5), indicating an almost constant GL retreat velocity of ~25 m/yr. In the viscoelastic runs, the GL velocity slows down due to the partial adjustment to the unloading. This transition is modest in the VE_L035_M21 run, whereas the time to cover the last 10 km distance in the VE_L035_M19 run is longer than 9 kyr, meaning that the GL velocity is only slightly above zero over this time span.
(3) The integrated GL flux is much higher in the RIGID simulation as a constantly high amount of ice is transported from the inland to the shelf. In the case of a viscoelastically adjusting Earth, the GL flux decreases as the ice dynamics approaches a steady state. After the GL retreat is decelerated such that there is no more GL migration on grid scale, the GL flux decays towards the limit of ~34 km^3/yr. In the case of the VE_L035_M21 layering, the respective time scale is much smaller than the time scale of RSL relaxation (high-viscous upper mantle). In the case of the VE_L035_M19 layering, the respective time scales appear to be of similar magnitude.

The slow adjustment of RSL in the case of a high-viscous upper mantle has further implications on the GL migration. Figure 6 shows time series of GL retreat along the central cross section for the S150 scenario, extending the time span from 20 kyr shown in Figure 3B to 50 kyr. Here, a gradual GL re-advance of the GL on the VE_L035_M21 Earth starts after the maximum distance is reached at $t \approx$ 5 kyr. After approximately 19 kyr, the GL re-advance reaches the grid scale and ends up at a final distance of 113 km away from the initial position and 57 km from the maximum retreat position. This prominent re-advance is, however, a feature of the deformational response of the thin lithosphere: A comparable evolution cannot be found for the VE_L100_M21 simulation before t = 50 kyr although a sub-grid scale re-advance occurs.

DISCUSSION

Our general finding, that viscoelastic deformation can decelerate and stop GL retreat, is in accordance with Gomez et al. (2012). The actual evolution through time depends on the solid-Earth parameters, namely thickness of the lithosphere and mantle viscosity. The first one determines how localised the solid-Earth responds to the unloading caused by an ice mass loss. As a more localised response leads to a more effective compensation of the former backward slopes, GL stability is reached at sites closer to the initial GL location. Mantle viscosity, in contrast, affects the time scale on which the solid-Earth reacts to the change in the loading: The fast response of a low-viscous upper mantle also leads to earlier GL stability than in case of the slower response of a high-viscous mantle and so to less GL retreat and ice mass loss.

In the studied situation, the mantle viscosity and the related time scales of solid-Earth response have the dominant impact on maximum GL retreat (Tab. 5) compared to lithosphere thickness. One should, however, state that the grounded ice flow is rather slow in this scenario compared to present-day Antarctic ice streams, which feed the surrounding shelf areas (e.g., ~500 m/yr in the catchment area of the Ross Ice Shelf (Thomas et al. 2013) vs. less than 150 m/yr here). Compared to that, the ice flow in this scenario is potentially less controlled by the underlying bedrock topography.

The initial magnitude of the backward slope also affects the time to reach stability. An ice sheet on a slope of different steepness might then also be more sensitive to lithospheric thickness as it is the case in this scenario. The possibility of GL re-advance yields a greater importance for the lithosphere thickness in later parts of the system's evolution in time.

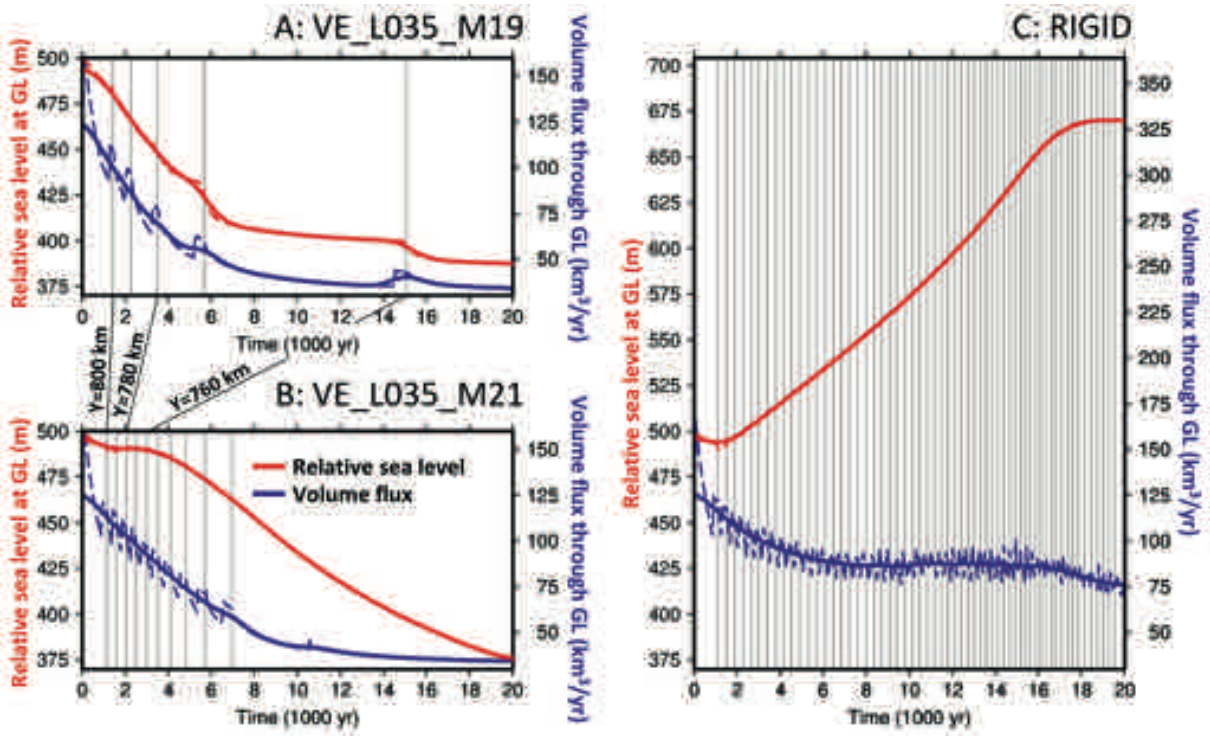

Fig. 5: Time series of RSL at the GL (red; left ordinate) and GL flux (blue; right ordinate); A: for the BASL scenario on the VE_L035_M19 Earth; B: on the VE_L035_M21 Earth and C: on the RIGID Earth. Each black vertical line indicates when the GL passes one of the *y*-grid nodes at $x = 0$. The GL flux is the integrated flux from the inland ice into the ice-shelf area. The GL retreat is considered along the central cross section ($x = 0$). The dashed coloured lines show the originally modelled data; the solid thick lines are obtained from these by running mean application and, hence, are less disturbed by numerical effects of the discrete GL retreat.

Abb. 5: Zeitreihen des relativen Meeresspiegels an der Aufsetzlinie (GL; rot, linke Ordinate) und Eisfluss über die Aufsetzlinie (GL; blau, rechte Ordinate) im Falle des BASL-Szenarios A: auf der VE_L035_M19-Erde, B: auf der VE_L035_M21-Erde und C: auf der RIGID-Erde. Jede senkrechte schwarze, gestrichelte Linie zeigt an, dass die Aufsetzlinie einen weiteren diskreten Punkt des *y*-Gitters entlang des Querschnittes bei $x = 0$ passiert. Der Fluss über die Aufsetzlinie ist integriert über die gesamte Grenzfläche zwischen Eisschild und Schelfeis. Die gestrichelten farbigen Linien zeigen die ursprünglichen Ergebnisse an; die entsprechenden durchgezogenen Linien sind durch Glättung (gleitender Mittelwert) erhalten und sind daher weniger durch den numerischen Effekt des diskreten Rückzuges beeinträchtigt.

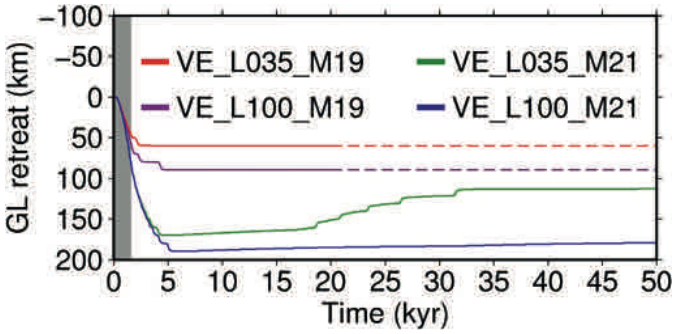

Fig. 6: Time series of grounding line (GL) retreat along the central cross section for the S150 scenario for 50 kyr (Fig. 3B: 15 kyr). The dashed parts in the VE_L035_M19 and VE_L100_M19 time series are extrapolated.

Abb. 6: Zeitreihen des Rückzuges der Aufsetzlinie (GL) entlang des Querschnittes bei $x = 0$ im Falle des Antriebsszenarios S150 über 50.000 Jahre hinweg (vgl. Abb. 3B: 15.000 Jahre). Die gestrichelten Passagen in den Zeitreihen der Erdparametrisierungen VE_L035_M19 und VE_L100_M19 sind extrapoliert.

The common method to account for a coupling between ice and solid-Earth dynamics, the ELRA method, shows similar behaviour as the ISM-SGVEM simulations, but has a major drawback when it comes to sea-level implications. The SLE is not solved within the ELRA approximation. The only possible way of accounting for sea-level rise or fall on glacial-interglacial time scales is to account for the eustatic sealevel. But this simplification overestimates (underestimates) the local sea-level in the ice sheet's vicinity during deglaciation (glaciation), because the gravitational attraction of the oceans by the ice mass is ignored. Hence, the ice sheet's response to sealevel change is amplified. The overestimated sea level can be compensated by an adequate choice of ELRA parameters (faster and more localized adjustment), from which in turn the physical meaning of the ELRA parameters τ_r and D would suffer. The adjustment of the ELRA parameters and the assessment against SGVEM simulations is an important issue even without the requirement of modelling interactions between ice sheets and sea level (VAN DEN BERG et al. 2008, KONRAD et al. 2014). The comparison of results from the VE_L035_M19 and VE_L100_M21 simulations to results from respective ELRA simulations shows that the a priori relaxation time in ELRA has to be chosen shorter than the related relaxation spectrum of a SGVEM in order to adequately model GL retreat in a sea-level rise scenario in general.

The relation between the time scales of solid-Earth relaxation and ice-flow adjustment is also very important for the retreat characteristics and potential re-advance of the GL. A slowly adjusting solid-Earth stabilises the disintegrating ice sheet gradually (VE_L035_M21 graphs in Fig. 5). Depending on the GL retreat velocity and on the delay of the solid-Earth response, the GL can even overshoot the later steady-state position and – after stopping further down-slope – re-advance

when the delayed fall of RSL creates the necessary conditions (Fig. 6). This, however, also depends on the lithosphere thickness: The thick lithosphere in the VE_L100_M21 simulation and the related long-wavelength pattern of RSL fall prevent the GL from re-advancing.

A fast adjusting solid-Earth interacts with the ice sheet in a more complex way. Depending on the ice-rheological parameters and the stress field in the ice, it takes the ice dynamics a certain time to adjust to new boundary conditions. In the case shown in Figure 5, these new conditions comprise the new SMB and the changed basal conditions (BASL), as well as the constantly adjusting ice-sheet geometry due to GL retreat. If the Earth beneath the ice sheet adjusts faster than or with similar time scales as the ice flow adjusts to the new conditions, the approach towards the final steady state becomes very slow. This manifests numerically in the long time spans between two grid-scale GL retreat events.

A general feature of the presented results is the insensitivity of the ice sheet to the applied forcing: The GL retreats over 190 km at most – under the most unrealistic condition of a 150 m rise of global mean sea level within 1500 yr (Tab. 5). Although this might be attributed to the specific set-up, it points at the inert representation of the GL, if this is not treated beyond the application of the SIA on the one and SSA on the other side of the GL and the floating criterion to separate these two areas (Pattyn et al. 2013). This drawback hinders clearer conclusions with respect to the relation of time scales of the ice and the Earth.

CONCLUSIONS

The feedback of RSL on GL migration has been treated extensively in this study. In the simplified situation considered here, the differences in the Earth representation – be it due to application of different approaches (ELRA *versus* SGVEM) or due to different choices for the viscoelastic parameters – lead to systematic differences in the ice sheet's evolution. In particular, the fast adjustment of an Earth with low mantle viscosities, as well as the high amplitudes of deformation of a relatively thin lithosphere yield a stronger negative feedback on GL migration than higher mantle viscosities and thicker lithospheric layers on glacial time scales. This indicates that a thorough consideration of the determining Earth parameters is necessary when studying ice dynamics, e.g., through past glacial cycles.

The simplified Earth dynamics of the ELRA approximation yield an essential conceptual drawback when it comes to the feedback of ice sheets with the solid Earth via the GL positioning and sealevel. Firstly, ELRA does not allow treating sea level gravitationally consistently, which leads to a possible overestimation of the related effects. Secondly, the dependence of the relaxation time on the load dimension and the viscoelastic stratification can become important, when it comes to GL migration in a MISI scenario; the usage of a single *a priori* relaxation time in ELRA, despite the wavelength-dependent relaxation spectrum associated with a more realistic Earth model description (e.g., Spada et al. 2011), introduces a bias in the evolution of the grounded ice, particularly if the ELRA parameters are not carefully tuned. Already in the simplified ice-sheet set-up in this study, it is difficult to define ELRA parameters, such that the effects from overestimated local RSL, inaccurate surface deformation and mantle relaxation are minimized. The problem becomes even more important for the simulation of an ice-sheet history through glacial cycles, as the ice sheet's response is sensitive to both, sea-level variations and atmospheric conditions. To avoid these drawbacks, a coupled model system such as the presented or that by Gomez et al. (2012, 2013) or de Boer et al. (2014) should be used, as it self-consistently accounts for sea-level variations and surface deformations.

ACKNOWLEDGMENTS

The authors wish to thank Heinz Miller for his thorough review and helpful suggestions and the editor Dieter Fütterer for handling the manuscript. HK is funded by the German Research Foundation (DFG) through grant SA 1734/6-1. This study has partially been funded in the framework of the DFG priority program SPP1257 "Mass transport and mass distribution in the Earth system" through grant SA 1734/2-2. IS acknowledges funding through DFG grant SA 1734/4-1. ZM acknowledges support from the Science Foundation of Ireland through the research program 11/RFP.1/GEO/3309. The study is also a contribution to the Helmholtz Climate Initiative REKLIM, a joint research project of the Helmholtz Association of German Research Centres (HGF).

References

Abramowitz M. & Stegun, I.A. (eds) (1964): Handbook of Mathematical Functions with Formulas, Graphs, and Mathematical Tables.- Dover 1-1046.

Beckmann, A. & Goosse, H. (2003): A parameterization of ice shelf-ocean interaction for climate models.- Ocean Model. 5(2): 157-170, doi: 10.1016/S1463-5003(02)00019-7.

Bindschadler, R.A. & 26 co-authors (2013): Ice-sheet model sensitivities to environmental forcing and their use in projecting future sea level (the SeaRISE project).- J. Glaciol. 59 (214): 195-224, doi: 10.3189/2013JoG12J125.

Brotchie, J.F. & Silvester, R. (1969): On crustal flexure.- J. Geophys. Res. 74: 5240-5252, doi: 10.1029/JB074i022p05240.

Cuffey, K.M. & Paterson, W.S.B. (2010): The Physics of Glaciers.- Elsevier Science, 4th edition, ISBN 9780080919126, 1-704.

de Boer, B., Stocchi, P. & van de Wal, R.S.W. (2014): A fully coupled 3-D ice-sheet – sea-level model: algorithm and applications.- Geosci. Model Dev. Discuss. 7: 3505-3544, doi: 10.5194/gmdd-7-3505-2014.

Dziewonski, A.M. & Anderson, D.L. (1981): Preliminary reference Earth model.- Phys. Earth Planet. Inter. 25: 297-356, doi: 10.1016/0031-9201(81)90046-7.

Farrell, W. & Clark, J. (1976): On postglacial sea level.- Geophys. J. Astr. Soc. 46: 647-667, doi: 10.1111/j.1365-246X.1976.tb01252.x.

Foldvik, A. & Kvinge, T. (1974): Conditional instability of sea water at the freezing point.- Deep-Sea Res. 21: 169-174, doi: 10.1016/0011-7471(74)90056-4.

Gomez, N., Pollard, D., Mitrovica, J.X., Huybers, P. & Clark, P.U. (2012): Evolution of a coupled marine ice sheet–sea level model.- J. Geophys. Res. 117: F01013, doi: 10.1029/2011JF002128.

Gomez, N., Pollard, D. & Mitrovica, J.X. (2013): A 3-D coupled ice sheet – sea level model applied to Antarctica through the last 40 ky.- Earth Planet. Sci. Lett. 384: 88-99, doi: 10.1016/j.epsl.2013.09.042.

Greve, R., Saito, F. & Abe-Ouchi, A. (2011): Initial results of the SeaRISE numerical experiments with the models SICOPOLIS and IcIES for the Greenland Ice Sheet.- Ann. Glaciol. 52(58): 23-30, doi: 10.3189/172756411797252068.

Gudmundsson, G.H., Krug, J., Durand, G., Favier, L. & Gagliardini, O. (2012): The stability of grounding lines on retrograde slopes.- The Cryosphere 6: 1497-1505, doi: 10.5194/tc-6-1497-2012.

Gudmundsson, G.H. (2013): Ice-shelf buttressing and the stability of marine ice sheets.- The Cryosphere 7: 647-655, doi: 10.5194/tc-7-647-2013.

Hagedoorn, J.M., Wolf, D. & Martinec, Z. (2007): An estimate of global mean sea-level rise inferred from tide-gauge measurements using glacial-iso-

static models consistent with the relative sea-level record.- Pure Appl. Geophys. 164: 791-818, doi: 10.1007/s00024-007-0186-7.

Haskell, N.A. (1935): The motion of a viscous fluid under a surface load.- J. Appl. Phys. 6: 265-269, doi: 10.1063/1.1745329.

Huybrechts, P. (1993): Glaciological modelling of the late Cenozoic East Antarctic Ice Sheet: stability or dynamism?- Geogr. Ann. Phys. Geogr. 75: 221-238, URL http://www.jstor.org/stable/521202.

Huybrechts, P., Goelzer, H., Janssens, I., Driesschaert, E., Fichefet, T., Goosse, H. & Loutre M.-F. (2011): Response of the Greenland and Antarctic Ice Sheets to multi-millennial greenhouse warming in the Earth system model of intermediate complexity LOVECLIM.- Surv. Geophys., 32(4-5): 397-416, doi: 10.1007/s10712-011-9131-5.

Konrad, H., Thoma, M., Sasgen, I., Klemann, V., Barbi, D., Grosfeld, K. & Martinec, Z. (2014): The deformational response of a viscoelastic solid earth model coupled to a thermomechanical ice sheet model.- Surv. Geophys. 35: 1441-1458, doi: 10.1007/s10712-013-9257-8.

Lambeck, K. & Nakiboglu, S.M. (1980): Seamount loading and stress in the ocean lithosphere.- J. Geophys. Res. 85B: 6403-6418, doi: 10.1029/JB085iB11p06403.

Le Meur, E. & Huybrechts, P. (1996): A comparison of different ways of dealing with isostasy: examples from modeling the Antarctic ice sheet during the last glacial cycle.- Ann. Glaciol. 23: 309-317.

Maris, M.N.A., de Boer, B., Ligtenberg, S.R.M., Crucifix, M., van de Berg, W.J. & Oerlemans, J. (2014): Modelling the evolution of the Antarctic Ice Sheet since the last interglacial.- The Cryosphere 8: 1347-1360, doi: 10.5194/tc-8-1347-2014.

Martinec, Z. (2000): Spectral-finite element approach to three-dimensional viscoelastic relaxation in a spherical Earth.- Geophys. J. Int. 142: 117-141, doi: 10.1046/j.1365-246x.2000.00138.x.

Mitrovica, J.X. & Milne, G.A. (2003): On post-glacial sea level: I. General theory.- Geophys. J. Int. 154: 253-267, doi: 10.1046/j.1365-246X.2003.01942.x.

Mitrovica, J.X., Tamisiea, M.E., Davis, J.L. & Milne, G.A. (2001): Recent mass balance of polar ice sheets inferred from patterns of global sea-level change.- Nature 409: 1026-1029, doi: 10.1038/35059054.

Oerlemans, J. (1980): Model experiments on the 100,000-yr glacial cycle.- Nature 287: 430-432, doi: 10.1038/287430a0.

Pattyn, F. & 27 co-authors (2013): Grounding-line migration in plan-view marine ice-sheet models: results of the ice/sea MISMIP3d intercomparion.- J. Glaciol. 59: 410-422, doi: 10.3189/2013JoG12J129.

Peltier, W.R. (1974): The impulse response of a Maxwell Earth.- Rev. Geophys. 12: 649-669, doi: 10.1029/RG012i004p00649.

Pollard, D. & DeConto, R.M. (2009): Modelling West Antarctic Ice Sheet growth and collapse through the past five million years.- Nature 458: 329-332, doi: 10.1038/nature07809.

Pollard, D. & DeConto, R.M. (2012): Description of a hybrid ice sheet-shelf model, and application to Antarctica.- Geosci. Model Dev. 5: 1273-1295, doi: 10.5194/gmd-5-1273-2012.

Schoof, C. (2007): Ice sheet grounding line dynamics: Steady states, stability, and hysteresis.- J. Geophys. Res. 112:, doi: 10.1029/2006JF000664.

Spada, G., Barletta, V.R., Klemann, V., Riva, R.E.M., Martinec, Z., Gasperini, P., Lund, B., Wolf, D., Vermeersen, L.L.A. & King, M.A. (2011): A benchmark study for glacial isostatic adjustment codes.- Geophys. J. Int. 185: 106-132, doi: 10.1111/j.1365-246X.2011.04952.x.

Spada, G., Bamber, J.L. & Hurkmans, R.T.W.L. (2013): The gravitationally consistent sea-level fingerprint of future terrestrial ice loss.- Geophys. Res. Lett. 40: 482-486, doi: 10.1029/2012GL053000.

Thoma, M., Grosfeld, K., Barbi, D., Determann, J., Goeller, S., Mayer, C. & Pattyn, F. (2014): RIMBAY – a multi-approximation 3D ice-dynamics model for comprehensive applications: model description and examples.- Geosci. Model Dev. 7: 1-21, doi: 10.5194/gmd-7-1-2014.

Thomas, R., Scheuchl, B., Frederick, E., Harpold, R., Martin, C. & Rignot, E. (2013): Continued slowing of the Ross Ice Shelf and thickening of West Antarctic Ice streams.- J. Glaciol. 59: 838-844, doi: 10.3189/2013JoG12J122.

Thomas, R.H. & Bentley, C.R. (1978): A model for Holocene retreat of the west Antarctic Ice Sheet.- Quat. Res. 10: 150-170, doi: 10.1016/0033-5894(78)90098-4.

van den Berg, J., van de Wal, R.S.W., Milne, G.A. & Oerlemans J. (2008): Effect of isostasy on dynamical ice sheet modeling: A case study for Eurasia.- J. Geophys. Res. 113: B05412, doi:10.1029/2007JB004994.

Weaver, A.J., Saenko, O.A., Clark, P.U. & Mitrovica, J.X. (2003): Meltwater pulse 1A from Antarctica as a trigger of the Bølling-Allerød warm interval.- Science 299: 1709-1713, doi: 10.1126/science.1081002.

Weertman, J. (1957): On the sliding of glaciers.- J. Glaciol. 3: 33-38.

Wessel, P. & Smith, W.H.F. (1991): Free software helps map and display data.- Eos Trans. AGU 72: 441, doi: 10.1029/90EO00319.

Polarforschung 85 (2), 101–105, 2015 (erschienen 2016)

High Resolution Sea-Ice Modelling and Validation of the Arctic with Focus on South Greenland Waters, 2004–2013

by Kristine Skovgaard Madsen[1*], Till Andreas Soya Rasmussen[1], Mads Hvid Ribergaard[1] and Ida Margrethe Ringgaard[1]

Abstract: We introduce an operational model system of the Arctic and Atlantic oceans with a horizontal resolution of about 10 km. The model system consists of the 3D ocean model HYCOM coupled with the sea-ice model CICE. This study presents a hindcast simulation from 2004–2013, which has been continued in operational mode, and is continuously updated with a 6-day operational forecast. We first focus on the general ice cover and thickness simulated by this hindcast. The Arctic Sea ice cover is to a large degree fixed by assimilation and the modelled total sea ice volume is within the uncertainty range of available observations and other models. Then, we zoom in on the ocean around Cape Farewell (the southern tip of Greenland), which is the main focus area for the Ice Charting by the Danish Meteorological Institute (DMI). Simulating the sea-ice conditions in this area is challenging, since it requires correct simulation of the ice export along the East Greenland coast, the interplay between cold Polar and warm Atlantic water masses within the East Greenland Current and the effects of local weather systems. The model replicates the seasonal and interannual ice variability as compared to the DMI ice chart index for Cape Farewell, but the total number of weeks with sea ice is underestimated by the model. Finally, *in situ* profile observations near Fylla Bank off West Greenland are used to validate the properties of the Polar and Atlantic water masses within the West Greenland Current. Despite a warm bias originating at the sea surface, the hindcast reproduces the pulsating nature of the interplay between the two water masses and demonstrates interannual variability in the same range as observed.

Zusammenfassung: Es wird ein operationelles Modellsystem für die Arktis und den Atlantischen Ozean mit einer horizontalen Auflösung von 10 km vorgestellt. Das Modellsystem besteht aus dem 3D Ozeanmodell HYCOM, gekoppelt mit dem Meereismodell CICE. Die Arbeit zeigt eine auf die Periode 2004 bis 2013 zurückschauende Simulation (Hindcast), die im operationellen Modus fortgeführt und kontinuierlich mit sechstägigen operationellen Vorhersagen aktualisiert wurde. Schwerpunkt liegt hierbei auf der Untersuchung der Eisbedeckung und der Eisdicke. Die arktische Meereisbedeckung ist im Modell zu einem Großteil durch Assimilation festgelegt. Das hiermit modellierte, totale Meereisvolumen liegt innerhalb des Unsicherheitsbereiches der vorhandenen Beobachtungen und von anderen Modellen. Der Ozean rund um das Kap Farewell (der südlichste Punkt Grönlands) ist die Hauptfokusregion der Eiskartierung des Dänischen Meterologischen Instituts (DMI). Die Meereissituation dieser Region zu simulieren, stellt eine Herausforderung dar, da korrekte Simulationen des Eisexportes entlang der Ostküste Grönlands benötigt werden und Kenntnisse über das Zusammenspiel zwischen kaltem Polar- und warmem Atlantikwasser innerhalb des Ostgrönlandstroms und Einflüsse lokaler Wettersysteme eine Rolle spielen. Das Modell bildet die saisonale und zwischenjährliche Eisvariabilität, verglichen mit der DMI Eiskarte des Kap Farewell gut ab. Jedoch wird die Gesamtzahl der Wochen mit Meereis durch das Modell unterschätzt. *In situ* Beobachtungen nahe Fylla Bank an der Küste Westgrönlands werden genutzt, um die Eigenschaften des Polar- und Atlantikwassers innerhalb des Westgrönlandstroms zu validieren. Abgesehen von einer Tendenz zu wärmeren Meeresoberflächentemperaturen, bildet die zurückschauende Simulation (Hindcast) den pulsierenden Charakter der Wechselwirkungen zwischen den zwei Wassermassen gut ab und spiegelt die zwischenjährliche Variabilität in derselben Größenordnung wie die Beobachtungen wider.

doi:10.2312/polfor.2016.006

[1] Danish Meteorological Institute, Lyngbyvej 100, 2100 Copenhagen OE Denmark;
[*] Corresponding author <kma@dmi.dk>

This extended abstract was presented as a poster contribution at the Inter-national Conference "Our Climate – Our Future: Regional perspectives on a global challenge", 6–9 October 2014 in Berlin, Germany.
Manuscript received 22 June 2015; accepted in revised form 16 October 2015.

INTRODUCTION

Over the past ten years, the annual Arctic minimum sea-ice extent has been observed to be low and highly variable compared to the 1979–2000 climatology, with record low years in 2007 and again in 2012 (Lavergne et al. 2010, Eastwood et al. 2011, Meier et al. 2013, Peng et al. 2013). The sea-ice volume is not well observed, but model studies of the Arctic show a steady decrease throughout the last decade (e.g., Zhang & Rothrock 2003, updated), making the sea ice weaker and more sensitive to weather and upper ocean heating (Parkinson & Comiso 2013, Zhang et al. 2013). Warming is observed in the Polar Waters that reach tidewater glaciers of the Greenland Ice Sheet, enhancing their retreat (Myers & Ribergaard 2013, Straneo & Heimbach 2013). With the reduction in sea ice, an increasing interest and need is seen for detailed data of the Arctic Ocean and sea-ice conditions for applications in ecology, ice-sheet modelling, shipping, ice charting, oil-spill preparedness, etc. Here, we present a high-resolution ten year ocean and sea-ice hindcast of the Arctic. We place a special focus on the south Greenland Waters, which is one of the hotspots for Arctic development and change, and focus on three research questions:

(1) Is the model suitable to estimate the total sea-ice volume in the Arctic?
(2) Is the model a suitable tool for assessing the sea-ice extent at Cape Farewell (the southern tip of Greenland)?
(3) Are the temperature and salinity properties of the water masses at Fylla Bank, west of Greenland, represented in the model?

In all three cases we discuss the operational aspects. We consider the seasonal and interannual variability of the daily mean variables, except for the sea-ice extent of Cape Farewell, where we match the weekly resolution of the observational index.

MODEL AND MATERIALS, INCLUDING OBSERVATIONS FOR VALIDATION

The model system consists of the HYbrid Coordinate Ocean Model (HYCOM, e.g., Chassignet et al. 2007) and Community Ice CodE (CICE, Hunke & Dukowicz 1997, Hunke 2001) models, coupled with the ESMF coupler. The model resolution is about 10 km to ensure an eddy-permitting model and resolve the coastal shelf, while balancing computational resources and the domain covers the Arctic Ocean and the Atlantic Ocean to approximately 20°S (Fig. 1). The sea-ice model, CICE v4.0, is a Hibler-type model with five ice thickness categories. The thermodynamics of CICE allows for a vertical tempera-

ture profile with a resolution of four thermodynamic layers and one layer of snow. The ocean model, HYCOM v2.2.55, explores a hybrid coordinate system, combining isopycnals with z-level coordinates. The vertical mixing is defined by the K-profile parameterisation (KPP) scheme (LARGE et al. 1994). Our setup of HYCOM has 40 vertical levels, it includes tides, and we have modified the input radiation scheme to correct for inconsistencies of the ice cover between the atmospheric forcing and the model (RASMUSSEN et al. 2010).

The model is initialized in 1997 with a combined climatology, using the Polar Science Center Hydrographic Climatology (PHC, STEELE et al. 2001) in the Arctic and World Ocean Atlas 2001 in 0.25° resolution (CONKRIGHT et al. 2002) in the Atlantic, with a 100 km linear transition. The first seven years were considered as spin-up. ERA-Interim was used for atmospheric forcing (DEE et al. 2011). The model domain has two open boundaries in the Barents Strait and in the South Atlantic Ocean, where temperature and salinity are prescribed from the combined climatology, while no volume transports were prescribed at the boundaries. Similarly, tidal forcing is prescribed from Oregon State University TOPEX/Poseidon Global Inverse Solution (TPXO71, EGBERT & EROFEEVA 2002). In the model interior, body tides are induced using eight constituents.

The model assimilates Ocean and Sea Ice Satellite Application Facility (OSISAF) reanalysed sea-ice concentration (EASTWOOD et al. 2011) and sea-surface temperature from the Operational SST and Sea Ice Analysis (OSTIA) system (DONLON et al. 2011) for 1997-2010 and from Global Ocean Data Assimilation Experiment High Resolution SST (GHRSST) Level 4 DMI_OI (DMI 2007, HØYER et al. 2014) from 2011 onward, using a nudging scheme with 10 and 30 days relaxation time, respectively. Surface salinity is relaxed towards climatology with 30 days relaxation time. More than 100 rivers are included as monthly climatological discharges obtained from the Global Runoff Data Centre GRDC) and scaled as in DAI & TRENBERTH (2002).

Only non-flagged OSISAF reanalysed sea-ice observation is used, therefore sea ice is not assimilated in a 20–50 km zone near the coast where the satellite footprint is affected by land. We also do not assimilate where the modelled and observed sea-ice concentration agrees within 10 %, to limit observationally induced noise effects. In these areas, the concentrations are determined purely by the sea ice model physics.

For validation of sea ice conditions in the Cape Farewell area on the southern tip of Greenland, we use an index based on weekly ice charts for south Greenland (pers. com. K. Qvistgaard 2014). The index is set to 1 if sea ice is present west of Cape Farewell at 44°W, and set to 2 if it is present at 48°W and thus fills the Julianehaab Bight (see Fig. 1 for locations).

For validation of the temperature and salinity profile in West Greenland Waters, we use annual in situ observations for Fylla Bank station 4 obtained in June/July (63.8833°N, 53.3683°W, Fig. 1). The data was collected and handled by DMI in collaboration with the Greenland Institute of Natural Resources (RIBERGAARD 2014).

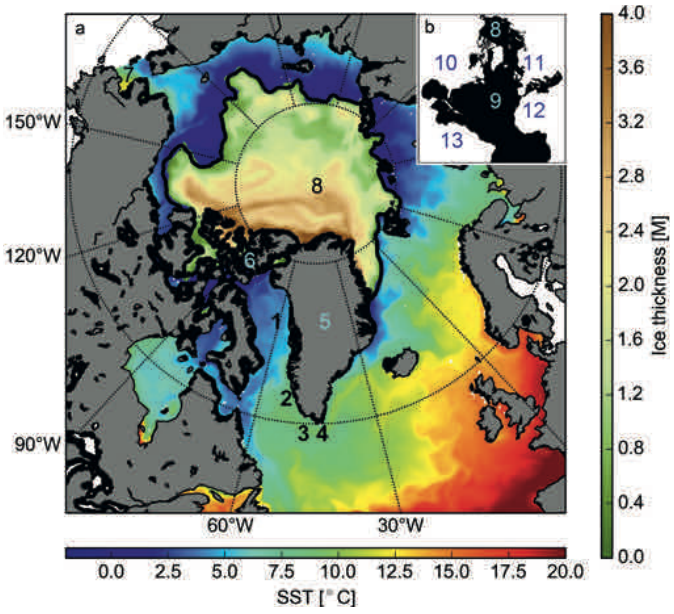

Fig. 1: a) September 2009 mean modelled SST (horizontal colour bar) and sea-ice thickness (vertical colour bar), overlaid with the 15 % contour of OSISAF ice concentration (black). The numbers indicate 1: Baffin Bay, 2: Fylla Bank, 3: Julianehaab Bay, 4: Cape Farewell, 5: Greenland, 6: Canadian Archipelago, 7: Barents Strait. b): Small insert marks the entire model domain. The numbers indicate 8: Arctic Ocean, 9: Atlantic Ocean, 10: North America, 11: Europe, 12: Africa, 13: South America.

Abb. 1: a) Mittlere modellierte Meeresoberflächentemperatur (SST) (horizontale Farbskala) und Meereisdicke (vertikale Farbskala) im September 2009 mit Kontourlinie der 15 % Eiskonzentration des OSISAF überlagert (schwarz). Die Nummern geben spezielle Regionen der Untersuchungen an: 1: Baffin Bay, 2: Fylla Bank, 3: Julianehaab Bay, 4: Cape Farewell, 5: Greenland, 6: Canadian Archipelago, 7: Barents Strait. b) Einlegekarte markiert das gesamte Modellgebiet. Die Ziffern dienen zur geographischen Orientierung 8: Arctic Ocean, 9: Atlantic Ocean, 10: North America, 11: Europe, 12: Africa, 13: South America.

RESULTS

General evaluation

The modelled sea-ice thickness and sea-surface temperatures (SST) averaged for September 2009 are shown in Figure 1.

For this month, the observed and modelled sea ice extents are similar, with small deviations in the western Arctic and the Canadian Archipelago. The SST general patterns indicate that the large-scale ocean currents are captured by the model, with the warm North Atlantic Current up along the European coast, the generally cold sea surface of Baffin Bay and the cold East Greenland Current. This current is responsible for the export of sea ice southwards along the coast of Greenland and down to Cape Farewell in winter and early spring.

The sea-ice thickness distribution in the Arctic is also reasonable with thick ice located near the Canadian Archipelago and the northern coast of Greenland. There are no continuous measurements of the distribution of the thick ice, however, remote sensing results by CryoSat-2 as well as point measurements from the IceBridge-campaign support the modelled ice-thickness distribution and total volume (FARRELL et al. 2009, FARRELL et al. 2012, TILLING et al. 2015).

The overall sea-ice extent closely follows sea ice observations independently processed by NSIDC (Fig. 2, CAVALIERI et al. 1996). The sea-ice volume, on the other hand, is not fixed by assimilation. At the start of the time series, the seasonal range is 10,000-30,000 km^3, but the volumes decrease to a new level from 2005 to 2008, following the observed loss of Arctic sea ice. The summer minima in 2008 and 2012 are both around 5,000 km^3.

As indicated by the sea-ice extent time series, there are large seasonal variations in the Arctic ice cover. Figure 3 shows the average modelled number of days with at least 15 % ice concentration, displaying how large parts of the Arctic, including coastal zones where satellite observations are lacking, is accessible for the summer season only.

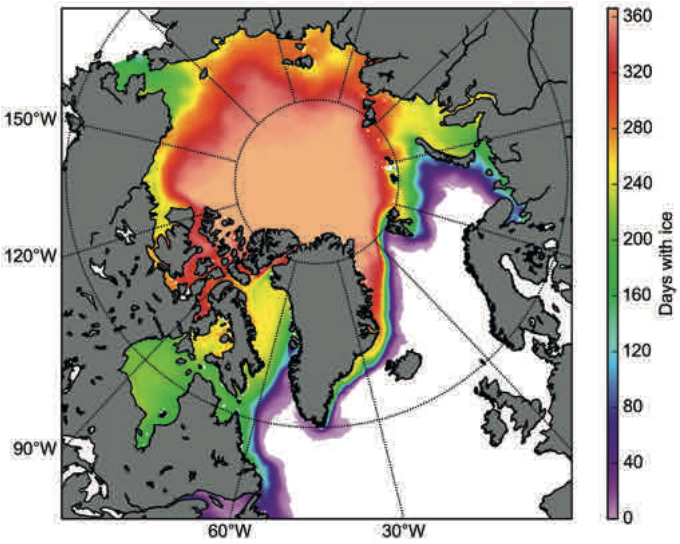

Fig. 3: Modelled average number of days with sea ice, 2004–2013. Points with only one model year with sea ice have been removed.

Abb. 3: Modellierte mittlere Anzahl der Tage mit Meereis, 2004–2013. Punkte mit Meereis in nur einem Modelljahr wurden ausgenommen.

Cape Farewell

In the challenging waters of Cape Farewell, sea-ice assimilation is almost absent due to land effects in the OSISAF products. Nevertheless, the weekly mean modelled sea ice extent captures most interannual variability seen in the ice chart based weekly sea ice index, including an almost complete absence of sea-ice in 2005 and a long period with sea ice in Julianehaab Bight in 2008 (Fig. 4). However, the model has a bias with too early breakup and a following lack of sea ice in June and July.

Fylla Bank

The model is able to reproduce the general vertical structure with low-saline shelf and Polar Waters in the upper ~200 m and warm and saline water masses of subtropical Atlantic origin below 400–500 m (Fig. 5). The seasonality in the two water masses and interannual variations are both captured by the model, but it is not possible to make solid conclusions on changes from one year to another, using one single observa-

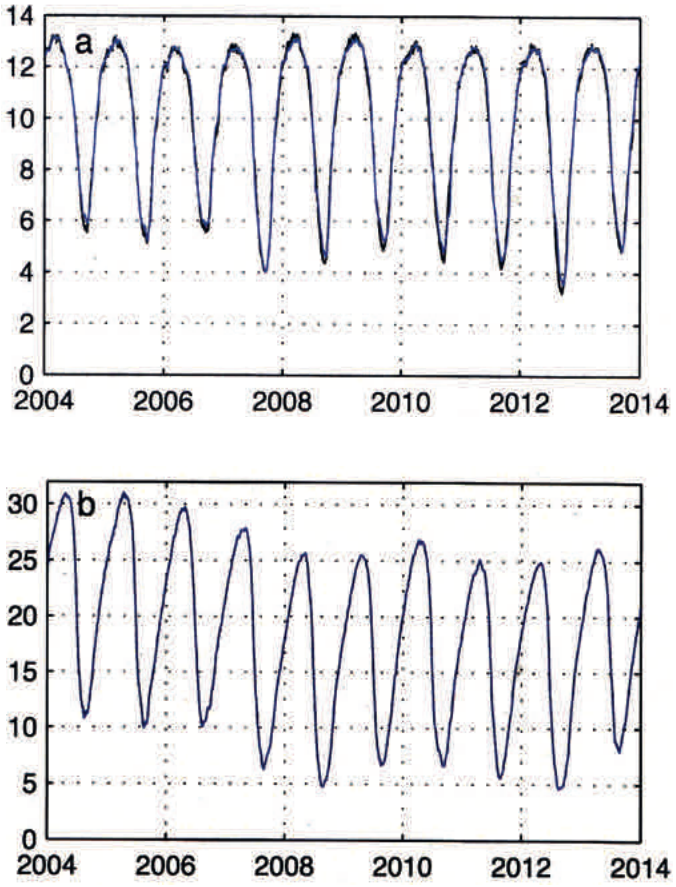

Fig. 2: a): Modelled (blue) and observed (CAVALIERI et al. 1996, black) sea-ice extent (15 % concentration limit) of the entire model domain, daily averages 2004–2013 (million km^2); b): Modelled total sea ice volume, daily average 2004–2013 (thousand km^3).

Abb. 2: a): Modellierte (blau) und beobachtete (CAVALIERI et al. 1996, schwarz) Meereisausdehnung (15 % Meereiskonzentration) im gesamten Modellgebiet, tägliche Mittelwerte 2004–2013 (in Mio. km^2), b): modelliertes Meereisvolumen, tägliche Mittelwerte 2004–2013 (in 1000 km^3).

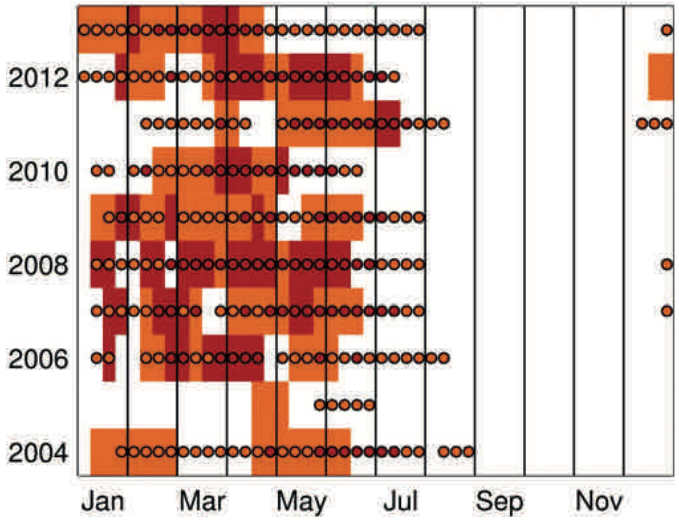

Fig. 4: Weekly sea ice index at Cape Farewell as observed (circles) and as modelled (patches), 2004–2013. White: no sea ice. Orange: sea ice at Cape Farewell. Red: sea ice fills Julianehaab Bight.

Abb. 4: Wöchentlicher Meereisindex am Kap Farewell aus Beobachtungen (Kreise) und Modellierung (farbliche Hintergrundfüllung), 2004–2013. Weiß: kein Meereis. Orange: Meereis am Cape Farewell. Rot: Meereis füllt die Julianehaab Bucht.

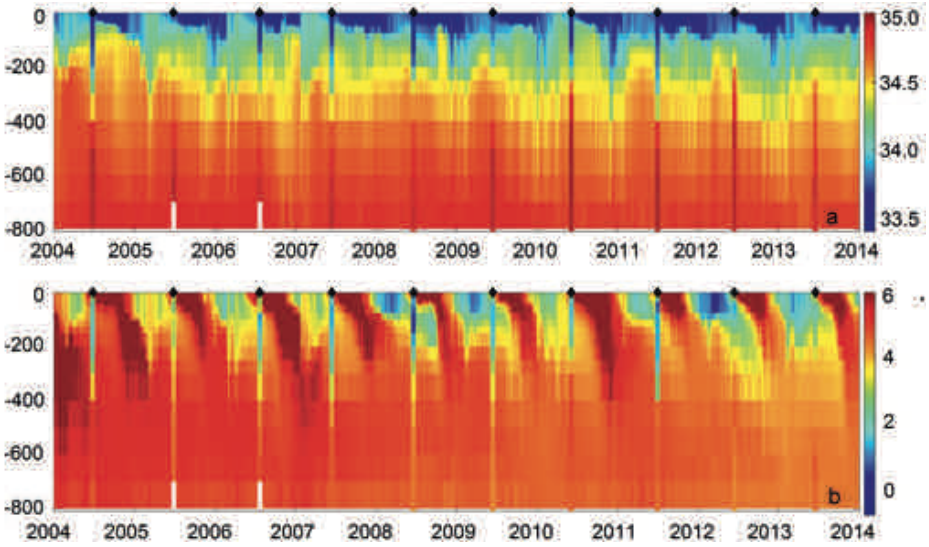

Fig. 5: Hovmöller diagram of modelled salinity (a) and temperature (b) (°C) as a function of depth (m) and time (years). Annual in situ observations in June/July (RIBERGAARD 2014) are interpolated to the same vertical axis, shown with 20 days width, and marked with black markers at the top.

Abb. 5: Hovmöllerdiagramm der modellierten (a) Salinität und (b) Temperatur (in °C) als Funktion der Tiefe (in m) und Zeit (in Jahren). Jährliche Beobachtungen im Juni/Juli (RIBERGAARD 2014) wurden auf dieselbe vertikale Achse interpoliert, gezeigt mit 20 Tagen Bandbreite und gekennzeichnet mit schwarzen Markierungen an der Spitze.

tion per year. For example, the observed low temperature and salinity down to almost 400 m in 2011 is likely due to a cold-water eddy. However, compared to June/July observations, the model has higher salinities in the surface waters and slightly lower salinities in the deeper waters. This leads to a lower stratification, as it is mainly determined by its salinity. Likewise, the modelled temperatures are in general higher than observed. This is especially true for the upper waters and is likely related to a too thin and too saline surface layer. In contrast, the Atlantic Water temperature is much closer to the observations.

DISCUSSION AND SUMMARY

The total sea-ice volume (Fig. 2b) is comparable to that of the PIOMAS model (Schweiger et al. 2011, not shown). The seasonality is very similar, but our maximum values are about 4.000 km^3 higher than the PIOMAS estimate, in line with observations by CryoSat-2 (TILLING et al. 2015). Our model reproduces more short-term variability than PIOMAS. The two models differ on the interannual variability of the annual minimum volumes; in particular, the PIOMAS model simulates a larger ice volume in 2008 than in 2012. However, the differences are within the uncertainties of this very poorly constrained parameter.

The model is able to correctly position the ocean currents in the water column off West Greenland, despite bias in the water mass characteristics compared to observations. The differences are likely related to an overly weak stratification due to underestimated fresh water discharge from the Greenland Ice Sheet. An update of the runoff is an obvious improvement of the model performance.

When analysing the sea ice, we have paid special attention to the coastal regions, where the satellite observations have an increased level of uncertainty. Based on the unassimilated model results by MADSEN et al. (2016), the model physics are expected to maintain a realistic ice edge without assimilation. This is confirmed by the validation against ice charts at Cape Farewell. However, the modelled amount of summer sea ice in this area is too low, possibly relating to the warm bias detected off West Greenland.

The simulation presented here serves several purposes. It is a scientific baseline for studies of the physical environment of the ocean and the sea ice and its effect on and interaction with the atmosphere, the ecosystem, the cryosphere, etc. It is also the foundation for operationally interesting statistics on ocean and sea-ice conditions that are valuable for ice charting, shipping, and oil-spill response planning among other activities. Since the simulations are continued seamlessly to the present, complete with twice-daily forecasts, the results also serve as a first validation of the operational forecast. However, the assessment of forecast skill and of the impact of the required change of atmospheric forcing to an operational product is left for future studies.

ACKNOWLEDGMENTS

We acknowledge the Ocean and Sea Ice Satellite Application Facility (OSISAF) High Latitude Processing Centre for producing and making available their reprocessing data sets and derived products from the Danish Meteorological Institute (DMI) and the Norwegian Meteorological Institute (MET Norway). We would like to thank Paul Meyers and an anonymous reviewer for fruitful comments improving this manuscript and R. Mottram for language support.

References

GRDC <http://grdc.bafg.de>

Cavalieri, D.J., Parkinson, C.L., Gloersen, P. & Zwally, H.J. (1996: updated yearly): Sea Ice Concentrations from Nimbus-7 SMMR and DMSP SSM/I-SSMIS Passive Microwave Data, Version 1 [2004-2013].- NASA National Snow and Ice Data Center Distributed Active Archive Center. Boulder, Colorado USA, doi:10.5067/8GQ8LZQVL0VL.

Chassignet, E.P., Hurlburt, H.E., Smedstad, O.M., Halliwell, G.R., Hogan, P. J., Wallcraft, A.W., Baraille, R. & Bleck, R. (2007): The HYCOM (HYbrid Coordinate Ocean Model) data assimilative system.- J. Marine Syst. 65: 60-83, doi:10.1016/j.jmarsys.2005.09.016.

Conkright, M.E., Locarnini, R.A., Garcia, H.E., O'Brien, T.D., Boyer, T.P., Stephens, C. & Antonov, J.I. (2002): World Ocean Atlas 2001: Objective Analyses, Data Statistics, and Figures, CD-ROM Documentation.- National Oceanogr. Data Center, Silver Spring, MD, 1-17.

Dai, A. & Trenberth, K.E. (2002): Estimates of freshwater discharge from continents: Latitudinal and seasonal variations.- J. Hydrometeorol. 3: 660-687.

Dee, D.P. & 35 co-authors (2011): The ERA-Interim reanalysis: configuration and performance of the data assimilation system.- Quat. J. Royal Meteorol. Soc., 137: 553-597, doi:10.1002/qj.828.

DMI (2007): GHRSST Level 4 DMI_OI Global Foundation Sea Surface Temperature Analysis (GDS version 2). Ver. 1.0.- PO.DAAC, CA, USA, doi:10.5067/GHGDM-4FD02.

Donlon, C.J., Martin, M., Stark, J.D., Roberts-Jones, J., Fiedler, E. & Wimmer, W. (2011): The Operational Sea Surface Temperature and Sea Ice analysis (OSTIA).- Remote Sensing of the Environment, doi:10.1016/j.rse.2010.10.017.

Eastwood, S., Larsen, K.R., Lavergne, T., Nielsen, E. & Tonboe, R. (2011): Global Sea Ice Concentration Reprocessing.- Product User Manual. Product OSI-409. Document version: 1.3. Data set version: 1.1. Available online <http://osisaf.met.no/docs/pum_seaicereproc_ss2_v1p3.pdf>

Egbert, G.D. & Erofeeva, S.Y. (2002): Efficient inverse modeling of barotropic ocean tides.- J. Atmos. Oceanic Technol. 19: 183-204.

Farrell, S.L., Laxon, S.W., McAdoo, D.C.. Yi, D. & Zwally, H.J. (2009): Five years of Arctic sea ice freeboard measurements from the Ice, Cloud and land elevation Satellite.- J. Geophys. Res. 114: C04008, doi: 10.1029/2008JC005074.

Farrell, S.L., Kurtz, N., Connor, L.N., Elder, B.C., Leuschen, C., Markus, T., McAdoo, D.C., Panzer, B., Richter-Menge, J. & Sonntag, J.G. (2012): A first assessment of IceBridge snow and ice thickness data over Arctic sea ice.- IEEE Transactions on Geoscience and Remote Sensing 50: 2098-2111, doi:10.1109/tgrs.2011.2170843,

Hunke, E.C. (2001): Viscous–plastic sea ice dynamics with the EVP model: linearization issues.- J. Comp. Phys. 170: 18-38, doi: 10.1006/jcph.2001.6710.

Hunke, E.C. & Dukowicz, J.K. (1997): An elastic–viscous–plastic model for sea ice dynamics.- J. Phys. Oceanogr. 27: 1849-1867, doi:10.1175/1520-0485(1997)027<1849:AEVPMF>2.0.CO;2,

Høyer, J.L., Le Borgne, P., & Eastwood, S. (2014): A bias correction method for Arctic satellite sea surface temperature observations.- Remote Sensing of Environment 146: 201-213, doi: 10.1016/j.rse.2013.04.020.

Large, W.G., McWilliams, J.C. & Doney, S.C. (1994): Oceanic vertical mixing: A review and a model with a nonlocal boundary layer parameterization.- Rev. Geophys. 32: 363-403, doi:10.1029/94RG01872.

Lavergne, T., Killie, M.A., Eastwood, S. & Breivik, L.-A. (2010): Extending the CryoClim Arctic sea ice extent time series with operational OSI SAF products from 2008 onwards.- Met. no Note 07/2010.

Madsen, K.S., Mottram, R., Rasmussen, T.A.S. & Ribergaard, M.H. (2016): High resolution sea-ice modelling and validation of the Arctic with focus on South Greenland Waters, 2004–2013.- Polarforschung 85: 85–88.

Meier, W., Fetterer, F., Savoie, M., Mallory, S., Duerr, R. & Stroeve, J. (2013): NOAA/NSIDC climate data record of passive microwave sea ice concentration. Version 2.- Natl. Snow Ice Data Center, Boulder, USA, doi:10.7265/N55M63M.1.

Myers, P.G. & Ribergaard, M.H. (2013): Warming of the Polar water layer in Disko Bay and potential impact on Jakobshavn Isbrae.- J. Phys. Oceanogr., 43: 2629-2640, doi:10.1175/JPO-D-12-051.1.

Parkinson, C.L. & Comiso, J.C. (2013): On the 2012 record low Arctic sea ice cover: Combined impact of preconditioning and an August storm.- Geophys. Res. Lett. 40: 1356-1361, doi:10.1002/grl.50349.

Peng, G., Meier, W., Scott, D. & Savoie, M. (2013): A long-term and reproducible passive microwave sea ice concentration data record for climate studies and monitoring.- Earth Syst. Sci. Data 5: 311-318, doi: 10.5194/essd-5-311-2013.

Rasmussen, T.A.S., Kliem, N. & Kaas, E. (2010): Modelling the sea ice in the Nares Strait.- Ocean Modelling 35: 161-172, doi:10.1016/j.ocemod.2010.07.003.

Ribergaard, M.H. (2014): Oceanographic investigations off West Greenland 2013.- NAFO Scientific Council Documents, 14/001.

Schweiger, A., Lindsay R., Zhang J., Steele M., Stern H. & Kwok, R. (2011): Uncertainty in modelled Arctic sea ice volume.- J. Geophys. Res. 116: C00D06, doi:10.1029/2011JC007084 (Updated to version 2.1).

Steele, M., Morley, R. & Ermold, W. (2001): PHC: A global ocean hydrography with a high quality Arctic Ocean.- J. Climate 14: 2079-2087 (Updated to PHC 3.0 in 2005).

Straneo, F. & Heimbach, P. (2013): North Atlantic warming and the retreat of Greenland's outlet glaciers.- Nature 504, 36-43, doi: 10.1038/nature12854.

Tilling, R.L., Ridout, A., Shepherd, A. & Wingham, D.J. (2015): Increased Arctic sea ice volume after anomalously low melting in 2013.- Nature Geosci. 8: 643-646, doi:10.1038/ngeo2489.

Zhang, J. & Rothrock, D.A. (2003): Modelling global sea ice with a thickness and enthalpy distribution model in generalized curvilinear coordinates.- Mon. Weath. Rev. 131: 681-697 (Updated data available from <http://psc.apl.washington.edu/zhang/IDAO/data_piomas.html>).

Zhang, J., Lindsay, R., Schweiger, A. & Steele, M. (2013): The impact of an intense summer cyclone on 2012 Arctic sea ice retreat.- Geophys. Res. Lett. 40: 720-726, doi:10.1002/grl.50190.

Polarforschung 85 (2), 107–115, 2015 (erschienen 2016)

Geodatabase and WebGIS Project for Long-Term Permafrost Monitoring at the Vaskiny Dachi Research Station, Yamal, Russia

by Yury Dvornikov[1,2*], Marina Leibman[1,3], Birgit Heim[2], Annett Bartsch[4,5,6], Antonie Haas[2], Artem Khomutov[1,3], Anatoly Gubarkov[7], Maria Mikhaylova[7], Damir Mullanurov[1], Barbara Widhalm[4,5], Tatiana Skorospekhova[8], and Irina Fedorova[8,9,10]

Abstract: The research station Vaskiny Dachi (VD) in central Yamal, Western Siberia was established in 1988. Continuous monitoring of the permafrost state is conducted since 25 years, which allows collecting a large amount of data related to permafrost state and environment of this region. To store and visualise the geospatial data, containing our knowledge of the research area and research topic, we created a geodatabase (GDB) to operatively process different types of geospatial data. The produced GDB contains so far 11 vector feature datasets and raster data in the same coordinate system. The vector data represent: 1) bathymetry; 2) social-economic objects; 3) field data; 4) geomorphology; 5) hydrography; 6) landscapes; 7) permafrost; 8) snow; 9) topography; 10) vegetation; 11) long-term measurement grids and transects (Circumpolar Active Layer Monitoring (CALM) transect, CALM measurement grid). All these feature datasets contain 60 feature classes of spatial data in total. Some of the geodata layers are directly linked to data bases of field data. The raster data contain 37 layers, including a digital elevation model with derivatives, a map of snow distribution for the key site, bathymetric maps and other maps of different scale. Moreover, the key area is a site for international research projects and the ongoing exchange of the data is supported by the VD GDB. Geographical Information System (GIS) allows collecting, storing and processing geospatial data from different sources in a wide range of types and formats. WebGIS platforms allow displaying the geospatial data for different users, giving the impression of the general processes on the certain geographic area. Also, we use the WebGIS service to publish the data and to make it available for the larger community. This paper is an overview on the permafrost studies at the VD research station, the GDB for permafrost monitoring as well as the established Yamal WebGIS project.

Zusammenfassung: Im Bereich der Forschungsstation Vaskiny Dachi (VD), in der zentralen Yamal-Region in West-Sibirien, werden seit 25 Jahren zahlreiche Messungen zur Überwachung des Zustande des Permafrost, der Vegetation, und der kryogenen Prozesse durchgeführt. Während dieser Zeit wurde eine große Menge verschiedener Informationen gesammelt, die strukturiert archiviert wurden. Für diese Aufgabe wurde eine spezielle Datenbank erstellt. Die Datenbank enthält sowohl Vektor- als auch Rasterdatensätze von Geoinformationen in einem einheitlichen Koordinatensystem. Insgesamt liegen 11 Vektordatensätze vor: 1) Bathymetrie, 2) soziale/wirtschaftliche Einrichtungen, 3) Geomorphologie, 4) Felddaten in Form von GPS-Koordinaten und Attribute, 5) Hydrographie, 6) Landschaften, 7) Permafrost, 8) Relief, 9) Schneedecke, 10) Vegetation, 11) lokale Daten (Transekte des Circumpolar Active Layer Monitoring (CALM). Diese Datensätze enthalten wiederum 60 Klassen von räumlichen Daten, wobei in einigen Fällen die Tabellen der Geodaten mit Daten von Geländemessungen verknüpft sind. Die Rasterdatensätze in der Datenbank umfassen ein Höhenmodell und verschiedene Derivate, die auf der Grundlage des Höhenmodells gemacht wurden, sowie die Verteilung der Schneedecke für Schlüsselbereiche und Rasterkarten verschiedener Maßstäbe. Des Weiteren enthält die Datenbank auch Aufnahmen von verschiedenen Fernerkundungs-Sensoren unterschiedlicher räumlicher Auflösung in einer einheitlichen Projektion. Die Struktur ermöglicht es, schnell verschiedene Daten zusammenzustellen und zu vergleichen, Untersuchungen von Abhängigkeiten zwischen Parametern durchzuführen und die Datenbank mit neuen Daten zu erweitern. Auch nutzen wir ein WebGIS, um die Geodaten zu publizieren und einem größerem Publikum zur Verfügung zu stellen. In dieser Veröffentlichung werden die Permafrostuntersuchungen, die darauf aufbauende Geodatenbank und das Yamal WebGIS Projekt in der VD Untersuchungsregion vorgestellt.

INTRODUCTION

The research station Vaskiny Dachi (VD) in central Yamal, West Siberia, Russia was established in 1988. Since then monitoring of permafrost-related and environmental parameters is on-going, which results in a large data collection related to permafrost state and environment of this region (Leibman et al. 2015). Management of the collected data is important and also needed for the exchange of the data within on-going international research projects.

The long-term permafrost monitoring site VD is run by the Earth Cryosphere Institute, Siberian Branch of Russian Academy of Sciences (Leibman et al. 2015) and an established site for the international Global Terrestrial Network for Permafrost (GTN-P) program (Biskaborn et al. 2015), including international CALM (Circumpolar Active Layer Monitoring, since 1993) (Brown et al. 2000) and TSP (Thermal State of Permafrost, since 2011) (Brown et al. 2010) programs. In 2007, VD became a part of the North Eurasian Transect within the Land Cover Land Use Change for Yamal Peninsula (LCLUC-Yamal) project with three more LCLUC-CALM grids and shallow boreholes established (Leibman et al. 2012). Since 2013 also the technogenic impact due to high impact of the Bovanenkovo gas field development on the tundra environment and on permafrost state is investigated (Khomutov & Khitun 2014). Permafrost and environmental monitoring is also part of the on-going Russian-Austrian COLD Yamal (COmbining remote sensing and field studies for assessment of Landform Dynamics and permafrost state on Yamal) project that focuses on radar remote sensing

doi:10.2312/polfor.2016.007

[1] Earth Cryosphere Institute Siberian Branch Russian Academy of Sciences, Malygina 86, 625000 Tyumen, Russia;
[*] Corresponding author: <ydvornikow@gmail.com>
[2] Alfred Wegener Institute Helmholtz Center for Polar and Marine Research, Telegrafenberg A43, 14473 Potsdam, Germany.
[3] University of Tyumen, Volodarskogo 6, 625003 Tyumen, Russia.
[4] Zentralanstalt für Meteorologie und Geodynamik ZAMG, Hohe Warte 38, 1190 Vienna, Austria.
[5] Austrian Polar Research Institute, Althanstrasse 14, 1090 Vienna, Austria.in
[6] Vienna University of Technology, Gusshausstrasse 27-29, 1040 Vienna, Austria.
[7] Tuymen Industrial University, Volodarskogo 38, 625000 Tyumen, Russia.
[8] Arctic and Antarctic Research Institute AARI, Beringa 38, 199397 St. Petersburg, Russia.
[9] Institute of Earth Science, Saint-Petersburg State University, 10th line of Vasiljevsky Island 33–35, 199178 Saint-Petersburg, Russia.
[10] Kazan Federal University, Kremlyovskaya 18, 420008 Kazan, Russia.
This paper was presented as a poster presentation at the International Conference "Our Climate – Our Future: Regional perspectives on a global challenge", 6–9 October 2014 in Berlin, Germany.
Manuscript received 22 June 2015; accepted in revised form 16 March 2016.

applications for thermokarst lakes and permafrost landscape dynamics in Yamal. In 2011 first tentative water sampling for organic matter concentration in thermokarst lakes started and transformed to an ongoing Russian-German research project, POLYAR (Process of Organic matter transport to the Lakes of Yamal Region, DVORNIKOV et al., 2014). The main purpose of this project is to extract the environmental characteristics of lake catchments and the geochemistry of lake water bodies in Central Yamal. Geographical information systems are a useful tool for management of geodata, i.e. data with an assigned geo-referencing. Existing geodatabases in geocryology aim to collect and store historical data and ongoing monitoring data (e.g., Global Terrestrial Network for Permafrost (GTNP), BISKABORN et al. 2015), collect knowledge on permafrost (ROMANOVSKII & LEIBMAN 1994) as well as saving old data gathered before the "digital revolution" (e.g., CAPS, INTERNATIONAL PERMAFROST ASSOCIATION 2003). The requirements for the creation of a geodatabase in geocryology may differ in terms of its object basis (MELNIKOV & MINKIN 1998, MINKIN et al. 2001). For the geodata of the VD region we collected all available geospatial data in the GeoDataBase (GDB), undertook GIS-oriented modelling and mapping, to analyse the linkages in the "permafrost dynamics – landscape change" system.

Note that acronyms of projects and associated websites are listed in Table 7 at the end of this paper.

STUDY AREA

The Vaskiny Dachi (VD) research region is located in the western Siberian Arctic (Fig. 1). The area belongs to the continuous permafrost zone with thickness down to 500 m and is characterised by a wide distribution of tabular ground ice (LEIBMAN 1996, KHOMUTOV et al. 2012). The presence of tabular ground ice in connection with active layer dynamics is responsible for the cryogenic landsliding and thermal denudation in this area (LEIBMAN & KIZYAKOV 2007). In 2012, a considerable activation of thermal denudation was observed in the VD region (LEIBMAN et al. 2015) due to an extremely warm summer accompanied by active layer deepening. At least six wide exposures along the lake shore line of thermokarst lakes were documented during 2012 and 2013 field expeditions.

DATA AND METHODS

Several datatypes are used to collect the geospatial data including:

(i) *in-situ* field observations and measurements (active layer on 4 established grids and at additional sites, ground temperature-depth profiles in 11 boreholes, geodetic measurements for the cryogenic landslide monitoring, and ground control points (GCP) collection for satellite-image geometric correction, bathymetry surveys, description of exposures, snow survey (snow depth and snow depth measurements);

(ii) geochemical and geo-optical data from lakes, soils and ground ice (results obtained in the laboratory and linked to a specific sampling point which includes ground ice samples, water samples from thermokarst lakes, soil samples);

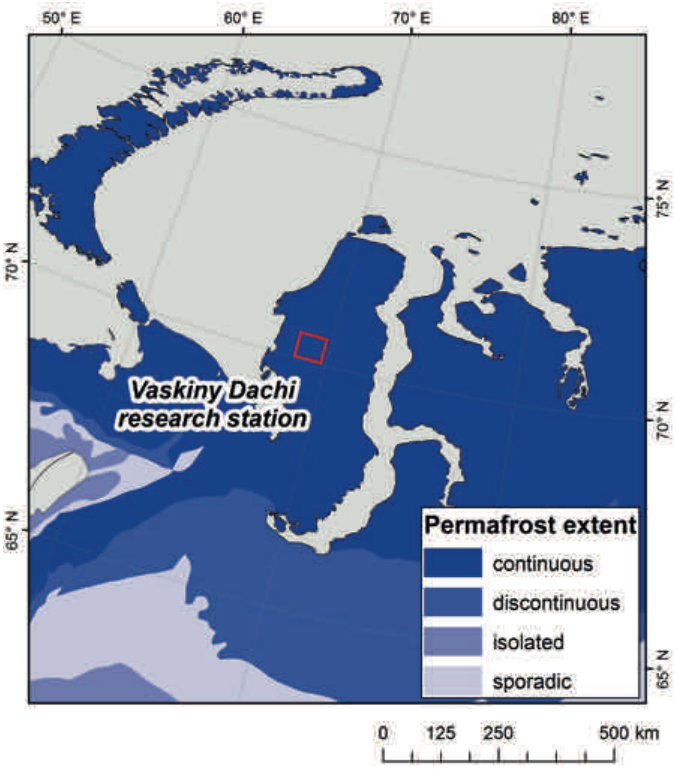

Fig. 1: Location of the region Vaskiny Dachi (VD) in central Yamal, Western Siberia. Background: Map of the permafrost extent (BROWN et al. 1998).

Abb. 1: Geographische Lage der Region Vaskiny Dachi (VD) in Zentral-Jamal, West Sibirien. Hintergrund: Karte der Permafrostausdehnung (BROWN et al. 1998).

(iii) data extracted from satellite images and aerial photographs taken in different years as well as data extracted from digital elevation models (DEM) (vegetation classes, landscape map, maps of the manifestation of cryogenic processes, maps of technogenic impact on the tundra (KHOMUTOV & KHITUN 2014), map of environmental hazards);

(iv) GIS-modelled data (snow water equivalent (SWE) map, DVORNIKOV et al. 2015). The sources of data for the GDB are presented in Table 1.

Field data collection

CALM and TSP data

Active layer depth is measured by a metal probe according to the CALM protocol within four grids. Such a grid is fundamental for the study of spatial and temporal variations of active layer depth and vegetation patterns. These include lithological and cryogenic controls and surface cover controls for spatial distribution. Temporal variations are controlled by climate fluctuations which are mediated by topography, lithology and surface covers (LEIBMAN 1998).

The VD CALM grid was established in 1993 on the top and slope of a highly dissected alluvial-lacustrine-marine plain, affected by landslides, with sandy to clayey soils. Within the LCLUC program "Greening Of the Arctic" (GOA) other three grids were established in 2007 in typical conditions of

1. Field data					
Type		**Number of sites**	**Number of points/units**	**Year**	**Equipment**
ALD (Active Layer Depth) **measurements**		1 (CALM)	121	1993-	
		3 (LCLUC)	165	2007-	
Boreholes			12	2006-	HOBO
Tachymetry		3	2246	2011	TopCon© GTS-235
DGPS measurements	**Static**		7	2014	Trimble© GNSS 5700
	Kinematic		199	2014	
Bathymetry		20	>25000	2012, 2014, 2015	Humminbird© 788cxi, points tracked with 5 seconds interval
Snow survey		3	233	2013	Metal ruler, snow sampler VS-43
Water samples		29	>100	2011-2015	
2. Remote sensing data / Digital maps					
Optical data	VHR			2009	GeoEye-1 (MS)
				2010	QuickBird (Pan, MS)
				2013	GeoEye-1, WorldView-2 (Pan, MS)
	HR			2015	SPOT-5 (MS)
Radar data				2008	TerraSAR-X, ALOS PALSAR
				2010	TerraSAR-X
				2014	Terrasar-X, TanDEM-X
DEM digital elevation model				2014	TanDEM-X IDEM 12 m
Topographic maps			2	1987	1:50000
3. Laboratory data					
CDOM coloured dissolved organic matter				2011-2015	Specord 200 (Jena Analytic©)
DOC dissolved organic carbon				2015	TOC-V-CPH Shimadzu©
SPM suspended particulate matter				2014-2015	0.45 µm CA filters
MI major ions				2014-2015	Ion Chromatography

Tab. 1: List of data sources for Vaskiny Dachi GDB. ALD: active layer depth; DEM: digital elevation model; CDOM: coloured dissolved organic matter, DOC: Dissolved organic carbon, SPM: suspended particulate matter, MI: major ions.

Tab. 1: Liste der Datenquelle für Vaskiny Dachi GDB. ALD: Tiefe der Auftauschicht; DEM: Digitales Höhenmodell; CDOM: Gelbstoff, DOC: gelöster organischer Kohlenstoff, SPM: Schwebstoff, MI: Hauptionen.

IVth Coastal-marine plain (VD-1), IIIrd Alluvial-marine plain (VD-2) and IInd River terrace of Mordyakha river (VD-3). Each 50 × 50 m measurement grid covers a homogeneous terrain.

Boreholes are equipped under the CALM and TSP Programs (Tab. 2) with HOBO data loggers. The depth of boreholes ranges from 0.8 m up to 10 m. Ground temperature was first measured to the depth of 10 m in 1993 in a borehole "LGT", which was drilled in 1988. This borehole was re-established in 2010 to the depth of only 7 m. Borehole "191-m" was drilled next to the CALM grid in 1990 to the depth 10 m and ground temperature was measured by mercury thermometers in summer only till 1996. In 2011, the borehole was replicated (new ID: "VD CALM_10") in the same place and equipped with HOBO data loggers. Ground temperature measurements in the shallow boreholes were used to understand the process of freeze back in various landscape conditions (Leibman et al. 2015).

Bathymetry

The depth of 19 lakes was measured during 2012, 2014 and 2015 field expeditions (Tab. 3). Chartplotter Humminbird 788 cxi with internal GPS was used to collect both distances between sonar and lake bottom and position coordinates. The readings were taken along several profiles for each lake and then were filtered with 5 seconds and converted to ASCII format. Bathymetric maps were produced by interpolation.

Snow measurements

Snow survey in the study area has been carried out in March 2013. Snow depth was measured by digging a snow pit and measuring the snow layer using a metal ruler. Samples for snow density were taken with the snow sampler VS-43 designed for snow density measurements during snow surveys (Slabovich 1985). The measurements are described in detail in Dvornikov et al. (2015).

Water sampling

Water samples from lakes were collected within the POLYAR research project in order to study a number of hydrochemical parameters of the lake water: coloured dissolved organic matter (CDOM) (Dvornikov et al. 2016), dissolved organic carbon

	Site ID	X	Y	N points	established
CALM	CALM grid	68.9072	70.2836	121	1993
	VD-1 (GOA)	68.8916	70.2755	55	2007
	VD-2 (GOA)	68.8835	70.2955	55	2007
	VD-3 (GOA)	68.8413	70.3014	55	2007
TSP	**Borehole ID**			**Max depth (cm)**	**Logger installed**
	VD 1 (GOA)	68.8916	70.2755	90	27-08-2007
	VD 2 (GOA)	68.8835	70.2955	100	27-08-2007
	VD 3 (GOA)	68.8413	70.3014	100	29-08-2007
	VD CALM	68.9072	70.2836	150	25-08-2006
	VD AG19/3	68.9091	70.2826	150	29-08-2007
	VD LGT	68.8916	70.2811	700	13-09-2010
	VD CALM_10m	68.8913	70.2811	1000	25-08-2011
	VD AGG1	68.9294	70.2943	100	20-08-2011
	VD AGG2	68.9300	70.2929	80	20-08-2011
	VD Gully	68.9271	70.2912	170	03-09-2012
	VD landslide	68.9238	70.2796	140	26-08-2013
	VD Gully_2	68.9271	70.2912	200	24-08-2014

Tab. 2: List of sites for ALD (Active Layer Depth) measurements and boreholes within CALM and TSP projects. GOA: Greening of the Arctic project.

Tab. 2: Liste der Standorte von der Tiefe der Auftauschicht (ALD) sowie der Bohrlöcher von CALM und TSP-Projekten, GOA: Greening of the Arctic project.

Lake_ID	Year	Area (ha)	Y	X	N points recorded
LK-001	2012	38.30	68.8829	70.2787	790
LK-002	2012	3.26	68.9045	70.2977	448
LK-003	2012	107.72	69.0019	70.2898	1652
LK-004	2012	74.96	68.9705	70.2809	2167
LK-006	2012	3.55	68.8991	70.2878	655
LK-007	2012	38.77	68.9912	70.2672	1000
LK-010	2012	4.75	68.8642	70.3012	412
LK-012	2012	2.24	68.9216	70.2825	473
LK-013	2012	212.46	68.8843	70.2563	1156
LK-014	2015	6.55	68.8736	70.2836	1121
LK-015	2015	8.58	68.9218	70.2651	2313
LK-016	2015	10.25	68.9335	70.2668	1472
LK-017	2015	6.37	69.0221	70.2326	1195
LK-018	2015	11.79	69.0061	70.2319	1782
LK-019	2015	13.60	68.9951	70.2301	2553
LK-035	2014	66.53	68.8738	70.2155	5254
LK-037	2014	2.02	68.9938	70.2498	549
LK-038	2014	3.84	68.9974	70.2448	925
LK-039	2014	2.69	69.0024	70.2494	928

Tab. 3: List of lakes in which bathymetry survey was conducted.

Tab. 3: Liste der Seen, in denen bathymetrische Messungen ausgeführt wurden.

(DOC), suspended matter (SPM), major ions (MI) (Tab. 4). Samples were collected in calm weather conditions (to avoid mixing effects) from upper 30 cm of water column close to the shore or in the centre of lakes from boat in August-September of the 2011–2015 field expeditions. Criteria for selecting the lakes were the difference in the visual (water colour in the satellite images in "true colour" RGB composite) as well as morphometric properties of coastal area (presence of high cliffs, thermal denudation or cryogenic landslides).

Remote sensing and GIS data processing

Optical satellite sensor data and synthetic aperture radar (SAR) satellite data are used to extract additional parameters. High-spatial resolution optical satellite data were used to analyse the vegetation as well as to detect activation of cryogenic processes. Time series of TerraSAR-X data are used to extract water bodies and to assess the seasonality of the thermokarst lakes (Bartsch et al. 2012, Trofaier et al. 2013). TanDEM-X digital elevation model (DEM) was used to delineate lake catchments, for topography analysis as well as to model snow distribution in the study area.

Optical satellite data processing

The optical satellite images from high-spatial resolution sensors (GeoEye-1, QuickBird, WorldView-2) obtained from Digital Globe Foundation© (DGF) in both, very high spatial resolution panchromatic (0.5–0.6 m) and lower spatial resolution multispectral (2.0–2.4 m) bands. All the acquisitions have been taken in the summer season: QuickBird on 2010-07-30, GeoEye-1 on 2013-07-05, WorldView-2 on 2013-07-21 (Tab. 5). Pan-sharpened images for all three acquisitions were obtained, applying PANSHARP2 fusion algorithm developed by Zhang (2004) with the PCI Geomatica 2014 software (PCI Geomatics©), where the multispectral and panchromatic bands were merged to obtain the high spatial resolution together with multispectral information in one image. The pan-sharpened very high resolution images were used to manually digitise streams, areas covered by shrubs and other visual analysis, but not for the spectral processing. The ortho-rectification procedure was performed within the OrthoEngine module in PCI Geomatica. The TanDEM-X IDEM (Tab. 5) was used to correct the images for relief distortions. ATCOR (Richter 1996) ground reflectance atmospheric correction module was used to correct the image data within PCI Geomatica software.

Multispectral processing is the base for the extraction of vegetation distribution based on vegetation indices. To calculate the vegetation indices, water masking, using a near infrared

Year	CDOM	DOC	SPM	MI
2011	11	–	–	–
2012	7	–	–	–
2013	13	–	–	–
2014	21	–	16	21
2015	24	24	24	24
Total	76	24	40	45

Tab. 4: Overview on the lake sampling in 2011 to 2015. CDOM: coloured dissolved organic matter; DOC: dissolved organic carbon; SPM: suspended particulate matter; MI: major ions.

Tab. 4: Überblick über die Wasserbeprobungen von 2011 bis 2015. CDOM: Gelbstoff, DOC: gelöster organischer Kohlenstoff, SPM: Schwebstoff, MI: Hauptionen.

	Sensor/ [bands]	Type*	Acquired	Source	Spatial resolution (m)
Optical data	GeoEye-1/ [4]	PS	2009-08-15	NASA NGA License UAF	0.5
	–	MS	2013-07-05	DGF**	2
		PS			0.5
	QuickBird/ [4]	MS	2010-07-30	–	2.4
		PS			0.6
	WorldView-2/ [8]	MS	2013-07-21	–	2
		PS			0.5
Radar data	TerraSAR-X/[1]		2008-07-11, 2008-09-15	DLR PI agreement LAN1706	2.5
	–		2010-07-29, 2010-08-31	–	–
	–		2014-07-04, 2014-08-10	–	2
	ALOS Palsar/ [1]		2008-08-14 2008-09-29	JAXA PI agreement 90 and 1200	16
DEM	TanDEM-X		2013-06-19	DLR PI agreement LAN1706	12

Tab. 5: List of remote sensing data. *different types of data used; MS: multispectral; PS: pan-sharpened (PANSHARP2 model, ZHANG 2004); DGF**: Digital Globe Foundation.

Tab. 5: Liste der Fernerkundungsdaten. *verschiedene Datentypen wurden genutzt; MS: multispectral, PS: pan-sharpened (PANSHARP2 Modell, ZHANG 2004); DGF**: Digital Globe Foundation.

(NIR) band threshold, was performed for the further spatial analysis. NDVI index (KRIEGLER et al. 1969), which describes the abundance and "greenness" of vegetation, is calculated using the following equation:

$$NDVI = \frac{NIR - R}{NIR + R}$$

where NIR and R are the reflectance values in near infrared and red bands, respectively.

The relative chlorophyll absorption vegetation index CHL is calculated as follows:

$$CHL = \frac{G + NIR}{2} - R$$

where G is the reflectance value in green band.

Radar satellite data processing

TerraSAR-X time series and the TanDEM-X DEM with 12 m resolution have been available via DLR PI agreement LAN1706. The time series of water-body extents make it possible to investigate the seasonal area change of thermokarst lakes (e.g., TROFAIER et al. 2013).

The TerraSAR-X data was derived as Level 1B SSC (Single-Look Slant Range Complex) Data with HH polarization. For data processing, the open source software NEST (Next ESA SAR Toolbox) was used. The data were multilooked and terrain corrected using Range Doppler Terrain Correction and the DEM product of TanDEM-X (12 m spatial resolution). The output pixel spacing was set to 2 m, resembling the source ground range pixel spacing and projected into UTM Zone 42, WGS-1984. Radiometric normalisation was applied and the resulting Sigma0 band was transferred to dB using the Software IDL. Water bodies were extracted by using a threshold method. Due to specular radar reflection on open water bodies, the resulting lower backscatter values can be used to differentiate between land and open water bodies.

ALOS PALSAR data have been available via JAXA PI agreement 90 and 1200 and were used to extract shrub contours for the study area. The data Level 1.1 HV data of two dates (14th Aug. and 29 Sep. 2008) were processed within NEST. The multilooked images were ellipsoid corrected using the Geolocation-Grid method. The resulting intensity images were multiplied by a factor of 10^{12} and converted into dB. The mean of the two dates was calculated and gamma filtered. To extract the shrub layer a threshold of -25 dB was used.

TanDEM-X IDEM was used to extract catchment polygons, for terrain analysis and as a source of relief derivatives for snow redistribution modelling. Delineation of the lake catchments requires the high quality DEM. To improve the model, the raster image is converted to the point data model and re-interpolated with interpolation method in ArcGIS 10.2.2. (ESRI Inc©). After interpolation procedure the DEM is levelled, i.e., the extracted lake polygons from TerraSAR-X 2014.08.10 are used as vector polygons for assigning the specific elevation to the lake areas. Extreme sinks are filled using ArcHydro module. The optimized DEM is used to calculate the flow direction raster model in ArcHydro (DJOKIC et al. 2011) and then for catchment delineation. All automatically calculated catchment areas are manually corrected for the outflows from the lakes.

DEM derivatives are curvature, aspect and slope. These parameters have been used as an input data for snow modelling together with field data and the shrub layer derived from ALOS Palsar data.

VD GDB database

The established GDB for the VD region enables the data management of all the different data sets: from the long-term GTN-P (CALM) program and all the vector and raster data produced within the POLYAR project.

Geodetic measurements (DGPS and tachymetry) in the area as well as the geocoded very high resolution images provide the high accuracy of the spatial location of the data. Geospatial data in the GDB is presented in two different data models: vector and raster. The vector data in GDB is divided into several feature classes, according to specific geographic objects (e.g., topography, vegetation, permafrost, hydrography etc.). Each feature dataset is filled with a number of feature classes (points, polylines and polygons). The data of similar types are linked to each other using unique object ID.

WebGIS application

WebGIS is a useful tool for visualising and analysing the geodata of different sources and types. For a WebGIS application GIS is compiled on a server and transferred to the user web-browser in interactive web viewers. Users can perform their own GIS visualization. The Alfred Wegener Institute, Helmholtz Centre for Polar- and Marine Research (AWI) offers a WebGIS service, an application based on JavaScript. The WebGIS core components are ArcGIS for Server 10.3 and PostgreSQL databases 9.3.1 including Spatial Database Engine (SDE). The AWI WebGIS server has been used for publishing selected GIS data layers of the Vaksiny Dachi GDB as the Yamal WebGIS Project. The selected GIS data are layers, reflecting the general state of the ongoing research in the station such as lake catchments, water sampling points, active layer grids, river network, DEM raster, snow map raster etc.

RESULTS

Vaskiny Dachi Geodatabase

The compiled GDB contains 11 vector feature datasets and raster data in the WGS-84 coordinate system, projection UTM Zone 42 North. The vector data represents: 1) bathymetry; 2) social-economic objects; 3) field data; 4) geomorphology; 5) hydrography; 6) landscapes; 7) permafrost; 8) snow; 9) topography; 10) vegetation; 11) long-term measurement grids and transects (CALM transect, CALM measurement grid). All the feature datasets contain 60 feature classes of spatial data in total (Tab. 6).

Bathymetry feature dataset contains measured depths in 19 lakes (Tab. 3) as well as GIS-derived isobaths. Social-economic objects feature dataset contains only polylines characterising the off-road tracks classified according to its impact on the landscape (low, medium, high) (KHOMUTOV & KHITUN 2014). The tracks are derived from the satellite images and aerial photographs (Tab. 5). Field data feature dataset contains the points of the field monitoring sites as well as the location of samples with the laboratory measured parameters as a supplementary information in the attribute table. Geomorphology feature dataset represents polygons of different geomorphic levels obtained from DEM and topographic maps (Tab. 5). In addition, this feature dataset contains lake-catchment polygons extracted from the TanDEM-X IDEM with the large amount of supplementary information (volume of snow in form of SWE, high shrubs percentage, occurrence of cryogenic processes etc.). Each catchment polygon is linked to a specific lake polygon, using the unique object ID.

Feature datasets	Number of feature classes	Number of points	Number of polylines	Number of polygons
Bathymetry	2	61851	261	–
Social-economic objects	2	–	170	–
Field data	6	459	–	–
Geomorphology	9	–	–	761
Hydrography	9	–	360	415
Landscapes	1	–	–	47
Permafrost	9	120	–	711
Snow	5	99	–	–
Topography	10	88	673	7
Vegetation	3	–	–	16143
Local data	4	2683	–	–
Total	60	65300	1464	18084

Tab. 6: Geospatial feature datasets in the Vaskiny Dachi GDB.

Tab. 6: Räumliche Datensätze in der Vaskiny Dachi GDB.

Hydrography – digitalized thermokarst lake polygons with the large attributive information including the transferred laboratory data (CDOM, IC, SPM, DOC; DVORNIKOV et al. 2016), seasonal area change derived from the TerraSAR-X time series etc. Landscapes feature dataset contains only one polygonal feature class representing the landscape map for the research station (KHOMUTOV & LEIBMAN 2014).

Permafrost - large dataset containing the location of boreholes with a certain attributes (depth, temperature values), remote sensing derived map of the cryogenic processes, location and characteristics of observed thermocirques. Snow feature dataset represents the *in-situ* measured snow depth in snow density points and the interaction with topography and vegetation parameters. Topography feature dataset contains the results of the tacheometry survey of the area.

Vegetation – mostly remote sensing derived contours of different vegetation classes (e.g., shrubs and sedges). Local data – CALM grid and GOA grids with a multiyear ALD measurements as well as a transect data. In total, about 80000 geometry objects in vector format are in the GDB (Tab. 6). Most of the objects are *in-situ* measured depths of thermokarst lakes and vegetation contours. The specific geospatial basis of all the data allows work with the data very fast, obtaining various geographic information and geographic interaction between objects, providing the local-scale permafrost modelling. One successful application of the GIS-based local scale modelling of SWE in the research station has been already carried out in DVORNIKOV et al. (2015).

Raster data in the VD GDB contains: DEM and different derivatives, SWE map, bathymetric maps of several lakes, raster maps of different map scales, aerial photographs, corrected and processed satellite images (Tab. 5). The raster data are often the base for the extraction of vector objects in the GDB (e.g., vector data from vegetation, topography, hydrography). The general structure of the VD GDB (Fig. 2) is very evolving and the new data is monthly uploaded. The spatial data analysis leads to creation of new feature classes and new attribute rows.

Yamal WebGIS

The majority of created geodata was published as the Yamal WebGIS service, which serves as a tool for the data visualization (Fig. 3). WebGIS is not a flexible tool for external users in terms of data processing but it provides a visualisation of topographic and environmental variables. The WebGIS enables visualisation on which lakes have in- and outlets, where landslides and wind-blown sandy areas are in catchments, or on what is the spatial distribution of shrubs.

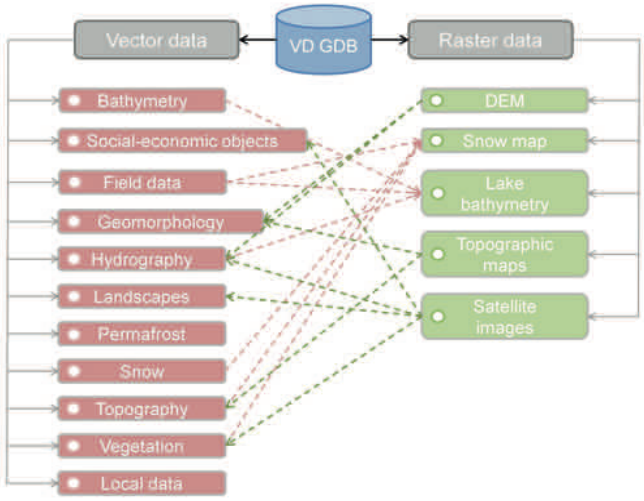

Fig. 2: Schematic structure of data layers of the Vaskiny Dachi (VD) database GDB).

Abb. 2: Schematische Struktur der Daten in der Vaskiny Dachi (VD) Datenbasis (GDB).

The Yamal WebGIS project is available and keeps the data structure form of the GDB also in the published WebGIS data sets (Fig. 4).

DISCUSSION

The created Vaskiny Dachi (VD) Geodatabase (GDB) is aimed to support the analyses of processes on this type of high-latitude tundra permafrost landscape. The GDB is adapted to fast data accumulation, processing and obtaining higher level geospatial products (e.g., SWE map, lake catchments, land cover map etc.), including spatial and temporal GIS-based modelling. The structure of GDB allows collecting the data from different sources, most of which are *in-situ* measured field parameters and remote sensing derived data. Field data is a main source for the GDB and, furthermore, is the ground truth data for validation of remote sensing products (Fig. 4). Ground truth validated environmental parameters derived from remote sensing data might be used for data extrapo -lation on the larger areas, enabling to produce new GIS layers and digital maps (Fig. 4). Both, *in-situ* measured and remote sensing data are suitable for GIS or spatial statistic based modelling. This combination is very important for the permafrost area, because the modelling of underground permafrost parameters such as ground temperature or active layer depth on the local or regional scale can only be done using landscape-based approach (e.g., STRELETSKIY et al. 2012).

Nowadays, existing databases for permafrost monitoring are predominantly oriented on global scale. For example: CAPS, which contains the information about several permafrost characteristics and supporting metadata (INTERNATIONAL PERMAFROST ASSOCIATION 2003). Another service is GTNP, collecting and disseminating the data on two major permafrost variables (ALT and permafrost temperature). National geocryological databases also exist (e.g., MINKIN et al. 2001). Many local-scale geodatabases are developed by various research groups on different objects and areas, because they significantly support the research process, providing interlinkages between environmental parameters and variables. It also

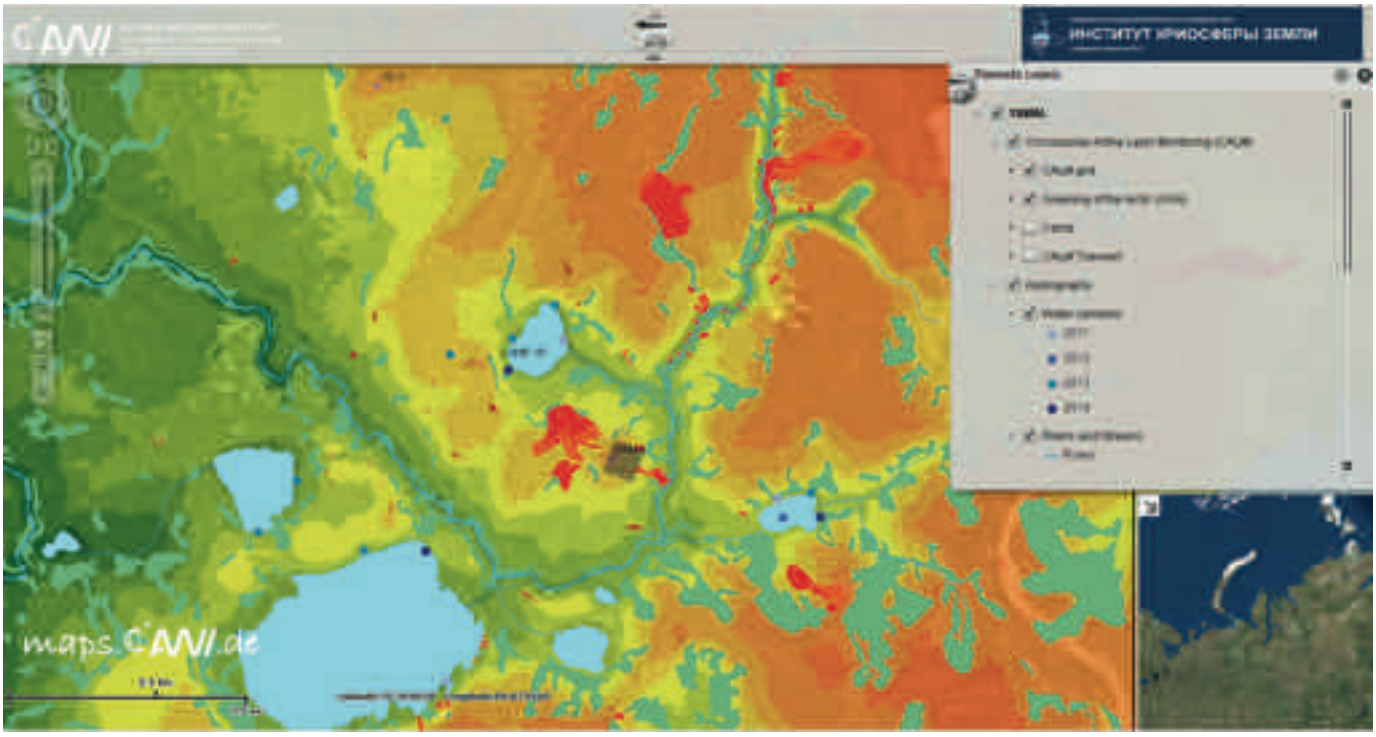

Fig. 3: Visualisation of the Vaskiny Dachi (VD) WebGIS <http://maps.awi.de/yamal/>. User-oriented interface allows to analyse the geodata. Thematic layers include field sampling points, raster surfaces and vector datasets.

Abb. 3: Visualisierung von Vaskiny Dachi (VD) WebGIS <http://maps.awi.de/yamal/>. Die benutzerorientierte Oberfläche erlaubt es, die Geodaten zu analysieren. Thematische Daten umfassen Beprobungspunkte, Rasterdaten und Vektordatensaten.

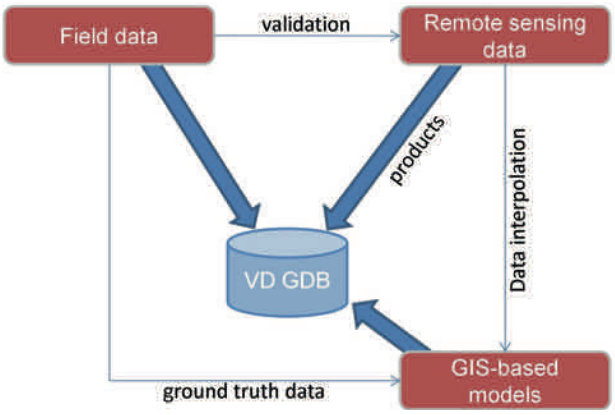

Fig. 4: Structure of data sources for the geodatabase (GDB) and its interconnection.

Abb. 4: Struktur von Datenquellen der Geodatenbasis (GDB) und deren Verbindung untereinander.

allows distributing the data within the research group members (joint research projects, international projects, PhD and master projects). The developed structure of the GDB allows fast extracting specific feature classes when it is considered as "completed" and publishing the data through world data centres such as PANGAEA. The international permafrost research covers different aspects (permafrost parameters, hydrology, geobotany, geomorphology etc.) and to establish a GDB is a very useful instrument to combine and process the knowledge of these different environmental parameters.

Both, desktop GIS and WebGIS enable visualisation. Related to the POLYAR project we visualise the location of the water sampling data related to the catchments size and properties. The Desktop GIS for example enables the combination from raster data such as the NIR band from a coarser scale resolution Landsat to optimally show the water bodies overlain by half-transparent color-coded DEM.

This raster dataset combination can be overlain by vector data of sampling points and lake catchments (Fig. 3). This combination or other possible combinations (e.g., snow depth map, vegetation indices distribution), supports the understanding of the results of the field data (different concentrations of CDOM, SPM, hydrochemistry in the lakes), and can guide the further statistical analyses. It is also possible to undertake area-based calculations to statistically derive the relationships from the range of catchment properties towards the geochemical composition in the Yamal lakes.

WebGIS is publicly available on the AWI Maps server, enabling users without technical GIS expertise to get an impression of the potential driving factors. Using the WebGIS visualisation, e.g., immediate interpretation is possible: *Which lakes have in- and outlets? Where are landslides and wind-blown sandy areas in catchments? What is the spatial distribution of shrubs?* The geomorphic spatial context is given with the GIS layer of the geomorphic terraces and the DEM (Fig. 5). The Yamal WebGIS is a very useful communication tool for the exchange between the international project partners and for the presentation of the VD study site. Recently, the developed regional scale geodatabase and WebGIS project were shown as a very useful tool for supporting big research

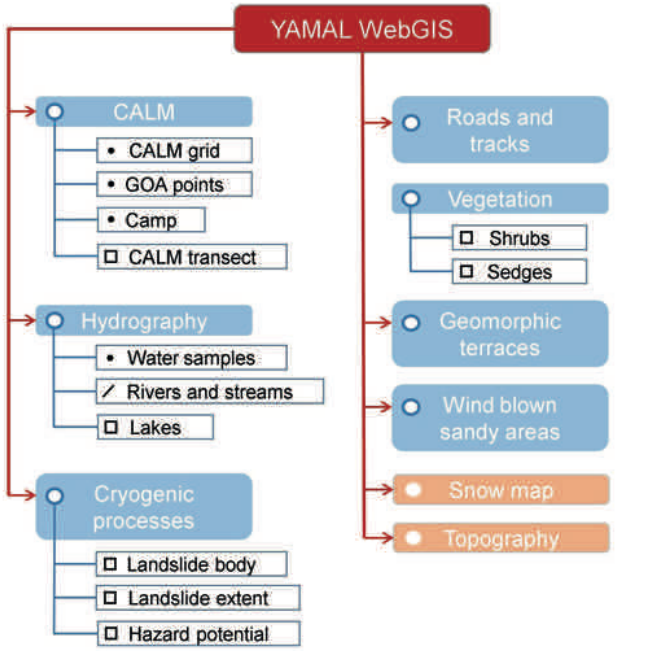

Fig. 5: Structure of the Yamal WebGIS (blue coloured boxes: vector data; orange coloured boxes: raster data).

Abb. 5: Struktur von Jamal WebGIS (blau gefärbte Felder: Vektordaten; orange gefärbte Felder: Rasterdaten).

projects, e.g., CONTINENT on Lake Baikal, and helped for obtaining new data using the existing open source datasets as well as data collected in the field (HEIM et al. 2008).

SUMMARY

1) The VD GDB contains 11 vector feature datasets with more than 80000 geometry objects as well as a raster data enriched with metadata. The GDB is the base for the Yamal WebGIS published on the AWI Maps platform.
2) Field data are a main source for the GDB and is supporting the interpretation and generation of remote sensing products and GIS-based modelling.
3) Ground truth validated environmental parameters derived from remote sensing data might be used for data extrapolation on the larger areas, enabling to produce new GIS layers and digital maps.
4) Both, *in-situ* measured and remote sensing data are suitable for GIS or spatial statistic based modelling.
5) The Yamal WebGIS visualizes the study region, studied objects, and *in-situ* monitoring and sampling for a larger community. Within the POLYAR project the Yamal WebGIS visualises the lakes and lake catchments and the sampling effort of the recent years, being a useful platform to support joint international projects.

ACKNOWLEDGMENTS

This research was conducted within the framework of the Program of Fundamental Research Department of Earth Sciences No. 12 "The processes in the atmosphere and cryosphere as factors of environment changes", the RFBR grant 13-05-91001-ANF_a, Presidential grant for scientific schools

No. 5582.2012.5 and 3929.2014.5, Russian Science Foundation Grant 16-17-10203, as well as International projects CALM and TSP. Authors would like to thank the German Academic Exchange Service (DAAD), Otto Schmidt Laboratory for Polar and Marine Research (OSL) and Helmholtz graduate school for Polar and Marine Research (POLMAR) for financial support; Digital Globe Foundation and German Aerospace Center (DLR) for providing satellite images. Authors also would like to thank two anonymous reviewers and the editor of this issue for provided comments to this manuscript.

References

Bartsch, A., Trofaier, A.M., Hayman, G., Sabel, D., Schlaffer, S., Clark, D.B. & Blyth, E. (2012): Detection of open water dynamics with ENVISAT ASAR in support of land surface modelling at high latitudes.- Biogeosci. 9: 703-714. doi: 10.5194/bg-9-703-2012.

Biskaborn, B.K., Lanckman, J.-P., Lantuit, H., Elger, K., Streletskiy, D.A., Cable, W.L. & Romanovsky, V.E. (2015): The new database of the Global Terrestrial Network for Permafrost (GTN-P).- Earth Syst. Sci. Data 7: 245-259, doi: 10.5194/essd-7-245-2015.

Brown, J., Ferrians, Jr., O.J., Heginbottom, J.A. & Melnikov, E.S. (1998, revised February 2001): Circum-arctic map of permafrost and ground ice conditions.- Boulder, CO, National Snow and Ice Data Center, Digital media <http://nsidc.org/data/docs/fgdc/ggd318_map_circumarctic/>.

Brown, J., Hinkel, K.M. & Nelson, F.E. (2000): The circumpolar active layer monitoring (CALM) program: Research designs and initial results.- Polar Geogr. 24: 166-258, doi: 10.1080/10889370009377698.

Brown, J., Kholodov, A., Romanovsky, V., Yoshikawa, K., Smith, S.L., Christiansen, H.H., Vieira, G. & Noetzli, J. (2010): The thermal state of permafrost: the IPY-IPA snapshot (2007-2009).- Proc. 63rd Canadian Geotechnical Conference & 6th Canadian Permafrost Conference Geo 2010, Calgary, Canada, 12-16 Sept. 2010.

Djokic, D., Ye, Z. & Dartiguenave, C. (2011): Arc hydro tools overview.- Redland, Canada, ESRI, 1-189.

Dvornikov, Y., Bartsch, A., Khomutov, A., Heim, B., Widhalm, B., Fedorova, I., Leibman, M., Mikhaylova, M. & Skorospekhova, T. (2014): Process of organic transport in lakes of the Yamal region (POLYAR).- Proc. of Arctic Change Conference 2014, Ottawa, Canada, 6-12 December 2014.

Dvornikov, Y., Khomutov, A., Mullanurov, D., Ermokhina, K., Gubarkov, A. & Leibman, M. (2015): GIS and field data based modelling of snow water equivalent in shrub tundra.- Fennia 193: 53-65.

Dvornikov, Y., Heim, B., Roessler, S., Leibman, M., Khomutov, A. & Bartsch, A. (2016): Colored dissolved organic matter (CDOM) absorption measurements in the Vaskiny Dachu region, Central Yamal, Russia.- Inst. Earth Cryosphere Siberian Branch Russian Acad. Sci. Tuymen, doi: 10.1594/PANGAEA.860049

IPA (2003): International Permafrost Association Standing Committee on Data Information and Communication, Circumpolar Active-Layer Permafrost System (CAPS), Vers. 1. Boulder, Colorado USA: National Snow and Ice Data Center, doi: http://dx.doi.org/10.7265/N5SF2T3B

Heim, B., Klump, J., Oberhänsli, H. & Fagel, N. (2008): Assembly and concept of a web-based GIS within the paleolimnological project CONTINENT (Lake Baikal, Russia).- J. Paleolimnol. 39: 567-584, doi: 10.1007/s10933-007-9131-0.

Khomutov, A.V. & Khitun, O.V. (2014): The dynamics of vegetation cover and the depth of seasonal thawing in the typical tundra of Central Yamal under technogenic impact.- Tyumen State University Herald 4: 17-27 [In Russian].

Khomutov, A.V. & Leibman, M.O. (2014): Assessment of landslide hazards in a typical tundra of Central Yamal, Russia.- In: W. SHAN et al. (eds): Landslides in Cold Regions in the Context of Climate Change, Springer International Publishing, 271-290, doi: 10.1007/978-3-319-00867-7_20.

Khomutov, A.V., Leibman, M.O. & Andreeva, M.V. (2012): Mapping of ground ice in Central Yamal.- Tyumen State University Herald 7: 68-76 [In Russian].

Kriegler, F.J., Malila, W.A., Nalepka, R.F. & Richardson, W. (1969): Preprocessing transformations and their effects on multispectral recognition.- Proc. 6th Internat. Sympos. Remote Sensing of Environment 97-131.

Leibman, M.O. (1996): Results of chemical testing for various types of water and ice, Yamal Peninsula, Russia.- Permafrost Periglacial Processes. 7: 287-296, doi: http://dx.doi.org/10.1002%2f(SICI)1099-1530(199609)7%3a3%3c287%3a%3aAID-PPP224%3e3.0.CO%3b2-A.

Leibman M.O. (1998): Active layer depth measurements in marine saline clayey deposits of Yamal Peninsula, Russia: Procedure and interpretation of results.- In: A. LEWKOWICZ & M. ALLARD (eds): Permafrost. Proc. 7th internat. Confer. 635-639. Collection Nordicana. Centre d'Etudes Nordiques, Université Laval, Yellowknife.

Leibman, M.O. & Kizyakov, A.I. (2007): Cryogenic landslides of the Yamal and Yugorsky Peninsulas.- Earth Cryosphere Inst. SB RAS, Moscow, 1-206 [In Russian].

Leibman, M.O., Khomutov, A.V., Gubarkov, A.A., Mullanurov, D.R. & Dvornikov, Y.A. (2015): The research station rVaskiny Dachiiny Dac DacYamal, West Siberia, Russia ia ion rVaskiny Dachivor. & Dvor. & Dvorlas.- Fennia 193: 3-30, doi: 10.11143/45201.

Leibman M.O., Khomutov, A.V., Orekhov, P.T., Khitun, O.V., Epstein, H., Frost, G. & Walker, D.A. (2012): Gradient of seasonal thaw depth along the Yamal transect.- In: D. DROZDOV & V. ROMANOVSKY (eds): Proc. 10th Internat. Confer. Permafrost 2. Translations of Russian Contributions, 237-242. The Northern Publisher, Salekhard.

Melnikov, E.S. & Minkin, M.A. (1998): About the strategy of developing geoinformational systems (GIS) and data bases in geocryology.- Kriosfera Zemli 2(3): 70-76 [In Russian].

Minkin, M.A., Melnikov E.S. & Leibman, M.O. (2001): Russian national geocryological database and a strategy for its development.- In: R. PAERE & V. MELNIKOV (eds): Permafrost response on economic development, environmental security and natural resources, 591-599, Kluwer Academic Publishers, Netherlands.

Romanovskii, N.N. & Leibman, M.O. (1994): Russian Contribution to the Global Geocryological Database. Glaciological Data, Report, GD-28, WDC-A for Glaciology, Boulder, Colorado, 24-27.

Richter, R. (1996): A spatially adaptive fast atmospheric correction algorithm.- Internat. J. Remote Sensing 17: 1201-1214, doi: 10.1080/01431169608949077.

Slabovich, G.I. (ed) (1985): Instructions for hydrometeorological stations and posts.- Gidrometeoizdat, Leningrad 1-301 [In Russian].

Streletskiy, D.A., Shiklomanov, N.I. & Nelson, F.E. (2012): Spatial variability of permafrost active-layer thickness under contemporary and projected climate in Northern Alaska.- Polar Geogr. 35: 95-116, doi: 10.1080/1088937X.2012.680204.

Trofaier, A.M., Bartsch, A., Rees, G. & Leibman M. (2013): Assessment of spring floods and surface water extent over the Yamalo-Nenets Autonomous District.- Environ. Res. Lett. 8: 045026, doi: 10.1088/1748-9326/8/4/045026.

Zhang, Y. (2004): Highlight Article: Understanding Image Fusion.- Photogrammetric Engineering & Remote Sensing 70: 657-661.

Acronym	Description	Website
AWIMAPS WebGIS Service	Alfred Wegener Institute GIS maps portal	<http://maps.awi.de/awimaps/>
YAMAL WebGIS	Alfred Wegener Institute GIS maps portal for YAMAL region	<http://maps.awi.de/yamal/>
CALM	Circumpolar Active Layer Monitoring network	<http://www.gwu.edu/~calm/>
COLD Yamal	COmbining remote sensing and field studies for assessment of Landform Dynamics and permafrost state on Yamal	<http://cold.zgis.net/>
GTN-P	Global Terrestrial Network for Permafrost Database	<http://gtnpdatabase.org/>
LCLUC-Yamal	Land-cover and Land-use Changes on the Yamal Peninsula, Russia	<http://www.geobotany.uaf.edu/yamal/>
NEST	NEST ESA SAR toolbox	<https://earth.esa.int/web/nest/home>
PANGAEA	Data Publisher for Earth & Environmental Science	<http://www.pangaea.de/>
TSP	Thermal State of Permafrost	<http://ipa.arcticportal.org/activities/gtn-p/tsp/15-tsp.html>

Tab. 7: List of projects and associated websites.

Tab. 7: Liste von Projekten und zugehörigen Webseiten.

Polarforschung 85 (2), 117–118, 2015 (erschienen 2016)

Rapid Melting of Fast-Ice in the Buor-Khaya Bay

by Peter V. Bogorodski[1*], Alexander P. Makshtas[1*] and Vasily Y. Kustov[1]

Abstract: In this extended abstract data of Buor-Khaya Bay fast-ice radiation measurements and thermodynamic properties are presented and analysed. The thermo-metamorphic transformations of fast-ice, including rapid melting of its upper surface layer, and melt pond formation are described. The data of observations are compared with estimations of the melting snow cover evolution from a conceptual thermodynamic model.

Zusammenfassung: Dieser Beitrag beschreibt die Ergebnisse von Strahlungsmessungen und thermodynamischen Eigenschaften des Festeises der Buor-Khaya-Bucht im Laptewmeer. Es werden thermo-metamorphe Veränderungen von Festeis einschließlich der Schmelzprozesse der Oberflächenschicht sowie die Entwicklung von Schmelztümpeln beschrieben. Die Daten der Beobachtungen werden mit Ergebnissen eines konzeptionellen thermodynamischen Modells zur Abschätzunge der Schmelzentwicklung der Schneedecke verglichen.

INTRODUCTION

The exclusive role of melt ponds in sea ice melting indicates that a further progress in climate prediction in the Arctic is partly defined by the development of melt-pond parameterisations and its incorporation into general sea-ice models. Certain advancements in the solution of this problem are described by, e.g., PEDERSEN et al. (2009) and FLOCCO et al. (2010). Nevertheless, to ensure that parameterisations are realistic it is necessary to understand and prove the physical mechanisms of melt-pond formation and evolution. This is possible only on the basis of remote sensing or field observations. The latter investigations are regularly performed on fast-ice of the Tiksi Gulf near Hydrometeorological Observatory Tiksi during spring. Below, the results of field observations and numerical calculations with a conceptual thermodynamic model of fast-ice melting in late spring 2011 are presented. The period was characterised by rapid melt-pond formation. During 72 hours, the whole visible area of fast-ice with thickness exceeding 2 m was covered by a meltwater layer of 20–25 cm depth.

FIELD OBSERVATION

The observations were conducted at the Sogo Bay, the southwest part of the Tiksi Gulf at the northeastern coast of Yakutia in late spring to early summer 2011. The Sogo Bay with an area of about 16 km^2, a mean water depth of 3–4 m, and salinity from 5 to 10 PSU (practical salinity unit) is part of the Tiksi Gulf connected with the Buor-Khaya Bay, Laptev Sea. The area is covered with fast sea ice from late of October to early July. Mean ice thickness before beginning of melting is 2.2 m. The maximal thickness is up to 2.5 m.

RESULTS AND CONCLUSIONS

The albedo of melt ponds changes from 0.1 to 0.5 (EICKEN et al. 2004) and is significantly smaller compared to the albedo of snow-covered and bare sea ice (0.84-0.87 and 0.6-0.65, respectively, PEROVICH 1996). Intensive absorption of solar radiation determines a specific role of melt ponds in the disintegration of sea ice. In spring 2011, extensive investigations of melt ponds evolution have been conducted on fast-ice of the Buor-Khaya Bay in the Laptev Sea. The results of field observations are presented in Figure 1. During May 28 to 29, 2011, a rapid increase of air temperature up to +12 °C took place. It led to the onset of snow cover melting accompanied by

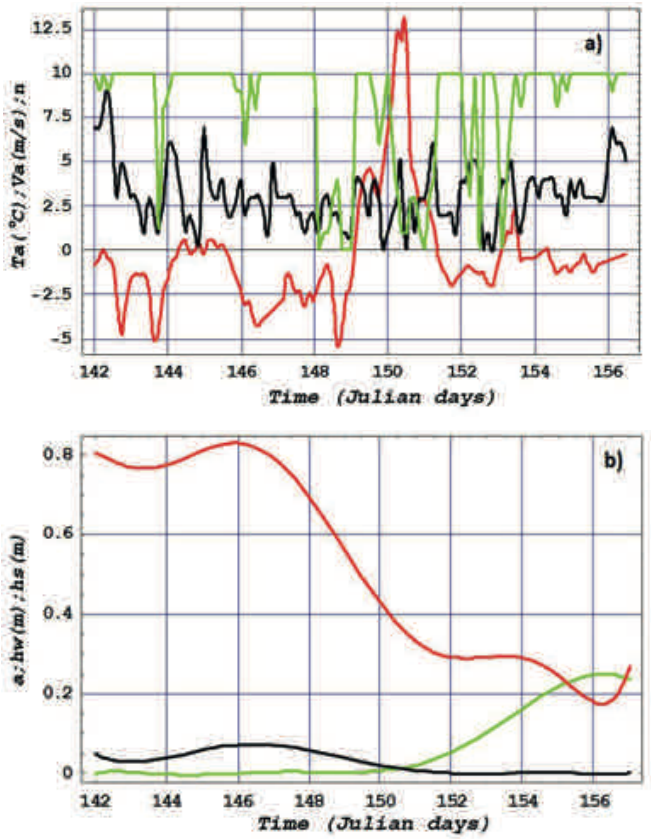

Fig. 1: Time series of (a): air temperature Ta (in °C) (red), wind velocity Va (in m/s) (black) and total cloudiness n (in 10/10 fraction) (green). (b): integral surface albedo a (red), snow thickness hs (in m) (black) and melt-pond depth hw (in m) (green).

Abb. 1: Zeitreihen (a): Lufttemperatur Ta (°C) (rot), Windgeschwindigkeit VA (in m/s) (schwarz) und Bewölkungsgrad n (in 10/10 Bedeckungsgrad) (grün). (b): integrale Oberflächenalbedo a (rot), Schneedicke hs (in Meter) (schwarz) sowie Schmelztümpel-Tiefe hw (in Meter) (grün).

doi:10.2312/polfor.2016.008

[1] Arctic & Antarctic Research Institute (AARI), St. Petersburg, Russia.
[*] Corresponding authors: <makshtas@yahoo.com>, <bogorodski@aari.ru>

This extended abstract was presented as an oral presentation at the International Conference "Our Climate – Our Future: Regional perspectives on a global challenge", 6–9 October 2014 in Berlin, Germany.
Manuscript received 01 June 2015; revised version 15 April 2016; accepted 28 April 2016.

a decrease of surface albedo from 0.8 to 0.25. The melt ponds formation started during May 30. During the next days, intensive surface melting continued, leading to melt ponds deepening and their subsequent joining into one pool. Practically during one day (May 31), the whole fast-ice surface in the visible area transformed to a giant melt pool with 20–25 cm depth.

For the description of the observed rapid fast-ice melting the conceptual thermodynamic model by BOGORODSKII & PNYUSHKOV (2000) is used. The model describes different stages of fast ice evolution: melting without forming of molten zones at the upper surface; melting of snow, melting of ice at the upper and bottom boundaries. The model is based on the heat diffusion equation and uses the following approximations: linear temperature profiles in snow and ice (assumption of quasi-stationarity); the temperatures of outer interfaces of sea ice correspond to the temperatures of thermodynamic equilibrium; shortwave radiation is absorbed by snow – ice upper surface, seepage is prescribed. The first assumption leads to the system of equations of the heat and mass balances of the upper and lower boundaries of sea ice. Boundary conditions and parameterisations of energy exchange processes on the outer interfaces are the same for all stages of ice transformation. The results of the modelling for different seepages are presented in Figure 2a.

Figure 2 illustrates that the seepage rate could be the important parameter for the description of melt-pond formation. Unfortunately, its values are still questionable. TAYLOR & FELTHAM (2004) proposed different seepage rate values for low (0-1.5 cm/day), average (1.5-2.0 cm/day), and high (>2.0 cm/day) sea-ice melting, but they specify its constant magnitudes for the whole period of melt-pond formation. However, for the initial period of sea-ice melting it is difficult to imagine that the drainage rates are constant, because during the formation of drainage channels the freezing of infiltrated water takes place under negative temperatures within the ice cover (TYSHKO et al. 2000). For this reason we determine seepage rates as linearly increasing from 0 cm/day at the beginning of melt-pond formation to a maximum value of 0 cm/day, 1 cm/day and 2 cm/day during the last day of observations. The comparison of Figures 1b and 2a show the best agreement between observed and calculated melt pond depth for seepage equal 0.

Using the data on melt-pond depth evolution, it is possible to compare estimations of the relative area covered with melt ponds, based on parameterisation as developed by PEDERSEN et al. (2009), with observational data. The results of the calculations with parameterisation, using our estimates of melt pond depth for different seepage rates, together with data of direct observations are shown in Figure 2b. The time lag of the relative area calculated with parameterisation is approximately 5 days. The reason of such delay could be due to the differences of the surface topography of sea-ice cover (flat or ridged), forming under different weather conditions. A full paper on this topic is published by MAKSHTAS et al. (2012) in Russian.

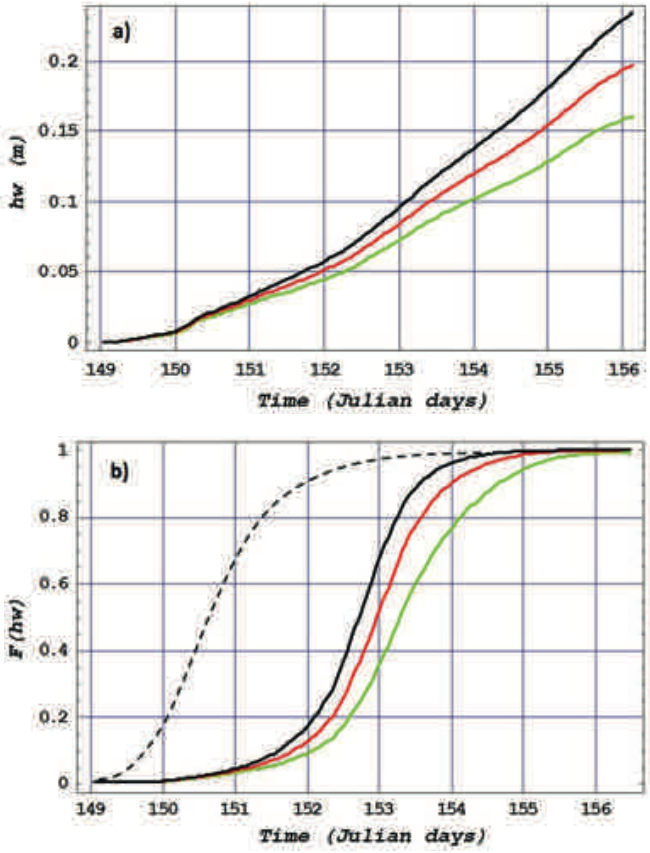

Fig. 2: Temporal evolution of (a): melt pond depth hw for seepage rates 0 cm/day (black), 1 cm/day (red), and 2 cm/day (green); (b): relative area occupied by melt ponds according to observational data (dashed line) and calculated with parameterisation (PEDERSEN et al. 2009) for seepage rates 0 cm/day (black), 1 cm/day (red) and 2 cm/day (green).

Abb. 2: Zeitliche Entwicklung (a): Schmelztümpel-Tiefe hw für Sickerraten von 0 cm/Tag (schwarz), 1 cm/Tag (rot) und 2 cm/Tag (grün); (b): der durch Beobachtungsdaten (gestrichelte Linie) abgeschätzten relativen Schmelztümpel-Fläche im Vergleich zu der mit Hilfe der Parametrisierungen nach PETERSEN et al. (2009) berechneten Fläche für Sickerraten von 0 cm/Tag (schwarz), 1 cm/Tag (rot) und 2 cm/Tag (grün).

ACKNOWLEDGMENTS

This study was supported by the Russian Foundation for Basis Research (Project 14-05-00408), Roshydromet (Project 14-05-00408), and the Otto Schmidt Laboratory (OSL). The authors would like to thank Aleksey Marchenko and an anonymous reviewer for helpful comments and suggestions on an earlier version of this extended abstract.

References

Bogorodskii, P.V. & Pnyushkov, A.V. (2011): Influence of melt pond on the formation of the multiyear sea ice cover.- Oceanology 51: 224-231 (in Russian).

Eicken, H., Grenfell, T.C., Perovich, D.K., Richter-Menge, J.A. & Frey, K. (2004): Hydraulic controls of summer Arctic pack ice albedo.- J. Geophys. Res. 109(C08007), doi: 10.1029/2003JC001989.

Flocco, D., Feltham, D.I. & Turner, A.K. (2010): Incorporation of a physically based melt pond scheme into the sea ice component of a climate model.- J. Geophys. Res. 115 (C08012), doi: 10.1029/2009JC005568.

Makshtas A.P., Bogorodsky P.V. & Kustov V.Yu. (2012): Quick melting of fast ice in the Sogo Bay (Tiksi Bay) in spring 2011.- Problemy Arctic and Antarctic 1(91): 37-47 (in Russian).

Pedersen, C.A., Roeckner, E., Lüthje, M. & Winter J.-G. (2009): A new sea ice albedo parameterization including melt ponds for ECHAM5 GCM.- J. Geophys. Res. 114 (D08101) doi: 10.1029/2008JD010440.

Perovich, D.K. (1996): The optical properties of sea ice.- Monogr. Ser. 96-1, Cold Region Res. and Eng. Lab., Hanover, N.H.

Taylor, P.D. & Feltham, D.L. (2004): A model of melt pond evolution on sea ice.- J. Geophys. Res. 109 (C12007), doi: 10.1029/2004JC002361.

Tyshko K.P., Cherepanov, N.V. & Fedotov V.I. (2000): Kristallicheskoe stroenie morskogo ledyanogo pokrova.- St.Petersburg, Gidrometeoizdat 1-66 (in Russian).

Polarforschung 85 (2), 119–133, 2015 (erschienen 2016)

Open Research Data, Data Portals and Data Publication – an Introduction to the Data Curation Landscape

by Kirsten Elger[1*], Boris Biskaborn[2], Heinz Pampel[1] and Hugues Lantuit[2]

Abstract: During the past decade, the relevance of research data stewardship has been rising significantly and data publication has become more familiar. Preservation of research data for long-term use, including its storage in adequate repositories has been identified as a key issue by the scientific community as well as by research agencies and the public. In practice, however, the current state of data sharing and re-use requires considerable improvement. This paper reviews recent developments in this area, and aims to provide some guidance to the increasing diversity of newly developed digital solutions, such as data journals, online data repositories, and citable digital object identifier (DOI) for datasets. We examine the differences and similarities between different examples of Arctic-related data management, including the newly created database of the Global Terrestrial Network for Permafrost GTN-P, a Canadian example of a (meta)data portal (Polar Data Catalogue), and examples of data repositories (e.g., PANGAEA, Nordicana D) and data journals (e.g., Earth System Science Data). We also describe the newly established Registry of Research Data Depositories (re3data.org) as a convenient resource for individual researchers to get an overview on and identify an appropriate repository for their scientific datasets as well for funding agencies during the evaluation process of the data management plan of research proposals.

Zusammenfassung: In den letzten zehn Jahren ist die Bedeutung des Zugangs und der Nachnutzung von Forschungsdaten gestiegen. Neue Publikationsstrategien für Forschungsdaten stellen sicher, dass wissenschaftliche Daten dauerhaft in geeigneten Daten-Repositorien gespeichert und zugänglich gemacht werden können. Auch wenn die Umsetzung dieser Publikationsstrategien von der wissenschaftlichen Community und von Forschungsförderorganisationen als zentrale Herausforderung für das Wissenschaftssystem benannt wird, ergeben sich in der Praxis noch viele Herausforderungen. Dieser Artikel gibt einen Überblick über aktuelle Entwicklungen im Bereich des Forschungsdatenmanagements. Exemplarisch werden einige Beispiele für den offenen Zugang vorgestellt und Publikationsstrategien für Forschungsdaten beschrieben. U.a. werden Aufgabe und Dienstleistung von Daten-Repositorien, Daten-Journalen sowie Daten-Portalen im Bereich der Arktisforschung erläutert. Exemplarisch werden folgende digitale Forschungsdateninfrastrukturen vorgestellt: Das kanadische (Meta)daten-Portal Polar Data Catalogue, die neue Datenbank des Global Terrestrial Network for Permafrost GTN-P (Metadaten und Daten), die Daten-Repositorien PANGAEA und Nordicana D sowie das Daten-Journal Earth System Science Data (ESDD). Darüber hinaus wird der Service des Registry of Research Data Repositories (re3data.org) vorgestellt. Dieses internationale Verzeichnis unterstützt Forschende und Forschungsförderer bei der Identifikation von geeigneten Daten-Repositorien zur Speicherung und Zugänglichmachung ihrer Forschungsdaten.

INTRODUCTION

Research data are fundamental for scientific research. Especially in the Geosciences, where observational data are not reproducible, and many historical data sets are important benchmarks, e.g., in the context of climate change, data curation and publication meets the needs for scientific reproducibility as well as offering potential for re-use.

For more than a decade, the free and open access to scientific results and research data has become more and more important, both by political expectations and technical possibilities. Especially the advent of the internet and new digital possibilities enabled the collection of high quantities of research data and often triggered a movement from empirical science towards data-driven science. Today, many datasets are available via the internet. Very often, however, these datasets are not used to their full extent because they are not systematically archived or made readily accessible or are not sufficiently described (COPDESS 2015). Another impediment to free and open data exchange is the reluctance of researchers to share their data in the absence of appropriate credit for the large investment of time and intellectual effort that went into collecting, processing, and describing the data, as well as concern that their data may be misused or misinterpreted.

This article reviews recent developments in the data curation landscape, and aims to provide some guidance to the increasing diversity of newly developed digital solutions, such as data journals, online data repositories, and citable digital object identifier (DOI) for datasets followed by presenting some exposed examples. We neither aim to provide a complete overview on the constantly increasing number of data repositories and portals, nor will we recommend or favour any of them. After a brief overview on the latest political developments, we introduce the key components for open research data (e.g., metadata, digital object identifier, different possibilities for data publication) and further examine the differences and similarities between them by introducing different examples of Arctic-related data management, including the newly created database of the Global Terrestrial Network for Permafrost GTN-P, the Polar Data Catalogue, a Canadian example of a (meta)data portal, and examples of data repositories (e.g., PANGAEA, Nordicana D) and data journals (e.g., Earth System Science Data). We also introduce the newly established Registry of Research Data Depositories (re3data.org) as a convenient resource for individual re-searchers to identify an appropriate repository for their scientific datasets as well for funding agencies during the evaluation process of the data management plan of research proposals. Note that all acronyms are listed (Tab. 2) at the end of this paper.

Politics

Following-up the Berlin Declaration on Open Access to Knowledge in the Sciences and Humanities (2003)

doi:10.2312/polfor.2016.009

[1] GFZ German Research Centre for Geosciences, Telegrafenberg, 14473 Potsdam, Germany;
[*] Corresponding author: <kelger@gfz-potsdam.de>
[2] Alfred Wegener Institute, Helmholtz Centre for Polar and Marine Research, Telegrafenberg, 14473 Potsdam, Germany.
This paper represents a supplement to the International Conference "Our Climate – Our Future: Regional perspectives on a global challenge", 6–9 October 2014 in Berlin, Germany.
Manuscript received 3 June 2015; revised version 17 January 2016; accepted 21 March 2016.

there are more and more initiatives to foster the free and open access not only to scientific journal articles but also to research data and metadata. Especially during the last about five years, there is an increasing expectation by research funding agencies and the public that close attention should be given to data management, and many research agencies and organisations require that grant proposals explicitly address the plans for metadata and data archiving e.g., the European Commis-sion, the German Research Foundation (DFG), the International Arctic Science Committee IASC, etc.). Internationally, the largest impact and a testimony for open science was the G8 Science Ministers Statement from June 2013. They claim that *"to the greatest extent and with the fewest constraints possible, publicly funded scientific research data should be open […] whilst acknowledging the legitimate concerns of private partners"* and that *"increasing free access to peer-reviewed, published research results will require sustainable solutions"* (G8 Science Ministers, 2013). This statement was followed by several national and international initiatives like the "EU Implementation of the Open Data Charter" (European Commission, 2013a), which requires, e.g., the use of open formats, semantic interoperability, to ensure data quality and documentation, and a clear definition of intellectual property rights, e.g., by using open licences for scientific data, etc. The "Digital Agenda 2014–2017 of the Federal Government of Germany" supports a *"comprehensive open access strategy designed to enhance incentives and ensure more efficient, ongoing access to publicly funded research publications and data"* (BMWi et al. 2014).

Several other countries adopted open science policies, like, e.g., G8 Open Data Charter – Canada's Action Plan (Government of Canada 2014), the memorandum on "Public Access to the Results of Federally Funded Research" (Office of Science and Technology Policy 2013) and the "US Open Data Action Plan" (US Government 2014), or the German Alliance of Science Organisations (2010) with a clear statement in favour of open research data in the preamble: *"Quality-assured research data are a cornerstone of scientific knowledge and […] can often serve as the basis for further research. […] Preserving research data over the long-term and making them available therefore does not only serve the verification of prior results, but also, to a large extent, the obtaining of future ones. It is a strategic task to which science and the humanities, politics as well as other parts of society, must contribute."*

An important step for open data in Arctic research is the "Statement of Principles and Practices for Arctic Data Management" of the International Arctic Science Committee that was released in April 2013 (IASC 2013). It states that all research projects seeking endorsement by IASC must adhere to the principle of full and open access to data, and must make metadata (basic descriptive information of collected data) available in an internationally recognised standard-format to an appropriate catalogue or registry. The policy further states that IASC should actively encourage adherence to the principles and may withdraw project endorsement if necessary (IASC 2013). The full open access to scientific results and research data, together with a comprehensive data management plan, is also required for every project funded within the new EU framework program Horizon 2020 (European Commission 2013b) and other funding agencies (e.g., National Science Foundation NSF, German Research Foundation DFG).

COPDESS and the Statement of Commitment

Founded in October 2014, a new initiative joins together major Earth and Space Science publishers with primary Earth and Space Science data repositories and related consortia, the Coalition on Publishing Data in the Earth and Space Sciences (COPDESS 2015, Hanson et al. 2015). To mark the launch of the new initiative they published a "Statement of Commitment" that signals *"an important progress and a continuing commitment by publishers, data facilities and unions to enable open data in the Earth and Space Sciences"* (COPDESS 2015). By the end of 2015 it is already signed by 38 of the leading publishers and data centres in Earth and Space Sciences, including Science, Nature, AGU, EGU, Springer, Copernicus, Elsevier, NSIDC, ICSU and many more. By committing to the proper citation of scientific datasets in scientific articles (see below), this statement is a major step forward for the acknowledgment and recognition of the important scientific work to make research data publicly available together with a comprehensive description of the published datasets and clear indications about where to find them. In addition and often as a consequence of their signature of the "Statement of Commitment", many institutions and publishers have released policies for full and open access to research data.

The consortium has pointed out that even though it is widely acknowledged that *"scholarly publication is a key high value entry point in making data available, open, discoverable, and usable." and "most publishers have statements related to the inclusion or release of data as part of publication […] the vast majority of data submitted along with publications are in formats and forms of storage that makes discovery and re-use difficult or impossible."* They further recommend that research datasets should preferably be stored in *"appropriate domain repositories"* (COPDESS 2015) and are currently developing an online registry for these.

The key message in favour of acknowledging and promoting data publications and important incentive to convince scientists to share and publish their data, is the commitment *"to promote referencing of data sets using the Joint Declaration of Data Citation Principles"* (Data Citation Synthesis Group 2014), in which *"citations of data sets should be included within reference list"* (COPDESS 2015).

In addition they agreed to make sure to *"include in research papers concise statements indicating where data reside and clarifying availability"* and *"to promote and implement links to data sets in publications and corresponding links to journals in data facilities via persistent identifiers"*, ideally by registered DOI's (COPDESS 2015).

DATA PUBLICATION WITH DIGITAL OBJECT IDENTIFIER (DOI)

Publishing research datasets with assigned digital object identifier (DOI) has emerged as convenient solution for publishing citable and persistently accessible research data. By rules of

the International DOI Foundation the registration of a DOI requires the submission of at least a minimum set of metadata. In the following we will give a brief introduction to DOI, metadata and different formats for the DOI-referenced data publication.

Digital Object Identifier (DOI)

A DOI is an *"online reference (digital), pointing to (identifying) a resource (object). The DOI system links, through a directory, references and web addresses of an object to a "landing" page providing information on access and metadata about that object — at a minimum its creator, title, publisher, year of publication, and DOI. This allows DOIs to provide a stable, persistent, resolvable reference taking users to an object, even if web addresses or other references to the location of an object, or its content, change"* (HORTON 2015). Using DOIs brings stability to data referencing in the digital era where scientific sources and references are much more than printed paper (e.g., databases, websites, audio, blogs, video, social media, etc.). A DOI persistently directs to the related text or data set, independent of website changes, servers getting switched off or other changes of sources.

Digital Object Identifiers are well established for scientific articles since the early 2000s. The concept to also cite data sets, archived in data repositories, with a persistent DOI, has been developed in Germany within the STD-DOI project funded by the German Science Foundation between 2004-2007 with the participation of the Technical Information Library Hannover (TIB), the GFZ German Centre for Geosciences, PANGAEA, OKRZ, and the German Space Agency DLR (KLUMP et al. 2006). Following this was the foundation of DataCite in December 2009, which is a world-wide nonprofit organisation for DOI for research data, under the realms of the "International DOI Foundation". Among other ways to persistently identify references to digital objects, DOIs have emerged as the leading system for text and data publication (COPDESS 2015).

Nevertheless, even if a DOI guarantees the discovery of research data, it may not guarantee the data quality or enable data re-use. Therefore, high-quality research data must be accomplished by metadata for data discovery and re-use. Assuming the scientifically correct and careful acquisition and processing of a dataset, the scientists, the data repository or the publisher should make sure that the dataset is accompanied by an adequate and sufficient description suitable for data discovery and re-use.

Metadata

To meet the requirements for intelligent openness standards that published data sets must be intelligible and usable by others for both, verification of research results and data re-use, data sets must be supported by explanatory metadata (ROYAL SOCIETY LONDON 2012). Metadata, or data about data, is *"structured information that describes, explains, locates, or otherwise makes it easier to retrieve, use, or manage an information resource"*. (NATIONAL INFORMATION STANDARDS ORGANIZATION 2004).

There is a general difference between structural metadata which is essential for data re-use (e.g., the information of instruments or sensors used to measure the data, applied functions or processing steps, quality control, etc.) and the more descriptive metadata for data discovery (e.g., the information of the existence of a dataset, the brief description of the data and the project, i.e. in form of an abstract, measurement period, contact information of the data originator and distributor, and information about where to obtain the datasets). Metadata for data discovery aims to discover research data via search engines, data portals, etc., whereas structural metadata is essential for data re-use and often directly attached to the datasets (e.g., in form of a README file).

Metadata Standards

Using international metadata standards, that mainly exist for metadata for data discovery allow database interoperability and are a sign of quality. Prominent metadata schemes for geo-referenced datasets and services are, e.g., the ISO19115 Schema accessed on 28 December 2015, the DATACITE (2014) Metadata Schema, or outcomes of the European INSPIRE initiative, the "Infrastructure for Spatial Information in the European Community". To facilitate data discovery and re-use, it is strongly recommended to not only provide the minimum set of obligatory metadata, that is usually very small in number and designed to fit to every type of data, but to make sure to describe the datasets as good as possible, e.g., by using the recommended fields in the Datacite Metadata Schema 3.1 (DATACITE 2014, see Tab. 1).

In addition, there are more and more initiatives to define standards for structural metadata. These are always discipline-specific and often developed in large collaboration projects, or global networks, e.g., as metadata forms, protocols or data models that are often accomplished by detailed instruction for the data collection in the field. Examples are the GTN-P metadata forms (BURGESS 2000), the ADAPT standard protocols of the "Canadian permafrost research programme Arctic Development and Adaptation to Permafrost in Transition" or the recommendations for seismic metadata of the INTERNATIONAL FEDERATION OF DIGITAL SEISMOGRAPH NETWORKS (FDSN, 2014) that are a combination of structural metadata and metadata for data discovery and are now recommended for all seismic networks worldwide.

Data Publication formats

Research data may be published supplementary to journal articles, with a descriptive article in one of the new Data Journals, or as independent entities (KATZ & STRASSER 2015) with accompanying structural metadata, e.g., in form of a readme or a data report. For curation purposes and data re-use it is always recommended to store the data in open access data repositories and not to submit them to the journals as supplementary material. This is also a recent recommendation of publishers within the COPDESS consortium. An open access repository enables data re-use even if the corresponding articles was not published in an Open Access Journal.

Category	Sub-category
Resource information	**DOI, publisher, publication year**, licences
People involved	**Authors: name**, affiliation, role (e.g.: data manager, distributor, editor, hosting institution, project leader, project member, researcher, research groups, etc.), authors-id type and number (ORCID-ID), Contact person: name, email, affiliation, Contributors: name, affiliation, email, authors-id and number (authors and contributors may be people or institutions),
Description	**Abstract**, methods, table of contents, series numbers, others
Keywords	Free **keywords** and controlled vocabulary via thesauri to fulfil metadata standards
Spatial & temp. coverage	Visual control via a mapping tool and the possibility to enter bounding boxes and or point values, each with different temporal domains and descriptions,
Dates	e.g. created, embargo until, valid from … to
Related reference	e.g. for documentation, supplements, references, new versions, etc.

Tab. 1: Metadata for data discovery used in the Data Repository of the GFZ German Research Centre for Geosciences. Bold fields are obligatory, the others "recommended for data discovery" in the DataCite (2014) Metadata Scheme 3.1. While the metadatabase is designed to produce DataCite, ISO19115, and other standards, the user interface in which the scientists enter their metadata uses a language that is understandable for scientists (e.g. creators are named authors, geoLocationPoints or geoLocationBoxes are inserted via the mapping tool or direct entry of coordinates, etc.). Every field that may be automatically generated (e.g., the URL of the metadataset or rights, dates of submission or acceptance) and is not visible for the scientist.

Tab. 1: Übersicht über die Metadaten für Data Discovery, die im Repositoi-um des Deutschen GeoForschungsZentrums GFZ erhoben werden. Es han-delt sich sowohl um die Pflichtfelder (fett) als auch die für die Data Dis-covery empfohlenen zusätzlichen Metadatenfelder, wie sie im DataCite (2014) Me-tadaten Schema 3.1 definiert werden. Das GFZ Datenrepositorium unterstützt darüber hinaus auch ISO19115 und andere Metadatenstandards. Bei der Ge-staltung des Metadatenerhebungsformular wurde besonderer Wert auf die Nut-zerfreundlichkeit gelegt. Das Formular ist in einer für Wissen¬schaftler ver-ständlichen Sprache angelegt, was sich z.B. in der Bezeichnung der beteiligten Wissenschaftler als Autoren (und nicht als "creators") widerspiegelt. Auch die Eingabe der geografischen Koordinaten der Daten¬sätze erfolgt mit Hilfe einer interaktiven Karte und es wurde Wert darauf gelegt, dass automatisch generier-bare Informationen, wie z.B. die URL einer gewählten Lizenz oder auch das Datum der Einreichung eines Datensatzes, automatisch bezogen wird und nicht durch die Wissenschaftler eingetragen werden müssen.

METADATA PORTALS, REPOSITORIES, DATA JOURNALS, DATA REPORTS – A DATA PUBLICATION TOOLBOX

Metadata Portals

Metadata portals are the most important source to get information about projects, data, activities, and people involved (by metadata for data discovery). They usually have search engines and provide standardised metadata that may be exchanged with other portals via standard application programming interfaces (API), like, e.g., the Open Archives Initiative Protocol for Metadata Harvesting (OAI-PMH). Metadata portals provide information about where to find the data and aim to give as much information about data and project that a potential user is able to decide whether the described datasets are fitting his needs or not before accessing or downloading the data. Metadata portals are very often the entry point to data repositories (e.g., PANGAEA, NSIDC Data Search) and exist for the whole range from collections of information stored in Excel sheets and published via a list on a website to large inter-institutional object-oriented databases, like, e.g., the Canadian Polar Data Catalogue with various search options and partly access to the datasets (see below). New developments are overarching national and international metadata portals that are retrieving their metadata not from individual scientists, but by harvesting it from other metadata portals and data repositories. Examples for these metadata catalogues of research data collections are, e.g., B2FIND, which was developed within the EU FP7 project EUDAT or the new "Arctic Data Explorer of the National Snow and Ice Data Center NSIDC". The US initiative "Earth Cube" aims to develop a common cyberinfrastructure for the purpose of collecting, accessing, analysing, sharing, and visualizing all forms of data and related resources for solid Earth, hydrosphere, atmosphere, and space environment.

Data Repositories

Data repositories are digital research infrastructures for archiving and distributing research data sets. They *"ensure a maximum of accessibility, stability and reliability to facilitate working with and sharing of research data."* (Pampel et al. 2013) and often have a data discovery metadata portal as entry point. The landscape of data repositories is very heterogeneous. Datasets are accompanied by descriptive metadata and often have links to related scientific articles. Data repositories may or may not provide DOIs to their datasets and the completeness of metadata is quite variable. There are institutional, disciplinary, multidisciplinary, and project specific data repositories (Pampel et al. 2013), however, it is recommended to archive datasets preferably in open access, theme-specific or institutional data repositories that provide DOIs to the archived datasets, hence making them citable (COPDESS 2015, European Commission 2013b).

Data Journals

Data journals publish articles about original research datasets, collections or data portals. The articles mainly describe datasets, data collections or databases without giving an interpretation of the data itself. Most data journals, e.g., Earth System Science Data (ESSD) or Nature's Scientific Data follow a distributed way for the actual data; i.e., the data are not accessible attached to the journal article but stored in a data repository and will be reviewed together with the scientific article. Data journals are rapidly evolving in all scientific disciplines and some have already been indexed in the Web of Science (e.g., ESSD).

Data Reports

For many datasets, the standardised metadata fields for data discovery are not suitable alone for an appropriate data description and many datasets are accompanied by readme files for the technical description of the datasets. These readme files, however, are usually only accessible after downloading and unzipping a dataset. Discovering in the readme file that the dataset does not fit the needs of the researcher,

e.g., because the temporal coverage is not fitting, requires the deletion of the dataset and a second or third trial and often leads to the decision of not using the data set at all.

An additional option for the description of datasets is to pub-lish the dataset description in form of a data report. They have a flexible format, are fully readable before downloading the datasets (in contrast to many readme files) and especially attractive for datasets that are not large enough to be described in a data article.

For many years, German Research Centre for Geosciences (GFZ) publishes "Scientific Technical Reports (STR)" as a report series which is electronically persistent available and citable with assigned DOIs. Typical contents for STRs were PhD theses or project reports. In 2011, this series was opened for the description of datasets as Scientific Technical Report Data. These data reports offer a full and consistent overview and description to all relevant parameters of linked published datasets. They have a flexible format that is applicable to descriptions of datasets for all scientific fields and are internally reviewed. Whenever possible, we are developing templates for different types of datasets (e.g., for descriptions of seismological experiments realised with instruments of the Geophysical Instrument Pool Potsdam (GIPP, e.g., ASCH et al. 2014).

Furthermore, it is possible to publish one data report for several published datasets that are all referring to the same data report as description (e.g., different runs of a climate model). With the newly developed project-specific design of data reports and specific content of landing pages, (e.g., ICDP Operational Reports and datasets, LORENZ et al. 2015a, b) they have qualified as helpful tool to fill the gap between basic metadata and restricted readme information on the one hand and preparing extended journal articles on the other hand.

EXAMPLES FOR DATA DISCOVERY AND PUBLICATION

Polar Data Catalogue: Canadian portal for interdisciplinary Arctic Research

The Canadian Polar Data Catalogue (PDC) is an online portal for data discovery (and partly data access) covering a wide range of scientific fields from natural sciences to policy, health, and social sciences (FRIDDELL et al. 2014a, 2014b). It has been developed during the International Polar Year (IPY) 2007/2008 and is co-financed by the ArcticNet at the University Laval and the Canadian Cryospheric Information Network (CCIN) at the University of Waterloo. Each scientist who is funded by ArcticNet or any of its partners or is doing research at any field station supported by ArcticNet partners, is supposed to submit their metadata for data discovery to PDC on an annual base. PDC metadata follows ISO19115 standards (see FRIDDELL et al. 2014a for an overview) and metadata standards of the Federal Geographic Data Committee (FGDC, listed in ELGER et al. 2014).

In June 2015, the portal has more than 2100 metadata entries. In addition, PDC hosts about 250 datasets from the International Polar Year 2007/2008 and almost 28.000 Radarsat 1 satellite images from both Polar Regions, Radarsat-2 satellite mosaics of Antarctica, and sea-ice charts of the Canadian Ice Service.

In addition to full-text and advanced search options with various parameters, the catalogue has a geospatial web-based mapping system that can be used in combination with various search options (Fig. 1). The geospatial search tool in PDC has been developed with consultation of northern communities who were especially interested to search for projects that have taken place in their regions. This interest also led to the development of a PDC-lite version that is fully operational under low internet bandwidth connections that are abundant in many parts of the Canadian North (see ELGER et al. 2014 for an extended description).

The new Database of the Global Terrestrial Network for Permafrost GTN-P – an example for a thematic database

Permafrost is formally defined as perennial frozen ground that remains at or below 0 °C for at least two consecutive years. Some 25 % of the global land mass is underlain by permafrost, and is increasingly vulnerable to degradation as a result of global climate change. The Global Terrestrial Network for Permafrost (GTN-P) is the prime international program concerned with permafrost monitoring. Initiated in 1999 by the Global Climate Observing System (GCOS) and the Global Terrestrial Observing System (GTOS) of the World Meteorological Organisation (WMO) and managed by the International Permafrost Association (IPA), GTN-P is dedicated to long-term monitoring of permafrost temperature and active-layer thickness, with the goal of obtaining a comprehensive view of the spatial structure, trends, and variability of changes in the active layer and permafrost in both Hemispheres.

GTN-P has two international components with very different data in temporal and spatial resolution:

(1) The Thermal State of Permafrost (TSP) programme is a circumpolar network of more than 1000 boreholes ranging from 1 m to about 1000 m depths located in the polar re-gions of both Hemispheres and in mountainous permafrost areas (Fig. 2 for GTN-P sites in the northern Hemisphere). The temperature data have a high temporal resolution (hourly to daily measurements, annual for deep boreholes, BISKABORN et al. 2015a).

(2) The Annual Thaw Depth (ALT) is mainly observed by the Circumpolar Active Layer Monitoring (CALM) program. This network incorporates 240 sites in Arctic, sub-Arctic, Antarctic, and mountainous regions. About 70 % of the sites are located in Arctic and Subarctic lowlands underlain by continuous permafrost. Discontinuous and mountainous permafrost areas contain 20 % and 11 % of ALT sites respectively. The distribution of ALT sites is not uniform, a circumstance attributable to historical circumstances and logistical constraints. The active layer is measured within grids with side lengths between 10, 100, and 1000 m on an annual basis (BISKABORN et al. 2015b).

Since the beginning, GTN-P adopted an open data policy and developed standardised metadata forms for both programmes (BURGESS et al. 2000). However, more than a decade after the implementation of GTN-P, the data was not used as much as it was intended. Reasons for this were, e.g., the large vari-

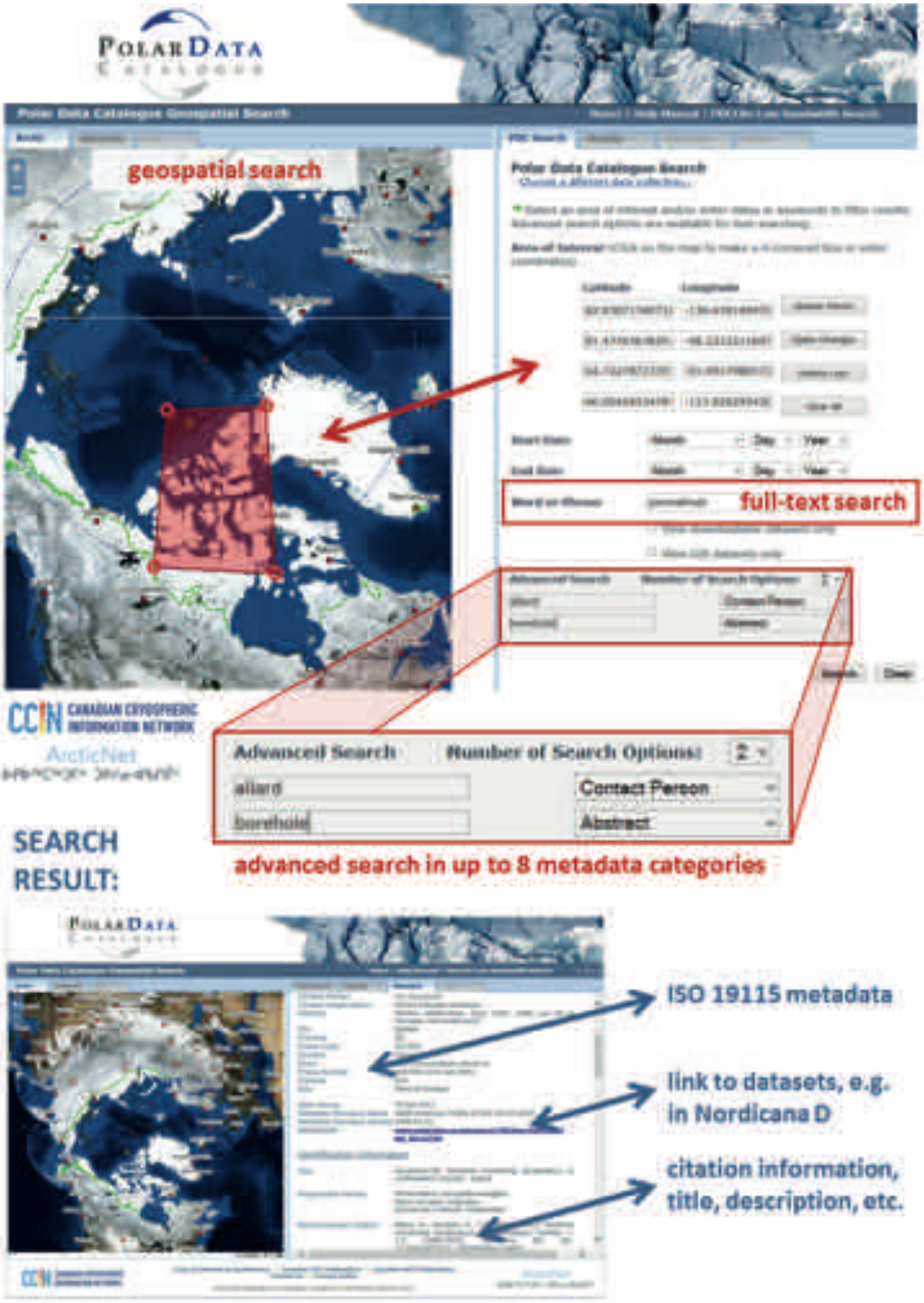

Fig. 1: Example from the Canadian Polar Data Catalogue. The map-based geospatial search is linked with the geographic coordinates and allows search for a certain region. Alternatively and additional, users may use the full-text search or the advanced search with specific search in up to eight categories (e.g., contact person, responsible parties, abstract, title, etc.). The results show classical metadata for data discovery in ISO19115 and FGDC standards and show links to the data sets if applicable. An overview on all ISO19115 metadata fields in PDC is given in FRIDDELL et al. (2014a). The figure is a combination of different snapshots from PDC websites accessed in June 2015.

Abb. 1: Darstellung einiger Funktionalitäten des kanadischen Polar Data Catalogue. Die Suche von Metadatensätzen erfolgt entweder über die Karte als Geodatendienst (links oben) oder durch die Eingabe von Suchparametern. Neben der Volltextsuche gibt es auch erweiterte Sucheinstellungen, die die Suche innerhalb von acht Kategorien erlaubt (Kontaktperson, Autoren, Kurzbeschreibung, Titel, usw.). Die Metadaten folgen Metadatenstandards gemäß ISO19115 und FGDC und beinhalten Verknüpfungen („link“) zu den vorhandenen Datensätzen, sofern diese existieren. FRIDDELL et al. (2014a) geben eine vollständige Übersicht über die im Polar Data Catalogue geführten ISO19115 Metadatenfelder. Die Abbildung ist eine Kombination verschiedener Momentaufnahmen der Websites mit zusätzlichen grafischen Elementen und wurde im Juni 2015 erstellt.

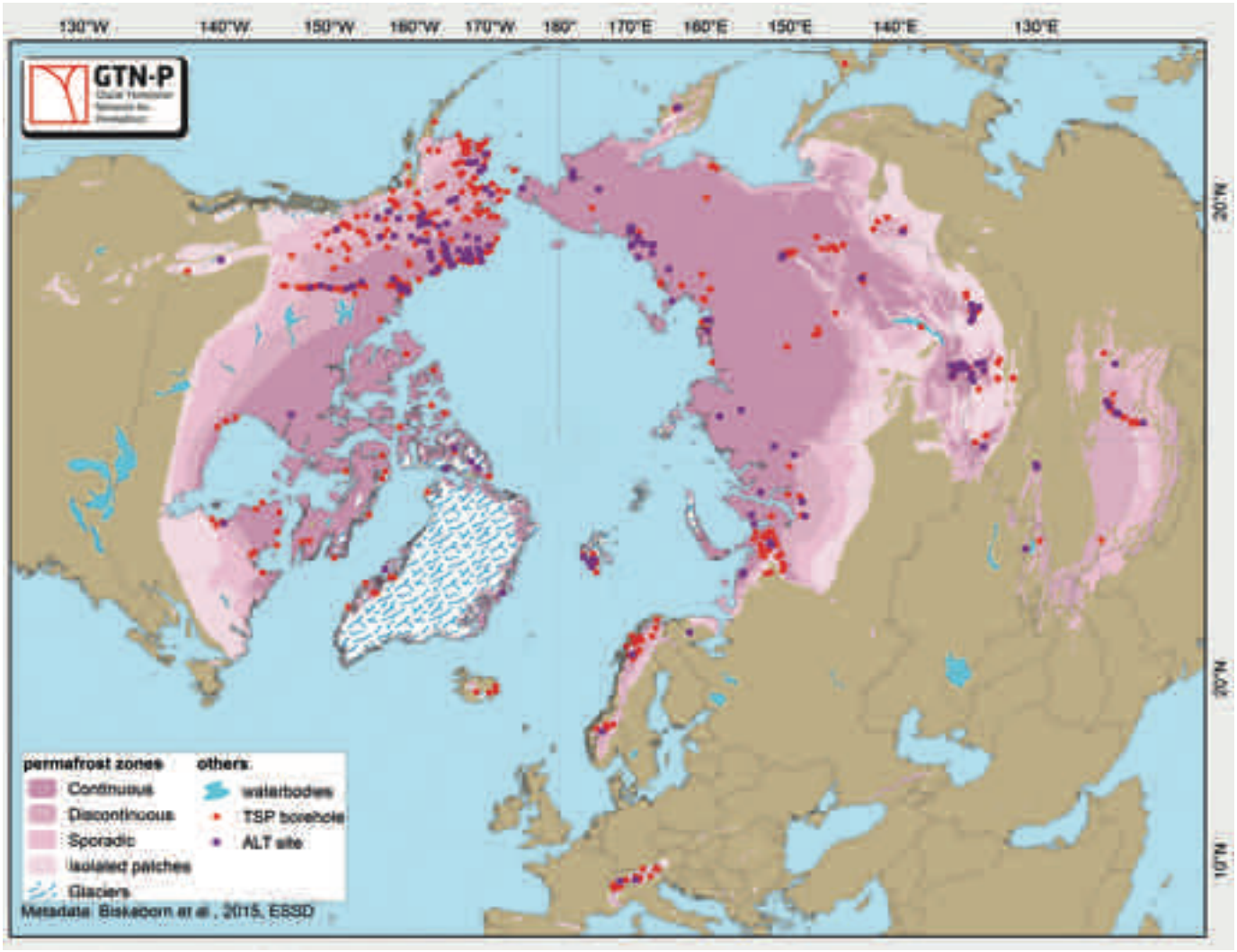

Fig. 2: Monitoring sites of the Global Terrestrial Network for Permafrost (GTN-P) in the Northern Hemisphere and their location within permafrost zones, as defined by the International Permafrost Association IPA. Red dots show permafrost boreholes of the Thermal State of Permafrost (TSP) programme, purple dots active-layer thickness (ALT) monitoring sites of the Circumpolar Active Layer Monitoring (CALM) programme.

Abb. 2: Übersicht über die Messstationen und -flächen des Global Terrestrial Networks for Permafrost (GTN-P) der nördlichen Hemisphäre und deren Lage in den jeweiligen Permafrost Zonen, welche von der International Permafrost Association IPA definiert wurden. Rote Punkte markieren Permafrost-Bohrlöcher, die im Rahmen des Thermal State of Permafrost (TSP) Programms gebohrt wurden. Violette Punkte zeigen die Lage langjähriger Messfelder der Tiefe der sommerlichen Auftauschicht des Permafrostes an, welche im Rahmen des Programms Circumpolar Active Layer Monitoring (CALM) angelegt wurden.

ability of data description in different countries (even despite the availability of standardised metadata sheets) and the lack of a central repository for borehole data (especially for the TSP component). While CALM data was accessible via the central CALM website (as mainly as Excel spreadsheets and txt files), borehole temperatures of the TSP network could only be partially accessed via national data portals, e.g., the Norwegian NORPERM database (for TSP data from Norway and Svalbard) or the National Snow and Ice Data Centre (NSIDC) and the Permafrost Laboratory at the University of Alaska Fairbanks (for many boreholes in Alaska and Russia). In November 2011, the necessity to build a joint database for both components of the Global Terrestrial Network for Permafrost was identified and the EU FP7 program Changing Permafrost in the Arctic and its Global Effects in the 21st Century (PAGE21) provided the frame for developing a GTN-P governance structure and a state-of-the-art data management system. This central GTN-P database was released in April 2014 and is fully described in Biskaborn et al. (2015b) and at the corresponding website (see Tab. 1). It contains data, metadata, a search engine with specific filters for permafrost researchers and an automated data visualisation including quality control. Metadata information is entered into the Data Management System following the ISO19115 documentation by developing a metadata frame-work suitable for permafrost monitoring sites. Upload of both, data and metadata, is coordinated and quality checked by 36 GTN-P National Correspondents from 25 different countries.

PANGAEA: Data Publisher for Earth and Environmental Science

World Data Systems (WDS) reformed the former World Data Centres (WDC) of the International Council of Science (ICSU), which were created to host and distribute scientific

data sets during the 1957–1958 International Geophysical Year. WDCs originally were mono-disciplinary, e.g., WDC Climate, WDC Mare, etc. but as a whole covered a broad range of disciplines from the natural and social sciences to humanities. As all data held in WDC's were available for the cost of copying and sending the requested information, they were the first "open access" data centres. Today, many former WDC's changed to the multi-disciplinary ICSU World Data System. The World Data System (WDS) is an interdisciplinary body of the ICSU with the vision to promote long-term stewardship of, and universal and equitable access to, quality-assured scientific data and data services, products, and information across a range of disciplines in the natural and social sciences, and the humanities.

PANGAEA is a certified member of the ICSU-WDS system and one of the first data repositories, assigning DOI to data sets. It is hosted by two German institutes: the Alfred-Wegener Institute Helmholtz Centre for Polar and Marine Research (AWI) and the Centre for Marine Environmental Sciences

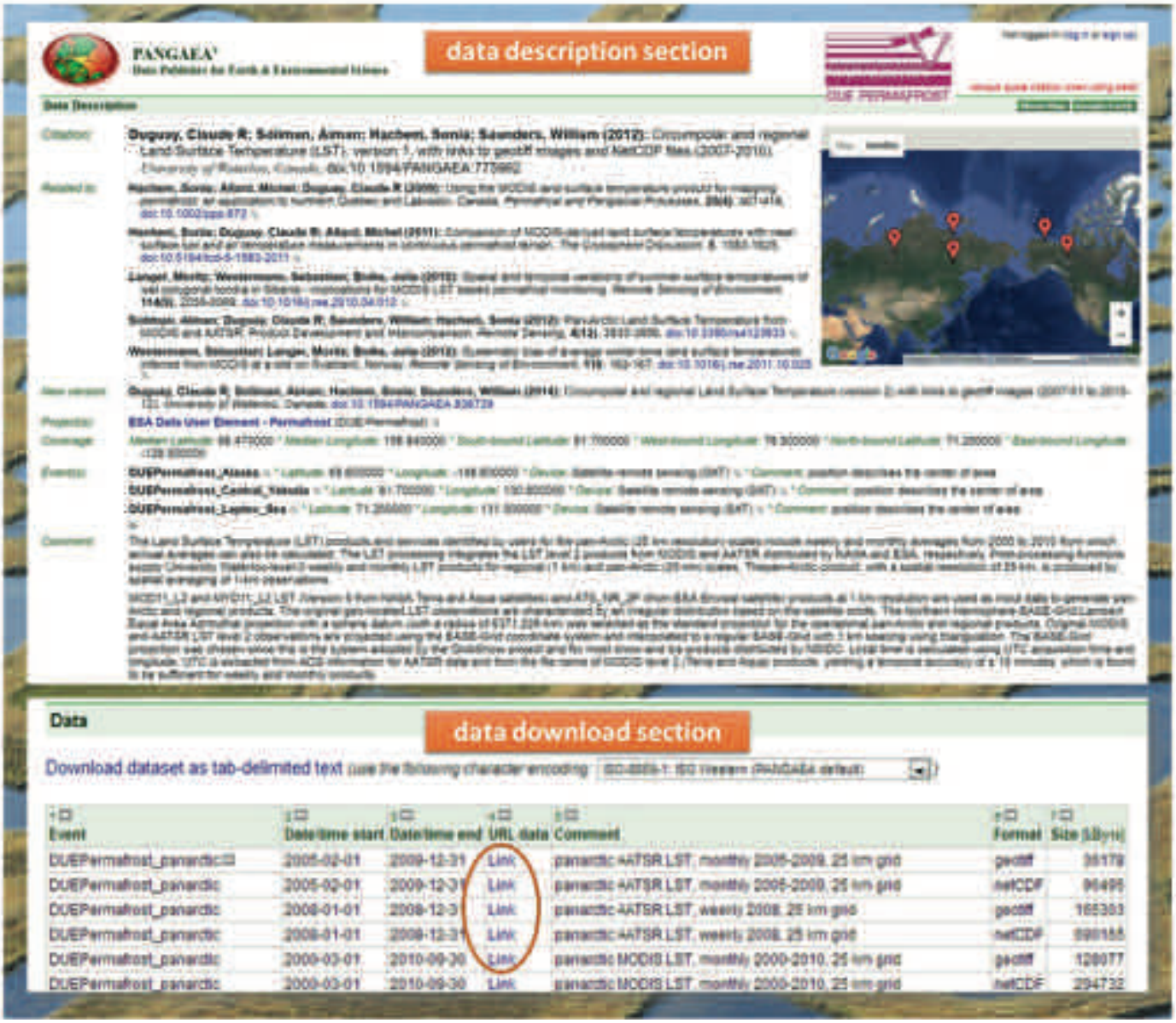

Fig. 3: Example of a PANGAEA landing page for a data collection of remotely sensed land surface temperature products from the ESA Data User Element DUE Permafrost Project (Duguay et al. 2012). The metadata fields in the data description section (upper part) include information about how to cite the datasets (citation), cross-references to related journal articles or other datasets (related to), the project name, spatial coverage, a data/ project description section (comment), the parameter description (here: bands, periods, time series), licence for working with the data, and the file size. The data download section (lower part) has information on the temporal domain and links to data download in different formats (geotiff, NetCDF) and the download link to the Product guide with the full description of the dataset (not schown in the figure).

Abb. 3: Beispiel einer DOI Landing Page des PANGAEA Datenrepositoriums. Bei dem gezeigten Datensatz handelt es sich um eine Kollektion von Fernerkundungsprodukten (Land Surface Temperature), die im Rahmen des ESA Data User Element (DUE) Permafrost Projekt entstanden sind (Duguay et al., 2012). Die Metadaten im beschreibenden Teil oben beinhalten neben der Zitationsvorgabe auch Querverweise zu wissenschaftlichen Artikeln oder anderen relevanten Datensätzen, den Projektnamen, die geographische Abdeckung der Datensätze, eine kurze Projektbeschreibung, die Lizenz zur Nachnutzung der Daten und die Dateigröße. Im unteren Teil sind die Verknüpfungen ("link") zu den Datensätzen gegeben, welche in zwei unterschiedlichen Formaten (geotiff und NetCDF) verfügbar sind. Darüber hinaus gibt es hier einen "link" zu der vollständigen Produktbeschreibung (nicht in der Abbildung sichtbar).

(MARUM). The free and open access international data library aims at archiving, publishing and distributing geo-referenced data from Earth system research with guaranteed long-term data availability. The datasets are accomplished by standardised metadata (ISO19115) and can be fully read before downloading the datasets (Fig. 3). The policy of data management and archiving follows the Principles and Responsibilities of ICSU World Data Systems and the OECD "Principles and Guidelines for Access to Research Data from Public Funding". Authors submitting data to the PANGAEA data repository for archiving agree that all data are provided under a Creative Commons License. Each dataset can be identified, shared, published, and cited by using a DOI. After editorial review, datasets are archived by data curators as supplements to journal articles or independent datasets or data collections. At the end of 2015, there are more than 34.000 dataset DOIs registered by PANGAEA.

Nordicana D

Nordicana D is a DOI-referenced, open access, online data repository that was launched in February 2013 at the Centre d'études Nordiques (Centre for Northern Studies, CEN), Québec, CA. Until December 2015 they have published 23 data collections, mostly with long-term meteorological time-series from climate stations and (shallow) boreholes in the Canadian North, provided by CEN scientists and project partners. Nordicana D is following a versioning strategy, i.e. whenever there is an update to the datasets, e.g., by adding another year to the data or relocating stations, etc., a new version number will be published for the same DOI. As required by the DOI assignment, all version numbers are accessible and the website provides a history of changes for each version (Fig. 4). For each Nordicana D collection standardised metadata for data discovery are archived in the Polar Data Catalogue (see above for details in the respective section).

The description of the datasets allows easy identification of a suitable dataset before downloading the data. Data download is possible for different temporal resolutions, from measured data every hour, to daily, monthly, and annual averages. It has started with mostly micro-meteorological data from local climate stations (air and ground temperatures, wind speed and direction, net radiation, snow height), but also, more recently, other types of data. These are, e.g., permafrost soil geochemical and geophysical data from the ADAPT project, and lemming monitoring data, with additional data entries in progress, including for circumpolar diatoms and microbial DNA.

Earth System Science Data (ESSD) – the first data journal for the Geosciences

Launched in 2008 as one of Copernicus' Open Access Journals, ESSD is an international, interdisciplinary journal for the publication of articles on original research data (sets), furthering the re-use of high-quality data of benefit to Earth system sciences (Pfeiffenberger & Carlson 2011). It is an ideal place to publish scientific articles on research datasets or collections, data portals and repositories as well as new-developed nontrivial statistical and other methods. Any interpretation of the datasets or comparison of the described methods with others is beyond the focus of the journal. ESSD is open for various formats, ranging from regular articles, to brief communications (e.g., on additions to datasets) and commentaries, to review articles and special issues.

ESSD uses a distributed approach with the datasets being stored in recognised data repositories with an assigned DOI (e.g., PANGAEA) and cross-referenced in the respective ESSD article. The interactive public peer-review with discussion papers is also open for comments from the scientific community and includes the review of the published datasets or portals described in the articles, especially with respect to the data description and usability. On March 17, 2015, ESSD was the first data journal that has been indexed by Thomson-Reuters' Web of Science (ESSD news 2015).

RE3DATA.ORG – A REGISTRY OF RESEARCH DATA REPOSITORIES

With the increasing relevance for appropriate storage of research data, more and more data repositories and archives are evolving across all scientific fields. Funding agencies require the formulation of a data management plan for each research proposal in which they often want to know in which repository the newly measured or produced data will be stored. Since 2012 re3data.org (Registry of Research Data Repositories) offers researchers, funding organisations, libraries and publishers a comprehensive overview of the heterogeneous landscape of research data repositories. Project partners in re3data.org include the GFZ German Research Centre for Geosciences, Humboldt-Universität zu Berlin, Purdue University, and Karlsruhe Institute of Technology (KIT). The work of re3data.org has been funded by the German Research Foundation (DFG) in Germany and the Institute of Museum and Library Services (IMLS) in the United States. The re3data.org registry cooperates with other Open Science initiatives like BioSharing and OpenAIRE.

In January 2016 re3data.org lists more than 1,400 research data repositories from around the world covering all academic disciplines (Fig. 5). The databases, repositories and data infrastructures are described, following the "Metadata Schema for the Description of Research Data Repositories" that has been developed within the project (Rücknagel et al. 2015). Besides the detailed description, re3data.org summarises the properties of a repository into a user-friendly icon system helping researchers to easily identify an adequate repository for the storage of their datasets (Pampel et al. 2013, and see Fig. 6). More than 5,000 unique visitors are using the registry per month. At present, an average of ten repositories is added weekly to the registry.

The registry offers two search possibilities: free text search through a simple search box and filters for more specific searches (Fig. 7). In the list of results each record includes the name of the repository, the subjects covered, a brief description of the content and a set of icons visualizing key properties of the repository (Fig. 6). A comprehensive view of the descriptive record of the repository can be obtained by clicking on the name of the repository in the search results. It is also possible to simply browse through the list of indexed data repositories. An Application Programming Interface (API) enables machine access to the registry.


Nordicana D
Nordicana D1:
DOI : 10.5885/44985SL-8F203FD3ACCD4138
Environmental data from Northern Ellesmere Island in Nunavut, Canada
Links to PDC
Version history
Site overview
Data download: hourly, daily, monthly, yearly
Download section

Fig. 4: Commented elements of a DOI landing page for the online data repository Nordicana D (number D1). It contains climate station data from 2002 to 2014 from three sites in Northern Ellesmere Island in Nunavut, Canada (CEN, 2015). In addition to the required metadata for data discovery (map, citation, abstract, key references, contributors) it provides links to additional metadata in the Polar Data Catalogue, the version history, the site overview table with key information on the time series, and the data download section at the bottom. Each data download is a life query into the database with the possibility to choose different temporal resolutions for data download (hourly: measured data or daily, monthly or annual averages). The dataset is updated on an annual basis. The figure is a compilation of different snapshots and explanations from the Nordicana D website, accessed in June 2015.

Abb. 4: Kommentierte Ausschnitte einer DOI Landing Page des kanadischen Datenrepositoriums Nordicana D (Datensatz D1). Der Datensatz enthält mikrometeorologische Daten (Lufttemperatur, und -feuchtigkeit, oberflächennahe Bodentemperaturen) von drei Messstationen im nördlichen Ellesmere Island in Nunavut, Kanada (CEN, 2015). Die DOI Landing Page enthält die obligatorischen Metadaten für Data Discovery, wie eine Karte, die Zitationsvorgabe, die Kursbeschreibung („abstract"), Querverweise zu wissenschaftlichen Artikeln mit weiterführenden Informationen über die hier publizierten Datensätze und die beteiligten Wissenschaftler. Darüber hinaus gibt es Querverweise zu den entsprechenden Metadatensätzen im Polar Data Catalogue und eine Übersichtstabelle mit detaillierten Informationen zu jeder einzelnen Station. Im unteren Bereich befinden sich die direkten Verknüpfungen („link") zum Herunterladen der Datensätze. Jeder Datensatz wird in unterschiedlicher zeitlicher Auflösung angeboten: stündliche Werte (wie sie vom Sensor aufgezeichnet wurden), sowie tägliche, monatliche und jährliche Mittelwerte. Jedes Jahr kommt eine weitere Jahreszeitreihe hinzu (und die DOI bekommt eine neue Version). Die Abbildung ist eine Kombination verschiedener Momentaufnahmen der Websites mit zusätzlichen grafischen Elementen und wurde im Juni 2015 erstellt.

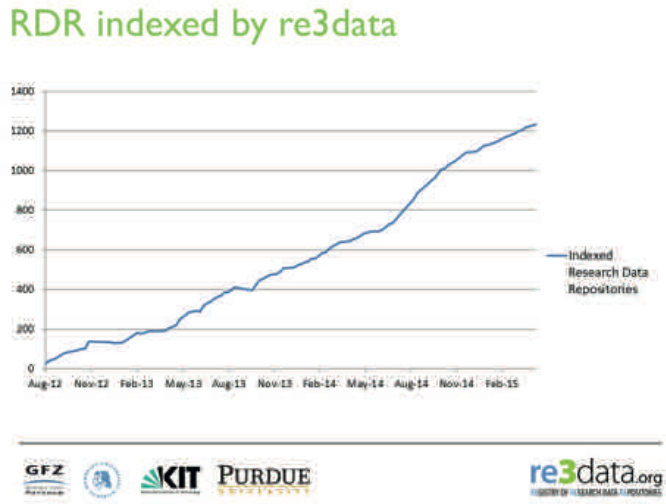

Fig. 5: Number of research data repositories indexed in re3data.org between August 2012 and May 2015.

Abb. 5: Anzahl der in re3data.org gelisteten Forschungsdaten Repositorien zwischen August 2012 und Mai 2015.

Fig. 6: The icon system of re3data.org provides quick information about the availability of metadata, if the repository provides a data policy, legal aspects for reuse (e.g., licences), the type of persistent identifier provided by the repository, and whether the repository is certified or supports repository standards (see also Fig. 7).

Abb. 6: Die Symbole von re3data.org bieten einen schnellen Überblick über die Daten-Repositorien. Durch die Symbole werden folgende Informationen graphisch angezeigt: Sind die Repositorien beschrieben? Haben sie eine Data Policy auf ihrer Website? Sind die Nachnutzungsregeln geklärt (Lizenzen)? Vergeben sie persistente Identifikatoren für ihre Datensätze und wenn ja welche? Ist ein Repositorium zertifiziert und wenn ja nach welchem Standard? (vgl. Fig. 7).

Fig. 7: Search options and features of re3data.org. In addition to a simple full-text search, several filters may be used. The first overview on the results already provide information on subjects, content types and countries for each repository, as well as the icons visualising key properties for each repository. An extended overview is available after selecting a result.

Abb. 7: Beispiel eines Suchergebnisses auf re3data.org mit Erläuterungen der einzelnen Optionen. Zusätzlich zur Volltextsuche, können verschiedene Filter gesetzt werden (erweiterte Sucheinstellungen). Das Suchergebnis zeigt eine kurze Übersicht über die jeweiligen Repositorien, die bereits die wichtigsten Parameter wie wissenschaftliche Disziplin, Inhaltstypen und das Land, welches das Repositorium betreibt, aber auch die re3data.org Symbole enthält. Bei der Auswahl eines der Suchergebnisse öffnet sich eine Unterseite mit der vollständigen Übersicht über das Repositorium (unten in der Abbildung).

A growing numbers of funders and research institutions recommend the use of re3data.org for the identification of appropriate repositories, e.g., during the composition of a research proposal. For example: Projects, funded under HORIZON 2020 are advised by the European Commission's "Guidelines on Open Access to Scientific Publications and Research Data in Horizon 2020" (EUROPEAN COMMISSION 2013b) to use re3data.org.

Operators of data repositories can suggest their infrastructures to be listed in re3data.org by filling in an online application form. A repository is indexed by re3data.org when a minimum set of requirements are met. These are, e.g., that the mode of access to the data and repository as well as the terms of use must be clearly explained on the repository websites and the repository must have a focus research data. Before a new record of a research data repository is published in re3data.org, all gathered information is reviewed by a second team member. An editorial board is currently being formed to add a scientific quality check via an online form. The repository has to inform users about the mode of access to the data and state the terms of use on the repository websites, since these statements are essential pieces of information for researchers either searching for or depositing data.

From 2016 on re3data.org will be included into DataCite. Bringing this service together with DataCite, who mints and manages DOIs for datasets, will yield new opportunities to explore in combining a registry of data repositories with information about persisted datasets to create new value for the research community.

DISCUSSION AND CONCLUSIONS

The increasing relevance and importance of open access to research data for the scientific community, funding agencies and the public together with new technical opportunities in the digital era triggered the development of an increasing number of data repositories, metadata portals and data journals, enabling both, the discovery and persistent and citable

access to research data sets in all scientific fields. Based on examples for Arctic data sets, we have described the functionality and differences of different possibilities to make research data open available via the internet as well as for data journals.

Re3data.org, the Registry of Research Data Repositories offers guidance in the constantly increasing number and very heterogeneous landscape of research data repositories. The structured description of each repository is accomplished by a user-friendly icon system, helping researchers to easily identify an adequate repository for the storage of their datasets. The inclusion of re3data.org into DataCite from January 2016 on emphasizes its relevance and the necessity for this service.

We recommend to always choose a DOI-referenced discipline-specific or institutional data repository to make research datasets publicly available. DOI-referenced datasets are citable, permanent accessible, and accompanied by at least a minimum set of metadata for data discovery, improving the usability of a published data set. Seeing the recent developments towards metadata portals combining metadata of several databases (e.g., NSIDC Data Explorer), we recommend to not only submit the obligatory metadata to the registration agency, data repository or portal, but to make sure that the metadata provides a usable description of a published dataset, e.g., by adding the recommended fields of the DataCite Metadata Scheme (DataCite 2014).

For curation purposes and data re-use datasets should preferably be stored in open access data repositories and not be submitted to the journals as supplementary material, as it is recommended by the COPDESS consortium. An open access repository facilitates data re-use even if the corresponding articles were not published in an Open Access Journal.

Moreover, by signing the Statement of Commitment (COP-DESS 2015), many publishers have agreed to list dataset DOIs in reference lists of journal articles. Attaching DOI to research datasets and citing them in reference lists is a major step towards the recognition of the important work of data producers for the scientific community and bring data providers the recognition they deserve (International DOI Foundation, 2012).

In addition, because reference lists are always targets for evaluation metrics, it is also possible to assess the number of citations for DOI-referenced datasets, which provides an independent proof for the re-use of a published dataset. Consequently, whenever possible, we recommend following the recommendations of the "Joint Declaration of Data Citation Principles" (Data Citation Synthesis Group 2014) and always cite DOI-referenced data publications in journal articles and list them in the reference lists, and not, as it was common practice for many years, in the acknowledgments.

ACKNOWLEDGMENTS

We like to thank Birgit Heim from the Alfred Wegener Institute in Potsdam and Warwick Vincent from the University Laval and the Centre d'étudues nordiques in Québec, Canada for valuable discussions and feedback that greatly improved the manuscript. We also thank two anonymous reviewers for their careful review and constructive comments.

References

Asch, G., Tilmann, F., Schurr, B. & Ryberg, T. (2014): MINAS, temporary MINi ArrayS within the frame of IPOC.- Scientific Technical Report - Data 14/03, Potsdam: Deutsches GeoForschungsZentrum GFZ: 1-13, doi: 10.2312/GFZ.b103-14036.

Berlin Declaration on Open Access to Knowledge in the Sciences and Humanities (2003): Available online: <http://oa.mpg.de/lang/enuk/berlin-prozess/berliner-erklarung/> (accessed on 05 July 2015).

Biskaborn, B.K., Lantuit, H., Dreßler, A., Lanckman, J.P, Jóhannsson, H., Romanovsky, V., Cable, W., Sergeev, D., Vieira, G., Pogliotti, P., Nötzli, J. & Christiansen, H.H. (2015a): Quality assessment of permafrost thermal state and active layer thickness data in GTN-P.- GEOQuébec 2015, Conference Paper, Québec.

Biskaborn, B.K., Lanckman, J.P., Lantuit, H., Elger, K., Streletskiy, D.A., Cable, W.L. & Romanovsky, V.E. (2015b): The new database of the Global Terrestrial Network for Permafrost (GTN-P).- Earth Syst. Sci. Data 7: 245-259, 2015, doi: 10.5194/essd-7-245-2015.

BMWi et al. (2014): Bundesministerium für Wirtschaft und Energie, Bundes-ministerium des Innern und Bundesministerium für Verkehr und digitale Infrastruktur (2014): Digitale Agenda 2014-2017.- August 2014. URL: <http://www.bmwi.de/BMWi/Redaktion/PDF/Publikationen/digitale-agenda-2014-2017,property=pdf,bereich=bmwi2012,sprache=de,rwb= true.pdf> (accessed on 10 June 2015).

Burgess, M., Smith, S., Brown, J., Romanovsky, V. & Hinkel, K. (2000): The Global Terrestrial Network for Permafrost (GTNetP): permafrost monitoring contributing to global climate observations.- Current Research 2000 E14, Geol. Survey Canada, Ottawa, Canada, URL: <http://wmsmir.cits.rncan.gc.ca/index.html/pub/geott/ess_pubs/211/211621/cr_2000_e14.pdf> (accessed on 23 December 2015).

CEN (2014): Environmental data from Northern Ellesmere Island in Nuna-vut, Canada, 1.2 (2002-2014).- Nordicana D1, doi: 10.5885/44985SL-8F203FD3ACCD4138.

COPDESS (2015): Coalition on Publishing Data in the Earth and Space Sciences: Statement of Commitment from Earth and Space Science Publishers and Data Facilities.- URL: <http://www.copdess.org/statement-of-commitment/> (accessed on 22 December 2015).

Data Citation Synthesis Group (2014): Joint Declaration of Data Citation Principles.- M. MARTONE (ed) San Diego CA: FORCE11, URL: <https://www.force11.org/datacitation> (accessed on 10 June 2015).

DataCite (2014): DataCite Metadata Schema 3.1 XML Schema.- doi: 10.5438/0011.

Duguay, C.R., Soliman, A., Hachem, S. & Saunders, W. (2012): Circumpolar and regional Land Surface Temperature (LST),Version 1, with links to geotiff images and NetCDF files (2007-2010).- University Waterloo, Canada, doi: 10.1594/PANGAEA.775962.

Elger, K., Vincent, W.F. & Barnard, C. (2014): Chapter 11: Knowledge capture and data management (p. 233-254).- In: E. Topp-Jørgensen et al. (eds): INTERACT - Management planning for Arctic and northern alpine research stations – Examples of good practices. DCE – Danish Centre for Environment and Energy, Aarhus University, 1-324, doi: 10.2312/GFZ.LIS.2014.001.

ESSD News (2015): ESSD indexed by Thomson Reuters as first data journal in Earth sciences.- URL: <http://www.earth-system-science-data.net/about/news_and_press/2015-03-17_essd-indexed-in-the-wos.html> (ac-cessed on 23 June 2015).

European Commission (2013a): EU Implementation of the G8 Open Data Charter.- URL: <http://ec.europa.eu/information_society/newsroom/cf/dae/document.cfm?doc_id=3489> (accessed on 10 June 2015).

European Commission (2013b): Guidelines on Open Access to Scientific Publications and Research Data in Horizon 2020. Version 1.0, 11 December 2013.- URL: <http://ec.europa.eu/research/participants/data / ref/h2020/grants_manual/hi/oa_pilot/h2020-hi-oa-pilot-guide_en.pdf> (accessed on 06 May 2015).

Friddell, J., LeDrew, E. & Vincent, W.F. (2014a): The Polar Data Catalogue: Data Management for Polar and Cryospheric Science.- 70th Eastern Snow Conference, Huntsville, Ontario, Canada, 4-6 June 2013.

Friddell, J., LeDrew, E. & Vincent, W.F. (2014b): The Polar Data Catalogue: Best practices for sharing and archiving Canada's Polar Data.- Data Sci. J. 13(0): PDA1-PDA7, doi: 10.2481/dsj.IFPDA-01.

G8 Science Ministers (2012): G8 Science Ministers Statement; June 12, 2013.- URL: <https://www.gov.uk/government/news/g8-science-ministers-statement> (accessed on 10 June 2015).

German Alliance of Science Organisations (2010): Schwerpunktiniti-ative "Digitale Information": Principles for the Handling of Research Data; June 24, 2010.- URL: <http://www.allianzinitiative.de/en/core-activities/research-data/principles.html> (accessed on 10 June 2015).

Government of Canada (2014): G8 Open Data Charter – Canada's Action Plan.- URL: <http://open.canada.ca/en/g8-open-data-charter-canadas-action-plan> (accessed on 10 June 2015)..

Hanson, B., Lehnert, K. & Cutcher-Gershenfeld, J. (2015): Commit-

Acronym	Meaning	Web address
ADAPT	Canadian permafrost research programme Arctic Development and Adaptation to Permafrost in Transition	<http://www.cen.ulaval.ca/adapt/protocols/adapt.php>
AGU	American Geophysical Union	<https://sites.agu.org/>
Arctic Data Explored	"Arctic Data Explorer" of the National Snow and Ice Data Center NSIDC	<http://nsidc.org/acadis/search/>
ArcticNet	Network of Centres of Excellence of Canada	<http://www.arcticnet.ulaval.ca/>
AWI	Alfred Wegener Institute Helmholtz Centre for Polar and Marine Research	<www.awi.de>
BioSharing	A curated, searchable portal of inter-related data standards, databases, and policies in the life, environmental and biomedical sciences	<https://biosharing.org/>
B2FIND	Discovery service based on metadata steadily harvested from research data collections from EUDAT data centres and other repositories.	<www.eudat.eu/services/b2find>
CALM	Circum Polar Active Layer Monitoring	<http://www.gwu.edu/~calm/>
CCIN	Canadian Cryospheric Information Network at the University of Waterloo	<https://www.ccin.ca/home/>
CEN	Centre for Northern Studies, Québec, CA	<http://www.cen.ulaval.ca/en/page.aspx?lien=index>
COPDESS	Coalition on Publishing Data in the Earth and Space Science	<http://www.copdess.org/>
DataCite	International not-for-profit organization, which aims to improve data citation	<www.datacite.org>
DFG	German Science Foundation / Deutsche Forschungsgemeinschaft	<http://www.dfg.de/en/index.jsp>
DKRZ	Deutsches Klimarechenzentrum	<https://www.dkrz.de/>
DOI	Digital Object Identifier	<www.doi.org>
EarthCube	Earth Cube	<www.earthcube.org>
EGU	European Geosciences Union	<http://www.egu.eu/>
ESSD	Earth System Science Data	<http://www.earth-system-science-data.net/>
EU	European Union	<http://europa.eu >
EUDAT	Collaborative Pan-European infrastructure providing research data services, training and consultancy	<www.eudat.eu>
FDSN	International Federation of Digital Seismograph Networks	<www.fdsn.org>
FGDC	Federal Geographic Data Committee	<https://www.fgdc.gov/>
GCOS	Global Climate Observing system	<http://www.wmo.int/pages/prog/gcos/>
GTOS	Global Terrestrial Observing System	<http://www.fao.org/gtos/>
GFZ	Helmholtz Centre Potsdam German Research Centre for Geosciences	<http://www.gfz-potsdam.de>
GIPP	Geophysical Instrument Pool Potsdam	<http://www.gfz-potsdam.de/gipp>
GTN-P	Global Terrestrial Network for Permafrost	<http://www.gtnp.org>, <http://gtnpdatabase.org/>
IASC	International Arctic Science Committee	<http://iasc.info/>
ICDP	International Scientific Drilling Program	<http://www.icdp-online.org/home/>
ICSU	International Council for Science	<http://www.icsu-wds.org/>
IMLS	Institute of Museum and Library Services, US	<https://www.imls.gov/>
INSPIRE	Infrastructure for Spatial Information in the European Community	<http://inspire.ec.europa.eu>
IPA	International Permafrost Association	<http://ipa.arcticportal.org/>
ISO19115	ISO Standards Catalog	<http://www.iso.org/iso/home/store/catalogue_ics/catalogue_detail_ics.htm?csnumber=53798>
KIT	Karlsruhe Institute of Technology	<http://www.kit.edu/>
MARUM	Centre for Marine Environmental Sciences	<https://www.marum.de/>
Nature's Scientific Data	Nature.Com Scientific Data	<http://www.nature.com/sdata/>
NORDICA D	The Nordica D collection	<http://www.cen.ulaval.ca/nordicanad/en_index.asp>
NORPREM	Norwegian data base for TSP from Norway and Svalbard	<http://www.tspnorway.com/20090301%20NEWS%20NORPERM%20DATABASE%20open.htm>
NSF	National Science Foundation	<http://www.nsf.gov/>
NSIDC	National Snow and Ice Data Center	<http://nsidc.org/acadis/search/>
OAI-PMH	Open Archives Initiative Protocol for Metadata Harvesting	
OECD	Organisation for Economic Co-operation and Development	<http://www.oecd.org/>
OpenAIRE	Network of Open Access repositories, archives and journals that support Open Access policies	<https://www.openaire.eu/>
PAGE21	Changing Permafrost in the Arctic and its Global Effects in the 21st Cent.	<www.page21.eu>
PANGAEA	Data Publisher for Earth & Environmental Sciences	<www.pangaea.org>
Permafrost Laboratory	Permafrost Laboratory at the University of Alaska Fairbanks	<http://permafrost.gi.alaska.edu/>
PDC	Polar Data Catalogue: Canadian portal for interdisciplinary Arctic Research	<https://www.polardata.ca/>
re3data.org	Registry of research data repositories	<www.re3data.org>
TIB	Technical Information Library Hannover	<https://www.tib.eu/en/>
TSP	Thermal State of Permafrost	<http://ipa.arcticportal.org/activities?catid=0&id=15>
WDS	ICSU World Data System	<https://www.icsu-wds.org/>
WMO	World Meteorological Organization	<http://public.wmo.int/en>

Tab. 2: List of all used acronyms and associated websites.

Tab. 2: Liste aller verwendeter Abkürzungen und zugehörigen Webseiten.

ting to publishing data in the Earth and Space Sciences.- Eos 96; doi: 10.1029/2015EO022207.

Horton, L. (2015): Digital Object Identifiers: Stability for citations and referencing, but not proxies for quality. April 23, 2015, The London School of Economics and Political Science.- URL: <http://blogs .lse.ac.uk/impactofsocialsciences/2015/04/23/digital-object-identifiers-stability-for-citations> (accessed on 6 October 2015).

IASC (2013): Statement of Principles and Practices for Arctic Data Management; April 16, 2013.- URL: <http://www.innovation.ca/sites/default/files/Rome2013/files/IASC%20Statement%20on%20Arctic%20Data%20Management_2013.pdf> (accessed on 6 October 2015).

International DOI Foundation (2012): DOI handbook, version 5.- URL: <http://www.doi.org/hb.html> (accessed on 30 December 2015).

International Federation of Digital Seismograph Networks FDSN (2014): FDSN recommendations for seismic network DOIs and related FDSN services [WG3 recommendation].- doi: 10.7914/D11596.

Kratz, J. & Strasser, C. (2014): Data publication consensus and controversies (version 3; referees: 3 approved).- F1000Research, 3:94; doi: 10.12688/f1000research.3979.3.

Klump, J., Bertelmann, R., Brase, J., Diepenbroek, M., Grobe, H., Höck, H. & Wächter, J. (2006): Data publication in the open access initiative.- Data Sci. Journal 5: 79-83; doi: 10.2481/dsj.5.79.

Lorenz, H., Rosberg, J.-E., Juhlin, C., Bjelm, L., Almqvist, B., Berthet, T., Conze, R., Gee, D.G., Klonowska, I., Pascal, C., Pedersen, K., Roberts, N.M.W. & Tsang, C.F. (2015a): COSC-1 operational report - Operation-al data sets.- GFZ German Research Centre for Geosciences, <http://dx.doi.org/10.1594/GFZ.SDDB.ICDP.5054.2015>.

Lorenz, H., Rosberg, J.-E., Juhlin, C., Bjelm, L., Almqvist, B., Berthet, T., Conze, R., Gee, D.G., Klonowska, I., Pascal, C., Pedersen, K., Roberts, N.M.W. & Tsang, C.F. (2015b): COSC-1 operational report Explanatory remarks on the operational data sets.- Deutsches GeoForschungsZentrum GFZ, doi: 10.2312/ICDP.2015.001.

National Information Standards Organization (2004): Understanding Metadata.- NISO Press, Bethesda, MD 20814 USA, URL: <http://www.niso.org/publications/press/UnderstandingMetadata.pdf>.

Office of Science and Technology Policy (2013): Increasing Access to the Results of Federally Funded Scientific Research.- URL: <https://www.whitehouse.gov/sites/default/files/microsites/ostp/ostp_public_access_memo_2013.pdf> (accessed on 6 October, 2015).

Pampel, H. & Dallmeier-Tiessen, S. (2014): Open Research Data: From Vision to Practice. - In: S. BARTLING & S. FRIESIKE (eds): Opening Science. The Evolving Guide on How the Internet is Changing Research.- Collaboration and Scholarly Publishing, Heidelberg, Springer, 213-224, doi: 10.1007/978-3-319-00026-8.

Pampel, H., Vierkant, P., Scholze, F., Bertelmann, R., Kindling, M., Klump, J., Goebelbecker, H.-J., Gundlach, J., Schirmbacher, P. & Dierolf, U. (2013): Making Research Data Repositories Visible: The re3data.org Registry.- PLOS ONE 8, e78080 (2013), doi: 10.1371/journal.pone. 0078080.

Pfeiffenberger, H., & Carlson, D. (2011): Earth System Science Data (ESSD) - A Peer Reviewed Journal for Publication of Data.- D-Lib Magazine 17(1/2), doi: 10.1045/january2011-pfeiffenberger.

Rücknagel, J., Vierkant, P., Ulrich, R., Kloska, G., Schnepf, E., Fichtmüller, D., Reuter, E., Semrau, A., Kindling, M., Pampel, H., Witt, M., Fritze, F., van de Sandt, S., Klump, J., Goebelbecker, H.-J., Skarupianski, M., Bertelmann, R., Schirmbacher, P., Scholze, F., Kramer, C., Fuchs, C., Spier, S. & Kirchhoff, A. (2015): Metadata Schema for the Description of Research Data Repositories .Version 3.- doi: 10.2312/re3.008.

Royal Society London (2012): Science as an open enterprise.- The Royal Society Science Policy Centre report 02/12.- ISBN: 978-0-85403-962-3. URL: <https://royalsociety.org/~/media/Royal_Society_Content/policy / projects/sape/2012-06-20-SAOE.pdf (accessed on 30 December 2015).

US Government (2014): U.S. Open Data Action Plan; May 9, 2014.- URL: <https://www.whitehouse.gov/sites/default/files/microsites/ostp/us_open_data_action_plan.pdf > (accessed on 6 October 2015).

Polarforschung 85 (2), 135–141, 2015 (erschienen 2016)

Assembly of the CarboPerm WebGIS for the Laptev Sea Region, Arctic Siberia – Data Visualisation as a WebGIS Service

by Antonie Haas[1*], Birgit Heim[2], Sebastian Zubrzycki[3], Kirsten Elger[4], Christian Schäfer-Neth[1], Anne Morgenstern[2] and Irina Fedorova[5]

Abstract: Permafrost regions are highly sensitive to climate change. Bringing research data and metadata from diverse sources together and visualising them within a publicly available worldwide system would have an enormous impact on data accessibility and availability and would significantly promote scientific work. The CarboPerm WebGIS, a case study focusing on the Lena River Delta in the Laptev Sea Region (Siberia), shows how a WebGIS infrastructure can support scientific work, data management, data visualisation, and data publication. CarboPerm is an interdisciplinary German project with Russian cooperation, investigating the formation, turnover and release of carbon in Siberian permafrost landscapes. There, the Lena River formed the largest delta in the Arctic and is place of long-term Russian-German scientific cooperation in permafrost research. The CarboPerm WebGIS is being set up to visualise and emphasise the spatial context of local samples, measurements, and analyses versus the thematic background information (e.g., geomorphology, pedology, geology and vegetation), using the WebGIS infrastructure "maps@awi" at the Alfred Wegener Institute, Helmholtz Centre for Polar and Marine Research (AWI). The CarboPerm WebGIS database includes historical data from long-term Russian-German cooperation and recent field campaigns as well as environmental datasets that are freely available via the internet or research data repositories.

Zusammenfassung: Permafrost-Landschaften reagieren sehr sensibel auf den Klimawandel. Die Synthese von Forschungsdaten und Metadaten über diese Gebiete und deren Visualisierung in einem interoperablen, weltweit zugänglichen System ist von hohem Nutzen für Wissenschaft und Gesellschaft. Innerhalb des Permafrost-Forschungsprojektes CarboPerm wird für das Lena-Delta und die Laptevmeer-Region ein WebGIS-Projekt entwickelt, welches die wissenschaftliche Forschertätigkeit durch Datenmanagement, Datenvisualisierung und Datenpublikation unterstützt. CarboPerm ist ein interdisziplinäres deutsch-russisches Kooperationsprojekt, das die Bildung, den Umsatz und die Freisetzung von Kohlenstoff in sibirischen Permafrost-Landschaften untersucht. Der Fluss Lena hat das größte Delta in der Arktis ausgebildet und ist gleichzeitig ein Kerngebiet langjähriger russisch-deutscher Kooperation in der Permafrost-Forschung. Das CarboPerm WebGIS wurde ins Leben gerufen, um den räumlichen Bezug von lokalen Probennahmen, Messergebnissen und Analysen mit thematischen Hintergrundinformationen, wie z.B. Geomorphologie, Pedologie, Geologie und Vegetation zu visualisieren. Die CarboPerm-WebGIS-Datenbank entstand unter Nutzung der WebGIS-Infrastruktur „maps@awi" am Alfred-Wegener-Institut, Helmholtz-Zentrum für Polar- und Meeresforschung (AWI). Sie beinhaltet sowohl historische Daten aus der langjährigen russisch-deutschen Kooperation als auch von aktuellen Geländekampagnen, sowie umweltrelevante räumliche Datensätze, die aus öffentlich zugänglichen Datenquellen und Daten-Repositorien stammen.

doi:10.2312/polfor.2016.010

[1] Alfred Wegener Institute Helmholtz Centre for Polar and Marine Research, Am Handelshafen 12, 27570 Bremerhaven, Germany.
[*] Corresponding author: <antonie.haas@awi.de>
[2] Alfred Wegener Institute Helmholtz Centre for Polar and Marine Research, Telegrafenberg, 14473 Potsdam, Germany.
[3] University of Hamburg, Allende-Platz 2, 20146 Hamburg, Germany.
[4] German Research Centre for Geosciences GFZ, Telegrafenberg, 14473 Potsdam, Germany.
[5] Arctic and Antarctic Research Institute AARI, St. Petersburg and St. Petersburg State University, Russia.

This paper represents a supplement to the International Conference "Our Climate – Our Future: Regional perspectives on a global challenge", 6–9 October 2014 in Berlin, Germany.
Manuscript received 17 June 2015; revised version 3 March 2016; accepted 5 April 2016.

MOTIVATION AND CHALLENGES

Permafrost research in Siberia has been carried out by Russian scientists for centuries, and for decades, Russian-German collaboration has initiated joint expeditions and established long-term measurements, specifically in the Laptev Sea region. The research subjects are diverse and range from specific permafrost-related to paleoclimate or environmental studies, to measurements of vertical and lateral fluxes of carbon, energy, and water, or assessing the permafrost landscape stocks of carbon and nutrients. Geophysical, geomorphological, pedological, geobotanical, cryological, hydrological, geochemical, biogeochemical, and biological data have been collected on the land, along the coast, and in the sea. In the central Lena Delta, a multi-parameter, long-term measurement field for permafrost-related parameters has been installed on the Island Samoylov. Here, long-term time series have been published (Boike et al. 2013, 2015). Supported by bilateral and international programmes and by the modern research basis "Samoylov Station" (Fig. 1) in the Lena Delta since 2013 (operated by the Trofimuk Institute for Petroleum Geology and Geophysics, Siberian Branch, Russian Academy of Sciences), the data collection by interdisciplinary international teams in the Lena Delta Region has intensified.

Large-scale research programmes focusing on the Laptev Sea region are for example: CarboPerm, the EU FP7 project PAGE21 and PETA-CARB "Rapid Permafrost Thaw in a Warming Arctic and Impacts on the Soil Organic Carbon Pool". CarboPerm is funded by the German Federal Ministry of Education and Research (BMBF) 2013-2016 and combines multi-disciplinary investigations by Russian and German permafrost scientists, focusing on the formation, turnover and release of carbon and nutrients. PAGE21 is a large-scale international collaborative project within the research field "Vulnerability of Arctic permafrost to climate change and implications for global GHG emissions and future climate", funded within the Seventh Framework Programme of the European Union between 2013 and 2015, co-ordinated by the Alfred Wegener Institute Helmholtz Centre for Polar and Marine Research (AWI). Results of PAGE21 were the optimisation of monitoring processes, process studies and modelling for permafrost landscapes. The European Research Council (ERC) is funding PETA-CARB from 2013–2018 to investigate and quantify the permafrost organic carbon pools and to build up the Arctic Permafrost Geospatial Centre (APGC), a data centre for the collection and visualisation of permafrost-related data. To strengthen the communication between all the partners, there is the need for data curation and, especially, data visualisation in the Laptev Sea region.

Fig. 1: Approaching the Russian research station Samoylov on Samoylov Island, Lena River Delta by helicopter (photo A. Morgenstern AWI, June 2015). "Samoylov Station" is the logistic base for permafrost research in the Laptev Sea Region, operated by the Trofimuk Institute for Petroleum Geology and Geophysics, Siberian Branch, Russian Academy of Sciences.

Abb. 1: Schrägaufnahme aus dem Hubschrauber im Anflug auf die russische Forschungsstation „Samoylov Station" auf der Samoylov-Insel im Lena-Delta (Foto A. Morgenstern, AWI, Juni 2015). Die „Samoylov Station" ist die logistische Basis für Permafrostforschung in der Laptewmeer-Region, die durch das Trofimuk Institute for Petroleum Geology and Geophysics, Siberian Branch, Russian Academy of Sciences betrieben wird.

However, which technology/platform would support this intention? Geographic Information System (GIS) server technology has been improving greatly and web-based data visualisation has been expanding steadily. Furthermore, desktop GIS' fundamental advantage is its feasibility to store and operate, besides raster data, three different feature data types (points, lines and polygons) that are put into relation by their geographic position. Regardless of their scientific source, data integration solely depends on its position. In environmental science, a large variety of data can be represented by these three feature types, and desktop GIS have become very popular during the last decade. Additionally, desktop GIS software is not only capable of data analysis and map creation, but also provides tools for data management, such as data catalogue functionalities and metadata editing. This implies that GIS server and desktop GIS technology support scientific work at all levels, from data collection and data processing to data management and data visualisation, by the publication of web services. Based on this, AWI has established a comprehensive GIS infrastructure. The GIS architecture offers an easy-to-use pathway from desktop GIS to GIS server, by sharing a data base management system and a specific folder system. Scientists may manage their data and layers either as a single data layer or as a collection of specific data layers, using desktop GIS. All data products are published as web services and embedded and displayed within a GIS viewer application.

In this case study, we illustrate the implementation of the CarboPerm WebGIS project, using the AWI GIS infrastructure and data originating from the long-term Russian-German cooperation, recent field campaigns as well as environmental datasets that are freely available via the internet or published via research data repositories (e.g., PANGAEA). Elger et al. (2016) give an overview on DOI-referenced data publication and selected data repositories.

CARBOPERM WEBGIS AT MAPS@AWI

The CarboPerm WebGIS is continuously developed within the AWI GIS infrastructure, which enables the development of WebGIS services for project-specific data. The core components are ArcGIS for Server, a PostgreSQL database including Spatial Database Engine (SDE), and desktop GIS software. Data uptake, editing and manipulation can be accomplished by using the ArcGIS desktop application. An intuitive editor ensures that metadata and project descriptions follow ISO standards. Published WebGIS projects and related descriptions are added to "maps@awi", the openly accessible unit for searching and displaying WebGIS projects at AWI. Here, data can be actively visualised by zooming, panning or enabling/disabling layers on appropriate background maps. The CarboPerm WebGIS can be accessed from "maps.awi.de" or via the respective project website.

In 2015, the CarboPerm WebGIS database contained nine feature layers focusing on three major subjects:

(I) Field data from joint Russian-German investigations,
(II) regional datasets from joint Russian-German investigations,
(III) circumpolar or large-scale publicly available spatial datasets.

In addition to the project-specific data, a high-resolution world imagery web service was implemented as background map (World Imagery). At present, multi-point vector-data layers are displayed to visualise the locations of samples or measurements, such as, "discharge measurements" (FEDOROVA et al. 2013) and "sediment cores (carbon, nitrogen)" (ZUBRZYCKI et al. 2013b). Additionally, line and polygon vector-layers represent features related to geomorphology, geology, cryology, or botany, including "Lena Delta terraces" (MORGENSTERN et al. 2011) and "Yedoma" (GROSSE et al. 2013).

In what follows, we give an overview on the visualized GIS layers that have been implemented:

I Field data from joint Russian-German investigations (Fig. 2):
  a) Geochemical data from sediment cores (ZUBRZYCKI et al. 2013b) published as a data supplement to ZUBRZYCKI et al. (2013a) in PANGAEA.
  b) Long-term time series of hydrographic measurements (e.g., discharge) measured in different Lena River branches and published in PANGAEA (FEDOROVA et al. 2013), and later linked as a data supplement to FEDOROVA et al. (2015).

II Regional datasets from joint Russian-German investigations:
  • Second and third geomorphological main terraces of the Lena Delta published in PANGAEA as GIS-compatible vector layers (MORGENSTERN et al. 2011). Detailed lithology and overview on the main geomor-

Fig. 2: Regular water sampling of meltwater from the Yedoma cliffs in the Lena Delta in late summer 2014 during maximum of ground-ice thaw and run-off of melt waters. Water samples will be analysed for dissolved organic carbon (DOC), coloured dissolved organic matter (cDOM), water isotopes (hydrogen and oxygen) and anorganic hydrochemistry (cations and anions) (photo B. Heim, AWI, 2014).

Abb. 2: Regelmäßige Beprobung des Schmelzwassers der Yedoma-Klippen im Lena-Delta im Spätsommer 2014 zur Zeit des maximalen Tauens des Yedoma-Grundeises und stärksten Schmelzwasserabflusses. Untersucht wird auf gelösten organischen Kohlenstoff (DOC), Gelbstoff (cDOM), Wasserisotope (Wasserstoff und Sauerstoff) und anorganische Hydrochemie (Kationen, Anionen) (Foto B. Heim, AWI, 2014).

phological terraces of the Lena Delta is described in Schwamborn et al. (2002b) with sedimentological data published in PANGAEA (Schwamborn et al. 2002a) that are being prepared for CarboPerm WebGIS visualisation in group I.

- Lena Delta lakes (>20 ha) published in PANGAEA as GIS-compatible vector layers (Morgenstern et al. 2011).

These regional geomorphological and hydrographic GIS data layers are frequently downloaded from PANGAEA and already widely used within the research groups working in the Laptev Sea region.

III Freely available environmental data from the World Wide Web:

Feature layers with geomorphological, pedological, land cover, and permafrost units were selected due to beneficial aspects in visualising environmental data. These datasets are publicly available, but not well known outside the actively working communities.

- The "Yedoma" GIS layer displays a geomorphological, organic-rich (about 2 % carbon by mass), Pleistocene-age permafrost layer with an average ice content of 50-90 % by volume. The data for the Siberian "Yedoma" areas was made publicly available by the USGS (Grosse et al. 2013).
- The "Soil Organic Carbon Content" GIS layer is derived from the Northern Circumpolar Soil Carbon Database produced by Hugelius et al. (2013).
- The Land Cover unit ("Soil Types", "Vegetation Ecosystems" and "Wetland Ecosystems") GIS layers are derived from the Land Resources of Russia (Stolbovoi & Savin 2002). This resource, first published in 2002, houses a collection of geo-referenced databases for socio-economics, environmental conditions and land endowment of the Russian territory, compiled by the International Institute for Applied Systems Analyses (IIASA).
- The "Permafrost Zones" (continuous, discontinuous and sporadic) GIS layer is derived from the circumpolar permafrost and ground ice unified international data based on the original 1:10,000,000 paper map called "Circum-Arctic map of permafrost and ground-ice conditions". The corresponding GIS data are published as revised digital datasets by the National Snow and Ice Data Center (NSDIC) (Brown et al. 2001).
- The Data User Element (DUE) Permafrost Digital Elevation Model (DEM) (Santoro & Strozzi 2012) with a high spatial resolution of 100 × 100 m cell size published in PANGAEA as (DUE Permafrost Project Consortium 2012). Up to date, there exists no global DEM data north of 60° with such high resolution, the default spatial resolution of available global DEM data sets being 1 km x 1 km cell size.

Figure 3 shows the WebGIS visualisation with selected datasets for the major themes: I) field data II) regional data sets and III) global data sets.

DISCUSSION

Environmental researchers, especially those working in remote locations, have become increasingly aware of the vast potential of GIS and WebGIS technologies. Hence, it is no surprise that the number of datasets in GIS-specific formats and the availability of GIS data are raising continuously. Several data repositories, such as PANGAEA or data portals like the EMODnet central portal, make research data freely accessible in usable formats for GIS applications.

Publishing research data as WebGIS services offers several advantages. GIS focuses on well-designed, highly informative maps and data layers, and not on written text. Subsequently, WebGIS layers of any scale and information density transport information through visualisation. This not only promotes the attractiveness of the data products but allows displaying the data and information in an environment that is often very interdisciplinary and, in varying degrees, technically interactive.

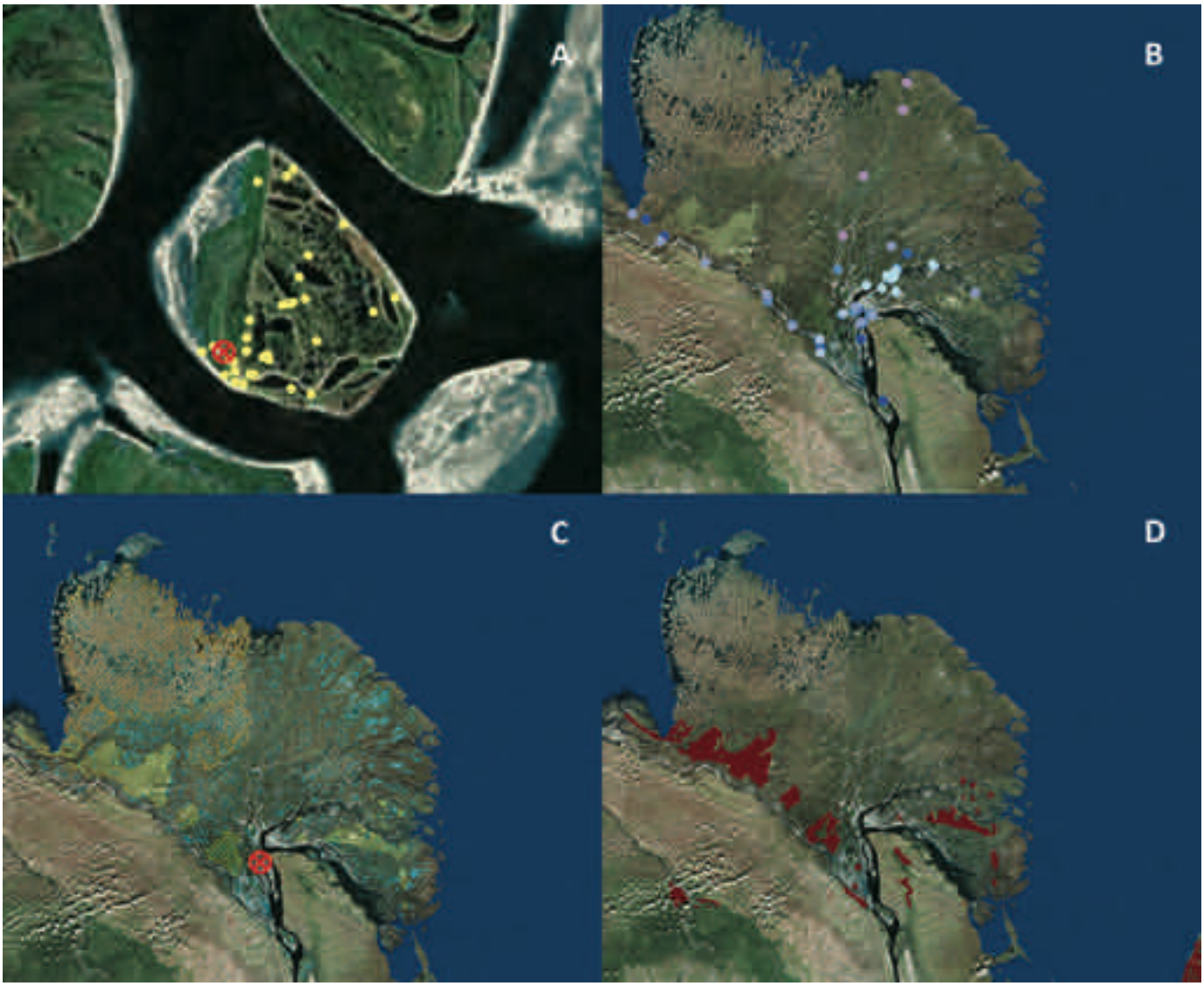

Fig. 3: CarboPerm WebGIS features overlay the background map (World Imagery) focusing on the Lena River Delta. A: Samoylov Island (horizontal scale about 2.3 km), yellow symbols show soil geochemical sampling locations (ZUBRZYCKI et al. 2013b); red-crossed circle indicates location of "Samoylov Station". B-D: Lena River Delta (horizontal scale about 250 km); B: blue symbols show discharge measurement sites for different years (FEDOROVA et al. 2013); C: yellow and orange hatched polygons display geomorphological terraces and blue polygons display lakes (MORGENSTERN et al. 2011); D: brown polygons display Yedoma units (GROSSe et al. 2013).

Abb. 3: Verschiedene CarboPerm WebGIS Informationsebenen für den Bereich Lena-Delta, dargestellt auf der WebGIS Hintergrundkarte (World Imagery). A: Insel Samoylov (horizontaler Maßstab ca. 2,3 km), gelbe Punkte zeigen die Probenahmestellen für geochemische Bodendaten (ZUBRZYCKI et al. 2013b); roter Kreis mit Kreuz zeigt die Position „Samoylov-Station". B-D: Übersichten über das Lena-Delta (horizontaler Maßstab ca. 250 km); B: blaue Symbole zeigen die Messstellen für Durchfluss-Messungen über verschiedene Jahre (FEDOROVA et al. 2013); C: gelb und orange schraffierte Polygone zeigen geomorphologische Terrassen und blaue Polygone die Seen (MORGENSTERN et al. 2011); D: rot-braune Polygone beschreiben die Yedoma-Einheiten (GROSSE et al. 2013).

However, scientists prepare their data products to comply with their own or scientific standards. Data products intended to be visualised and published as WebGIS services have also to satisfy specific technical requirements, including standardised metadata and are primarily operated by experienced GIS and administrative personnel. The development of specific WebGIS services like CarboPerm by a broader community, therefore, requires predefined data-management structures and how-to-use/preparation information. At AWI, a user manual was created to guide scientists through the data preparation and editing process, to provide insights into internal data structuring and related layout requirements. Additionally, a GIS-viewer template, including test data, was published to demonstrate GIS-viewer functionalities and show existing data-manipulation tools that may be plugged into the respective GIS project. Both, the user manual and the GIS-viewer template are easy-to-use services that shall encourage even colleagues who are less experienced in GIS to visualise and publish their data as WebGIS services. To guarantee sufficient metadata for re-use, scientists are encouraged to archive their (GIS) datasets in a data repository such as PANGAEA, preferably with a product guide to ensure documentation and sustainability, before adding them to the WebGIS. Most data repositories are attaching digital object identifier (DOI) to their dataset, thereby guaranteeing their long-term availability and citability. For more than a year now, the citation of dataset DOIs and their integration in reference lists of journal articles are widely accepted by most publishers and data centers. A

major step for this development that is also described in Elger et al. (2016), was the "Statement of Commitment by the Coalition for Publishing Data in the Earth and Space Sciences" (COPDESS, Hanson et al. 2015) and the FORCE11 initiative that developed a set of principles for data citation that is widely endorsed (Data Citation Synthesis Group 2014).

Once all GIS data layers are prepared, scientists just have to drop their project descriptions into a specific folder, which is shared with the GIS administrator, who subsequently operates the GIS data layer publishing process and creates the WebGIS project. Finally, the newly established WebGIS project and its description are added to "maps@awi" and made publicly accessible.

In addition to the CarboPerm WebGIS project, WebGIS projects for the Southern Ocean, Antarctica, the North and the Baltic Seas are available at "maps@awi". Some WebGIS projects have already been completed, whereas others are going on. The CarboPerm WebGIS is an ongoing project for which data preparation has recently started. It is an initial starting point to demonstrate the capabilities and benefits of such systems in a practical way while targeting a specific scientific community. It subsequently encourages scientists to contribute their own data. Despite being a project-related WebGIS, selected GIS layers in the CarboPerm WebGIS are already accessible via data portals of the United States Geological Survey (USGS), the National Snow and Ice Data Center (NSDIC), the International Institute for Applied System Analysis (IIASA) or published through data repositories or described in journal articles like, e.g., Earth Systems Science Data (ESSD).

The data assembly of the CarboPerm WebGIS follows the strategy of a previous international-Russian WebGIS project, the EU CONTINENT Baikal WebGIS (Heim et al. 2008). Within the EU CONTINENT Baikal WebGIS, a variety of already openly accessible data were preselected to provide mesoscale environmental background information together with the project-specific field data. Within the CONTINENT Baikal WebGIS data assembly, datasets from the Land Resources of Russia (IIASA; Stolbovoi & Savin 2002) provided relevant environmental background information.

Within the CarboPerm WebGIS data assembly activities, AWI is currently assessing the usability of various openly accessible datasets whose thematic content is reliable and usable, since they are reviewed by our user communities or have even been produced by collaborating research teams. Grosse et al. (2013) mapped the Yedoma areas and Hugelius et al. (2013) compiled the Circum-Arctic map of organic soil content. Morgenstern et al. (2011) derived the lake water objects of the Lena Delta and mapped in cooperation with Russian scientists the extent of the Lena Delta terraces. Bringing these already published data together within a broader spatial and thematic context provides an added-value to the interdisciplinary scientific communities. However, data visualisation and compilation sometimes exposes artefacts and inconformi-

Fig. 4: "Maps@awi" – Web access to all AWI WebGIS projects including CarboPerm and Yamal WebGIS projects.

Abb. 4: „Maps@awi" – Webzugang zu allen AWI WebGIS-Projekten einschließlich der CarboPerm- und Yamal-WebGIS-Projekte.

ties, such as geometric misfits unrelated to coordinate system transformations. In these instances, further detailed investigations are required. Over time, these data revisions will help to maintain homogenous and interoperable datasets. Therefore, specific WebGIS projects can support these processes substantially.

OUTLOOK

A further mesoscale AWI-based WebGIS project, focusing on Russian-German permafrost research, is currently being implemented for the central Yamal Region in cooperation with the Earth Cryosphere Institute in Tyumen, Russia: the Yamal WebGIS (Dvornikov et al. 2016, see also Fig. 4). The Yamal and the CarboPerm WebGIS projects will be explored and further enhanced by our user communities.

Furthermore, both WebGIS projects highlight the Russian-German scientific activities in Siberia, raising the scientific and political awareness. At the moment, these WebGIS projects are in an initial state, but their scalability is guaranteed by the AWI-GIS infrastructure.

In the future, freely accessible data will be published in formats, complying with standards of the Open Geospatial Consortium (OGC), the OpenGIS® Web Map Service Interface Standard (WMS) or Web Feature Service (WFS), and therefore will further support data exchange. The integration of additional functionalities within the GIS-viewer is planned to include simple data manipulation tools (e.g., select, search and download) and links to data providers such as institutes, repositories and portals like the Arctic Permafrost Geospatial Centre (coordinated by the ERC PETA-CARB project) or Russian information websites.

ACKNOWLEDGMENTS

The authors would like to thank Jens Klump and one anonymous reviewer for their careful review and helpful suggestions. We are grateful to Klaus Grosfeld for his ongoing assistance. We also would like to thank Frauke Thiele-Wolff for her support with the graphics and Laura Hehemann for proof reading. The authors acknowledge the Helmholtz Climate Initiative REKLIM (Regional Climate Change), a joint research project of the Helmholtz Association of German Research Centres (HGF). The Russian-German expeditions are supported and organized by the AWI (Germany) and the AARI (Russia).

List and Explanation of Acronyms

AARI	Arctic and Antarctic Research Institute
ArcGIS	Geographical information system for working with maps and geographical information developed by the Economic and Social Research Institute ESSRI
APGC	Arctic Permafrost Geospatial Centre
AWI	Alfred Wegener Institute Helmholtz Centre for Polar and Marine Research
BMBF	German Federal Ministry of Education and Research
COPDESS	Statement of Commitment by the Coalition for Publishing Data in the Earth and Space Sciences
CarboPerm	Interdisciplinary German project with Russian cooperation, investigating the formation, turnover and release of carbon in Siberian permafrost landscapes
DEM	Digital Elevation Model
DOI	Digital object identifier
DUE	Data User Element
EMODnet	Central portal of the European marine observation and data network
ERC	European Research Council
ESSD	Earth Systems Science Data
FORCE11	Future of research communication and e-scholarship
GHG	Greenhouse gase
GIS	Geographic Information System
IIASA	International Institute for Applied Systems Analyses
USGS	United States Geological Survey
NSDIC	National Snow and Ice Data Center
OGC	Open Geospatial Consortium
PAGE21	Changing Permafrost in the Arctic and its Global Effects in the 21st Century.
PANGAEA	Data Publisher for Earth & Environmental Science
PETA-Carb	Rapid Permafrost Thaw in a warming Arctic and Impacts on the Soil Organic Carbon Pool
PostgreSQL	Object-oriented database management system
SDE	Spatial Database Engine
USGS	United States Geological Service
WMS	OpenGIS® Web Map Service Interface Standard
WFS	Web Feature Service

References

CarboPerm <www.carboperm.net> Interdisciplinary Russian-German project on the formation, turnover and release of carbon in Siberian permafrost landscapes (accessed 18 April 2016).

Data Citation Synthesis Group (2014): Joint Declaration of Data Citation Principles.- M. Martone (ed), San Diego Canada, FORCE11, URL: <https://www.force11.org/datacitation> (accessed 11 December 2015).

COPDESS <www.copdess.org> Coalition for Publishing Data in the Earth and Space Sciences (accessed 18 April 2016).

EMODnet <www.emodnet.eu> Central Portal of the European marine observation and data network (accessed 18 April 2016).

maps@awi <http://maps.awi.de> Alfred Wegener Institute GIS maps portal (accessed 18 April 2016).

Northern Circumpolar Soil Carbon Database <www.bolin.geo.su.se/data/ncscd/> Bolin Centre Database (accessed 18 April 2016).

PAGE21 <www.page21.eu> Changing Permafrost in the Arctic and its Global Effects in the 21st Century (accessed 18 April 2016).

PANGAEA <www.pangaea.de> Data Publisher for Earth & Environmental Sciences (accessed 18 April 2016).

World Imagery <http://services.arcgisonline.com/> ArcGIS - Geographic information system of the Environmental Systems Research Institute (ESRI) (accessed 18 April 2016).

Yamal WebGIS <maps.awi.de/yamal> Yamal WebGIS at the Alfred Wegener Institute GIS maps portal (accessed 18 April 2016).

Boike, J., Kattenstroth, B., Abramova, K., Bornemann, N., Chetverova, A., Fedorova, I., Fröb, K., Grigoriev, M., Grüber, M., Kutzbach, L., Langer, M., Minke, M., Muster, S., Piel, K., Pfeiffer, E.-M., Stoof, G., Westermann, S., Wischnewski, K., Wille, C. & Hubberten, H.-W. (2013): Baseline characteristics of climate, permafrost and land cover from a new permafrost observatory on Samoylov Island, Lena River Delta, Siberia.- Data citation, doi: 10.1594/PANGAEA.806233.

Boike, J., Georgi, C., Kirilin, G., Muster, S., Abramova, K.A., Fedorova, I.A., Chetverova, A., Grigoriev, M.N., Bornemann, N. & Langer, M. (2015): Temperature, water level and bathymetry of thermokarst lakes in the continuous permafrost zone of northern Siberia - Lena River Delta, Siberia.- Data citation, doi: 10.1594/PANGAEA.846525.

Brown, J., O.J. Ferrians, O.I. Jr., Heginbottom, J.A. & E.S. Melnikov, E.S. (2001): Circum-Arctic map of permafrost and ground ice conditions.- National Snow and Ice Data Center. Digital media, Boulder, Colorado, USA. DUE Permafrost Project Consortium (2012): ESA Data User Element (DUE) Permafrost: Circumpolar Remote Sensing Service for Permafrost (Full Product Set) with links to data sets, doi: 10.1594/PANGAEA.780111.

Dvornikov, Y., Leibman, M., Heim, B., Bartsch, A., Haas, A., Khomutov, A., Gubarkov, A., Mikhaylova, M., Mullanurov, D., Widhalm, B., Skorospekhova, T. & Fedorova, I. (2016): Geodatabase and WebGIS project for long-term permafrost monitoring at the Vaskiny Dachi research station, Yamal, Russia.- Polarforschung 85: 107–115.

Elger, K., Biskaborn, B., Pampel, H. & Lantuit, H. (2016): Open research data, data portals and data publication – an introduction to the data curation landscape.- Polarforschung 85: 119–133.

Fedorova, I., Bolshiyanov, D. Y, Chetverova, A., Makarov, A. & Tretiyakov, M. (2013): Measured water discharges, suspended supply and morphometric parameters of cross-sections in the Lena River Delta during summer period 2002-2012.- Data citation, doi: 10.1594/PANGAEA.808854.

Fedorova, I., Chetverova, A., Bolshiyanov, D., Makarov, A., Boike, J., Heim, B., Morgenstern, A., Overduin, P.P., Wegner, C., Kashina, V., Eulenburg, A, Dobrotina, E. & Sidorina, I. (2015): Lena Delta hydrology and geochemistry: long-term hydrological data and recent field observations.- Biogeosci. 12: 345-363, doi: 10.5194/bg-12-345-2015.

Grosse, G., Robinson, J.E., Bryant, R., Taylor, M.D., Harper, W., DeMasi, A., Kyker-Snowman, E., Veremeeva, A., Schirrmeister, L. & Harden, J. (2013): Distribution of late Pleistocene ice-rich syngenetic permafrost of the Yedoma Suite in east and central Siberia, Russia.- U.S. Geol. Survey Open-File Report 2013-1078, 1-24.

Hanson, B., Lehnert, K. & Cutcher-Gershenfeld, J. (2015): Committing to publishing data in the Earth and space sciences.- Eos 96, doi: 10.1029/2015EO022207.

Heim, B., Klump, J., Oberhaensli, H. & Fagel, N. (2008): Assembly and concept of a web-based GIS within the paleoclimate project CONTINENT.- J. Paleolimnol. 39: 567-584, doi: 10.1007/s10933-007-9131-0.

Hugelius, G., Tarnocai, C., Broll, G., Canadell, J.G., Kuhry, P. & Swanson, D.K. (2013): The Northern Circumpolar Soil Carbon Database: spatially distributed datasets of soil coverage and soil carbon storage in the northern permafrost regions.- Earth Syst. Sci. Data 5: 3-13, doi: 10.5194/essd-5-3-2013.

Morgenstern, A., Röhr, C., Grosse, G. & Grigoriev, M.N. (2011): The Lena River Delta - inventory of lakes and geomorphological terraces.- Alfred Wegener Institute - Research Unit Potsdam, doi: 10.1594/PANGAEA.758728.

Schwamborn, G., Rachold, V. & Grigoriev, M.N. (2002a): Sedimentation and mineral analysis on sediment cores from the Lena Delta.- Data citation, doi: 10.1594/PANGAEA.728539.

Schwamborn, G., Rachold, V. & Grigoriev, M.N. (2002b): Late Quaternary Sedimentation History of the Lena Delta.- Quat. Internat. 89: 119-134, doi: 10.1016/S1040-6182(01)00084-2.

Santoro, M. & Strozzi, T. (2012): Circumpolar digital elevation models >55° N with links to geotiff images.- Data citation, doi: 10.1594/PANGAEA.779748.

Stolbovoi, V. & Savin, I. (2002): Land Resources of Russia compiled by the International Institute for Applied Systems Analyses (IIASA) and the Russian Academy of Sciences (RAS Maps of Land Cover.- In V. STOLBOVOI & I. MCCALLUM (eds), CD-ROM Land Resources of Russia, Laxenburg, Austria: International Institute for Applied Systems Analysis and the Russian Academy of Science, CD-ROM, available at <http://www.iiasa.ac.at/Research/FOR/russia_cd/guide.htm>.

Zubrzycki, S., Kutzbach, L., Grosse, G., Desyatkin, A. & Pfeiffer, E.-M. (2013a): Organic carbon and total nitrogen stocks in soils of the Lena River Delta.- Biogeosci. 10: 3507-3524, doi: 10.5194/bg-10-3507-2013.

Zubrzycki, S., Kutzbach, L., Grosse, G., Desyatkin, A. & Pfeiffer, E.-M. (2013b): Organic carbon and total nitrogen stocks in soils of the Lena River Delta.- Data citation, doi: 10.1594/PANGAEA.826958.

Polarforschung 85 (2), 143–155, 2015 (erschienen 2016)

Online Sea-Ice Knowledge and Data Platform <www.meereisportal.de>

by Klaus Grosfeld[1*], Renate Treffeisen[1], Jölund Asseng[1], Annekathrin Bartsch[1], Benny Bräuer[1], Bernadette Fritzsch[1], Rüdiger Gerdes[1], Stefan Hendricks[1], Wolfgang Hiller[1], Georg Heygster[2], Thomas Krumpen[1], Peter Lemke[1], Christian Melsheimer[2], Marcel Nicolaus[1], Robert Ricker[1] and Marietta Weigelt[1]

Abstract: The combination of multi-disciplinary sea ice science and the rising demand of society for up-to-date information and user customized products on climate change emphasis the need for addressing the challenges posed by environmental change in the Polar Regions by means of creating new ways of communication.
The new knowledge platform "meereisportal.de" is a contribution to the cross-linking of scientifically qualified information on climate change and focuses deliberately on the theme: "sea ice" in both Polar Regions. With "meereisportal.de" the science opens to changing societal demands and goes new ways of communication between science and society. "meereisportal.de" is the first comprehensive German speaking knowledge platform on sea ice that went online 2013. It was developed in the frame of the Helmholtz Climate Initiative, Regional Climate Change (REKLIM) as a joint project of the University of Bremen (Institute of Environmental Physics) and the Alfred Wegener Institute, Helmholtz Centre for Polar and Marine Research under the management of the Helmholtz Regional Climate Office for Polar Regions and Sea Level change. This paper describes the concept and the development of the knowledge platform, different usage examples and user-specific products. Moreover, an outlook on the planned activities in the future will be given.

Zusammenfassung: Die Kombination der zunehmend multi-disziplinären Meereisforschung und die steigende Nachfrage der Gesellschaft nach aktuellen Informationen und benutzerorientierten Produkten zum Thema Klimawandel erfordert neue Wege der Wissenskommunikation, um den Herausforderungen der zunehmenden Umweltveränderungen, insbesondere in den Polarregionen, zu begegnen.
Die neue Wissensplattform "meereisportal.de" ist ein Beitrag zum Vernetzen von wissenschaftlich qualifizierten Fachinformationen zum Thema Klimawandel und fokussiert dabei bewusst auf ein Thema: "Meereis" in beiden Polargebieten. Mit "meereisportal.de" öffnet sich die Wissenschaft gegenüber sich verändernden gesellschaftlichen Anforderungen und geht neue Wege der Kommunikation zwischen Wissenschaft und Gesellschaft. "meereisportal.de" ist 2013 als erste umfassende, deutschsprachige Wissensplattform rund um das Thema Meereis in der Arktis und Antarktis online gegangen. Sie wurde im Rahmen des Helmholtz-Verbundes Regionale Klimaveränderungen (REKLIM) als Gemeinschaftsprojekt der Universität Bremen (Institut für Umweltphysik) und des Alfred-Wegener-Institutes, Helmholtz-Zentrum für Polar- und Meeresforschung unter der Federführung des regionalen Helmholtz Klimabüros für Polargebiete und Meeresspiegelanstieg entwickelt. Dieser Beitrag beschreibt die Entstehung, das Konzept und die Entwicklung der Wissensplattform, verschiedene Anwendungsbeispiele sowie nutzerspezifische Produkte. Darüber hinaus wird ein Ausblick über die in Zukunft geplanten Aktivitäten gegeben.

INTRODUCTION

Stopping or at least slowing down climate change with its far-reaching and regionally varying consequences for humanity and nature is one of the great challenges of the 21st century. The Earth is undergoing profound climate change. Particularly, the Polar Regions are very sensitive to even slight climate changes. They play a paramount role for the global climate system. Whether we are able to adapt in time to the imminent changes will largely depend on whether the results from research and science are communicated and processed to an adequate degree and, hence, will be useful for government, economy and society in decision-making. Therefore, the importance of knowledge transfer of research results has grown in recent decades. Research institutes are obliged to disseminate their research results and knowledge to society and enter into a dialogue with society.

The need for the development of "meereisportal.de" was driven by various aspects, which will be shortly addressed in the following. The increasing interest of society to benefit from research results leads to the pressure to transfer research results into application and to interact directly with its users, as there is a big agreement that citizens get easy access to the results of research they have paid tax for. Policies and measures that mobilise these intellectual assets for a use through a broader access can accelerate scientific breakthroughs, increase innovation, and promote economic growth. That's why it is of growing importance to ensure that results of public-funded scientific research are made available to and useful for the public, industry, and the scientific community (Scott 2000).

Therefore, for example the European science policy as well as that of national governments has more and more set priorities for research to serve the requirements of society and have set increasingly ambitious targets for public research funding bodies in terms of the impact or application of their research. Communicating and interacting with the public about research outcomes presents a novel type of challenge and is of vital importance. However, it is clear that the landscape of scientific research communication is being transformed as the web gains increasing influence and alters how we interact with information. However, in facing urgent global issues like climate change, researchers cannot continue to share their findings only with their colleagues and scientific community through peer-reviewed scientific journals.

While the purpose of restricted-access, peer-reviewed journals is to ensure scientific quality and to communicate research outcomes to peers, the goal of open access, web-based dissemination is also to promote widespread public debate and to increase the speed of research feedback. Both, the restrict-

doi:10.2312/polfor.2016.011

[1] Alfred Wegener Institute, Helmholtz Centre for Polar and Marine Research (AWI), Bussestraße 24, D-27570 Bremerhaven, Germany.
[*] Corresponding authors: <klaus.grosfeld@awi.de> <renate.treffeisen@awi. de>
[2] Institute of Environmental Physics (IUP) University of Bremen, PO Box 330440, D-28334 Bremen, Germany.
This paper was presented as a poster presentation at the International Conference "Our Climate – Our Future: Regional perspectives on a global challenge", 6–9 October 2014 in Berlin, Germany.
Manuscript received 31 July 2015; accepted in revised form 28 December 2015.

ed-access and the open access are legitimate approaches and can co-exist effectively. Consequently, one major objective has to be to encourage scientists not to limit themselves to journals, but to engage with the public via other channels (Barett et al. 2014).

Another important point to be taken into account is that 'the public' is not a homogeneous population; rather it encompasses numerous sub-groups such as policy makers, researchers, journalists, environmentalists and many others. Each of these groups forms a distinct audience, looking for information that answers their questions and concerns with an appropriate level of detail. For this reason it is necessary that information fits the expectations, needs, interests, and knowledge background of these various potential user groups. Different users will require knowledge presented and visualised in different ways. Briefly this means: getting the right knowledge, in the right form, in the right place, to the right person, at the right time. There are many ways to channel information of scientific research results. Among these, the Internet plays a major role in contributing to improve public awareness (Breyer et al. 2007). The advantage of web-based methods compared with conventional communications channels is a huge opportunity to share the outcomes of scientific research more extensively and quickly across the entire society.

Sea ice was chosen for implementation of these communication and dialogue processes described above because it plays an important role in the climate system and so far mostly English based web platforms with focus on sea ice exist. Furthermore, information in German is scattered on webpages of various research institutes (Tab. 1). For example, the portal of the University of Bremen provides daily updated hemispherical and regional maps of sea-ice concentration and an archive of this data since 2002 when the satellites sensor AMSR-E became operational. The portal is in English and gives little background information beyond the map explanations. Considering language barriers, this fact prevents a considerable group from the access to information and data products. As a consequence science-based tailored information, customized products and services on sea ice are hardly asked for and various possible important target groups are not reached. For this reason, the public perception about sea ice, its variability and its role in the climate system is rather incomplete.

Platform Language	Responsible institutions	Target group	Services
nside.org English	[1)]NSIDC, USA	scientists, public	NSIDC manages and distributes scientific data, creates tools for data access, supports data users, performs scientific research, and educates the public about the cryosphere.
fram-data.awi.de English	[2)]AWI, Germany	scientists	The content displayed in this webpage consists mainly of validated track lines, publications and reports from EPIC repository and primary data from PANGAEA-Data Publisher for Earth & Environmental Science.
iup.uni-bremen.de:8084/amsr2 English	[3)]IUP, Germany	scientists	Provides daily updated hemispherical and regional maps and an archive starting with the sensor AMSR-E in 2002.
icdc.zmaw.de/daten/cryosphere.html English / German	Universität Hamburg, Germany	scientists, public	Extensive data collection on various data products but only very small background information.
aoos.org/ice-atlas English	[4)]AOOS, USA	scientists, public	AOOS represents a network of critical ocean and coastal observations, data and information products that aid our understanding of the status of Alaska's marine ecosystem and allow stakeholders to make better decisions about their use of the marine environment.
seaiceatlas.snap.uaf.edu English	[4)]AOOS, [5)]ACCAP, [6)]SNAP, USA	scientists, public	Simultaneously view multiple sources of historical sea ice data from the oceans surrounding northern Alaska.
climate4you.com English	Ole Humlum, Depart. of Geosciences, University of Oslo, Norway	scientists, public	Main emphasis of this web site is to provide the interested reader with data and other information on meteorology and climate. No large back-ground information. Data from various data sources.
seaice.dk English	Technical University of Denmark, DTU space, Denmark	operators, ice services, scientists	An Internet based distribution system for ice, weather and ocean information. The system provides near real time access to a large variety of data about the polar environment in a standard user environment.
Imb.erdc.dren.mil/newdata.htm English	[7)]CRREL, USA	scientists	All data from active and past Sea Ice Mass-Balance Buoys.
Driftnoise.com/data-portal.html English	Drift & Noise Polar Services GmbH Germany	public, scientists, stakeholders, operators	Open Data Portal with service oriented near real time sea-ice concentration maps.
cpom.ucl.ac.uk/csopr/seaice.html English	Centre for Polar Observation and Modelling at [8)]UCL, U.K.	scientists, stakeholders, operators	Near real time Arctic sea ice thickness processed at UCL from CryoSat's SAR mode data.

Tab. 1: Selection of sea ice related websites. The websites portrayed are exemplary and do not claim to be complete. The used acronyms of the institutes represent: [1)]NSIDC = National Snow and Ice Data Center; [2)]AWI = Alfred Wegener Institute, Helmholtz Centre for Polar and Marin Research; [3)]IUP = Institut für Umweltphysik, Universität Bremen; [4)]AOOS = Alaska Ocean Observing System; [5)]ACCAP = Alaska Center for Climate Assessment and Policy; [6)]SNAP = Scenarios Network for Alaska and Arctic Planning; [7)]CRREL = Cold Regions Research and Engineering Laboratory; [8)]University College London.

Tab. 1: Exemplarische Auswahl einiger meereisbezogener Websites. Die Tabelle erhebt keinen Anspruch auf Vollständigkeit. Die verwendeten Abkürzungen der Institute bedeuten: [1)]NSIDC = National Snow and Ice Data Center; [2)]AWI = Alfred Wegener Institut Helmholtz Zentrum für Polar- und Meeresforschung; [3)]IUP = Institut für Umweltphysik, Universität Bremen; [4)]AOOS = Alaska Ocean Observing System; [5)]ACCAP = Alaska Center for Climate Assessment and Policy; [6)]SNAP = Scenarios Network for Alaska and Arctic Planning; [7)]CRREL = Cold Regions Research and Engineering Laboratory; [8)]University College London.

These constraints led to the idea to create a German web platform about sea ice to meet the abovementioned demands and requests. "meereisportal.de" is the first comprehensive German online knowledge and data platform on sea ice. The knowledge platform is designed as an open portal and aims to bundle expertise around sea ice, especially utilising mainly the expertise of German research institutes. However, all research institutions from every country can use the platform as multiplier for their sea ice related data and research results. At the same time, we aim to provide updated links to ongoing international research activities and datasets.

Before going into the detailed description of the concept and idea, the implementation and finally the current application of "meereisportal.de", the following paragraphs of this paper give a short introduction about the importance and role of sea ice in the climate system.

THE ROLE OF SEA ICE IN THE CLIMATE SYSTEM

Sea ice in the Arctic and Antarctica covers approximately seven percent of our planet's surface, which is equivalent to the size to Europe. From a climate perspective, it serves as both, an indicator and an amplifier of climate change. Sea ice is a barrier, limiting the exchange of heat, moisture, and momentum between the atmosphere and the ocean, and in addition it hosts a rich marine ecosystem. Changes in ice cover affect a wide range of human activities from hunting and fishing, shipping and resource extraction.

Sea ice is a naturally occurring material with an intricate and highly variable structure; it consists of gas bubbles, ice platelets, brine pockets, brine channels, and crystals of various sizes and orientations, all of which exert large effects on the transport of solar radiation within sea ice. Furthermore, sea ice phenomena cover broad scales in time and space. Despite its relatively small volume compared to ocean and atmosphere, sea ice plays an important role in the Earth's climate system. Sea ice is sensitive to global climate change, and in turn it is a driver and amplifier of climate change. Sea ice represents a thin blanket covering the ocean surface, which controls, but is also controlled by, the fluxes of heat, moisture and momentum across the ocean-atmosphere interface.

Sea ice reflects solar radiation due to its high albedo and is, therefore, an important element determining the Earth's radiation budget. Furthermore, changes in sea-ice thickness and/or extent interact with dynamical processes in the atmosphere and the ocean, related to changes in atmospheric wind and temperature fields, ocean currents and heat storage as well as to thermodynamic and radiative processes connected with water vapor, cloud and aerosol feedbacks. In spite of the apparent extreme conditions it also provides a habitat for living organisms. Consequently, sea ice research spans many scientific disciplines including, among others, geophysics, glaciology, chemistry and numerous branches of biology.

The sea-ice cover in both hemispheres is characterized by large seasonal variability, with an Arctic extent maximum of approximately 15 million km^2 in March and to some 6 million km^2 in September. In the Antarctic, the sea ice cover varies from 17 million km^2 in September to 3 million km^2 in February. Sea ice exhibits a high spatial variability of different surface types, floe sizes, and snow and ice thicknesses.

Due to a number of feedbacks, sea-ice extent is a sensitive indicator of climate. Because sea ice is relatively thin, its vulnerability and sensitivity to small perturbations in the state of ocean and atmosphere is high.

Shifts in Arctic sea-ice indicate regional and global climate change. In recent years, Arctic sea ice retreated in summer extensively, leading to large areas of thin first-year ice during the subsequent freeze up season, an ice type that is more vulnerable to melting in the next summer (Stroeve et al. 2012). Sea-ice extent shows decreasing trends in all months and in almost all regions in the Arctic with the exception of the Bering Sea during winter (Perovich et al. 2014). The September average trend (Fig. 1b), representing the annual sea ice minimum extent, is now -13.3 % per decade relative to the 1981–2010 average. The trend for the annual winter maximum during March is smaller (-2.6 % per decade), but is still decreasing at a statistically significant rate (Fig. 1a). A complete demise of Arctic sea ice in summer during coming decades is projected around 2060, while some models predict this event as early as 2040 (Overland & Wang 2013).

In contrast to the sea-ice decline in the Arctic, Antarctic sea ice has undergone a spatial redistribution. Since the start of regular satellite observations in 1979, total Antarctic sea ice has increased by about 1.5 % per decade. Whether the increase is a sign of sustained change is uncertain because ice extents vary considerably from year to year around Antarctica. Antarctic climate is influenced by, among other factors, changes in radiative forcing and Pacific climate variability. It is likely that the gradual warming of the North and tropical Atlantic Ocean is contributing to climate change in Antarctica (Li et al. 2014). There are also indications that the Antarctic sea ice cover is slowly extending due to an intensification of the polar vortex caused by intensified interactions between troposphere and stratosphere (Fan et al. 2014).

The temperature gradient from the Tropics to the Polar Regions has a strong influence on the wind systems, their variability and ocean currents. It is one of the main drivers of the global atmospheric circulation. Strong warming in the Arctic has the potential to impact, e.g., storm tracks, patterns of precipitation and the frequency and severity of cold-air outbreaks in middle latitudes. Arctic processes can feed back on the global climate system. Disturbances in the wintertime Arctic sea-ice and snow cover may induce perturbations in the zonal and meridional planetary wave train from the Tropics over the Mid-Latitudes into the Arctic (Dethloff et al. 2006, Jaiser et al. 2012).

Beside physical changes of sea ice, also the ecosystem in Polar Regions is largely affected by sea-ice changes. Observations support the hypothesis that the current sea-ice thinning and increasing melt-pond cover may be enhancing under-ice productivity and ice-algae export to the benthos, with ecological consequences ranging from the surface ocean to the deep sea (Boetius et al. 2013).

In addition to its role in global climate change, the Arctic is receiving enhanced attention for economic reasons. Among these is the fact that large amounts of oil and gas are deposited

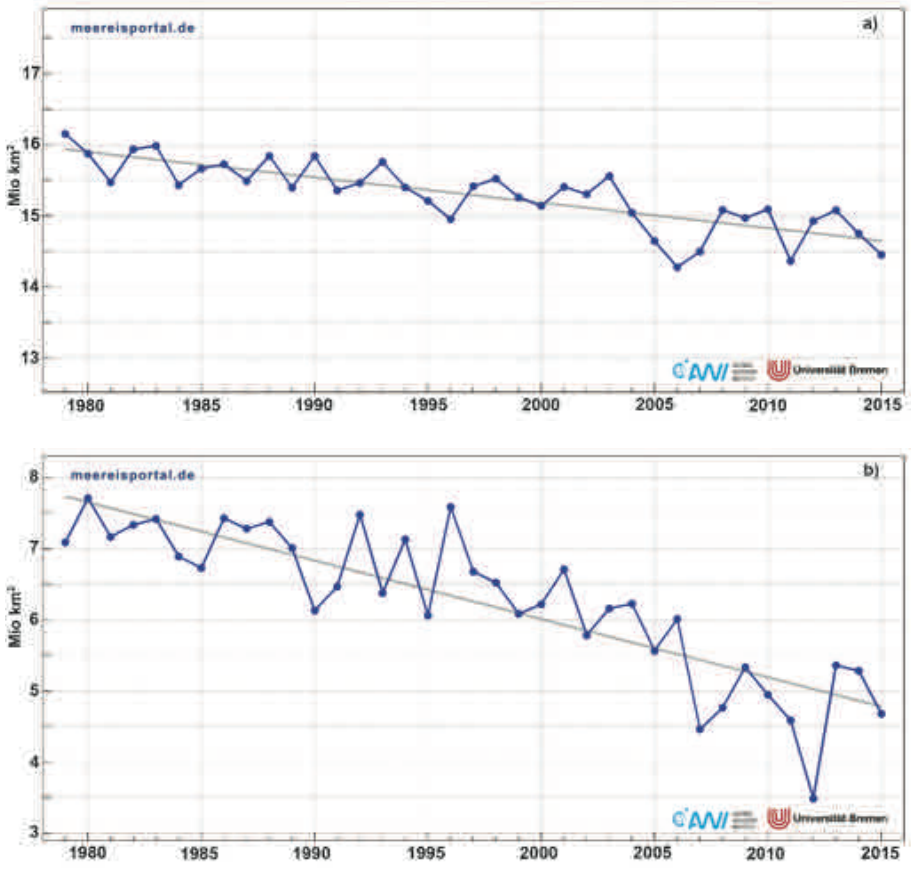

Fig. 1: Trend of Arctic sea ice minimum in March (a) and sea ice maximum in September (b) derived from satellite observations 1979–2015.

Abb. 1: Entwicklung des arktischen Meereisminimums im März (a) und Meereismaximum im September (b) aus Satellitenmessungen von 1979–2015.

in high Northern Latitudes. Other economic sectors depending on the sea-ice cover are transportation, fisheries and extraction of mineral resources. The potential for resource development and associated potential ecosystem risks is of increasing concern to the Arctic nations and to all concerned about the region's fragile environments (GAUTIER et al. 2009). Activities in the Polar Regions, e.g., research or economic planning strongly depends on a timely provision of accurate sea-ice data. Thus, there is an increasing need to provide various real time sea-ice data. Furthermore, stakeholders from different fields have a growing interest in expert commented sea-ice assessments. Consequently, sea ice becomes an increasing focus in the general public.

IDEA, REALIZATION AND CONCEPT OF "meereisportal.de"

The combination of multi-disciplinary sea-ice science and the rising demand of society for up-to-date information and user customized products emphasis the need for addressing the challenges posed by environmental change in the Polar Regions by means of creating new ways of communication. Therefore, research institutes are obliged to disseminate their scientific results and knowledge and enter into a dialogue with society. Disseminating and facilitating access to science-based information is a necessity to enable the public to make informed decisions. To provide information in this sense means process it appropriately to make it attractive and accessible to the intended audience. Accordingly, the development of "meereisportal.de" was governed by the following guiding principles:

- Simplicity, comprehensibility, and professional presentation.
- Topics and themes addressed through various approaches.
- Credibility by means of independence and reliability.
- User-friendliness, clear navigation.
- Differentiated access, depending on knowledge and experience.

In 2013 "meereisportal.de" was the first comprehensive German speaking knowledge platform on sea ice that went online. It was developed under the lead of the Helmholtz Regional Climate Office for Polar Regions and Sea Level Rise as a joint project of the University of Bremen (Institute of Environmental Physics) and the Alfred Wegener Institute, Helmholtz Centre for Polar and Marine Research within the frame of the Helmholtz Climate Initiative, Regional Climate Change (REKLIM).

The website delivers popularised information for the general public as well as scientific data meant primarily for the more expert readers and scientists. It also provides for various permanent tools allowing interaction with its visitors. Content is displayed using a web-based platform, based on a Typo 3 Content Management System. First results indicate a high level of interest from the general public and from experts, showing that the content of this website can contribute by communicating science-based information to improve awareness and understanding of sea ice related research. The principle concept of the new knowledge platform is based on three pillars:

(i) background information;
(ii) map and data archive and
(iii) expert knowledge.

The first pillar of the new knowledge platform is primarily providing comprehensive and understandable information about sea ice in German. This part of the website provides popularised information for the general public. Questions like *"How does sea ice form?", "How is it explored?"* or *"Which role does it play in the Earth's climate system?"* are answered here. All topics are described in various levels of detail. Particular emphasis is given to the description of new measurement methods, addressing general overview information up to detailed expert knowledge. This part also contains insight into latest research topics, project and methods. This is the main entrance door to the scientific results of sea-ice research for non-specialists.

The second pillar constitutes the extensive map and data archive. There are currently more than 10,000 graphically edited sea-ice maps of the past fourteen years and the associated datasets for processing available for download. Furthermore, this portal provides the first maps worldwide about sea-ice thickness as data products of the European Space Agency (ESA) satellite CryoSat-2. In addition to that, datasets of snow and thermistor buoys for the Arctic and Antarctic are found in the data portal. This part of the portal is presented in English in order to make contents also easy accessible to the international scientific community. Accordingly, the English version of "meereisportal.de" is directly accessible through the second domain name "seaiceportal.de".

The third pillar of "meereisportal.de" represents the outstanding expert knowledge of the partner institutions for different subject areas of sea-ice. This constitutes the main foundation of the platform and feeds into all parts of the portal. Consequentially, there are different essential quality features for the platform such as the accompanying assessments and evaluation of the sea-ice measurements, which are performed directly by the experts. These experts are also available to answer questions. Additionally, the direct connection to actual scientific questions guarantees a high level of competence and relevance of the topics represented on "meereisportal.de", where sea-ice physicists, oceanographers and sea-ice modellers discuss and explain sea ice research from various points of view.

The portal is complemented by appealing reports on sea-ice expeditions, which are performed by the Alfred Wegener Institute, Helmholtz Centre for Polar and Marine Research. Initial ideas about this have already been realised. So far, several expeditions of the research icebreaker RV "Polarstern" in both Polar Regions have been documented on "meereisportal.de" through photographs, reports, blogs and background information and are thus available for the general public.

IMPLEMENTATION EXAMPLES

Sea ice maps and products

Continuous and areal observations of the Arctic (Antarctic) sea ice requires satellite observation – *in situ* or airborne sensors do not allow observing the sea ice cover daily and monitor the seasonal variation between 6 and 15 million km^2 (3 and 17 million km^2) as average values between 1979 and 2014. Among the various types of satellite sensors, passive microwave instruments offer the advantage of being able to observe also during the (polar) night and not being hampered by clouds. Spaceborne passive microwave sensors on polar orbits belong to the most important tools for global sea-ice observations as they have been observing the complete Earth surface daily for over 30 years. A series of different sensors was involved in these observations, mainly the Nimbus-7 Scanning Multichannel Microwave Radiometer (SMMR, 1978–1987), the Defense Meteorological Satellite Program (DMSP)-F8, -F11 and -F13 Special Sensor Microwave/Imagers (SSM/Is, 1987–2003) and the DMSP-F17 Special Sensor Microwave Imager/Sounder (SSMIS, since 2003). The sensors with the highest resolution are the AMSR (Advanced Microwave Scanning Radiometer) instruments, namely AMSR-E (2002-2011) on AQUA and AMSR2 since 2012. In the data portal, sea-ice concentration maps starting from 2002 are available; in addition, monthly mean areal extent is provided from 1979 (Fig. 1 & 2).

All these instruments observe at a set of several microwave frequencies where the atmosphere is nearly transparent. The resolution on ground varies with frequency, e.g., for the AMSR instruments the resolution varies from 5 to 50 km as the frequency varies from 89 to 7 GHz. From the set of microwave observations of a given surface area, the sea-ice concentration, that is the percentage of the surface area covered by sea ice, is determined with so-called retrieval algorithms. The sea-ice concentrations are determined based on the difference between the vertically and horizontally polarised brightness temperatures at 89 GHz of the retrieved signal, called polarization difference. It is high with values around 47 K for open water (ice concentration 0), and low with values around 11.7 K for closed sea-ice cover (ice concentration 100 %). For values in between these range, intermediate sea ice-concentration are retrieved (Spreen et al. 2008). Various algorithms have been suggested over the years, and their results agree within about 5 %, which is among the best precisions of global time series of geophysical parameters. Most of the algorithms use the observations near 19 and 37 GHz. However, on "meereisportal.de" the ASI algorithm (Spreen et al. 2008) based on the 89 GHz observations of AMSR2 are used which offer a higher spatial resolution (5 × 5 km^2).

However, at 89 GHz the atmospheric influence from water vapor and clouds is higher than at 18 and 37 GHz which requires careful "weather filtering" based on other, lower frequency channels of the same sensor and validation of the retrieved sea-ice concentrations (Spreen et al. 2008). Figure 2 shows as an example of the obtained sea-ice-concentration map. Over the ocean, the colour represents the sea-ice concentration. According to the scale, 0 % ice concentration (open water) is represented in blue. As the ice concentration increases, the colour code changes gradually to lighter blue (50 % ice concentration) and then through blue tones to white, which corresponds to 100 % ice concentration (i.e., closed ice cover). Intermediate ice concentrations only occur near the ice edge, especially in those parts pointing towards the Siberian coast. In the inner ice pack, the ice cover is practically everywhere closed (100 %, white). The map shows the ice concentration on 16 September 2012, the day of the smallest ice extent ever observed (3.3 million km^2) in the satellite era since 1972. For comparison, the coloured lines show three more sea-ice extent contours, in blue the contour of the second-lowest sea-ice minimum of September 2007 with 4.3 million km^2, in green the average minimum extent of the years 1979–1983

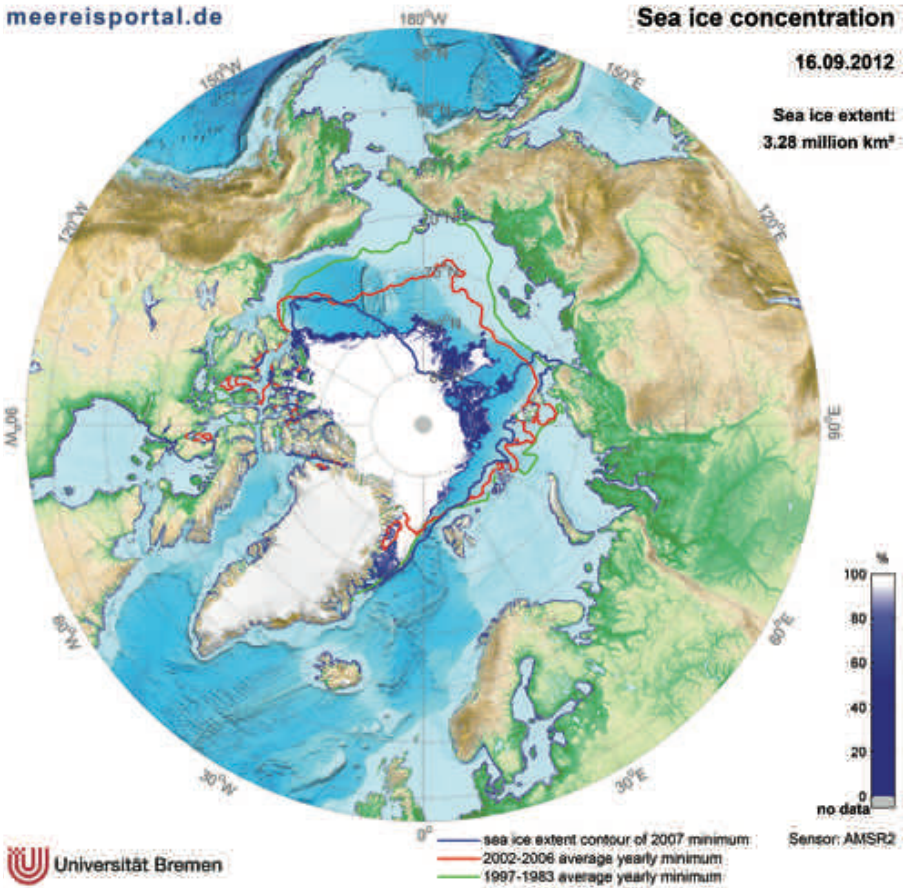

Fig. 2: Example map: sea-ice concentration of the historic minimum on 16 September 2012. Blue line: sea-ice extent contour of 2007 minimum; red: 2002–2006 average yearly minimum; green: 1997–1983 average yearly minimum. (Source contour lines: http://www.iup.uni-bremen.de: 8084/amsr2/; algorithm: SPREEN et al. 2008).

Abb. 2: Beispielkarte des historischen Meereisminimums am 16. September 2012; blau: Meereisminimum 2007; rot: mittleres jährliches Minimum von 2002–2006; grün: mittleres jährliches Minimum von 1997-1983 (Quelle: Linien: http://www.iup.uni-bremen.de:8084/amsr2/; Algorithmus: SPREEN et al. 2008).

and in red the average mean from 2002–2006: the extent of the yearly sea-ice minimum in September has reduced to less than 50 % from 1980 to 2012. The sea-ice concentration maps can be downloaded either as png-images as shown in the portal, or as original hdf5-files suitable for further processing by the users in the context of their specific applications. The files contain maps of the sea-ice concentration in percent. They use a polar stereographic projection with equal area at 70° latitude. The geographical coordinates of the pixels are given in separate files to be found at the data portal of "meereisportal.de". The data can also be found in more data formats (pdf, geotiff) on the pages of the cooperating portal of the University of Bremen (www.iup.uni-bremen.de:8084/ amsr2).

The most important applications of the maps are strategic planning of ship routing, especially for cruise ships and research vessels going to less frequented waters. Moreover, in combination with maps of earlier microwave sensors, various types of time series can be investigated. Figure 3 shows as an example of the daily Arctic sea-ice extent since 1972 together with the yearly maxima and minima. The horizontal line shows that all minima of 2007 and later were lower than all minima before: although the sea ice-minima of 2013 and 2014 were clearly higher than the historic minimum of 2012, the Arctic is still in a state of low sea ice.

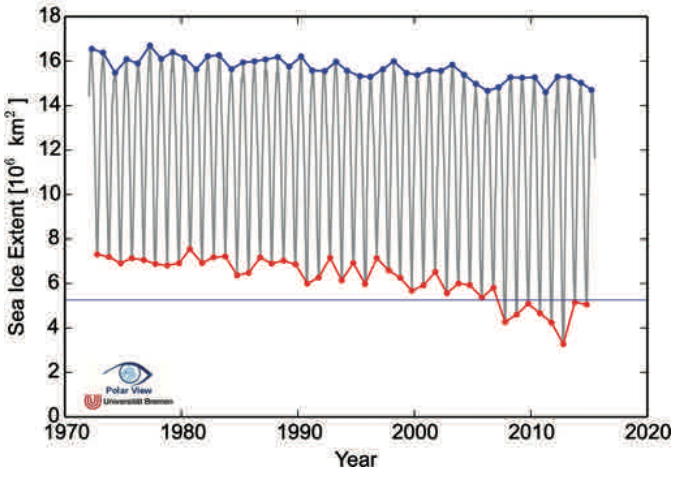

Fig. 3: Arctic sea ice extent 1972–2015. Data from various sensors combined according to iup.uni-bremen.de:8084/amsr2. Connected blue dots: winter sea-ice maximum values; connected red dots: summer minimum sea-ice extent values. The horizontal red line shows that all minima of 2007 and later were lower than all minima before.

Abb. 3: Arktische Meereisausdehnung von 1972-2015. Die Daten stammen von verschiedenen Sensoren die entsprechend iup.uni-bremen.de:8084/amsr2 kombiniert wurden. Die verbundenen blauen Punkte kennzeichnen das Wintermeereismaximum während die roten Punkte das Sommermeereisminimum kennzeichnen. Die horizontale rote Linie zeigt, dass alle Minima von 2007 und später niedriger sind als alle Minima davor.

Buoys data and maps

One main service of "meereisportal.de" is the near real-time access to measurements from autonomous platforms that measure sea-ice and sea-ice related parameters. Although these platforms are mostly not floating, but are deployed on sea ice (ice tethered), we use the common expression of "buoys" for them. The portal provides complete datasets of

all buoys (beside metadata and latest position), including all measured data of the operating sensors of the different buoys. Datasets are updated daily for all active, still reporting, buoys. Past buoys, which do not report data any more, are archived in the portal and also transferred into the Pangaea data publishing and archiving system ›http://www.pangaea.de‹. This is of particular interest, because the data get a digital object identifier (DOI) and a publication abstract, allowing proper citation of the dataset.

Currently, "meereisportal.de" processes measurements from five different types of buoys/autonomous platforms (Fig. 4). Here we describe the standard configuration of these buoys, while single units may have slightly different specifications or sampling intervals:

- Snow Depth Buoys (MetOcean, Canada) measure snow depth at four points, air temperature at 1.5 m height, body temperature, and barometric pressure in hourly intervals (Fig. 4a).
- Thermistor String Buoys (SRSL, Scotland) consist of a thermistor chain with 256 elements with 2 cm spacing on a 5 m long chain to measure air, snow, sea ice, and water temperatures as well as thermal conductivity through an internal heating mode (Hoppmann et al. 2015). Temperature profiles are measured and transmitted every three hours, heating mode data daily (Fig. 4b).
- Surface Velocity Profilers (SVP) and CALIBS (Compact Air-Launch Ice Buoys) both from MetOcean, Canada measure surface temperature and barometric pressure. Their main difference is the buoy design (Fig. 4c).
- Ice Beacons (MetOcean, Canada) measure water tempera–ture and conductivity in 5 and 10 m depth (Fig. 4d).
- CALIBS (Compact Air-Launch Ice Buoys) may be launched by air drop from planes, while SPVs are deployed manually on the ice. Depending on the exact purpose and design, SVPs differ in size and specifications, e.g., may have a drogue or not (Fig. 4e).

Beyond these key scientific parameters, all buoys transmit their geographic position and timestamps based on internal GPS receivers, as well as additional control parameters, like battery voltage and satellite transmission duration, to monitor the status of the buoy and satellite connection with every recording. Data transmission is realised through the Iridium telecommunication system for all units, except CALIBS, which transfer their data though the Argos system.

The backbone of the buoy data processing and archiving is a database of metadata. These metadata include information on:

1) the buoy owner (institute, contact person, project);
2) the buoy deployment (expedition, sea ice and snow conditions, co-location with other buoys, additional measurements and observations);
3) connections to buoy networks (see below);
4) the sensors on the buoy and their individual reporting times;
5) photos of the buoy;
6) additional information and comments.

In addition, the output of this database controls various processing routines (mostly Matlab scripts). The processing includes data retrieval from the data provider (currently JouBeh, Canada, and SRSL, UK), merging of individual datasets, processing into final physical quantities (e.g., from distance measurements into snow depth), plotting of data and maps. Pre-processed data plots and maps as well as pre-processed datasets are available from the "meereisportal.de" website. Data tables and figures use a consistent

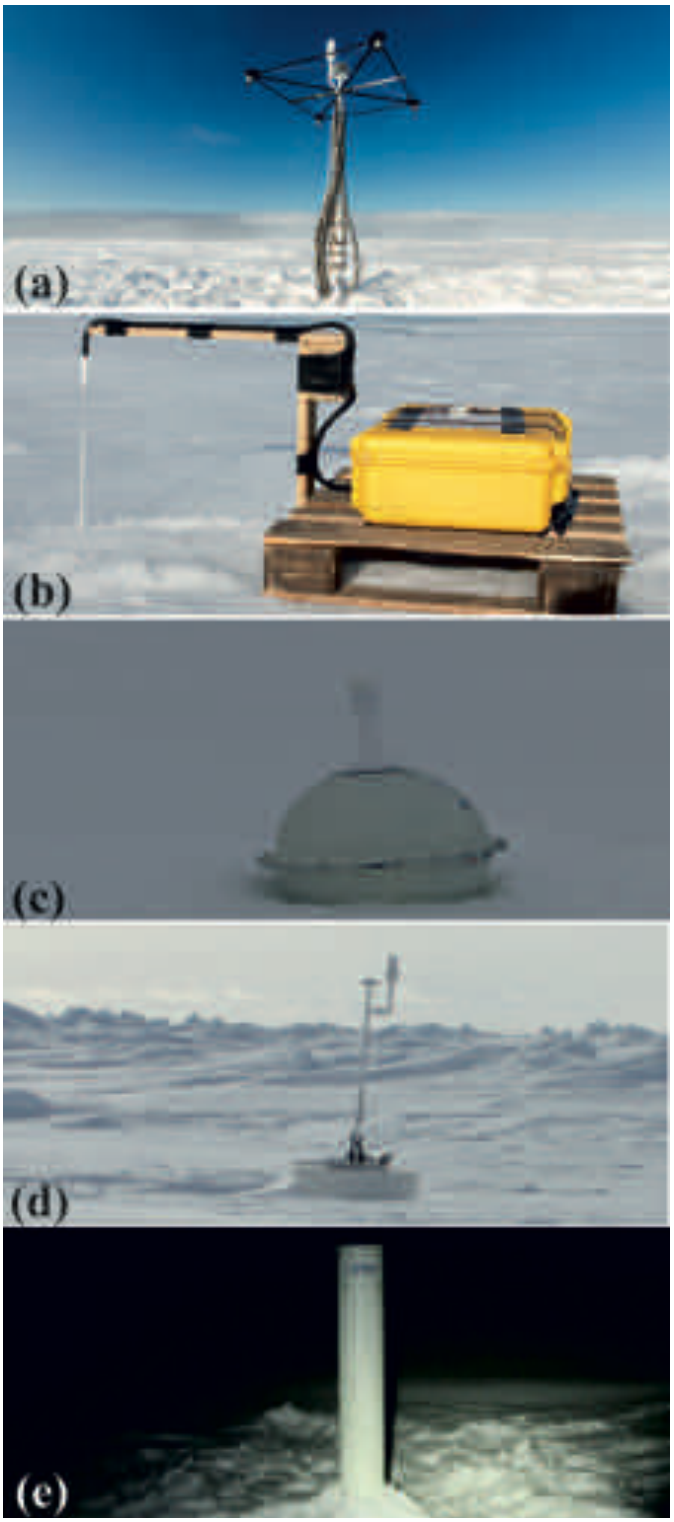

Fig. 4: Photographs of different buoy types; (a): Snow depth buoy; (b): Thermistor string buoy; (c): Surface Velocity Profiler, SVP; (d): Ice Beacon; (e): CALIBS (Compact Air-Launch Ice Buoys).

Abb. 4: Fotos verschiedener Bojentypen; (a): Schneeboje, (b): Thermistorboje, (c): Surface Velocity Profiler, SVP; (d): Ice Beacon; (e): CALIBS (Compact Air-Launch Ice Buoys).

naming of all buoys, based on the year of deployment (e.g., 2014), the buoy type (S for Snow Depth Buoys, T for thermistor string buoys, C for CALIBS, B for Ice Beacons, P for SVPs), and a running number per buoy type. Buoy 2014S11 is the eleventh Snow Depth Buoy in the system that was deployed in 2014.

The platform "meereisportal.de" reports position and temperature data into the Global Telecommunication System (GTS), since December 2014. The International Arctic Buoy Program (IABP, http://iabp.apl.washington.edu/) receives all buoy data and necessary metadata since August 2012. Data forwarding to GTS and IABP is coordinated in collaboration with the respective buoy owner.

Figure 5 shows an example of a drift and data plot for Snow Depth Buoy 2014S11. The buoy was deployed in the Weddell Sea, Antarctic, on 29 January 2014 and reported data until 02

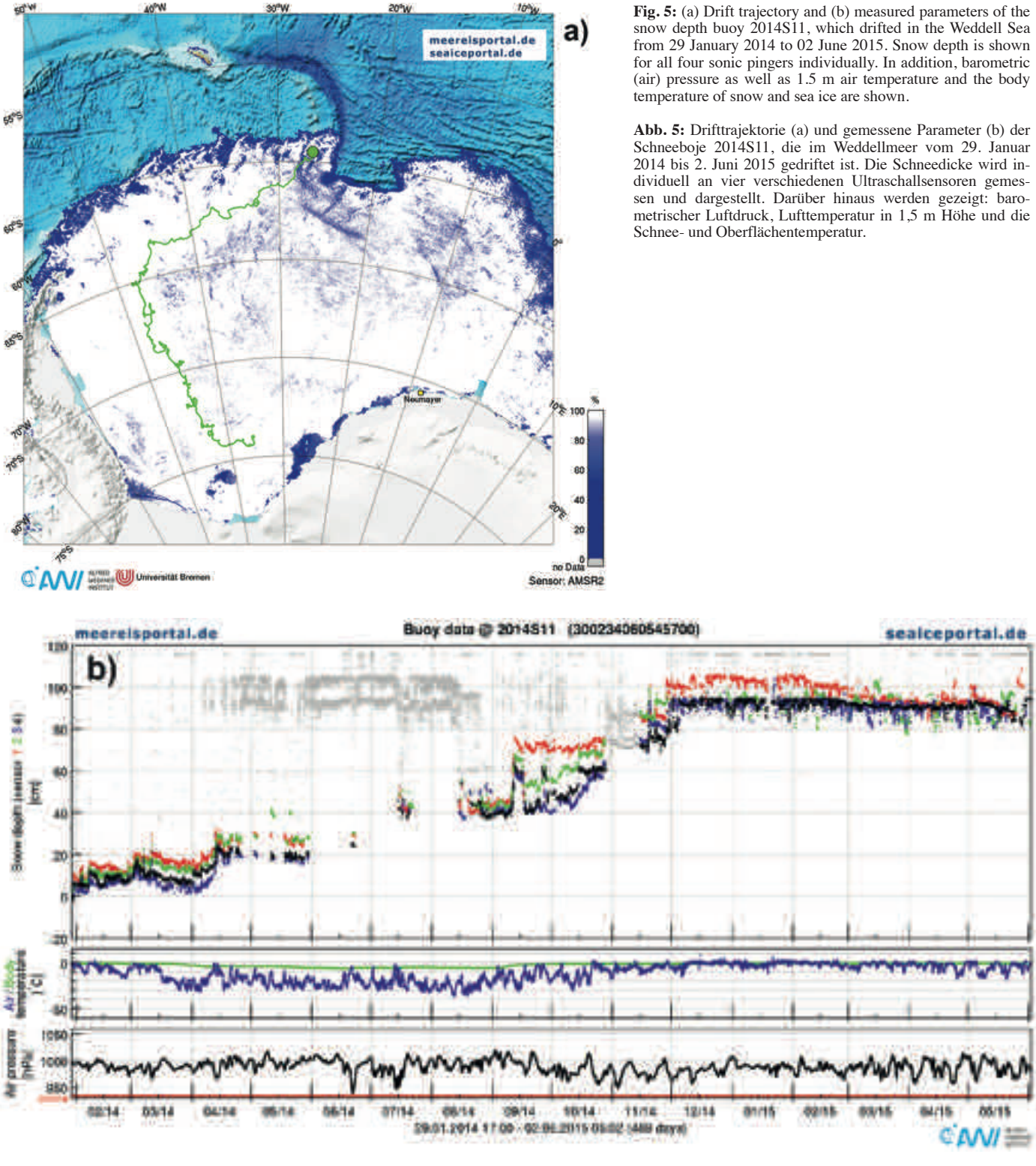

Fig. 5: (a) Drift trajectory and (b) measured parameters of the snow depth buoy 2014S11, which drifted in the Weddell Sea from 29 January 2014 to 02 June 2015. Snow depth is shown for all four sonic pingers individually. In addition, barometric (air) pressure as well as 1.5 m air temperature and the body temperature of snow and sea ice are shown.

Abb. 5: Drifttrajektorie (a) und gemessene Parameter (b) der Schneeboje 2014S11, die im Weddellmeer vom 29. Januar 2014 bis 2. Juni 2015 gedriftet ist. Die Schneedicke wird individuell an vier verschiedenen Ultraschallsensoren gemessen und dargestellt. Darüber hinaus werden gezeigt: barometrischer Luftdruck, Lufttemperatur in 1,5 m Höhe und die Schnee- und Oberflächentemperatur.

June 2015, when it (most likely) drowned in the marginal ice zone (Fig. 5a). In the meanwhile, snow depth has increased from below 10 to over 80 cm. Different snow fall events characterise the increase of snow depth, while also a slight decrease over the austral summer 2014/15 is visible (Fig. 5b). All four sonic sensors are shown and indicate the small-scale variability of snow depth in the area around the buoy (approximately 4 m^2) as well as uncertainties in the measurements. Grey dots show reported observations that got filtered during data processing and are removed from the final data set. In addition, air and body temperature show the seasonal cycle with air temperatures as low as -30 °C, while the body (snow and surface ice) temperature only drops to -15 °C. Air pressure is recorded along over the entire observation period of 489 days.

An example of Thermistor String Buoy 2014T14 is shown in Figure 6. This buoy was deployed close to the North Pole on 26 August 2014 (Fig. 6a). The buoy reported temperature and heating profiles through the entire Arctic winter 2014/15 (Fig. 6b). An automatic conversion of temperature profiles into sea-ice thickness is not possible yet, but different projects are currently working on methods that will allow time-series calculation of sea-ice thickness in the near future.

Different to the two very long lifetimes of the exemplary buoys from Figures 5 and 6, other buoys have much shorter lifetimes and periods of data transmission. Figure 7 shows the lifetimes of all snow depth (Fig. 7a) and thermistor string buoys (Fig. 7b) that are currently registered in "meereisportal.de". Average lifetime of snow depth buoys and thermistor string buoys are currently (status 24 November 2015) 200 and 153 days, respectively. Lifetimes on Antarctic sea ice are generally longer (snow buoys: 323 days, thermistor string buoys: 260 days) then on Arctic sea ice (snow buoys: 116 days, thermistor string buoys: 84 days), but this statistic is still weak due to the limited number of buoys (Arctic: 32 buoys, Antarctic: 28 buoys). The exact reason of buoy failure is often unknown. However, some reasons may be derived

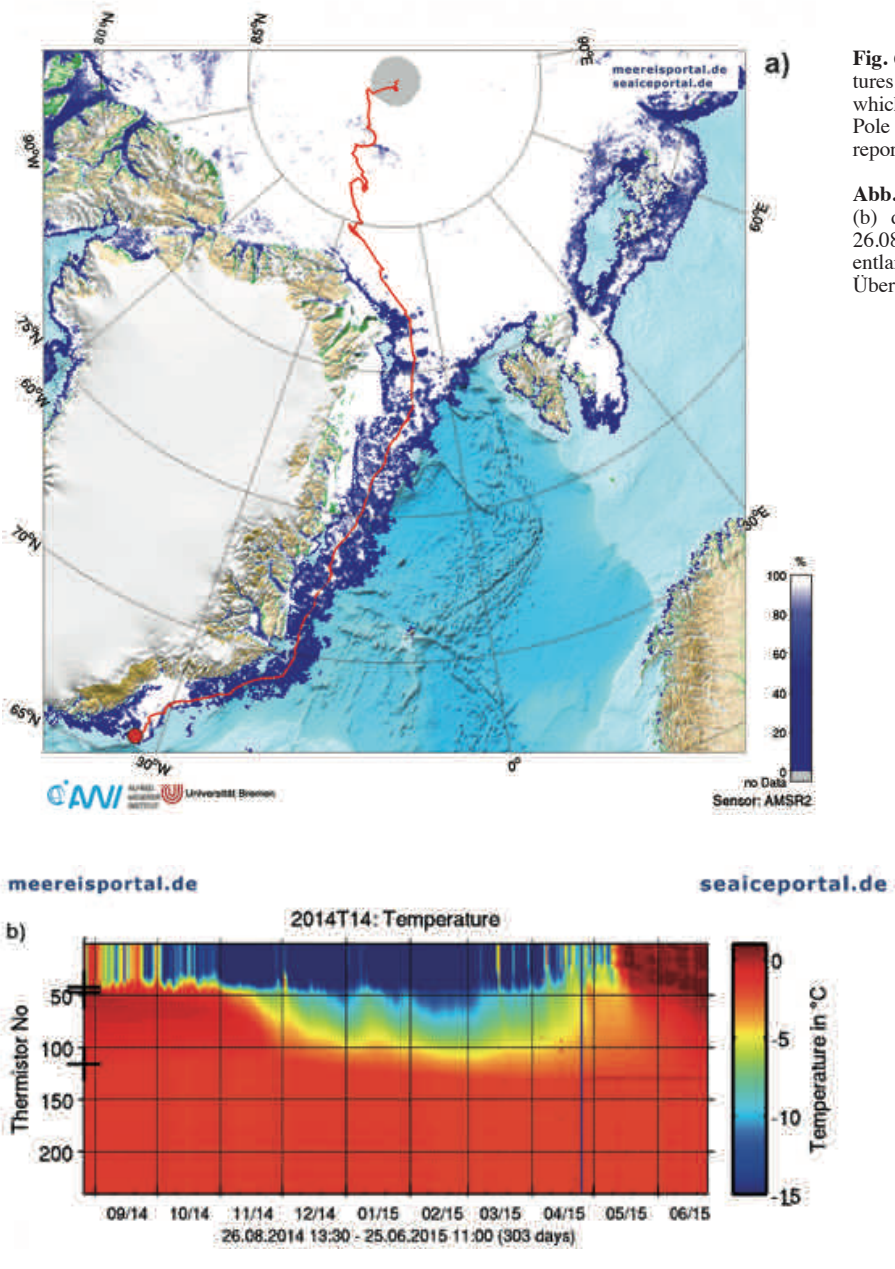

Fig. 6: (a) Drift trajectory and (b) measured sea ice temperatures of the thermistor string (mass balance) buoy 2014T14, which was deployed on 26 August 2014 close to the North Pole and drifted along the coast of Greenland until it stopped reporting after 265 days on 18 May 2015.

Abb. 6: Drifttrajektorie (a) und gemessene Meereistemperatur (b) der Thermisterboje (Massenbilanz) 2014T14, die am 26.08.214 nahe des Nordpols eingesetzt wurde. Sie driftete entland der Küste Grönlands und die Übertragung stoppte die Übertragung nach 265 Tagen am 18. Mai 2015.

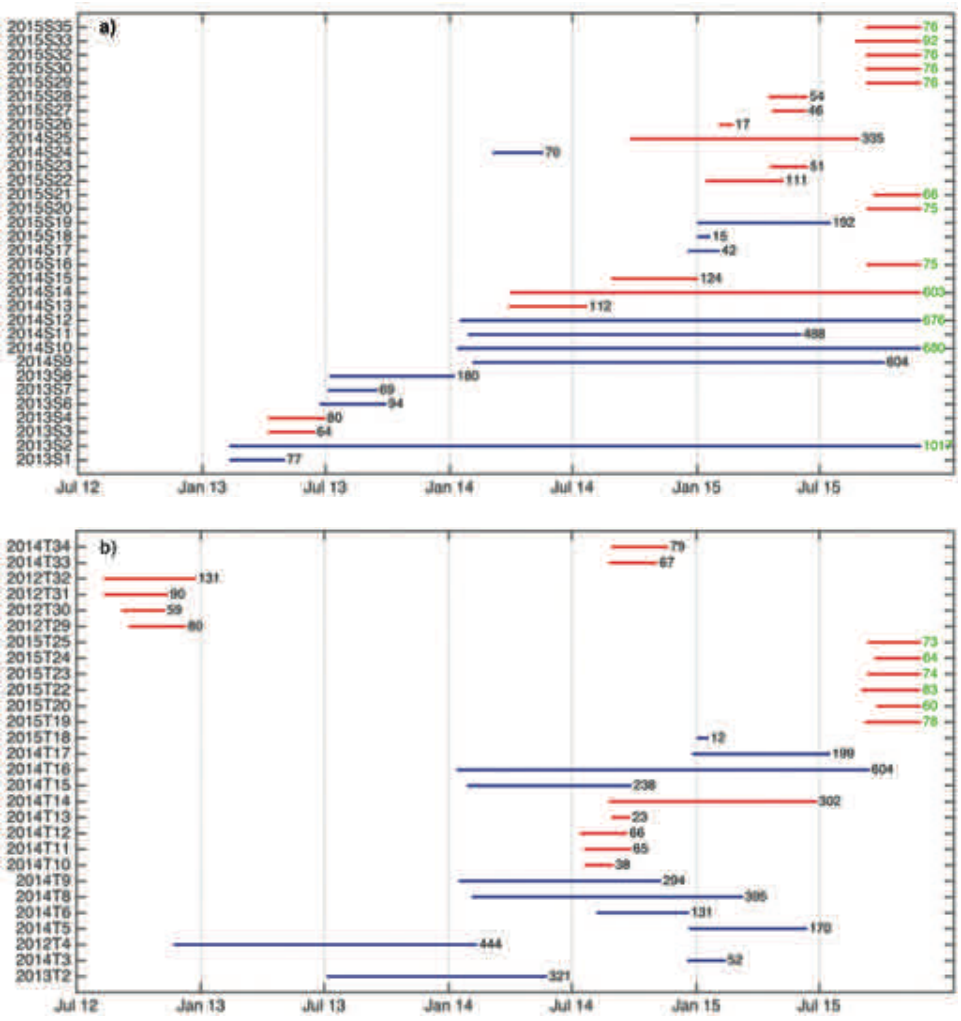

Fig. 7: Lifetimes of (a) all 32 snow depth and (b) all 28 thermistor string buoys recorded in "meereisportal.de" (status 24 November 2015). Numbers give the life time in days, while green numbers indicate buoys that were still transmitting. Blue (red) bars indicate Antarctic (Arctic) buoys, respectively.

Abb. 7: Lebenszeit aller (a) 32 Schneebojen und (b) 28 Thermistorbojen, die in "meereisportal.de" dokumentiert werden (Status 24. November 2015). Die Zahlen geben die Lebenszeit in Tagen an, während grüne Zahlen Bojen anzeigen, bei denen die Datenübertragung noch besteht. Blaue (rote) Balken stehen für antarktische (arktische) Bojen.

from the datasets themselves or in connection with sea-ice concentration data. Some snow depth buoys seem to have strongly tilted or even fallen over (e.g., 2013 S4; not depicted here, for details see website). This may be derived from the sudden spread of the measurements of single sensors. In this and similar cases, the buoy continued to send data, but not the entire suite of possible parameters is useful over the entire lifetime. However, the dataset may still be used for drift studies. Other buoys have simply melted out of the ice. In this case, the buoy does not send any data from one to the next moment and sea-ice concentration shows a position in the marginal ice zone (e.g., 2015 S22; not depicted here, for details see website). For the Thermistor String Buoys, the thermistor chain itself is the weakest element, causing most failures, while these units also report their position much longer (e.g., 2014 T9; not depicted here for details see website). Drifting buoys (SVP and CALIB) without masts or chains are the most robust systems.

CryoSat data product

The estimation of sea-ice thickness using data from the satellite radar altimeter mission CryoSat-2 of the European Space Agency (ESA) is a field of active research and developing processing schemes. Preliminary products, mainly monthly gridded fields of Arctic sea-ice thickness, are nevertheless of interest for model evaluation (Stroeve et al. 2014) and forecast initialisation. These products are based on a processing chain that has been developed at the Alfred Wegener Institute, Helmholtz Centre for Polar and Marine Research with the aim to investigate and evaluate optimal strategies for sea-ice thickness retrieval, using high resolution radar altimeters with the ultimate goal of quantifying the global sea-ice volume budget.

The underlying principle of CryoSat-2 sea-ice thickness retrieval is the estimation of freeboard, the height of the sea-ice surface above the local sea level and its conversion into thickness using isostatic principles. Freeboard values are obtained by means of differential radar range measurements between the elevation of the sea level over leads between floes and the elevation of the ice surface (Fig. 8). Main research question and reason for evolving processing schemes is the interpretation of radar echoes of CryoSat-2's synthetic aperture radar altimeter over rough and snow covered ice surfaces (Ricker et al. 2015). In addition, several auxiliary input parameters such as snow depth or snow and ice density cannot be measured on a relevant scale for CryoSat-2 sea-ice thickness retrieval and must be substituted by assumptions or parametrisations. It is therefore imperative for the scientific usability of data products to include an inventory of all parameter fields used with uncertainty estimations when possible. A detailed overview of the underlying assumptions and processing steps is available in a user guide (Hendricks et al. 2013) or in the scientific literature (Ricker et al. 2014).

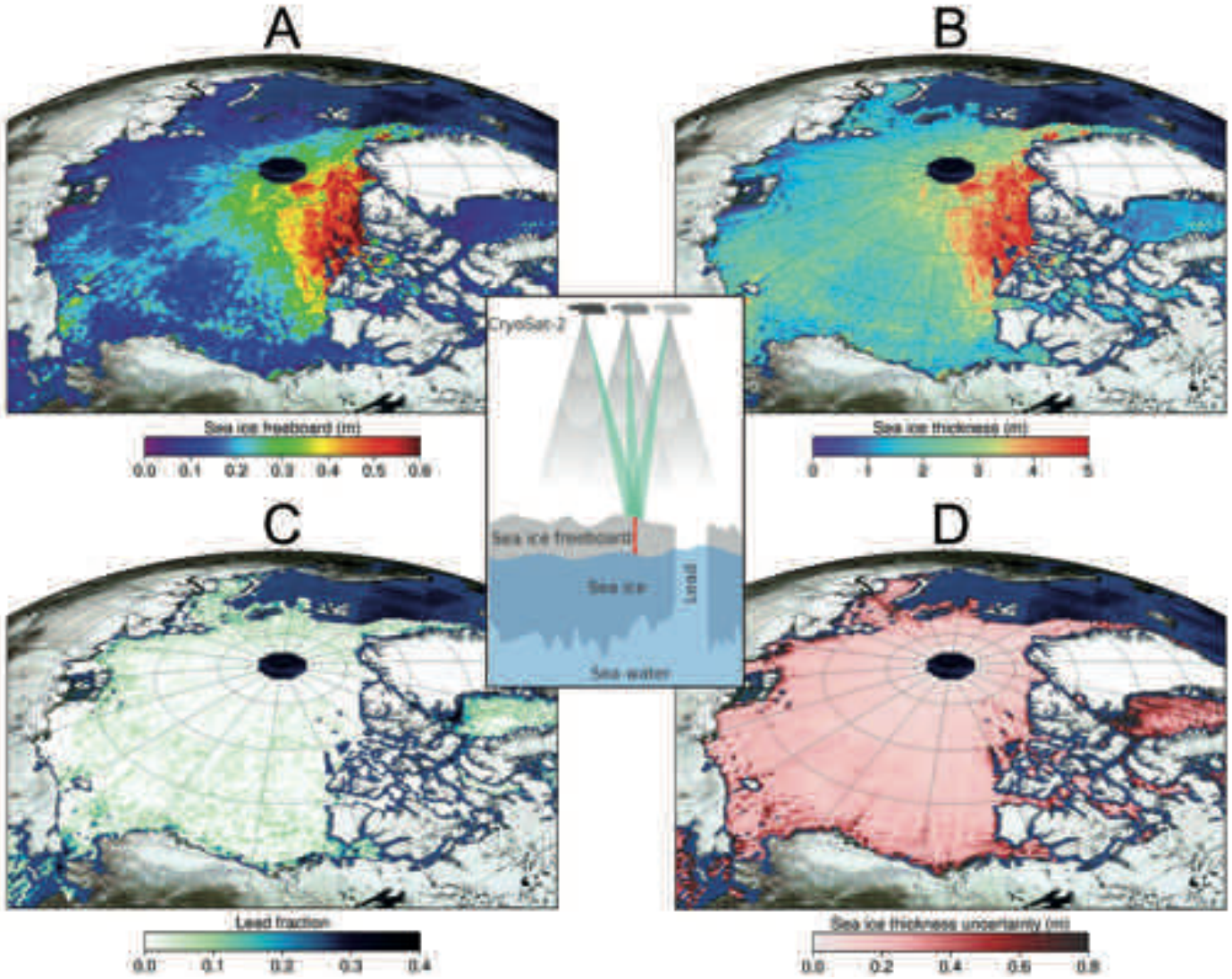

Fig. 8: Exemplary sea-ice parameters of the CryoSat-2 Arctic sea-ice data product. A: sea-ice freeboard, the height of ice floes above sea level, B: sea-ice thickness, derived from freeboard with the assumption of a snow climatology. C: The fraction of identified leads between sea-ice floes, whose elevation is used to obtain freeboard from the CryoSat-2 range measurements. D: The geographical distribution of sea-ice thickness uncertainty. The sketch in the middle of the figure demonstrates the principal behind CryoSat-2 sea-ice measurements.

Abb. 8: Exemplarische Meereis-Parameter aus dem CryoSat-2 Meereis-Produkt. A: Eis-Freibord, die Höhe der Meeresoberfläche über dem Meeresspiegel. B: Meereisdicke, abgeleitet aus Freibord unter Annahme einer Schneeklimatologie. C: Anteil der innerhalb der Eisfläche als offenes Wasser detektierten Messungen, deren Höhe genutzt wird, um das Freibord zu berechnen. D: Geographische Verteilung der Eisdicken-Unsicherheiten. Die Skizze in der Mitte der Abbildung beschreibt das Messprinzip von CryoSat-2.

Currently "meereisportal.de" hosts the Arctic CryoSat-2 sea-ice data product from spring 2011 to spring 2015 as gridded monthly means. Data from June to September are not shown because summer melt conditions strongly impact even prohibit reliable measurements (e.g., Ricker et al. 2014). An Antarctic CryoSat-2 sea-ice data product is under development and is planned to be included into "meereisporatal.de" in 2016 (Schwegmann et al. 2015). The data are available also during summer when the properties of the melting surface do not allow the retrieval of freeboard. Gridded fields on an Equal-Area Scalable Earth Grid (EASE2-Grid) with a 25 km resolution are available for a modified snow-depth climatology that is used in the processing as well as the density of ice and snow. In the future these fields shall be extended not only to recent monthly means but also with additional parameters such as the sea-surface height estimation. The height of the sea surface, that is a byproduct of the freeboard estimation, is usually described as the sum of mean sea-surface height and the anomaly of the actual sea surface relative to its mean value at the location of the individual record. The sea-surface anomaly is a valuable parameter since it may be used for sea-level budget estimations and Arctic wide measurements in ice-covered waters are sparse.

Changing baseline algorithm versions of the lower level data products at ESA and improvements in the sea-ice thickness retrieval are the reasons that the CryoSat-2 data product requires infrequent update. Subsequently, the data product on "meereisportal.de" will need to be updated as data and processing algorithms mature. Though CryoSat-2 data show a good agreement with independent validation data (Laxon et al. 2013) the sea-ice thickness grids should not be taken as an operational product. The intention is rather to distribute a science dataset that shall promote the use of CryoSat-2 data

products over sea ice and enable tests and improvements of the processing chain by the wider scientific community.

EXAMPLES OF "meereisportal.de" DATA PRODUCTS, THEIR APPLICATIONS, AND SPECIFIC USER REQUESTS

The following paragraph shortly describes the variety usage of information, data and products based on "meereisportal.de". Since its start in 2013, these services are used and incorporated in various applications and in many ways. This encompasses the answer of question by an interested public as well as data input for scientific analysis. In Table 2 we compiled a brief overview of some example applications to demonstrate the capability and the potential of the website and its provided direct data access.

CONCLUSION AND OUTLOOK

The website "meereisportal.de" represents an example of the knowledge transfer process of science to different stake–holders, which could be scientists for specific data demand or the society in general, with respect to sea ice as an important climate indicator. The platform is maintained by institutional support from different departments and partners and is embedded in the frame of the Helmholtz Climate Initiative, Regional Climate Change (REKLIM). The platform "meereisportal.de" offers scientific qualified information focused on sea ice to a German audience. It provides comprehensive, high quality and up-to-date data and information. The portal aims at user specified and individually tailored information and services. Through the multilevel structure (breadth and depth) of the data and information portal and its user specified products "meereisportal.de" responds to the increasing demands of various user groups. Following this approach, knowledge relevant for the society is derived from scientific results and supports activities in the fields of information, education and decision-making. In recognition of its excellent service the platform "meereisportal.de" received an award in 2015 within the "Germany – Land of Ideas" initiative.

The platform "meereisportal.de" is intended as a lively platform, providing preprocessed data, expert assessment of the current sea-ice situation and information from different perspectives around the topic of sea ice. However, beyond this service and products "meereisportal.de" is intended to be used from the scientific community as a multiplier forum for their research results and data. The website "meereisportal.de" invites scientists to upload their data on the portal, providing successively a full range of all sea ice related data. As a next step, ice thickness information on thin ice from SMOS satellite measurements (Tian-Kunze et al. 2014), complementing CryoSat-2 information on thin sea ice between 50-100 cm, as well as ice drift information and its uncertainty for the period 2003–2007 (Sumata 2015) will be made available. In addition, an evaluation of the Coupled Model Intercomparison Project phase 5 (CMIP5) with respect to sea-ice variability and projections will be provided by University of Hamburg

Area of application	Service	Example description and according references
Education	Support data set usage, including the extraction of custom-made datasets on demand	Sub-sampling sea ice concentration data over longer time periods related to past expeditions are used in different Bachelor and PhD theses which are realized in close cooperation with various universities (e.g., University of Hamburg, Jade Hochschule), where "meereisportal.de" is directly involved in providing processed data. These studies comprise data analysis about ship routing in the Russian Arctic and the comparison of EM bird measurements of sea-ice thickness with sea-ice concentration data.
Scientific papers	Access to various sea ice related data and data products for further own processing	Data input of "meereisportal.de": Rutgers van der Loeff et al (2014) used sea-ice concentration data in order to relate their findings of gas transfer through sea ice with the ice conditions prior to and during their expedition. Mutsa Roca-Marti et al (pers. com. 2015) used sea-ice concentration data to illustrate the results on "carbon fluxes and export efficiency in the Central Arctic at different time scales during summer 2012". Buoy data have been used for sea-ice drift product validation (Lavergne pers. com. 2014). Sea ice concentration data were analysed for different sectors in order to determine the impact of oceanic ^{222}Rn emissions (Weller et al. 2014).
Expedition support	Support route planning, provide for expedition operation areas, custom-made datasets and products on demand	This includes both the statistical analysis of data prior to the expedition as well as routinely providing current daily sea-ice concentration maps for specific operational areas via E-Mail during the expedition. These activities effectively support the on-site station planning (e.g., three RV "Polarstern" expedition into the Weddell Sea have been supported). Another example is a touristic shipping company, which downloaded sea-ice maps of the Weddell Sea area to derive average conditions of the sea ice to support their expedition planning, focussing on routes along the potential sea-ice edge.
General public	Provide answers for questions or provide input for books, exhibitions etc., custom-made data products on demand	For example in Lemke & von Neuhoff (2014), a popular science book, historical expedition maps and modern sea-ice concentration maps were specially adopted for this publication. Furthermore, "meereisportal.de" provided a customized animation of sea-ice concentration evolution of the Antarctic and Arctic for an exhibition in the International Maritime Museum Hamburg.
Policy support	Contribute to policy processes	"meereisportal.de" was directly asked for a contribution to a "kleine parlamentarische Anfrage 18/5692" of the party fraction "Bündnis90/Die Grünen" about sea ice in summer 2015.

Tab. 2: Overview on application examples of "meereisportal.de" services.

Tab. 2: Exemplarischer Überblick über einige Anwendungen von "meereisportal.de".

(Dirk Notz pers. com), offering data and maps for a thorough comparison of observational and modelled data up to present day and an expert assessment of the potential future development of sea-ice evolution in the Artic and Antarctica.

ACKNOWLEDGMENT

The authors thank Max König for his thorough review and helpful suggestions on the manuscript and the editor Dieter Fütterer for the manuscript handling. This work has been funded by the Helmholtz Climate Initiative REKLIM (Regional Climate Change), a joint research project of the Helmholtz Association of German research centers (HGF) under grant: REKLIM-2012-04. Use of any provided sea-ice data is free. Please refer to "meereisportal.de" and this grant number when downloading and publishing data from "meereisportal.de". Additional funding was retrieved through University Bremen, the Alfred Wegener Institute, Helmholtz Centre for Polar and Marine Research and the Helmholtz Initiative Earth System Knowledge Platform (ESKP).

References

IABP (2016): <http://iabp.apl.washington.edu> International Arctic buoy programme; function tested on 01 March 2016.

<http://meereisportal.de> Wissens und Datenplattform rund um das Thema Meereis; function tested on 01 March 2016.

<http://seaiceportal.de> Knowledge and data platform on the topic sea ice; function tested on 01 March 2016.

PANGAEA <http://www.pamgaea.de/> Data publisher for Earth & Environ–mental Science; funtion tested on 01 March 2016.

University Bremen <http://www.iup.uni-bremen.de:8084/amsr2> Daily AMSR2 Sea Ive Maps; funtion tested on 01 March 2016.

Barrett, B.F.D., Notaras M. & Smith, C. (2014): Communicating scientific research through the web and social media: experience of the United Nations University with the Our World 2.0 Web Magazine.- In V.C.H. Tong (ed), Geoscience Research and Outreach, Springer Verlag: 91-101, doi: 10.1007/978-94-007-6943-4_7.

Boetius, A., Albrecht, S., Bakker, K., Bienhold, C., Felden, J., Fernández-Méndez, M., Hendricks, S., Katlein, C., Lalande, C., Krumpen, T., Nicolaus, M., Peeken, I., Rabe, B., Rogacheva, A., Rybakova, E., Somavilla, R. & Wenzhöfer, F. (2013): Export of algal biomass from the melting Arctic sea ice.- Science 339: 1430-1432.

Breyer, D., Daubresse, P. & Sneyers, M. (2007): Bringing scientists to the people – the Co-Extra website.- Biotechnol. J. 2: 1081-1085.

Dethloff, K., Rinke, A., Benkel, A., Køltzow, M., Sokolova, E., Kumar Saha, S., Handorf, D., Dorn, W., Rockel, B., von Storch, H., Haugen, J.E., Røed, L.P., Roeckner, E., Christensen, J.H. & Stendel, M. (2006): A dynamical link between the Arctic and the global climate system.- Geophys. Res. Lett. 33: L03703.

Fan, T., Deser, C. & Schneider, P. (2014): Recent Antarctic sea ice trends in the context of Southern Ocean surface climate variations since 1950.- Geophys. Res. Lett. 41: 2419-2426, doi: 10.1002/2014GL059239.

Gautier, D.L., Bird, K.J., Charpentier, R.R., Grantz, A., Houseknecht, D.W., Klett, T.R., Moore, T.E., Pitman, J.K., Schenk, C.J., Schuenemeyer, J. H., Sørensen, K., Tennyson, M. E., Valin, Z.C. & Wandrey, C.J. (2009): Assessment of undiscovered oil and gas in the Arctic.- Science 324: 1175-1179, doi: 10.1126/science.1169467.

Hendricks, S., Ricker, R. & Helm, V. (2013): AWI CryoSat-2 sea ice thickness data product – User Guide.- http://www.meereisportal.de/cryosat.

Hoppmann, M., Nicolaus, M., Hunkeler, P.A., Heil, P. Behrens, L.-K., König-Langlo, G. & Gerdes, R. (2015): Seasonal evolution of an ice-shelf influenced fast-ice regime, derived from an autonomous thermistor chain.- J. Geophys. Res. Oceans, 120: 1703-1724, doi: 10.1002/2014JCO10327.

Jaiser, R., Dethloff, K., Handorf, D., Rinke, A. & Cohen, J. (2012): Impact of sea ice cover changes on the Northern Hemisphere atmospheric winter circulation.- Tellus A 64:11595, doi: 10.3402/tellusa.v64i0.11595.

Tian-Kunze, X., Kaleschke, L., Maaß, N., Mäkynen, M., Serra, N., Drusch, M. & Krumpen T. (2014): SMOS derived sea ice thickness: algorithm baseline, product specifications and initial verification.- The Cryosphere 8: 997-1018.

Laxon S.W., Giles, K.A., Ridout, A.L., Wingham, D.J., Willatt, R., Cullen, R., Kwok, R., Schweiger, A., Zhang, J., Haas, C., Hendricks, S., Krishfield, R., Kurtz, N., Farrell, S. & Davidson, M. (2013): CryoSat-2 estimates of Arctic sea ice thickness and volume.- Geophys. Res. Lett. 40: 732-737, doi: 10.1002/grl.50193.

Lemke, P. & von Neuhoff, S. (2014): Der gefrorene Ozean - Mit FS POLARSTERN auf Winterexpedition in die Antarktis.- Koehlers Verlagsges., ISBN-10: 3782212223, ISBN-13: 9783782212229.

Li, X., Holland, D.M., Gerber, E.P. & Yoo, C. (2014): Impacts of the north and tropical Atlantic Ocean on the Antarctic Peninsula and sea ice.- Nature 505: 538-542, doi: 10.1038/nature12945.

Overland, J. E. & Wang, M. (2013): When will the summer Arctic be nearly sea ice free?- Geophys. Res. Lett. 40: 2097-2101.

Perovich, D., Gerland, S., Hendricks, S., Meier, W., Nicolaus, M. Tschudi, M. (2014): Sea ice.- Arctic Report Card, http://www.arctic.noaa.gov/reportcard/sea_ice.html

Ricker, R., Hendricks, S., Helm, V., Skourup, H. & Davidson M. (2014): Sensitivity of CryoSat-2 Arctic sea-ice freeboard and thickness on radar-waveform interpretation.- The Cryosphere 8:1607-1622, doi: 10.5194/tc-8-1607-2014.

Ricker, R., Hendricks, S., Perovich, D.K., Helm, V. & Gerdes, R. (2015): Impact of snow accumulation on CryoSat-2 range retrievals over Arctic sea ice: An observational approach with buoy data.- Geophys. Res. Lett. 42: 4447-4455, doi:10.1002/2015GL064081.

Rutgers van der Loeff, M.M., Cassar, N., Nicolaus, M., Rabe, B. & Stimac, I. (2014): The influence of sea ice cover on air-sea gas exchange estimated with radon-222 profiles.- J. Geophys. Res. Oceans 119: 2735-2751, doi: 10.1002/2013JC009321.

Schwegmann, S., Rinne, E., Ricker, R., Hendricks, S. & Helm, V. (2015): About the consistency between Envisat and CryoSat-2 radar freeboard retrieval over Antarctic sea ice.- The Cryosphere, Discuss. 9: 4893-4923.

Scott A. (2000): The dissemination of the results of environmental research.- Environmental issues series No 15, November, European Environment Agency, ISBN: 92-9167-262-9.

Spreen, G.L., Kaleschke, L. & Heygster, G. (2008): Sea ice remote sensing using AMSR-E 89 GHz channels.- J. Geophys. Res. 113: C02S03, doi: 10.1029/2005JC003384.

Stroeve, J.C., Serreze, M.C., Holland, M.M., Kay, J.E, Malanik, J. & Barret, A.P. (2012): The Arctic's rapidly shrinking sea ice cover: a research synthesis.- Climatic Change 3-4:1005-1027, doi: 10.1007/s10584-011-0101-1.

Stroeve, J., Barrett, A., Serreze, M. & Schweiger, A. (2014): Using records from submarine, aircraft and satellites to evaluate climate model simulations of Arctic sea ice thickness.- The Cryosphere 8: 1839-1854, doi:10.5194/tc-8-1839-2014.

Sumata, H., Kwok, R, Gerdes, R., Kauker, F. & Karcher, M. (2015): Uncertainty of Arctic summer ice drift assessed by high-resolution SAR data.- J. Geophys. Res.-Oceans 120, doi: 10.1002/2015JC010810.

Weller, R., Levin, I., Schmithüsen, D., Nachbar, M., Asseng, J. & Wagenbach, D. (2014): On the variability of atmospheric ^{222}Rn activity concentrations measured at Neumayer, coastal Antarctica.- Atmos. Chem. Phys. 14: 3843-3853, www.atmos-chem-phys.net/14/3843/2014/, doi: 10.5194/acp-14-3843-2014.

Polarforschung 85 (2), 157–160, 2015 (erschienen 2016)

New Evidence for Abrupt Sea-Ice Fluctuations in the Subpolar North Atlantic at the End of the Last Glacial in Relation with Thermohaline and Atmospheric Circulation

by Juliane Müller*

Abstract: A temporally highly resolved reconstruction of sea-ice conditions in eastern Fram Strait, using the sea-ice proxy IP_{25}, sheds new light on potential feedback mechanisms between sea-ice variability and ocean circulation changes during rapid deglacial climate shifts. While a post-LGM sea-ice maximum probably played an important role for the timing of Heinrich Event 1, distinct sea-ice discharge events seem to be intrinsically tied to perturbations in the oceanic overturning circulation. The herein presented sea-ice record is the hitherto only continuous documentation of sea-ice changes in the subpolar North Atlantic that covers the transition from the last glacial into the Holocene. These data strengthen the need for more studies of high-resolution sediment cores to better assess the short-term palaeoenvironmental development and the feedback mechanisms between sea-ice variability and oceanic/atmospheric circulation fluctuations during this crucial time of climate change.

Zusammenfassung: Eine auf dem Meereisproxy IP_{25} basierende, zeitlich hochauflösende Rekonstruktion der Meereisbedingungen in der östlichen Framstraße wirft ein neues Licht auf mögliche Wechselwirkungen zwischen Meereisschwankungen und Veränderungen der Ozeanzirkulation während schneller deglazialer Klimaänderungen. Während ein post-LGM Meereismaximum wahrscheinlich eine wichtige Rolle für den Beginn von Heinrich-Ereignis 1 gespielt hat, scheinen Intervalle eines verstärkten Meereisexports untrennbar mit der Schwächung der ozeanischen Umwälzzirkulation verbunden zu sein. Der hier präsentierte Datensatz ist die bisher einzige durchgehende Dokumentation der Meereisveränderungen im subpolaren Nordatlantik während des Übergangs vom letzten Glazial in das Holozän. Diese Daten belegen den Bedarf an weiteren Studien an ähnlich zeitlich hochaufgelösten Sedimentkernabfolgen, um die kurzzeitige Entwicklung der Paläoumweltbedingungen und die Wechselwirkungen zwischen Meereisveränderungen und der ozeanisch/atmosphärischen Zirkulation während dieser Zeit häufiger Klimaschwankungen besser abschätzen zu können.

INTRODUCTION

Arctic sea ice is a crucial element within the global climate system. It has a direct influence on thermohaline processes (governing ocean circulation) and the oceanic-atmospheric heat and gas exchange with considerable effects on atmospheric circulation and precipitation patterns (Dieckmann & Hellmer 2003). Reconstructions of the spatial-temporal variability of sea ice in the geological past provide important information on ocean-atmosphere feedback mechanisms and thus support a more detailed assessment of natural (i.e. non-anthropogenically induced) climate changes. In particular, the transition from the last glacial into the current interglacial was accompanied by significant climate perturbations. Only few studies, however, address the role that sea ice might have played during these (often abrupt) climate shifts. The sea-ice biomarker IP_{25} is an organic molecule exclusively produced by sea-ice diatoms and a robust indicator of previous sea-ice coverage when identified in marine sediments (Belt et al. 2007, Brown et al. 2014). Several studies from the (sub) Arctic Ocean strengthen the reliability of IP_{25} but also highlight the need for the complementary analysis of phytoplankton-derived biomarkers for an unambiguous and more quantitative reconstruction of the sea-ice conditions by means of the PIP_{25} index (Müller et al. 2011, Stein et al. 2012, Knies et al. 2014, Xiao et al. 2015). This index combines the environmental information of the sea-ice proxy IP_{25} and a phytoplankton biomarker – indicative of ice-free conditions – and provides a semi-quantitative estimate of the intensity of a paleo sea-ice cover (see Belt & Müller 2013 for further details). The Fram Strait, the only deep-water passage connecting the Arctic and the Atlantic Ocean and the major outlet for the export of sea ice into the North Atlantic (Kwok et al. 2004), is a strategic study area to identify past changes in sea-ice export associated with climate shifts. Sediment core MSM5/5-712-2 from the western continental margin of Svalbard provides an exceptional high temporal resolution. Organic geochemical analyses of this core hence enabled a detailed reconstruction of the variable sea-ice conditions during the past 30 ka BP (i.e. 30,000 years before present, Müller et al. 2012, Müller & Stein 2014). Analytical details and the calculation of the P_BIP_{25} index are described in Müller & Stein (2014).

RESULTS AND DISCUSSION

Distinct short-term fluctuations in the biomarker content of MSM5/5-712-2 reveal that the late glacial period and the Last Glacial Maximum (LGM; 23-19 ka BP) were characterised by recurrent advances and retreats of sea ice at the core site (see Müller & Stein 2014 for further discussion), which is in good agreement with earlier observations of a variable North Atlantic heat flow (Weinelt et al. 2003) and seasonally ice free conditions in the Norwegian Sea (de Vernal et al. 2006). These frequent oscillations in sea-ice cover (and associated changes in the heat and moisture flux) might have played an important role for the sustained growth of the Svalbard-Barents Sea Ice Sheet during the LGM.

A sudden rise towards maximum P_BIP_{25} values at 19.2 ka BP points to a significant increase in the sea-ice cover at the end of the LGM (Fig. 1). Probably in direct response to the onset of meltwater discharge from disintegrating ice sheets that covered Eurasia and North America (Clark et al. 2004) and a significant

doi:10.2312/polfor.2016.012

* Alfred Wegener Institute, Helmholtz Centre for Polar and Marine Re-search, Am Alten Hafen 26, 27568 Bremerhaven, Germany, <juliane.mueller@awi.de>

This extended abstract was presented as an oral contribution at the Inter-national Conference "Our Climate – Our Future: Regional perspectives on a global challenge", 6–9 October 2014 in Berlin, Germany.

Manuscript received 31 May 2015; revised version 18 January 2016; accepted 27 January 2016.

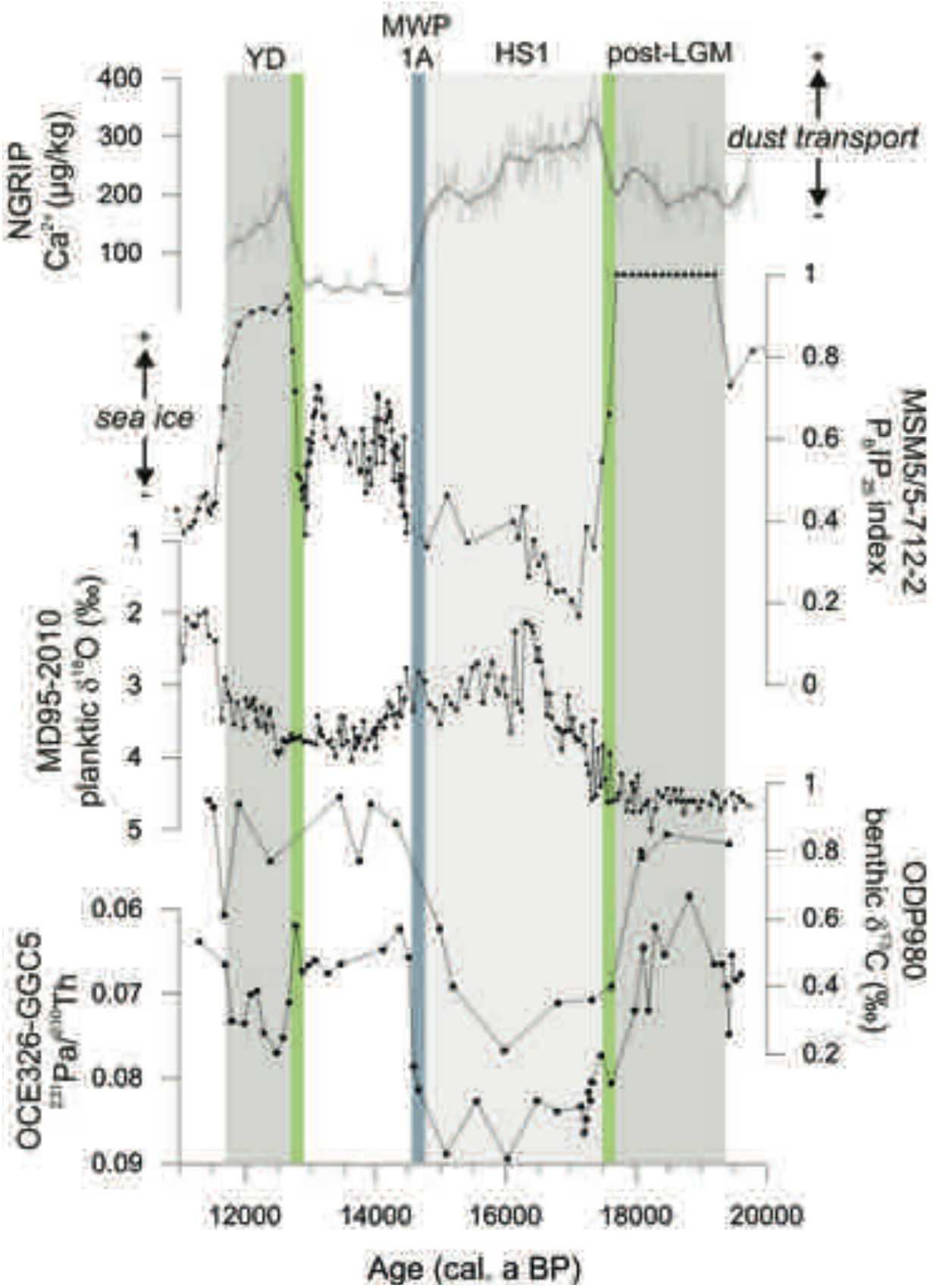

Fig. 1: Compilation of proxy data documenting deglacial changes in the Greenland ice core dust content (Ca^{2+}), sea-ice cover (P_BIP_{25}) in Fram Strait, ocean surface freshening ($\partial^{18}O$) at the Vøring Plateau, ocean ventilation ($\partial^{13}C$) in the eastern North Atlantic and AMOC (Atlantic Meridional Overturning Circulation) strength ($^{231}Pa/^{230}Th$) in the subtropical North Atlantic.

Abb. 1: Zusammenstellung von Proxydaten über deglaziale Änderungen im Staubgehalt in grönländischen Eiskernen (Ca^{2+}), in der Meereisbedeckung (P_BIP_{25}) in der Framstraße, in der Ozeanaussüßung ($\partial^{18}O$) am Vøringplateau, in der Ozeanventilierung ($\partial^{13}C$) im östlichen Nordatlantik und in der Stärke der AMOC (Atlantic Meridional Overturning Circulation) ($^{231}Pa/^{230}Th$) im subtropischen Nordatlantik.

salinity decrease of Arctic Ocean surface waters, a long lasting and perennial sea-ice cover developed. A southward expansion of this post-LGM sea-ice maximum into the subpolar North Atlantic (Fig. 2) and the formation of landfast sea ice might have reduced the further calving of icebergs from the adjacent ice sheets or, at least, it would have hampered the mobility of floating icebergs. Importantly, such a perennial sea-ice cover could have promoted an unusual heat accumulation in intermediate water depths CRONIN et al. 2012) which supports MARCOTT et al. (2011) who argued that only a subsurface warming in the subpolar North Atlantic could have triggered the massive release of icebergs from the Laurentide Ice Sheet during Heinrich Event 1 (17.5–16.8 ka BP, HEMMING 2004, MCMANUS et al. 2004). A post-LGM sea-ice maximum thus could have been a crucial prerequisite for such a scenario. By reducing the drift and thus the export of sea ice through Fram Strait, atmospheric blocking conditions could have favoured the accumulation of such a perennial (and "immobile") sea-ice cover in the Arctic Ocean (SCHOLZ et al. 2015).

An abrupt decline in P_BIP_{25} values at 17.6 ka BP, eventually marks a break-up of the post-LGM perennial sea ice and the return of ice-free summers in eastern Fram Strait during Heinrich Event 1 (Figs. 1, 2). At the same time, decreasing $\partial^{18}O$ values recorded at the Vøring Plateau (MD95-2010; DOKKEN & JANSEN 1999) reveal a rapid sea surface freshening in the Norwegian Sea that probably lead to a strong stratification and a reduced ocean ventilation as is indicated by a significant drop in benthic $\partial^{13}C$ values observed at ODP site 980 (Figs. 1, 2; MCMANUS et al. 1999). A rise in the $^{230}Pa/^{231}Th$ ratio in a sediment core from the subtropical North Atlantic finally depicts a large-scale weakening of the Atlantic Meridional Overturning Circulation (AMOC) during Heinrich Stadial 1 (Figs. 1, 2; MCMANUS et al. 2004). In regard of these observations it might be concluded that the abrupt break-up of a perennial sea-ice cover and the subsequent discharge of huge amounts of sea ice and icebergs into the North Atlantic very likely intensified the AMOC slow-down and/or the displacement of the locus of deep-water formation during Heinrich Stadial 1. At this stage, however, only sensitivity experiments performed with climate models may allow to disentangle (and quantify) the individual contribution of sea ice and icebergs to this AMOC perturbation. Interestingly, the sea-ice break-up coincides with a shift towards higher Calcium ion concentra-

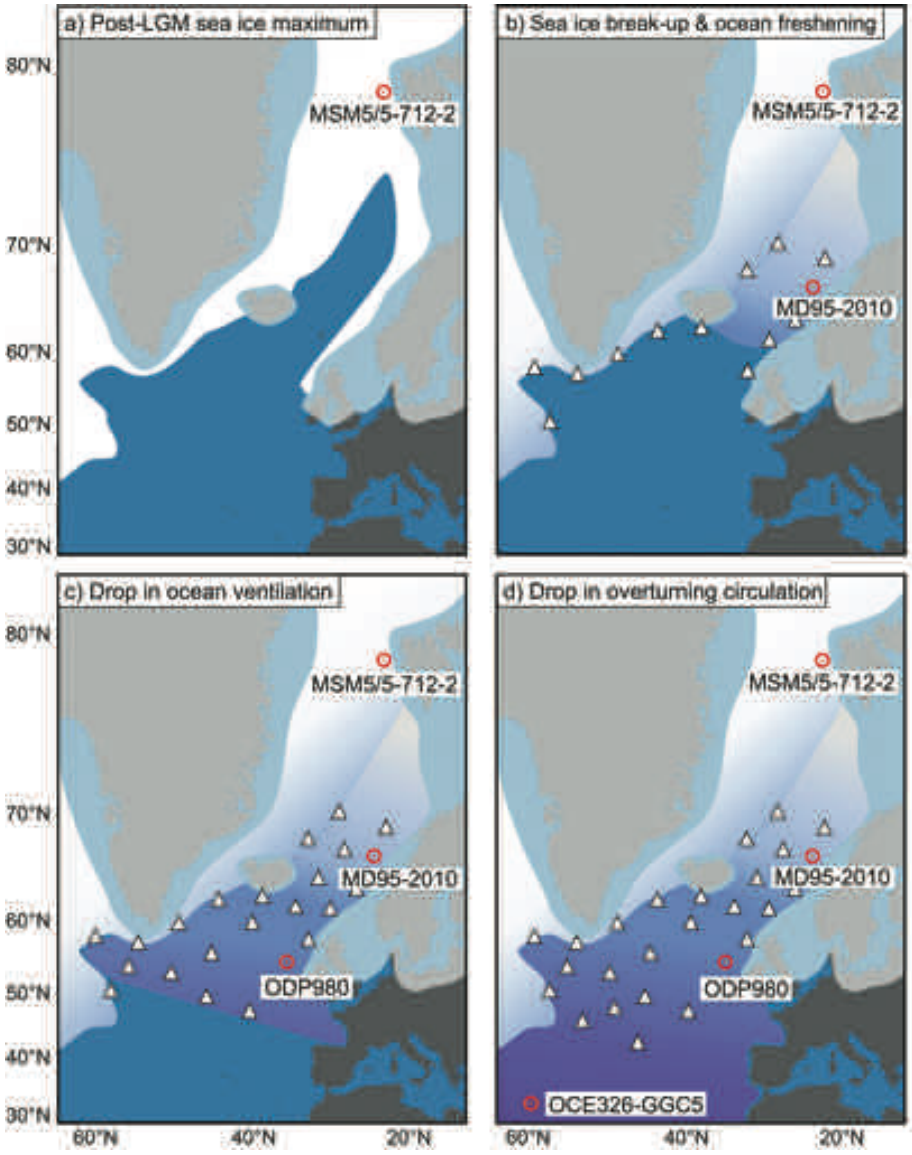

Fig. 2: Proposed scenario for the palaeoceanographic evolution in the subpolar North Atlantic during Heinrich Event 1. Extent of the Greenland, Iceland and Fennoscandian Ice Sheet (after MANGERUD et al. 2004, DYKE et al. 2002) and core sites of proxy records discussed in the text are indicated. White triangles refer to iceberg discharge.

Abb. 2: Mögliches Szenario der paläozeanographischen Entwicklung im subpolaren Nordatlantik während Heinrich-Ereignis 1. Die Ausdehnung der grönländischen, isländischen und fennoskandischen Eisschilde (nach MANGERUD et al. 2004, DYKE et al. 2002) und die Kernpositionen der Proxy-Datensätze, die im Text diskutiert werden sind angedeutet. Weiße Dreiecke zeigen den Eisbergtransport an.

tions (Ca^{2+}) in the NGRIP ice core (Fig. 1; RASMUSSEN et al. 2008). Variations in the Ca^{2+} content in ice cores are commonly interpreted to reflect variability in atmospheric dust transport in response to aridity changes in the source areas and/or atmospheric circulation patterns and wind strength (FISCHER et al. 2007, MCGEE et al. 2010). The rapid rise in the NGRIP dust content hence might be related to a strengthening of the westerlies, which, by carrying relatively warm air towards the subpolar North Atlantic, could have promoted the 17.6 ka sea-ice break-up. Further decreasing $\partial^{18}O$ values at the Vøring Plateau (reflecting a sustained freshening of the sea surface, DOKKEN & JANSEN 1999) are accompanied by continuously increasing P_BIP_{25} values that mark a successive re-expansion of sea ice in northern Fram Strait since 17.2 ka BP. Similar to the intensification of sea-ice coverage during the sea-level rise at 19 ka BP, this recovery seems to be boosted by another meltwater pulse 1A at ca. 14.6 ka BP (MWP-1A; DESCHAMPS et al. 2012) and potentially decreasing westerlies (Fig. 1).

A second sea-ice maximum prevailed at the core site during the Younger Dryas and coincided with another perturbation of the AMOC depicted by the $^{230}Pa/^{231}Th$ record from the subtropical North Atlantic (Fig. 1). In contrast to the perennial post-LGM "sea-ice plug", the Younger Dryas sea-ice maximum seems to result from an enormous discharge of drift ice via Fram Strait, which agrees with earlier observations of an increased export of sea ice into the subpolar North Atlantic (BRADLEY & ENGLAND 2008, NOT & HILLAIRE-MARCEL 2012, CABEDO-SANZ et al. 2013; see MÜLLER & STEIN 2014 for further discussion).

ACKNOWLEDGMENTS

Robert Spielhagen and an anonymous reviewer are acknowledged for their helpful comments on an earlier version of this extended abstract.

References

Belt, S.T., Massé, G., Rowland, S.J., Poulin, M., Michel, C. & Leblanc, B. (2007): A novel chemical fossil of palaeo sea ice: IP_{25}.- Organic Geochemistry 38: 16-27.

Belt, S.T. & Müller, J. (2013): The Arctic sea ice biomarker IP_{25}: a review of current understanding, recommendations for future research and applications in palaeo sea ice reconstructions.- Quat. Sci. Rev. 79: 9-25.

Bradley, R.S. & England, J.H. (2008): The Younger Dryas and the sea of ancient ice.- Quat. Res. 70: 1-10.

Brown, T.A., Belt, S.T., Tatarek, A. & Mundy, C.J. (2014): Source identification of the Arctic sea ice proxy IP_{25}.- Nature Commun. 5: 4197, doi:10.1038/ncomms5197.

Cabedo-Sanz, P., Belt, S.T., Knies, J. & Husum, K. (2013): Identification of contrasting seasonal sea ice conditions during the Younger Dryas.- Quat. Sci. Rev. 79: 74-86.

Clark, P.U., McCabe, A.M., Mix, A.C. & Weaver, A.J. (2004): Rapid rise of sea level 19,000 years ago and its global implications.- Science 304: 1141-1144.

Cronin, T.M., Dwyer, G.S., Farmer, J., Bauch, H.A., Spielhagen, R.F., Jakobsson, M., Nilsson, J., Briggs, W.M. & Stepanova, A. (2012): Deep Arctic Ocean warming during the last glacial cycle.- Nature Geosci. 5: 631-634.

Deschamps, P., Durand, N., Bard, E., Hamelin, B., Camoin, G., Thomas, A.L., Henderson, G.M., Okuno, J.I. & Yokoyama, Y. (2012): Ice-sheet collapse and sea-level rise at the Bolling warming 14,600 years ago.- Nature 483: 559-564.

de Vernal, A., Rosell-Melé, A., Kucera, M., Hillaire-Marcel, C., Eynaud, F., Weinelt, M., Dokken, T. & Kageyama, M. (2006): Comparing proxies for the reconstruction of LGM sea-surface conditions in the northern North Atlantic.- Quat. Sci. Rev. 25: 2820-2834.

Dieckmann, G.S. & Hellmer, H.H. (2003): The importance of sea ice: An overview.- In: D.N. THOMAS & G.S. DIECKMANN (eds), Sea ice: An introduction to its Pysics, Chemistry, Biology and Geology, Blackwell Publishing 1: 1-21.

Dokken, T.M. & Jansen, E. (1999): Rapid changes in the mechanism of ocean convection during the last glacial period.- Nature 401: 458-461.

Dyke, A.S., Andrews, J.T., Clark, P.U., England, J.H., Miller, G.H., Shaw, J. & Veillette, J.J. (2002): The Laurentide and Innuitian ice sheets during the Last Glacial Maximum.- Quat. Sci. Rev. 21: 9-31.

Fischer, H., Siggaard-Andersen, M.-L., Ruth, U., Röthlisberger, R. & Wolff, E. (2007): Glacial/interglacial changes in mineral dust and sea-salt records in polar ice cores: sources, transport, and deposition.- Rev. Geophys. 45: RG1002.

Hemming, S.R. (2004): Heinrich events: massive late Pleistocene detritus layers of the North Atlantic and their global climate imprint.- Rev. Geophys. 42 (1), doi:10.1029/2003RG000128.

Knies, J., Cabedo-Sanz, P., Belt, S.T., Baranwal, S., Fietz, S. & Rosell-Melé, A. (2014): The emergence of modern sea ice cover in the Arctic Ocean.- Nature Commun. 5: 5608.

Kwok, R., Cunningham, G.F. & Pang, S.S. (2004): Fram Strait sea ice outflow.- J. Geophys. Res. 109: C01009.

Mangerud, J., Jakobsson, M., Alexanderson, H., Astakhov, V., Clarke, G.K.C., Henriksen, M., Hjort, C., Krinner, G., Lunkka, J.-P., Möller, P., Murray, A., Nikolskaya, O., Saarnisto, M. & Svendsen, J.I. (2004): Ice-dammed lakes and rerouting of the drainage of northern Eurasia during the Last Glaciation.- Quat. Sci. Rev. 23: 1313-1332.

Marcott, S.A., Clark, P.U., Padman, L., Klinkhammer, G.P., Springer, S.R., Liu, Z., Otto-Bliesner, B.L., Carlson, A.E., Ungerer, A., Padman, J., He, F., Cheng, J. & Schmittner, A. (2011): Ice-shelf collapse from subsurface warming as a trigger for Heinrich events.- Proc. Nat. Acad. Sci. 108: 13415-13419.

McGee, D., Broecker, W.S. & Winckler, G. (2010): Gustiness: The driver of glacial dustiness?- Quat. Sci. Rev. 29: 2340-2350.

McManus, J.F., Oppo, D.W. & Cullen, J.L. (1999): A 0.5-million-year record of millennial-scale climate variability in the North Atlantic.- Science 283: 971-975.

McManus, J.F., Francois, R., Gherardi, J.M., Keigwin, L.D. & Brown-Leger, S. (2004): Collapse and rapid resumption of Atlantic meridional circulation linked to deglacial climate changes.- Nature 428: 834-837.

Müller, J. & Stein, R. (2014): High-resolution record of late glacial and deglacial sea ice changes in Fram Strait corroborates ice–ocean interactions during abrupt climate shifts.- Earth Planet. Sci. Lett. 403: 446-455.

Müller, J., Wagner, A., Fahl, K., Stein, R., Prange, M. & Lohmann, G. (2011): Towards quantitative sea ice reconstructions in the northern North Atlantic: a combined biomarker and numerical modelling approach.- Earth Planet. Sci. Lett. 306: 137-148.

Müller, J., Werner, K., Stein, R., Fahl, K., Moros, M. & Jansen, E. (2012): Holocene cooling culminates in sea ice oscillations in Fram Strait.- Quat. Sci. Rev. 47: 1-14.

Not, C. & Hillaire-Marcel, C. (2012): Enhanced sea-ice export from the Arctic during the Younger Dryas.- Nature Commun. 3: 647.

Rasmussen, S.O., Seierstad, I.K., Andersen, K.K., Bigler, M., Dahl-Jensen, D. & Johnsen, S.J. (2008): Synchronization of the NGRIP, GRIP, and GISP2 ice cores across MIS 2 and palaeoclimatic implications.- Quat. Sci. Rev. 27: 18-28.

Scholz, P., Ionita, M., Lohmann, G., Dima, M. & Prange, M. (2015): Abrupt shift of the Atlantic Ocean circulation induced by atmospheric blocking.- Geophys. Res. Abstr. 17: EGU2015-4651.

Stein, R., Fahl, K. & Müller, J. (2012): Proxy reconstruction of Cenozoic Arctic Ocean sea-ice history: From IRD to IP_{25}.- Polarforschung 82: 37-71.

Weinelt, M., Vogelsang, E., Kucera, M., Pflaumann, U., Sarnthein, M., Voelker, A., Erlenkeuser, H. & Malmgren, B.A. (2003): Variability of North Atlantic heat transfer during MIS 2.- Paleoceanography 18, 1071, doi: 10.1029/2002PA00077.

Xiao, X., Fahl, K., Müller, J. & Stein, R. (2015): Sea-ice distribution in the modern Arctic Ocean: Biomarker records from trans-Arctic Ocean surface sediments.- Geochim. Cosmochim. Acta 155: 16-29.

Polarforschung 85 (2), 161–170, 2015 (erschienen 2016)

Abrupt Climate Change Experiments: The Role of Freshwater, Ice Sheets and Deglacial Warming for the Atlantic Meridional Overturning Circulation

by Gerrit Lohmann[1,2,*], Xu Zhang[1], and Gregor Knorr[1]

Abstract: In this review paper we summarise a series of numerical abrupt climate change experiments in the context deglaciation. The effects of global warming, deglacial freshwater, and ice sheets for the termination of the last ice age are examined in a model of intermediate complexity and a fully coupled, coarse-resolution climate model. We find that gradual deglacial global warming induces an abrupt strengthening of the Atlantic Meridional Overturning Circulation (AMOC). More generally, if the system is in a bistable window, a linear forcing can yield non-linear AMOC changes. In this sense Northern Hemisphere freshwater hosing only modulates the timing of the AMOC onset. Furthermore, Northern Hemisphere freshwater hosing weakens the AMOC with a potential overshoot, after the freshwater forcing has stopped. Therefore, as a further hypothesis the onset of Bølling/Allerød (B/A) interstadial with warming over Greenland could be related to an increase in AMOC, which is induced by a declining freshwater forcing prior to or in parallel with the transition. In contrast, hosing in the Southern Hemisphere has a relatively minor influence on the AMOC. The associated climate signatures and mechanisms are explored and discussed in this study.

Zusammenfassung: In diesem Übersichtsbeitrag stellen wir eine Reihe von numerischen Experimenten zum abrupten Klimawandel am Ende der letzten Eiszeit vor. Die Auswirkungen der globalen Erwärmung, des deglazialen Süßwassers und der Eisschilde auf die Termination und Ozeanzirkulation werden in einem Modell mittlerer Komplexität und einem vollständig gekoppelten Klimamodell untersucht. Unsere Modellergebnisse vermitteln Einsichten in die abrupte Erwärmung in der Nordhemisphäre, das sogenannte Bølling/Allerød (B/A) Nordatlantik Interstadial, und der deglazialen Schmelzwasserpulse. Wir stellen fest, dass die deglaziale globale Erwärmung eine Verstärkung der atlantische Umwälzbewegung (Atlantic Meridional Overturning Circulation, AMOC) induziert. Wenn sich das System in einem bistabilen Fenster bewegt, kann ein linearer Antrieb zu einer nichtlinearen Antwort in der AMOC führen, wobei das Schmelzwasser den Zeitpunkt für das B/A verändern kann und die AMOC schwächt. Bei der Rückkehr in den Usprungszustand kann die AMOC überschwingen, d.h. sie zeigt stärkere Amplituden als unter ungestörten Bedingungen. Deglaziales Süßwasser in der südlichen Hemisphäre hat einen relativ kleinen Effekt auf die AMOC. Als weitere, alternative Hypothese zum Vorhandensein des B/A-Interstadials könnte auch die Abwesenheit von Süßwasser beigetragen haben. Dadurch wird die AMOC verstärkt und infolgedessen Grönland erwärmt. Signaturen und Mechanismen dieser Prozesse werden in diesem Beitrag untersucht und diskutiert.

INTRODUCTION

Within glacial periods, and especially well documented during the last one, there are dramatic climate transitions, including high latitude temperature changes approaching the same magnitude as the glacial cycle itself. Signals with world-wide teleconnections are recorded in archives from the polar ice caps, high to middle latitude marine sediments, lake sediments and continental loess sections (e.g., Bender et al. 1999). Flohn (1986) proposed as a concept of abrupt climate change to include both, singular events and catastrophes such as extreme El Niños, as well as discontinuities in paleoclimate indices. One hypothesis for explaining deglacial as well as Dansgaard-Oeschger climatic transitions is that the Atlantic meridional overturning circulation (AMOC) flips between different modes, with warm intervals reflecting periods of strong deep water formation in the northern North Atlantic and *vice versa* (Ganopolski & Rahmstorf 2001). As an alternative approach, the underlying dynamics with its bifurcation can directly be estimated from data (Kwasniok & Lohmann 2009, Livina et al. 2011, Kwasniok & Lohmann 2012). In this study we discuss several hypotheses of ocean dynamics during glacial terminations, including the effect of global warming, freshwater history, ice-sheet height, and orbital forcing.

The overarching goal of this article is to explore different hypotheses regarding abrupt millennial-scale deglacial climate variabilty and the glacial termination. In particular, the investigations aim at a better understanding of the Bølling/Allerød (B/A) (14,700–12,700 years before present) North Atlantic interstadial dynamics and their relation to deglacial meltwater pulses. To study the glacial dynamics, we use models with different level of complexity, an ocean general circulation model (OGCM) coupled to an energy balance of the atmosphere, as well as the Earth system model COSMOS, consisting of an atmosphere-ocean general circulation model (AOGCM), including a dynamical vegetation module.

There are numerous approaches to understand the last termination. The question is what causes the abrupt warming at the onset of the Bølling as seen in the Greenland ice cores. There is a clear antiphasing seen in the deglaciation interval between 20 and 10 ka. During the first half of this period, Antarctica steadily warmed, but little change occurred in Greenland. Then, at the time when Greenland's climate underwent an abrupt warming, the warming in Antarctica stopped. A possible hypothesis can be that a sudden increase of the northward heat transport draws more heat from the south, and leads to a strong warming in the north. This "heat piracy" from the South Atlantic has been formulated by Crowley (1992). A logical consequence of this heat piracy is the Antarctic Cold Reversal (ACR) during the Northern Hemisphere warm Bølling/Allerød.

Additional freshwater forcing complicates the situation. Roche et al. (2010) explored the impact of freshwater

doi:10.2312/polfor.2016.013

[1] Alfred-Wegener-Institut Helmholtz-Zentrum für Polar- und Meeresforschung, Bussestraße 24, 27515 Bremerhaven, Germany.
[*] Corresponding author <Gerrit.Lohmann@awi.de>
[2] University of Bremen, Bremen, Germany
This paper was presented as a poster contribution at the International Conference "Our Climate – Our Future: Regional Perspectives on a Global Challenge", 6–9 October 2014 in Berlin, Germany.
Manuscript received 03 June 2015; revised version 29 November 2015; accepted 21 December 2015.

pulses with respect to different geographical locations. Lohmann & Schulz (2000) performed freshwater sensitivity studies for different ocean states with and without North Atlantic overflow water. Liu et al. (2009) showed in their experiments, covering the deglaciation that a Bølling-type overshoot can be obtained when the freshwater hosing history has been prescribed in such a way that the reconstructed temperatures and AMOC are resembled. Other important parameters are the ice sheets and greenhouse gases. During times when the ice sheets were at intermediate ice-sheet volume, large millenial-scale warmings are accompanied by increases in atmospheric carbon dioxide with a global-scale impact (Schulz et al. 1999).

We summarize some numerical experiments when freshwater forcing or idealised background conditions are changed, which are helpful to explore the phase space of the complex dynamics of the climate system, especially during the last termination where abrupt changes are detected. It is also important to understand past warm climate states where models show a mismatch with data, e.g., for the Holocene (Lohmann et al. 2013, Liu et al. 2014, Lohmann 2016) or the Pliocene (Salzmann et al. 2013).

METHODS

Model of intermediate complexity

The three-dimensional ocean model is based on the large-scale geostrophic model (LSG, Maier-Reimer et al. 1993), which is part of the Bremen Earth System Model of intermediate complexity (Lohmann et al. 2003, Butzin et al. 2005, Knorr & Lohmann 2007). The horizontal resolution is 3.5° on a semi-staggered grid with 11 levels in the vertical. It includes a simple thermodynamic sea-ice model, a 3rd order advection scheme for temperature and salinity (Schäfer-Neth & Paul 2001) and a parameterisation of overflow (Lohmann 1998). The ocean is driven by monthly fields of wind stress, surface air temperature and freshwater flux, which are taken from a present day and Last Glacial Maximum (LGM) simulation of the atmospheric general circulation model ECHAM3 / T42 (Lohmann & Lorenz 2000, Roeckner et al. 1992). In order to close the hydrological cycle, a run-off scheme transports freshwater from the continents to the ocean. We employ a modelling approach, which allows an adjustment of surface temperatures and salinity to changes in the ocean circulation, based on an atmospheric energy balance model (Lohmann et al. 1996, Prange et al. 2003). The model (abbreviated as EBM-LSG in the following) belongs to the models of intermediate complexity (Claussen et al. 2002) and has been applied to glacial climate dynamics (Prange et al. 2002, 2004, Romanova et al. 2004, Knorr & Lohmann 2003, Knorr 2005, Knorr & Lohmann 2007), carbon isotopes (Butzin et al. 2005, Hesse et al. 2011, Butzin et al. 2012) and the Cenozoic climate (Butzin et al. 2011, Lohmann et al. 2015).

Comprehensive Earth System Model

We use a comprehensive fully coupled Earth System Model, COSMOS (ECHAM5-JSBACH-MPIOM) for this study. The atmospheric model ECHAM5 (Roeckner et al. 2003), complemented by a land-surface component JSBACH (Brovkin et al. 2009), is used at T31 resolution (~3.75°), with 19 vertical layers. The ocean model MPI-OM (Marsland et al. 2003), including sea-ice dynamics that is formulated using viscous-plastic rheology, has a resolution of GR30 (3° × 1.8°) in the horizontal, with 40 uneven distributed vertical layers. The climate model has already been used to simulate the last millennium (Jungclaus et al. 2010), internal climate variability (Wei et al. 2012), the Miocene warm climate (Knorr et al. 2011, Knorr & Lohmann 2014), the Pliocene (Stepanek & Lohmann 2012, Haywood et al. 2013), Holocene variability and trends (Wei & Lohmann 2012, Varma et al. 2012, Lohmann et al. 2013), the last interglacial (Lunt et al. 2013, Bakker et al. 2014, Felis et al. 2015, Pfeiffer & Lohmann 2016, Sutter et al. 2016), and the LGM climate (Zhang et al. 2013, 2014, Gong et al. 2015, Stärz et al. 2016), including hosing experiments (Kageyama et al. 2012, Gong et al. 2013). The model has recently been coupled to an ice-sheet model (Barbi et al. 2014, Gierz et al. 2015) and is enhanced with water-isotope modules (Werner et al. 2011, Langebroek et al. 2011, Xu et al. 2012, Haese et al. 2013, Dietrich et al. 2013, Goelles et al. 2014, Werner et al. 2015, Sutter et al. 2015). For another recent application of this model, see Stepanek & Lohmann 2016.

DEGLACIAL WARMING INDUCES AN ABRUPT AMOC TRANSITION: EBM-LSG EXPERIMENTS

The experiments with the EBM-LSG consist of two major parts. In the first part we simulate the deglacial climate between about 20 ka and the onset of the Bølling/Allerød (B/A) warm phase (experiments B1-B4). These experiments are identical to the ones published in Knorr & Lohmann (2007). Deglacial warming is implemented by a transition from glacial to interglacial background climate being accomplished within 15 ka. The background climate is provided by monthly fields of air temperature, sea ice (Southern Hemisphere) and wind stress, linearly interpolated between the LGM conditions at 20 ka before present and present day climatology (cf. Fig. 1a). We see how the linear warming of the background climate boundary conditions can induce a rapid intensification of the ocean circulation (Fig. 1a, b). The basic mechanism is related to a release of convectively unstable warm subsurface water in the northern North Atlantic.

The water gets vertically unstable due to changes in surface warming and sea-ice retreat. The warm subsurface water during weak overturning is released and provides a heat flush in the northern North Atlantic. This heat flush is related to the B/A transition as seen in ice cores. A similar mechanism of subsurface heat release is described in Knorr & Lohmann (2007), Kim et al. (2012), and Gong et al. (2013). The vertical structure can even be used to detect ocean circulation changes (Rühlemann et al. 2004, Lohmann et al. 2008).

In the second part of experiments attention is paid to investigating the effect of MWP-1A (deglacial melt water pulse 1A) on the AMOC and to evaluating its impact on the B/A and the subsequent deglacial meltwater. These freshwater perturbation experiments are denoted as MWP1–MWP5 (Fig. 2) and represent additional simulations to the experiments (B1-B4).

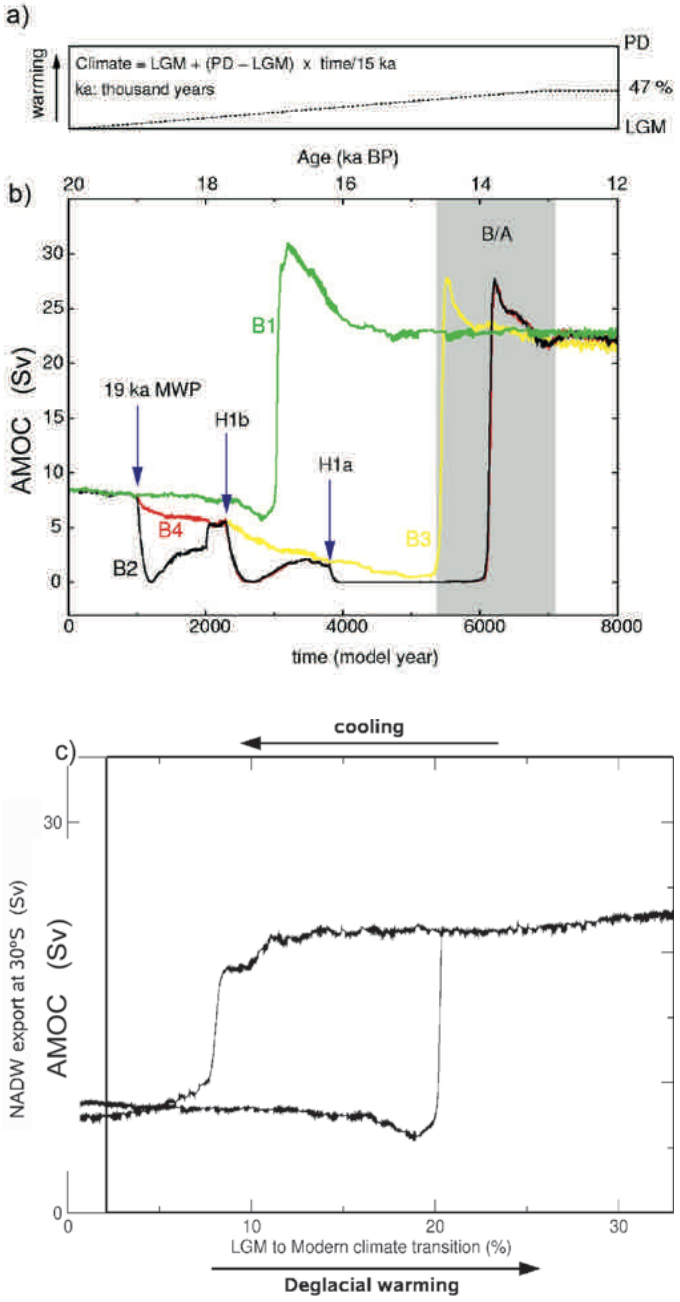

Fig. 1: a): Prescribed temporal changes in the global background climate and simulated Atlantic Meridional Overturning Circulation (AMOC) changes with the model of intermediate complexity. The background climate conditions are linearly interpolated between glacial and modern conditions. All experiments start from the glacial equilibrium and the gradual warming is stopped after 7000 model years. b): Green curve (B1) represents the experiment without any deglacial freshwater pulses. Experiments B2 (black curve), B3 (yellow curve), and B4 (red curve) exhibit different successions of deglacial meltwater pulse scenarios to the North Atlantic. The beginning of the respective freshwater perturbation is indicated by the blue arrows. c): Hysteresis diagram based on B1. The AMOC index is calculated from the export at 30°S in the Atlantic Ocean.

Abb. 1: (a): Vorgeschriebene zeitliche Veränderungen im globalen Hintergrundklima und simulierte AMOC (Atlantic Meridional Overturning Circulation) im EBM-LSG Modell mittlerer Komplexität. Die Hintergrundklimabedingungen werden linear zwischen Eiszeit und modernen Bedingungen interpoliert. Diese schrittweise Erwärmung wird nach 7000 Modelljahren gestoppt. b): Die grüne Kurve (B1) stellt das Experiment ohne deglaziales Süßwasser dar. Experimente B2 (schwarze Kurve), B3 (gelbe Kurve) und B4 (rote Kurve) weisen unterschiedliche Abfolgen von deglazialen Schmelzwasserpulsen aus. Der Beginn der jeweiligen Süßwasserstörungen wird durch die blauen Pfeile angezeigt. c): Hysterese Diagramm bezogen auf B1. Der AMOC Index wurde über den Wassermassenexport bei 30°S berechnet.

All meltwater discharge to the North Atlantic is uniformly applied between 20°N and 50°N. The timing and amplitude of the freshwater perturbations is depicted in Figure 2a. Figure 2a,b emphasizes the combined effect of hosing and AMOC strengthening due to global warming. The hosing provides only a second-order effect, modulating the timing of the transition. In MWP1, the release of the MPW-1A to the North Atlantic delays the abrupt AMOC amplification by about one decade, but does not inhibit the amplification of the AMOC. The rising freshwater flux of MWP-1A causes a drop back to

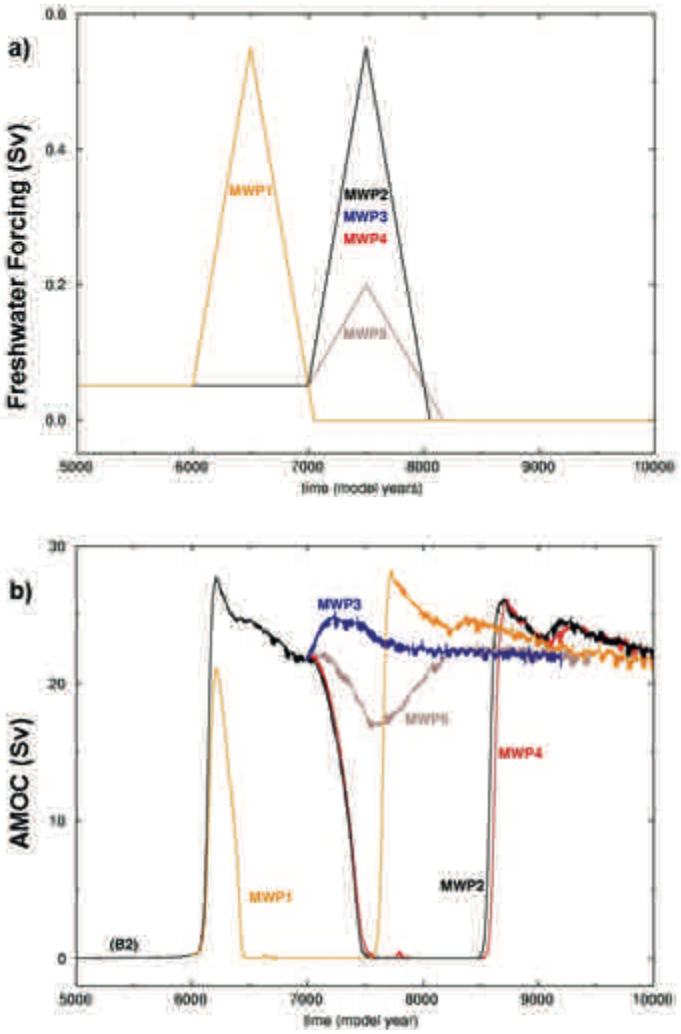

Fig. 2: a): Different deglacial hosing experiments with different timing and amplitude in the model of intermediate complexity. In experiment MWP1, the onset of the meltwater MWP-1A is after 6000 years prior to the onset of the Bølling/Allerød (B/A) in B2. In experiments MWP2-MWP5, MWP-1A is discharged after 7000 model years. In MWP2 and MWP3, it is released to the North Atlantic and the Weddell Sea, respectively. In MWP4 and MWP5 the pulses are discharged uniformly to both locations. b): Temporal signature of the AMOC (Atlantic Meridional Overturning Circulation) with respect to different meltwater scenarios with B2 as the base experiment (cf. Fig. 1b).

Abb. 2: a): Unterschiedliche deglaziale Experimente mit verschiedenen Süßwasserstörungen im EBM-LSG Modell mittlerer Komplexität. Im Experiment MWP1 wird der Schmelzwasserpulses 6000 Jahre vor den Beginn des Bølling/Allerød gelegt. In den Experimenten MWP2-MWP5 wird der Beginn des Schmelzwasserpulses nach 7000 Modelljahren realisiert. In MWP2 und MWP3 wird das Süßwasser im Norden bzw. im Süden eingebracht. Hingegen werden in den Experimenten MWP4 und MWP5 das Süßwasser zu gleichen Teilen in den Norden und Süden eingebracht. b): Zeitlicher Verlauf von AMOC (Atlantic Meridional Overturning Circulation) unter den verschiedenen Schmelzwasserszenarien mit B2 als Basisexperiment, welches auch in Abb. 1b gezeigt wird.

the "off-mode" simultaneously to the maximum meltwater magnitude. The AMOC remains stalled until the warming proceeds to more than 50 % of the total termination-I warming at 7500 years. In experiment MWP2, the MWP-1A is released 1000 years later than in MWP1 and the AMOC is also suppressed to the "off-mode", and the recovery to an interstadial AMOC occurs 500 years after the cessation of MWP-1A within a century. The application of MWP-1A only in the Weddell Sea results in a slight increase of the AMOC in experiment MWP3. The division of the meltwater inflow to both, the North Atlantic and the Weddell Sea region in MWP4 also ceases AMOC for about 1000 years with a minimal retarded model response compared to MWP2. The application of a weaker meltwater pulse than in MWP4 temporarily reduces, but does not shut down the AMOC in MWP5.

Again, the deglacial resumption of the AMOC is associated with heat release from the sub-surface ocean in the North Atlantic, as well as large-scale salinity advection of near-surface waters from the South Atlantic/Indian Ocean and the tropics to the formation areas of North Atlantic deep water. The restarted AMOC possesses a strong insensitivity to deglacial meltwater pulses (Figs. 1b, 2b), and coexistent, a distinct bistability in the hysteresis curve for cumulative positive freshwater fluxes to the North Atlantic (Fig. 1).

NORTHERN AND SOUTHERN HOSING AND OVERSHOOT IN THE AMOC IN COSMOS

A quite different concept for deglacial AMOC changes (compared to the previous section) is that a reduction of deglacial meltwater may induce a Northern Hemisphere warming after the meltwater has stopped (e.g., Liu et al. 2009, Gong et al. 2013, Zhang et al. 2013). In our COSMOS model integrations, a freshwater hosing of 0.2 Sv (1 Sv = 10^6 m^3/s) has been applied for 150 years in the North Atlantic (NA) in the ice-rafted debris (IRD) belt in the North Atlantic Ocean (40°N - 55°N) or in the Southern Ocean (SO) in the region (52° - 62°S, 40°W - 62°W), respectively (Fig. 3). The experiments LGM ctl and the North Atlantic hosing (LGM NA 0.2 Sv) have been used in Zhang et al. (2013).

The NA hosing experiments indicate an AMOC reduction, but the following recovery stages after 250 years exhibit a clear overshoot (Fig. 3a). One can subdivide the underlying dynamics of the overall recovery into two stages: one directly following the end of the freshwater perturbation that describes the initial resumption, and a superposed phase that coincides with the AMOC overshoot dynamics (Gong et al. 2013, Zhang et al. 2013): The deep-water formation in the South Labrador Sea reduces to 4-7 Sv, and a shutdown of deep-water formation in the Greenland-Iceland-Norwegian (GIN) Seas is diagnosed. Subsequently, an instant restart of deep-water formation in the South Labrador Sea is triggered, whereas the restart in the GIN Seas occurs 30 years later. The corresponding trigger mechanism is related to a modified salinity stratification and subsurface warming that quickly build up during the freshwater perturbation. The surface anomaly in surface temperature is shown in Figure 3b.

The SO hosing provides almost no change in AMOC (Fig. 3a, blue line), and the surface temperature signature shows only a minor cooling after 150 years in the North Atlantic (not shown).

INFLUENCE OF CO_2 AND NORTHERN HEMISPHERE ICE-SHEET HEIGHT

Here, we investigate the role of CO_2 changes on AMOC during times of intermediate glacial ice volume using COSMOS. Following Zhang et al. (2014), we perform a transient simulation in which we linearly increase atmospheric CO_2 concentration from 185 to 205 ppm within 500 years, under an intermediate ice-sheet height (40 % of the LGM ice-sheet level; Fig. 4a). Figure 4b indicates an abrupt onset of AMOC along the linear increase in CO_2 and thus surface temperature in the North Atlantic (Fig. 4c). The surface temperature

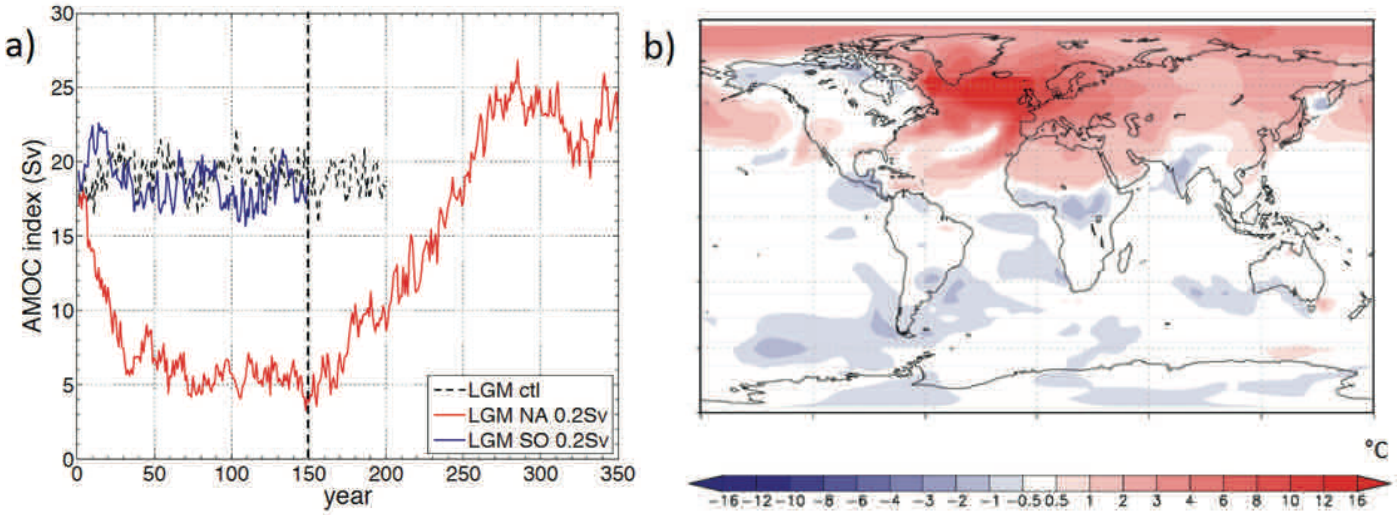

Fig. 3: Earth system model COSMOS experiments. a): AMOC response to freshwater hosing of 0.2 Sv in the North Atlantic Ocean (NA) or in Southern Ocean (SO), respectively. b): The NA hosing experiment indicates an AMOC reduction, but the following recovery stages after 250 years exhibit a clear overshoot.

Abb. 3: Experimente mit dem Erdsystemmodell COSMOS. a): AMOC Reaktion auf Süßwasserstörung von 0,2 Sv im Nordatlantik (NA) oder im Südlichen Ozean (SO). b): Das NA Experiment zeigt eine AMOC-Reduktion, aber die folgende Erholung nach 250 Jahren zeigt einen Überschwinger in der Atlantic Meridional Overturning Circulation (AMOC).

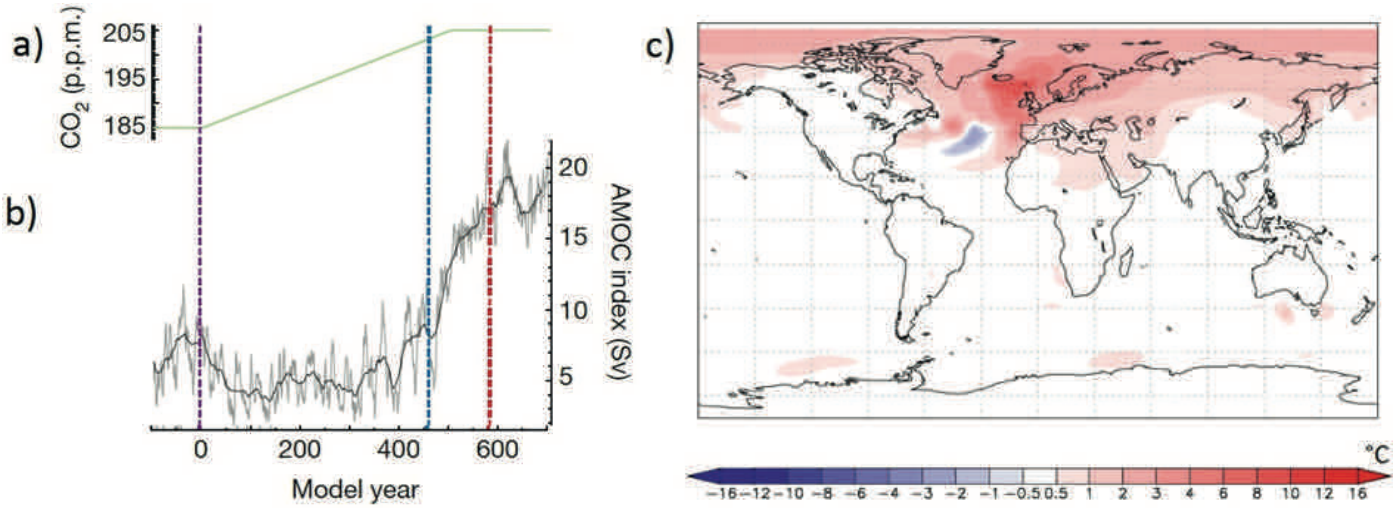

Fig. 4: Earth system model COSMOS experiments. a): Transient CO_2 forcing. b): Atlantic Meridional Overturning Circulation (AMOC) response. Bold lines show the 30-year running mean of the original data (grey lines). The vertical purple, blue and red dotted lines represent the starting points for the transient simulations, abrupt AMOC transitions and cooling in the Southern Hemisphere, respectively. Negative model years indicate the control simulation of a glacial state, but with 40 % Northern Hemisphere ice-sheet height, which is close to the height threshold. c): Surface temperature anomaly between year 600–700 (warming) and 300–400 (cooling) of panel 4b.

Abb. 4: Experimente mit dem Erdsystemmodell COSMOS. a): Transienter CO_2-Antrieb. b): Antwort der Atlantic Meridional Overturning Circulation (AMOC). Dicke Linien zeigen das 30-Jahresmittel der Originaldaten (graue Linien). Die vertikalen lila, blau und rot gestrichelten Linien stellen die Ausgangspunkte für die transiente Simulationen. Negative Modelljahre stehen für die Kontrollsimulation eines eiszeitlichen Zustands, der mit 40 % der Eisdeckenhöhe gerechnet wurde. 40 % ist in der Nähe der Schwelle der kritischen Eisschildhöhe. c): Oberflächen-Temperaturanomalie zwischen Jahr 600–700 (Erwärmung) und 300–400 (Abkühlung) bezogen auf Abb. 4 b.

in Figure 4c is shown as anomaly between the model year 600–700 (warming) and 300–400 (cooling) in this simulation (Fig. 4b). The response can be understood in terms of a transition in a bistable system with respect to the ice-sheet height (Zhang et al. 2014).

INFLUENCE OF STRONG SOUTHERN HOSING, CO_2, AND ORBITAL FORCING

Additional hypotheses related to Southern Hemisphere hosing from the Antarctic Ice Sheet (AIS) and warming are tested for deglaciation using COSMOS. The CO_2 and freshwater history used to force our transient runs is shown in Figure 5. The CO_2 concentration is fixed to LGM level (i.e. 185 ppm) before 18 ka BP. After that, the Antactic ice core EDC CO_2 record is imposed to force our transient simulations (Fig. 5a). Freshwater enters into the Southern Ocean (SO) where the freshwater input is linearly scaled by reconstructed marine records of iceberg-rafted debris (Weber et al. 2014). The freshwater forcing is determined by assuming that 50 % of the maximum sea-level rates during MWP-1A (40 mm/year) originated from Antarctica. The corresponding peak freshwater forcing around Antarctica is shown in Figure 5b. Because of the above mentioned sea-level assumption and the fact that we have to use the acceleration factor 5 for the transient integrations, the actual freshwater forcing is 5 times larger per time step than in runs without acceleration. The model runs were performed with COSMOS and the basic runs were published in Weber et al. (2014). Here, we present some analyses of the long-term climate scenarios.

Finally, we employed the transient orbital forcing in the experiments. The annual mean orbital forcing is due to obliquity (precession cancels out for the annual mean forcing) and is displayed in Figure 5c. As a caveat of our methodology due to computational resources, our runs were accelerated by factor 5 (cf. Lorenz & Lohmann 2004), implying the simulated warming and hosing in our runs might not directly represent the real Bølling warming and mechanisms of local freshwater input (e.g., Lunt et al. 2006, Timm & Timmermann 2007).

To determine the effect of different freshwater sources, three transient freshwater forcing experiments were conducted under glacial background conditions (Fig. 6). Freshwater flux is added to the coastal areas of the East Antarctic Ice Sheet (EAIS) (0° - 180°E) and the West Antarctic Ice Sheet (WAIS) (120°W - 60°W). In DG1, the forcing is assumed to originate from the EAIS. In DG2, EAIS (WAIS) forcing is used for the period 21–15 ka (15–14 ka). DG3 assumes EAIS forcing at 21–16 ka and WAIS forcing at 16–14 ka. Two other experiments (DG2C and DG2CO) were conducted to examine the effect of CO_2 (DG2C) as well as a combination of CO_2 and orbital forcing (DG2CO) on AMOC and surface temperature. DG2C and DG2CO show almost the same signature in time and space, indicating that the CO_2 effect is stronger than the effect by insolation.

Figures 6d, 6e show the surface temperature anomaly between 14.7-14.6 ka (warming in the north) and 15.55-15.4 ka (cooling in the north) in simulations DG2 and DG2CO. This bipolar seesaw is related to an AMOC increase (Fig. 6c). The SO meltwater pulse weakens the AMOC strength after a delay of 100 years when the large freshwater signal is transported to the North Atlantic. The AMOC increase and the related warming over Greenland after 14.7 ka are thus not due to the simultaneous SO meltwater pulse, but to a weakened SO freshwater forcing prior to this time (Fig. 5b).

For the water surrounding Antarctica, Weber et al. (2014) found a more pronounced halocline during periods of

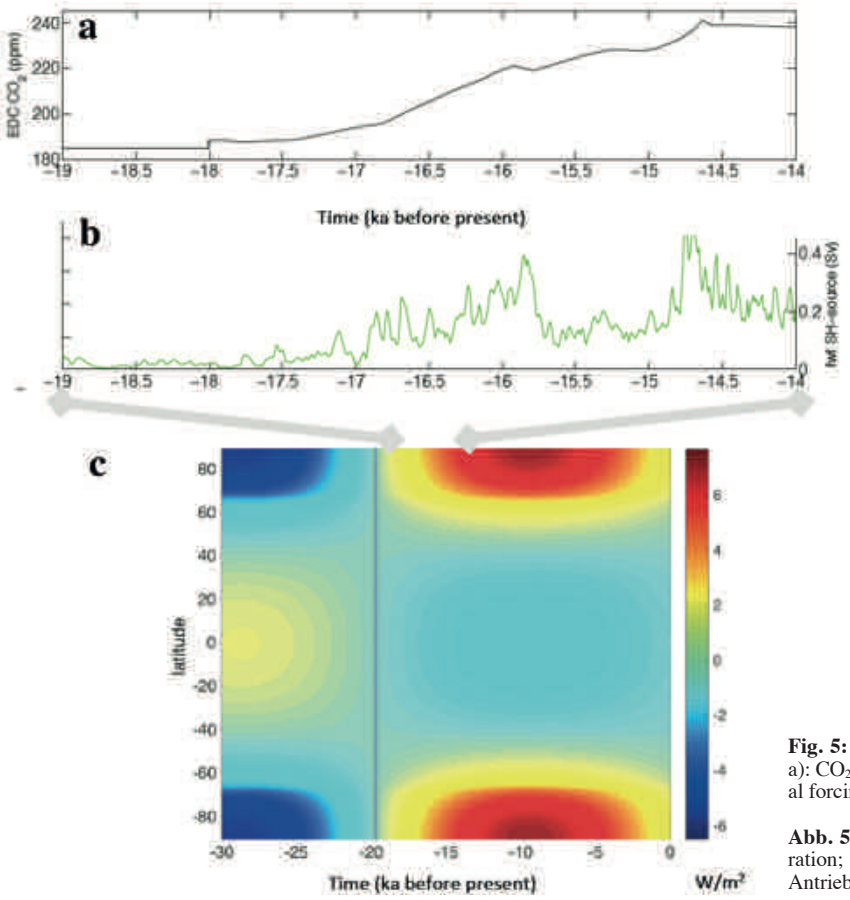

Fig. 5: Forcing for the Earth system model COSMOS experiments. a): CO_2 concentrations; b): Southern Ocean freshwater flux; c): orbital forcing (only annual mean is displayed).

Abb. 5: Antrieb für Erdsystemmodell COSMOS. a): CO_2-Konzentration; b): Deglaziales Süßwasser im Südlichen Ozean; c): orbitaler Antrieb für das jahreszeitlich gemittelte Signal.

strong freshwater forcing as the main cause for the subsurface warming in the SO during deglaciation. Such subsurface warming may have induced instabilities in the coupled atmosphere-ocean-ice system, which could be important for ice-shelf instabilities and shall be investigated in the future.

We furthermore mention that our models (COSMOS and EBM-LSG) show different full glacial overturning rates. For the EBM-LSG model, we validated the circulation model with carbon isotope data (HESSE et al. 2011) and find a good agreement with a stronger overturning circulation as used here as the LGM control state. A shallower than today circulation with about modern circulation strength is consistent with the carbon isotope data (HESSE et al. 2011). Zhang et al. (2013, 2014) compared the deep water and surface signatures in COSMOS with proxy data and found a general agreement with paleoclimate evidences (e.g., a salty and cold Antarctic Bottom Water).

DISCUSSION AND CONCLUSIONS

Our model experiments reveal insights for the Bølling/Allerød (B/A) North Atlantic interstadial dynamics and the impact of deglacial meltwater pulses. Robust features seem to be:

- Deglacial global warming induces stronger AMOC (Figs. 1b, 4b). If the system is in a bistable window, a linear forcing can yield non-linear AMOC changes (Fig. 1b, Fig. 2b, Fig. 4b). An abrupt onset of the AMOC can be triggered by a gradual global warming during deglaciation showing typical hysteresis behaviour (Fig. 1c). The intensification depends on its glacial mean state (KNORR & LOHMANN 2007), and this intensification is opposite to the weakening response of AMOC to increased CO_2, starting from the present to the future scenarios (e.g., LOHMANN et al. 2008). This dependence of the background state is caused by the large area of sea-ice cover under glacial conditions (ZHU et al. 2015). Northern Hemisphere freshwater hosing can affect the timing of the AMOC onset.

- Northern Hemisphere freshwater hosing weakens AMOC with a potential temperature and AMOC overshoot response after the freshwater forcing has stopped (Fig. 3a,b). However, the overshoot is just a transient phenomenon. Therefore, it cannot explain the B/A dynamics alone.

- Hosing in the Southern Hemisphere has a small effect on the AMOC if the perturbation is in the order of the Northern Hemisphere signal (Figs. 2b, 3a). This is in contrast to the findings of WEAVER et al. (2003), using a model of intermediate complexity – see also KERR 2003 and STOCKER 2003 for a discussion of southern and northern forcing. In our case the EBM-LSG shows a slight increase in AMOC due to a Southern Hemisphere signal (MWP3 in Fig. 2).

- If the Southern Hemisphere freshwater flux is strongly enhanced – in our case to mimic the possible sea-level contribution in the COSMOS run – it can affect the AMOC. An increase in AMOC and warming over Greenland can be simulated either by ending freshwater forcing in the Northern Hemisphere (Fig. 3) or as a delayed response to a weakened

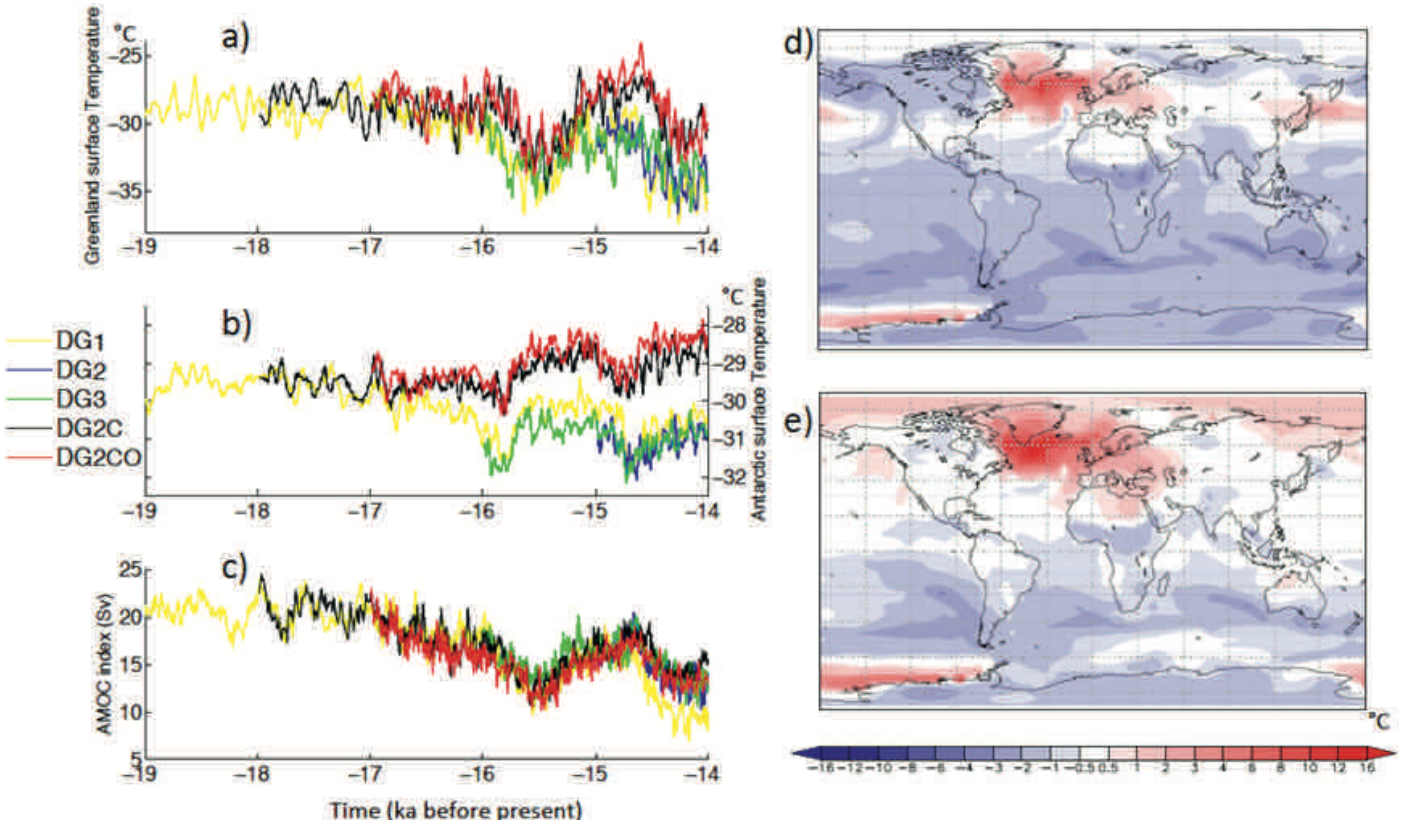

Fig. 6: Earth system model COSMOS experiments. a): History of original freshwater flux to the Southern Ocean. b) and c): Temperature and Atlantic Meridional Overturning Circulation (AMOC) response to external forcing. DG1: the freshwater forcing is assumed to originate from the East AIS. DG2: East (West) AIS forcing is used for the period 21–15 ka (15–14 ka). DG3: East AIS forcing at 21–16 ka and West AIS forcing at 16–14 ka. In DG2C, varied CO_2-concentrations were prescribed for the period 18–14ka. Orbital forcing covering the period from 17–14 ka were additionally used in DG2CO. d and e): show the surface temperature anomalies between 14.7–14.6 ka and 15.55-15.4 ka in simulations DG2 in (d) and DG2CO in (e), respectively.

Abb. 6: Experimente mit dem Erdsystemmodell COSMOS. a) Historie des originalen Süßwasserflusses im südlichen Ozean; b) und c): Temperaturantwort und Reaktion der Atlantic Meridional Overturning Circulation (AMOC) auf externe Randbedingungen. Verschiedene Szenarien DG1: Süßwasser stammt aus dem östlichen AIS. DG2: Östliches Süßwasser für den Zeitraum 21–15 ka, westliches für 15-14 ka. DG3: Östliches Süßwasser für 21–16 ka und westliches für 16–14 ka. In DG2C werden die CO_2-Konzentrationen für den Zeitraum 18–14 ka angenommen. Zusätzlich in DG2CO: Orbitaler Antrieb für 17–14 ka. Tafeln d und e) zeigen die Oberflächentemperatur-Anomalien zwischen 14,7–14,6 ka und 15,55–15,4 ka in Simulationen DG2 (6d) beziehungsweise DG2CO in (6e).

freshwater forcing in the Southern Hemisphere (Fig. 5, 6). Our finding is consistent with Swingedouw et al. (2009). They proposed the hypothesis that a SO freshwater pulse can impact the strength of the AMOC only when the amount of freshwater is larger than a certain value.

- Larger glacial Northern Hemisphere ice-sheet height produces stronger AMOC. The ice-sheet height seems to be an important parameter for multiple equilibria of the AMOC and possibly millenial variability at intermediate ice-sheet height. If the AMOC is in this bistable window, other parameters like CO_2 can cause abrupt transitions (Fig. 4). We speculate that for the termination, the change in ice-sheet height is most likely a second-order effect since the lowering of the Northern Hemisphere ice sheet will weaken the AMOC.

Using different types of models, it is important to explore the phase space of abrupt climate changes like the deglaciation, and to explore the separation between first and second order effects (Lohmann 2009). Several regional features like the subsurface warming (e.g., Rühlemann et al. 2004, Weber et al. 2014), seasonal sea-ice cover (Abelmann et al. 2015), and subsequent effects shall be studied, using different models with different levels of complexity. For example, in the intermediate complexity model EBM-LSG and the full AOGCM COSMOS, a smooth warming can produce an abrupt change of AMOC, while in Zhu et al. (2015) the AMOC intensification seems to be more gradual in their AOGCM. The change of AMOC in consequence to changes in ice-sheet height (higher ice sheet leads to stronger AMOC) is also qualitatively consistent with the finding in another fully coupled climate model in the sense that lowering the ice sheet reduces AMOC (Zhu et al. 2014). It is concluded that model experiments under different forcings (including single forcing experiments) are required for a wide range in the phase space of solutions.

Some general questions remain. As yet, it is not clear if the exact timing of transtions is partly phase-locked to an oscillating system (as seen e.g., in Winton 1993, Wang & Mysak 2006, Schulz et al. 1999, Kim et al. 2012), if the transitions are solely triggered by external forcing like freshwater or deglacial warming (Knorr & Lohmann 2007, Liu et al. 2009), or if noise-induced transitions play a role (e.g., Timmermann & Lohmann 2000). Others than oceanic processes can induce part of the long-term signal through modulations of atmospheric teleconnections and atmospheric bridges (Rodgers et al. 2003, Lohmann, 2016). All the different concepts and their underlying assumptions

might need to be revisited and to be carefully compared to paleoclimate proxy data. However, a further major difficulty for the validation of model results is the interpretation of the recorder systems since the paleodata may be biased towards different seasons or other recorder-related conditions (e.g., LAEPPLE et al. 2011, LOHMANN & WILTSHIRE 2012, LOHMANN et al. 2013, HESSE et al. 2014, WERNER et al. 2015, PFEIFFER & LOHMANN 2016), providing a source of uncertainty of forcing mechanisms and long-term climate variability.

ACKNOWLEDGMENTS

We acknowledge funding by the Helmholtz Climate Initiative Regional Climate Change (REKLIM), a joint research project of the Helmholtz Association of German Research Centres, the research programme "Polar regions and Coasts in a changing Earth System" (PACES) of the Alfred Wegener Institute Helmholtz Centre for Polar and Marine Research, and the BMBF funded projects SiGePax and PalMod. Finally, we thank Z. Liu and one anonymous referee for their detailed and constructive suggestions.

References

Abelmann, A., Gersonde, R., Knorr, G., Zhang, X., Chapligin, B., Maier, E., Esper, O., Friedrichsen, H., Lohmann, G, Meyer, H. & Tiedemann, R. (2015): The seasonal sea ice zone in the glacial Southern Ocean as a carbon sink.- Nature comm. 6, 8136. doi: 10.1038/ncomms9136.

Bakker, P., Masson-Delmotte, V., Martrat, B., Charbit, S., Renssen, H. Groger, M., Krebs-Kanzow, U., Lohmann, G., Lunt, D.J., Pfeiffer, M., Phipps, S.J., Prange, M., Ritz, S.P., Schulz, M., Stenni, B., Stone, E.J. & Varma, V. (2014): Temperature trends during the Present and Last interglacial periods - A multi-model-data comparison.- Quat. Sci. Rev. 99: 224-243, doi:10.1016/j.quascirev.2014.06.031.

Barbi, D., Lohmann, G., Grosfeld, K. & Thoma, M. (2014): Ice sheet dynamics within an Earth system model: coupling and first results on ice stability and ocean circulation.- Geosci. Model Dev. 7: 2003-2013, doi:10.5194/gmd-7-2003-2014.

Bender, M.L., Malaize, B., Orchardo, J., Sowers, T. & Jouzel, J. (1999): High precision correlations of Greenland and Antarctic ice core records over the last 100 kyr.- In: P.U. CLARK, R.S. WEBB, & L.D. KEIGWIN (eds): Mechanisms of global climate change at millennial time scales. Geophys. Monogr. 112: 149-164.

Brovkin, V., Raddatz, T., Reick, C.H., Claussen, M. & Gayler, V. (2009): Global biogeophysical interactions between forest and climate.- Geophys. Res. Lett. 36: 1-5.

Butzin, M., Prange, M. & Lohmann, G. (2005): Radiocarbon simulations for the glacial ocean: the effects of wind stress, Southern Ocean sea ice and Heinrich events.- Earth Planet. Sci. Lett. 235: 45-61, doi: 10.1016/j.epsl.2005.03.003.

Butzin, M., Lohmann, G. & Bickert, T. (2011): Miocene ocean circulation inferred from marine carbon cycle modeling combined with benthic isotope records.- Paleoceanography 26: PA1203, doi: 10.1029/2009PA001901.

Butzin, M., Prange, M. & Lohmann, G. (2012): Readjustment of glacial radiocarbon chronologies by self-consistent three-dimensional ocean circulation modeling.- Earth Planet. Sci. Lett. 317-318: 177-184, doi: 10.1016/j.epsl.2011.11.046

Claussen, M., Mysak, L.A., Weaver, A.J., Crucifix, M., Fichefet, T., Loutre, M.-F., Weber, S.L., Alcamo, J., Alexeev, V.A., Berger, A., Calov, R., Ganopolski, A., Goosse, H., Lohmann, G., Lunkeit, F., Mokhov, I.I., Petoukhov, V., Stone, P. & Wang, Z. (2002): Earth System Models of intermediate complexity: closing the gap in the spectrum of Climate System Models.- Clim. Dyn. 18: 579-586.

Dietrich, S., Werner, M., Spangehl, T. & Lohmann, G. (2013): Influence of orbital forcing and solar activity on water isotopes in precipitation during the mid and late Holocene.- Clim. Past 9: 13-26, doi: 10.5194/cp-9-13-2013.

Crowley, T.J. (1992): North Atlantic deep water cools the southern hemisphere.- Paleoceanography 7: 489-497.

Felis, T., Giry, C., Scholz, D., Lohmann, G., Pfeiffer, M., Pätzold, J., Kölling, M. & Scheffers, S.R. (2015): Tropical Atlantic temperature seasonality at the end of the last interglacial.- Nature Comm. 6: 6159, doi: 10.1038/ncomms7159.

Flohn, H. (1986): Singular events and catastrophes now and in climatic history.- Naturwissenschaften 73: 136-149.

Ganopolski, A. & Rahmstorf, S. (2001): Rapid changes of glacial climate simulated in a coupled climate model.- Nature 409: 153-158.

Gierz, P., Lohmann, G. & Wei, W. (2015): Response of Atlantic overturning to future warming in a coupled atmosphere – ocean – ice-sheet model.- Geophys. Res. Lett. 42, doi: 10.1002/2015GL065276.

Goelles, T., Grosfeld, K. & Lohmann, G. (2014): Semi-Lagrangian transport of oxygen isotopes in polythermal ice sheets: implementation and first results.- Geosci. Model Dev. 7: 1395-1408, doi: 10.5194/gmd-7-1395-2014.

Gong, X., Knorr, G., Lohmann, G. & Zhang, X. (2013): Dependence of abrupt Atlantic meridional ocean circulation changes on climate background states.- Geophys. Res. Lett. 40: 3698-3704, doi: 10.1002/grl.5070.1.

Gong, X., Zhang, X., Lohmann, G., Wei, W., Zhang, X. & Pfeiffer, M. (2015): Higher Laurentide and Greenland ice sheets strengthen the North Atlantic Ocean circulation.- Clim. Dyn. 45: 139-150, doi: 10.1007/s00382-015-2502-8,

Haese, B., Werner, M. & Lohmann, G. (2013): Stable water isotopes in the coupled atmosphere-land surface model ECHAM5-JSBACH.- Geosci. Model Dev. 6: 1463-1480, doi: 10.5194/gmd-6-1463-2013.

Haywood, A.M., Hill, D.J., Dolan, A.M., Otto-Bliesner, B., Bragg, F., Chan, W.-L., Chandler, M.A., Contoux, C., Jost, A., Kamae, Y., Lohmann, G., Lunt, D.J., Abe-Ouchi, A., Pickering, S.J., Ramstein, G., Rosenbloom, N.A., Sohl, L., Stepanek, C., Yan, Q., Ueda, H. & Zhang, Z. (2013): Large-scale features of Pliocene climate: results from the Pliocene Model Intercomparison Project.- Clim. Past, 9: 191-209, doi: 10.5194/cp-9-191-2013.

Hesse, T., Butzin, M., Bickert, T. & Lohmann, G. (2011): A model-data comparison of δ13C in the glacial Atlantic Ocean.- Paleoceanography 26: PA3220, doi: 10.1029/2010PA002085.

Hesse, T., Wolf-Gladrow, D., Lohmann, G., Bijma, J., Mackensen, A. & Zeebe, R.E. (2014): Modelling $\delta^{13}C$ in benthic foraminifera: insights from model sensitivity experiments.- Marine Micropal. 112: 50-61. DOI: 10.1016/j.marmicro.2014.08.001.

Jungclaus, J.H. Lorenz, S.J., Timmreck, C., Reick, C.H., Brovkin, V., Six, K., Segschneider, J., Giorgetta, M.A., Crowley, T.J., Pongratz, J., Krivova, N.A., Vieira, L.E., Solanki, S.K., Klocke, D., Botzet, M., Esch, M., Gayler, V., Haak, H., Raddatz, T.J., Roeckner, E., Schnur, R., Widmann, H., Claussen, M., Stevens, B. & Marotzke, J. (2010): Climate and carbon-cycle variability over the last millennium.- Clim. Past 6: 723-737.

Kageyama, M., Merkel, U., Otto-Bliesner, B., Prange, M., Abe-Ouchi, A., Lohmann, G., Roche, D.M., Singarayer, J., Swingedouw, D. & Zhang, X. (2012): Climatic impacts of fresh water hosing under Last Glacial Maximum conditions: a multi-model study.- Clim. Past. 9: 935-953, SRef-*ID:1814-9332/cp/2013-9-935.*

Kerr, R.A. (2003): Who pushed whom out of the Last Ice Age?.- Science 299: 1645, doi: 10.1126/science.299.5613.1645.

Kim, J.-H., Romero, OE., Lohmann, G., Donner, B., Laepple, T., Haam, E. & Damsté, J.S.S. (2012): Pronounced subsurface cooling of North Atlantic waters off Northwest Africa during Dansgaard-Oeschger interstadials.- Earth Planet. Sci. Lett. 339–340: 95-102, doi: 10.1016/j.epsl.2012.05.018.

Knorr, G. (2003): Collapse and resumption of the thermohaline circulation during deglaciation: insights by models of different complexity.- PhD Thesis, University of Hamburg, Germany. 1-107.

Knorr, G. & Lohmann, G. (2003): Southern Ocean origin for resumption of Atlantic thermohaline circulation during deglaciation.- Nature 424: 532-536.

Knorr, G. & Lohmann, G. (2007): Transitions in the Atlantic thermohaline circulation by global deglacial warming and melt-water pulses.- Geochem. Geophys. Geosyst. 8, doi:10.1029/2007GC001604.

Knorr, G. & Lohmann, G. (2014): A warming climate during the Antarctic ice sheet growth at the Middle Miocene transition.- Nature Geosci. 7: 376-381, doi: 10.1038/NGEO2119

Knorr, G., Butzin, M., Micheels, A. & Lohmann, G. (2011): A warm Miocene climate at low atmospheric CO_2 levels.- Geophys. Res. Lett. 38: 1-5.

Kwasniok, F. & Lohmann, G. (2009): Deriving dynamical models from paleoclimatic records: application to glacial millennial-scale climate variability.- Phys. Rev. E 80: 066104, doi: 10.1103/PhysRevE.80.066104.

Kwasniok, F. & Lohmann, G. (2012): A stochastic nonlinear oscillator model for glacial millennial-scale climate transitions derived from ice-core data.- Nonlin. Processes Geophys. 19: 595-603, doi: 10.5194/npg-19-595-2012.

Laepple, T., Werner, M. & Lohmann, G. (2011): Synchronicity of Antarctic temperatures and local solar insolation on orbital time-scales. Nature 471: 91-94, doi: 10.1038/nature09825

Langebroek, P., Werner, M. & Lohmann, G. (2011): Climate information imprinted in oxygen-isotopic composition of precipitation in Europe.- Earth Planet. Sci. Lett. 311: 144-154, doi: 10.1016/j.epsl.2011.08.049.

Liu, Z., Otto-Bliesner, B.L., He, F., Brady, E.C., Tomas, R., Clark, P.U., Carlson, A.E., Lynch-Stieglitz, J., Curry, W., Brook, E., Erickson, D., Jacob, R., Kutzbach, J. & Cheng, J. (2009): Transient simulation of last deglaciation with a new mechanism for Bolling-Allerod warming.- Science 325: 310-314, doi: 10.1126/science.1171041.

Liu, Z., Zhua, J., Rosenthal, Y., Zhang, X., Otto-Bliesner, B., Timmermann, A., Smith, R.S., Lohmann, G., Zheng, W. & Timm, O.E. (2014): The Holocene temperature conundrum.- Proc. National Acad. Sci. USA 111: 3501-3505, doi: 10.1073/pnas.1407229111.

Livina, V.N., Kwasniok, F., Lohmann, G., Kantelhardt, J.W. & Lenton, T.M. (2011): Changing climate states and stability: from Pliocene to present.- Clim. Dyn. 37: 2437-2453, doi: 10.1007/s00382-010-0980-2.

Lohmann, G. (1998): The influence of a near-bottom transport parameterization on the sensitivity of the thermohaline circulation.- J. Phys. Oceanogr. 28: 2095-2103.

Lohmann, G. (2009): Abrupt climate change modeling.- In R.A. MEYERS (ed): Encyclopedia of Complexity and Systems Science 1: 1-21, Springer, New York, doi:10.1007/978-0-387-30440-3_1.

Lohmann, G. (2016): Atmospheric bridge on orbital time scales.- Theoretical and Applied Climatology, doi: 10.1007/s00704-015-1725-2.

Lohmann, G. & Lorenz, S. (2000): On the hydrological cycle under paleoclimatic conditions as derived from AGCM simulations.- J. Geophys. Res. Atmos. 105: 17417-17436.

Lohmann, G. & Schulz, M. (2000): Reconciling Bølling warmth with peak deglacial meltwater discharge.- Paleoceanography 15: 537-540.

Lohmann, G. & Wiltshire, K.H. (2012): Winter atmospheric circulation signature for the timing of the spring bloom of diatoms in the North Sea.- Marine Biology 159: 2573-2581. doi: 10.1007/s00227-012-1993-7

Lohmann, G., Gerdes, R. & Chen, D. (1996): Sensitivity of the thermohaline circulation in coupled oceanic GCM-atmospheric EBM experiments.- Climate Dynamics 12: 403-416.

Lohmann, G., Butzin, M., Grosfeld, K., Knorr, G., Paul, A., Prange, M., Romanova, V. & Schubert, S. (2003): The Bremen Earth System Model of Intermediate Comlexity (BREMIC) designed for long-term climate studies. Model description, climatology, and applications.- University Bremen, techn. Rep. <www.geo.uni-bremen.de/~gerrit/ BREMIC .html>

Lohmann, G., Haak, H. & Jungclaus, J.H. (2008): Estimating trends of Atlantic meridional overturning circulation from long-term hydrographic data and model simulations.- Ocean Dyn. 58: 127-138, doi: 10.1007/s10236-008-0136-7.

Lohmann, G., Pfeiffer, M., Laepple, T., Leduc, G. & Kim, J.-H. (2013): A model-data comparison of the Holocene global sea surface temperature evolution.- Clim. Past 9: 1807-1839, doi: 10.5194/cp-9-1807-2013.

Lohmann, G., Butzin, M. & Bickert, T. (2015): Effect of vegetation on the Late Miocene ocean circulation.- J. Mar. Sci. Eng. 3(4): 1311-1333, doi: 10.3390/jmse3041311.

Lorenz, S. & Lohmann, G. (2004): Acceleration technique for Milankovitch typeforcing in a coupled atmosphere-ocean circulation model: method and application for the Holocene.- Climate Dyn. 23: 727-743, doi: 10.1007/s00382-004-0469-y.

Lunt, D.J., Williamson, M.S., Valdes, P.J., Lenton, T.M. & Marsh, R. (2006): Comparing transient, accelerated, and equilibrium simulations of the last 30000 years with the GENIE-1 model.- Clim. Past 2: 221-235, doi: 10.5194/cp-2-221-2006.

Lunt, D.J., Abe-Ouchi, A., Bakker, P., Berger, A., Braconnot, P., Charbit, S., Fischer, N., Herold, N., Jungclaus, J.H., Khon, V.C., Krebs-Kanzow, U., Lohmann, G., Otto-Bliesner, B., Park, W., Pfeiffer, M., Prange, M., Rachmayani, R., Renssen, H., Rosenbloom, N., Schneider, B., Stone, F. J., Takahashi, K., Wei, W. & Yin Q. (2013): A multi-model assessment of last interglacial temperatures.- Clim. Past 9: 699-717, doi: 10.5194/cp-9-699-2013.

Maier-Reimer, E., Mikolajewicz, U. & Hasselmann, K. (1993): Mean circulation of the Hamburg LSG OGCM and its sensitivity to the thermohaline surface forcing.- J. Phys. Oceanogr. 23: 731-757.

Marsland, S.J., Haak, H., Jungclaus, J.H., Latif, M. & Röske, F. (2003): The Max-Planck-Institute global ocean/sea ice model with orthogonal curvilinear coordinates.- Ocean Model. 5: 91-127.

Martrat, B., Grimalt, J.O., Shackleton, N.J., de Abreu, L., Hutterli, M.A. & Stocker, T.F. (2007): Four climate cycles of recurring deep and surface water destabilizations on the Iberian Margin.- Science 317: 502-507.

Pfeiffer, M. & Lohmann, G. (2016): Greenland Ice Sheet influence on Last Interglacial climate: global sensitivity studies performed with an atmosphere–ocean general circulation model.- Clim. Past 12: 1313-1338, doi:10.5194/cp-12-1313-2016.

Prange, M., Romanova, V. & Lohmann, G. (2002): The glacial thermohaline circulation: stable or unstable?.- Geophys. Res. Lett. 29: 2028, doi: 10.1029/2002GL015337.

Prange, M., Lohmann, G. & Paul, A. (2003): Influence of vertical mixing on the thermohaline hysteresis: Analyses of an OGCM.- J. Phys. Oceanogr. 33: 1707-1721.

Rühlemann, C., Mulitza, S., Lohmann, G., Paul, A., Prange, M. & Wefer, G. (2004): Intermediate depth warming in the tropical Atlantic related to weakened thermohaline circulation: Combining paleoclimate and modeling data for the last deglaciation.- Paleoceanography 19: PA1025, doi: 10.1029/2003PA000948.

Roche, D.M., Wiersma, A.P. & Renssen, H. (2010): A systematic study of the impact of freshwater pulses with respect to different geographical locations.- Clim. Dyn. 34: 997-1013, doi: 10.1007/s00382-009-0578-8.

Rodgers, K., Lohmann, G., Lorenz, S., Schneider, R. & Henderson, G. (2003): A tropical mechanism for Northern Hemisphere deglaciation.- Geochem. Geophys. Geosyst. 4: 1046, doi: 10.1029/2003GC0000508.

Roeckner, E., Arpe, K., Bengtsson, L., Brinkop, S., Dümenil, L., Esch, M., Kirk, E., Lunkeit, F., Ponater, M., Rockel, B., Sausen, R., Schleese, U., Schubert, S. & Windelband, M. (1992): Simulation of the present-day climate with the ECHAM model: Impact of model physics and resolution.- Max-Planck Institut für Meteorologie, Hamburg, 1-171.

Roeckner, E., Bäuml, G., Bonaventura, L., Brokopf, R., Esch, M., Giorgetta, M., Hagemann, S., Kirchner, I., Kornblueh, L., Manzini, E., Rhodin, A., Schlese, U., Schulzweida, U. & Tompkins, A. (2003): The Atmospheric General Circulation Model ECHAM5. Part 1: Model Description.- Max-Planck-Institut für Meteorologie, Report 349: 1-140.

Romanova, V., Prange, M. & Lohmann, G. (2004): Stability of the glacial thermohaline circulation and its dependence on the background hydrological cycle.- Clim. Dyn. 22: 527-538.

Salzmann, U., Dolan, A.M., Haywood, A.M., Chan, W.-L., Hill, D.J., Abe-Ouchi, A., Otto-Bliesner, B., Bragg, F., Chandler, M.A., Contoux, C., Jost, A., Kamae, Y., Lohmann, G., Lunt, D.J., Pickering, S.J., Pound, M.J., Ramstein, G., Rosenbloom, N.A., Sohl, L., Stepanek, C., Ueda, H. & Zhang, Z. (2013): Challenges in quantifying Pliocene terrestrial warming revealed by data-model discord.- Nature Clim. Change 3: 969-974, doi: 10.1038/nclimate2008.

Schäfer-Neth, C. & Paul, A. (2001): Circulation of the glacial Atlantic: a synthesis of global and regional modeling.- In: P. Schäfer, W. Ritzrau, M. Schlüter & J. Thiede (eds): The northern North Atlantic: A changing environment, Springer-Verlag, Berlin, Heidelberg, 446-462.

Schulz, M., Berger, W.H., Sarnthein, M. & Grootes, P.M. (1999): Amplitude variations of 1470-year climate oscillations during the last 100,000 years linked to fluctuations of continental ice mass.- Geophys. Res. Lett. 26: 3385-3388.

Stärz, M., Lohmann, G. & Knorr, G. (2016): The effect of a dynamic soil scheme on the climate of the mid-Holocene and the Last Glacial Maximum.- Clim. Past 12: 151-170. doi :10.5194/cp-12-151-2016.

Stepanek, C. & Lohmann, G. (2012): Modelling mid-Pliocene climate with COSMOS.- Geosci. Model Dev. 5: 1221-1243, doi: 10.5194/gmd-5-1221-2012.

Stepanek, C. & Lohmann, G. (2016): Towards a more exible representation of hydrological discharge transport in (paleo-)climate modelling.- Polarforschung, 85: 171–177.

Stocker, T.F. (2003): Global change: South dials north.- Nature 424: 496-499, doi: 10.1038/424496a.

Sutter, J., Thoma, M. & Lohmann, G. (2015): Integration of passive tracers in a three-dimensional ice sheet model.- In: G. LOHMANN, H. MEGGERS, V. UNNITHAN, D. WOLF-GLADROW, J. NOTHOLT, A. BRACHER (eds), Towards an Interdisciplinary Approach in Earth System Science, Springer Earth System Sciences, Heidelberg, 161-170, doi: 10.1007/978-3-319-13865-7_18.

Sutter, J., Gierz, P., Grosfeld, K., Thoma, M. & Lohmann, G. (2016): Ocean temperature thresholds for Last Interglacial West Antarctic Ice Sheet collapse.- Geophys. Res. Lett. doi: 10.1002/2016GL067818.

Swingedouw, D., Fichefet, T., Goosse, H. & Loutre, M.F. (2009): Impact of transient freshwater releases in the Southern Ocean on the AMOC and climate.- Clim. Dyn. 33: 365-381, doi: 10.1007/s00382-008-0496-1.

Timmermann, A. & Lohmann, G. (2000): Noise-induced transitions in a simplified model of the thermohaline circulation.- J. Phys. Oceanogr. 30: 1891-1900.

Timm, O. & Timmermann, A. (2007): Simulation of the last 21 000 years using accelerated transient boundary conditions.- J. Clim. 20: 4377-4401, doi: org/10.1175/JCLI4237.1.

Varma, V., Prange, M., Merkel, U., Kleinen, T., Lohmann, G., Pfeiffer, M., Renssen, H., Wagner, A., Wagner, S, & Schulz, M. (2012): Holocene evolution of the Southern Hemisphere westerly winds in transient simulations with global climate models.- Clim. Past. 8: 391-402. doi: 10.5194/cp-8-391-2012.

Wang, Z. & Mysak, L.A. (2006): Glacial abrupt climate changes and Dansgaard-Oeschger oscillations in a coupled climate model.- Paleoceanography 21: PA2001, doi:10.1029/2005PA001238.

Weaver, A.J., Saenko, O.A., Clark, P.U. & Mitrovica, J.X. (2003): Meltwater pulse 1A from Antarctica as a trigger of the Bolling-Allerod warm interval.- Science 299: 1709-1713, doi: 10.1126/science.1081002.

Weber, M.E., Clark, P.U., Kuhn, G., Timmermann, A., Sprenk, D., Gladstone, R., Zhang, X., Lohmann, G., Menviel, L., Chikamoto, M.O., Friedrich, T. & Ohlwein, C. (2014): Millennial-scale variability in Antarctic ice-sheet

discharge during the last deglaciation.- Nature 510: 134-138, doi: 10.1038/nature13397.

Wei, W. & Lohmann, G. (2012): Simulated Atlantic multidecadal oscillation during the Holocene.- J. Clim. 25: 6989-7002, doi: 10.1175/JCLI-D-11-00667.1.

Wei, W., Lohmann, G. & Dima, M. (2012): Distinct modes of internal variability in the global meridional overturning circulation associated to the Southern Hemisphere westerly winds.- J. Phys. Oceanogr. 42: 785-801, doi: 10.1175/JPO-D-11-038.1.

Werner, M., Langebroek, P.M., Carlsen, T, Herold, M. & Lohmann, G. (2011): Stable water isotopes in the ECHAM5 general circulation model: Towards high-resolution isotope modeling on a global scale.- J. Geophys. *Res. - Atmos. 116: D15109, doi: 10.1029/2011JD015681.*

Werner, M., Haese, B., Xu, X., Zhang, X., Butzin, M. & Lohmann, G. (2016): Glacial-interglacial changes of $H_2{}^{18}O$, HDO and deuterium excess – results from the fully coupled ECHAM5/MPI-OM Earth System Model.- Geosci. Model Dev. 9: 647-670, doi: 10.5194/gmd-9-647-2016.

Winton, M. (1993): Deep decoupling oscillations of the ocean thermohaline circulation.- In: W. PELTIER (ed): Ice in the Climate System, Springer, New York, 417-432.

Xu, X., Werner, M., Butzin, M. & Lohmann, G. (2012): Water isotope variations in the global ocean model MPI-OM.- Geosci. Model Dev. 5: 809-818.

Zhang, X., Lohmann, G., Knorr, G. & Purcell, C. (2014): Control of rapid glacial climate shifts by variations in intermediate ice-sheet volume.- Nature 512: 290-294, doi: 10.1038/nature13592.

Zhang, X., Lohmann, G., Knorr, G. & Xu, X. (2013): Different ocean states and transient characteristics in Last Glacial Maximum simulations and implications for deglaciation.- Clim. Past 9: 2319-2333, doi: 10.5194/cp-9-2319-2013.

Zhu, J., Liu, Z., Zhang, X., Eisenman, I. & Liu W. (2014): Linear weakening of the AMOC in response to receding glacial ice sheets in CCSM3.- Geophys. Res. Lett. 41: 6252-6258.

Zhu, J., Liu, Z., Zhang, J. & Liu, W. (2015): AMOC response to global warming: dependence on the background climate and response time scale.- Clim. Dyn. 44 (11): 3449-3468.

Polarforschung 85 (2), 171–177, 2015 (erschienen 2016)

Towards a More Flexible Representation of Hydrological Discharge Transport in (Paleo-)Climate Modelling

by Christian Stepanek[1*] and Gerrit Lohmann[1,2]

Abstract: In this extended abstract we motivate the development of the Flexible Hydrological Discharge Model (FHD-Model). We give a general overview on the FHD-Model's function and – based on a selection of case studies – we illustrate its application in the framework of climate modelling studies at a global scale. Furthermore, we offer an outlook to upcoming applications and a following publication. The new FHD-Model is required, both, in the field of future climate projections and paleoclimatology. In these research areas, it satisfies the emerging need for flexible discharge transport schemes that react to sea level variations, which are related to variability and evolution of ice sheets. Furthermore, the FHD-Model easily adapts to variations in topography. Therefore, this discharge model is suitable for climate modelling studies on time scales that involve the evolution of land surface, ice sheets, discharge basins, and river systems.

Zusammenfassung: In diesem Beitrag legen wir unsere Motivation zur Entwicklung des Flexiblen Hydrologischen-Abfluss-Modells (FHD-Modell) dar. Wir geben einen Überblick über die Funktion des FHD-Modells und illustrieren – auf der Grundlage von ausgewählten Fallstudien – die Anwendung im Rahmen von globalen Klima-Modell-Studien. Weiterhin weisen wir auf zukünftige Anwendungen des Modells und eine anstehende Publikation hin. Das neue FHD-Modell wird im Zusammenhang mit Projektionen des zukünftigen Klimas und der Paläoklimatologie benötigt. In diesen Forschungsgebieten bedient es den sich abzeichnenden Bedarf an flexiblen kontinentalen Abfluss-Schemata, die auf die Änderung des Meeresspiegels reagieren können, der mit der Variabilität und Entwicklung von kontinentalen Eisschilden verknüpft ist. Darüber hinaus ist das FHD-Modell leicht für geographische Änderungen adaptierbar, die folgende Charakteristika umfassen: Landoberfläche, Eisschilde, Einzugsgebiete der Abflusssysteme, Flussläufe. Das FHD-Modell ist daher anwendbar für Zeitskalen, auf denen sich solche Eigenschaften der Erdoberfläche verändern.

INTRODUCTION

In the hydrological cycle, vast amounts of water are moved between different parts of the climate system. Water that evaporates at the ocean surface may be transported over land masses, form clouds, and precipitate over continents. Excess water that cannot be stored in the soil by vegetation or in Polar Regions as land ice, forms runoff that is subsequently transported along the topographic gradient back to the ocean. Although the amount of water volume transported by rivers is small if compared to other pathways in the hydrological cycle (Chahine 1992, Trenberth et al. 2007), rivers need to be correctly represented in climate models. It has been stated that the lack of land-bound lateral water transfer in climate simulations leads to a misrepresentation of the hydrological cycle (Kite 1998). Furthermore, changes in coastal discharge volume have a profound influence on the ocean's regional salinity budget, and may subsequently impact on the buoyancy-driven part of ocean circulation at high latitudes (Manabe & Stouffer 1993, 1999). The exact region of high-latitude river discharge may potentially impact on the Atlantic Ocean meridional overturning circulation (Rennermalm et al. 2007) and may influence sea-ice formation (Dümenil & Todini 1992, p. 130) in Polar Regions.

Until recently, the focus of (paleo-)climatological modelling on a global scale has been on applications where land surface conditions, and particularly polar ice sheets, sea level, and river routes, do not dramatically change during the course of a simulation. Consequently, hydrological discharge routing in climate models has so far focused on high resolution discharge transport schemes, which are precise but often static, with prescribed and fixed river routes, while flexibility in discharge routing has so far not been of profound importance. Yet, the advent of fully coupled atmosphere – ocean – ice-sheet Earth System Models (e.g., Barbi et al. 2014), together with the emergence of scientific questions that focus on the state of the Arctic and the Antarctic, require dynamic consideration of variations in ice-sheets and sea-level height in the hydrological cycle, and represent a paradigm shift in (paleo)climatological modelling. This poses new challenges for hydrological discharge transport schemes. While there are already various discharge transport models in use in combination with general circulation models (for example Decharme et al. 2008, Alkama et al. 2010, Decharme et al. 2010, Yamazaki et al. 2011, Miguez-Macho & Fan 2012), these generally depend on high-resolution information of present-day river direction or elevation. Such information characteristic for present day is rarely a suitable choice for paleoclimatological applications at tectonic time scales, as assumptions on past or future land surface conditions that influence the discharge transport over land are uncertain and sparse. Consequently, for paleoclimatic applications of discharge transport schemes in climate models the importance is not so much on high resolution, while resolution is on the other hand of profound interest for the correct representation of watershed characteristics in present-day applications. In contrast, it is necessary for a discharge transport scheme in paleoclimatology to flexibly react to changes in boundary conditions, for example land-surface elevation of ice sheets as well as sea-level height. These considerations are the foundation for the development of the Flexible Hydrological Discharge Model (FHD-Model).

doi:10.2312/polfor.2016.014

[1] Section Paleoclimate Dynamics, Department of Climate Sciences, Alfred Wegener Institute Helmholtz Centre for Polar and Marine Research, Bussestraße 24, D-27570 Bremerhaven, Germany.
[2] University of Bremen, Institute of Environmental Physics, Otto-Hahn-Allee 1, 28359 Bremen, Germany.
* Corresponding author: <Christian.Stepanek@awi.de>
This paper was presented as a poster contribution at the International Conference "Our Climate – Our Future: Regional perspectives on a global challenge", 6–9 October 2014 in Berlin, Germany.
Manuscript received 03 June 2015; revised version 24 November 2015; accepted 22 December 2015.

In the following, we give a short first overview on design, validity, and performance of the FHD-Model as an optional part of the Community Earth System Models (COSMOS). The FHD-Model is designed to integrate into the main components of this climate model toolbox – the fifth generation of the European Centre Hamburg Model (ECHAM5, Roeckner et al. 2003) and the Max Planck Institute Ocean Model (MPIOM, Marsland et al. 2003). The new discharge scheme shall overcome some of the practical disadvantages of common hydrological discharge schemes with fixed river routes in (palaeo-) climatological applications of climate models.

The performance of the COSMOS in combination with the standard hydrological discharge scheme of ECHAM5 (HD-Model, Hagemann & Dümenil 1998), which is based on fixed river paths derived from high resolution orographic data, was evaluated for preindustrial conditions (Wei et al. 2012), the Holocene (Wei & Lohmann 2012, Lohmann et al. 2013), the last millenium (Jungclaus et al. 2010), glacial millenial-scale variability (Gong et al. 2013, Kageyama et al. 2013, Stärz et al. 2013, Zhang et al. 2013, Weber et al. 2014, Zhang et al. 2014, Gong et al. 2015), the Last Interglacial (Lunt et al. 2013, Felis et al. 2015, Pfeiffer & Lohmann 2016), and warm climates in the Miocene (Knorr et al. 2011, Knorr & Lohmann 2014) and Pliocene (Stepanek & Lohmann 2012, Haywood et al. 2013). In most of these publications, in particular those that investigate the climate of time slices earlier than the Preindustrial and the Holocene, various assumptions were necessary in adjusting the high resolution present-day topography setup of the HD-Model for the respective past land surface conditions. The availability of the FHD-Model as a flexible discharge transport scheme, which is able to accept reconstructed topography data of arbitrary resolution, would have been of help in such studies. This topic is of relevance particularly for paleoclimate modelling at tectonic time scales and with a focus on the evolution of ice sheets: At tectonic time scales there is no sufficient information on past global river networks that could be used as a constraint for the river routing in climate simulations, necessitating a more flexible approach as in the FHD-Model. For the evolution of ice sheets, the FHD-Model is able to automatically reroute river flow in response to changes in ice sheets and the related impact on the land surface. Furthermore, the FHD-Model is able to resolve the response of flow direction to any sea level variation that results from volume change of land ice.

METHODOLOGY

The FHD-Model's physical core is based on the Gauckler-Manning-Strickler formula (GMS), which describes the velocity of gravity-driven sheet-flow (e.g., Chow 1959, p. 99, Eq. 5–6). The GMS may be used to describe the flow rate Q in dependence of the water surface slope s (defined in Fig. 1a), the water height f in the flow bed, and a scalar real-valued flow capacity parameter c, which has the physical unit of $m^{4/3} \cdot s^{-1}$. This parameter is a system characteristic of the rectangular channel in which the computed discharge is assumed to occur – c is directly proportional to the width w of the flow bed, indirectly proportional to the roughness of the channel bed material (commonly referred to as Manning's roughness coefficient n), and describes how much volume may be transported by the channel in the four considered directions (Fig. 1b) for a given gravitational forcing that acts on the water volume along the topographic slope.

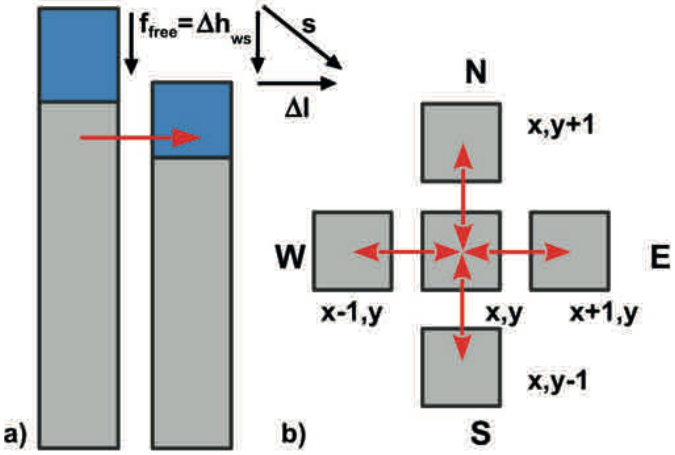

Fig. 1: Flow scheme of the FHD-Model. a): regulators of direction and strength of the flow include the slope of the water surface in the flow direction (red arrow), that is determined by time-depending height differences of water surfaces of neighbouring grid cells Δh_{ws} (in this case identical to the free flow height f_{free}) and the horizontal grid cell dimension Δl. b): currently, volume flow in the FHD-Model may occur between neighbouring grid cells along the four cardinal directions (N, E, S, W).

Abb. 1: Fluss-Schema des FHD-Modells. a): Regulatoren von Richtung und Stärke des Flusses enthalten das Gefälle der Wasseroberfläche in Flussrichtung (roter Pfeil), das durch die zeitabhängige Höhendifferenz der Wasseroberfläche benachbarter Gitterzellen Δh_{ws} (welche in diesem Fall identisch ist mit der freien Flusshöhe f_{free}) und die horizontale Ausdehnung einer Gitterzelle Δl bestimmt wird. b): in der aktuellen Version des FHD-Modells kann der Fluss zwischen benachbarten Gitterzellen entlang der vier Himmelsrichtungen (N, E, S, W) erfolgen.

Equation 1 is an adapted version of the GMS and suited for application on a discrete model grid: f is replaced by the free flow height f_{free}, which is defined by the difference between the flow heights of neighbouring grid cells (Fig. 1a).

$$Q = c \cdot f_{free}^{5/3} \cdot s^{1/2} \quad (1)$$

The simulation of hydrological discharge transport in the FHD-Model is performed by adding runoff and discharge at grid cell scale, which is computed in ECHAM5 by means of a bucket model, to the local value of f_{free}. Via an explicit time stepping method, this volume is subsequently transported between neighbouring grid cells as overland flow, as described by Equation 1, until it reaches either the coast or an unfilled endorheic basin. Choosing Equation 1 as the foundation of the discharge transport scheme has several advantages:

i) It enables flexibility of the flow simulation with respect to both, flow rate and flow direction of the hydrological discharge, which is a major difference to other common discharge schemes in climate models, that rather rely on prescribed and fixed flow paths – the highly accurate HD-Model, for example, which is the standard hydrological discharge scheme of ECHAM5, is strongly optimised for present-day topography as discussed in the literature (Hagemann & Dümenil 1998).

ii) The presence of directly observable physical quantities on the right hand side of Equation 1, namely f_{free} and s, enables easy application of the equation in climate models. The information necessary to derive a complete set of boundary conditions for the flow simulation (Fig. 2) is

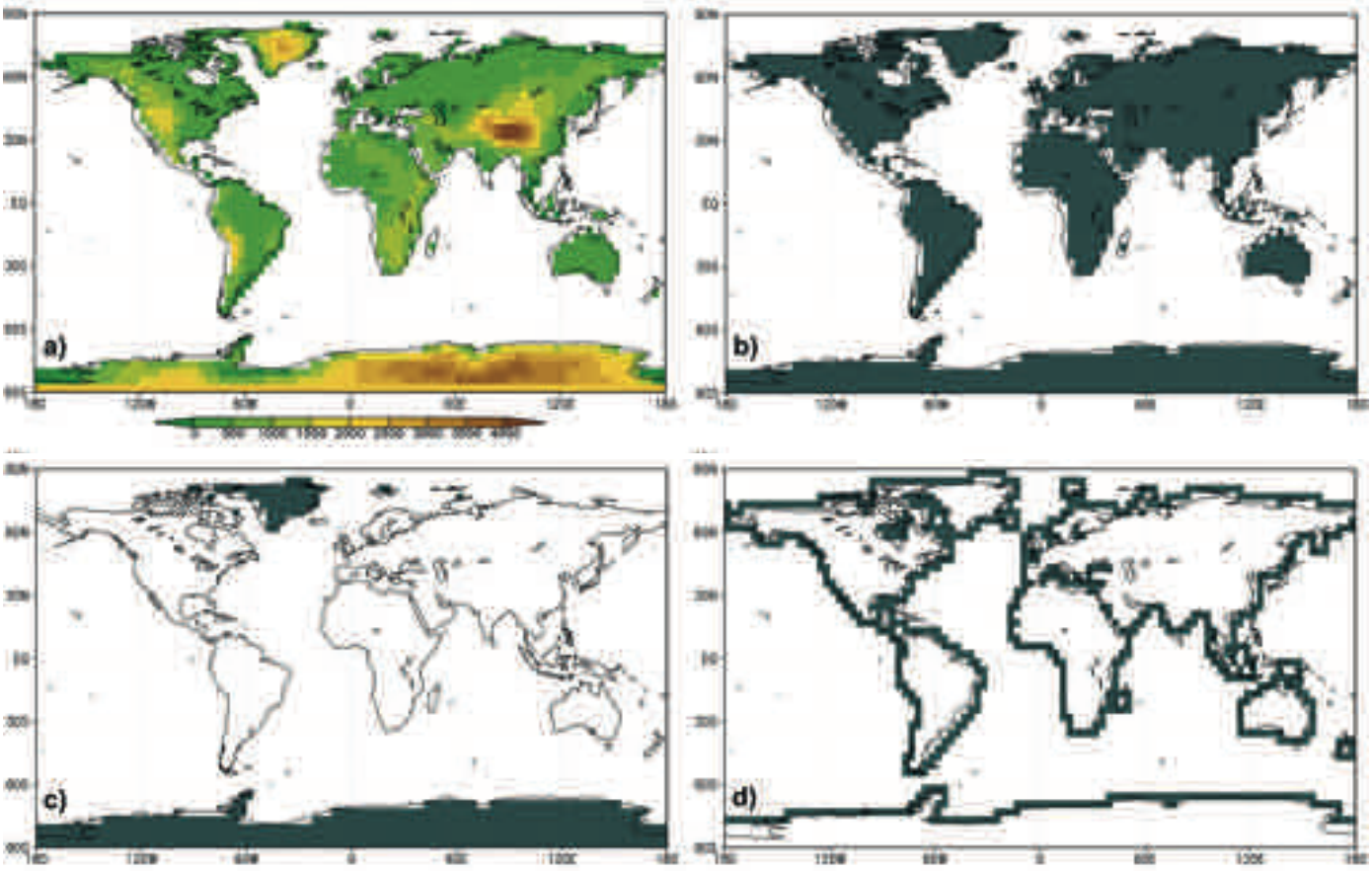

Fig. 2: A complete set of boundary conditions of the FHD-Model, here for present day at T31-resolution (3.75° × 3.75°). a): land topography (m); b): land-sea-mask; c): ice-sheet-mask (for coupling of the FHD-Model to an ice-sheet model); d): coastal discharge collection mask (for coupling the FHD-Model to an ocean model). a), b), and c) stem directly from the boundary conditions of the Atmosphere General Circulation Model ECHAM5, d) may be easily derived from b) based on a dedicated algorithm.

Abb. 2: Ein vollständiger Satz von Randbedingungen für das FHD-Modell, hier für heutige Bedingungen in T31-Auflösung (3.75° × 3.75°). a): Topographie über Land (m); b): Land–Ozean-Maske; c): Eisschild-Maske (zur Kopplung des FHD-Modells an ein Eisschild-Modell); d): Maske für die Sammlung des kontinentalen Abflusses an der Küste (zur Kopplung des FHD-Modells an ein Zirkulationsmodell des Ozeans). a), b) und c) entspringen direkt den Randbedingungen des Atmosphärenmodells ECHAM5; d) ist auf einfache Weise von b) mit Hilfe eines entsprechenden Algorithmus abgeleitet.

already present in common model setups of general circulation models, and the formulation of Equation 1 does not depend on a preferred resolution of the considered physical quantities. Therefore, the derivation of these quantities does not impose a significant amount of additional workload during the generation of a model setup, as it is often the case for common discharge transport schemes in climate models.

RESULTS AND DISCUSSION

Calibration of the model parameter c

The model parameter c in Equation 1 is an integrated quantity at grid-cell scale. There is no evident analytical method to find a value that is suitable for a global hydrological discharge simulation, where many different environmental conditions – for example sand, soil, vegetation, snow, and ice – pose various different background characteristics for the flow. Therefore, a parameter calibration against a benchmark is performed for spatially integrated coastal discharge at the spatial scale of interest for global climate simulations – that is catchments of major ocean basins. A simulation of hydrological discharge transport of the model ECHAM5 with the HD-Model is chosen as a benchmark. The calibration is shown here for present-day conditions, and it is principally necessary to repeat the calibration for any set of land surface conditions that shall be used as a boundary condition for the discharge transport simulation. Later, we will shortly discuss why we assume the derived value of c to be a good first-order guess also for other time slices than present day.

Results shown here refer to a present-day topography and ice sheet distribution at T31-resolution (3.75° × 3.75°) – a resolution that is still common for paleoclimatological application of global climate models. Ocean-basin-integrated coastal discharge, derived from a comparable discharge transport simulation with the HD-Model, serves as benchmark and reference dataset for the calibration. The model configuration, from which we derive, both, the benchmark and the hydrological forcing for the discharge simulation with the FHD-Model, is based on the ECHAM5 model with a horizontal resolution of 3.75° × 3.75° and 19 vertical layers, complemented by a land-surface scheme, including dynamic vegetation (Brovkin et al. 2009). The ocean component MPIOM, including the dynamics of sea ice formulated using viscous-plastic rheology, has an average horizontal resolution of 3.0° × 1.8° with 40 vertical layers of differing thickness.

Details of the calibration must be omitted here due to space limitations and will be presented in detail in a later publication that focuses on the model description. However, the three main results of the calibration are summarized in the following:

i) For every considered catchment (Arctic Ocean, Atlantic Ocean, Indian Ocean, and Pacific Ocean), a distinct optimum value of the model parameter *c* exists, for which the root mean square deviation (FHD-Model *versus* benchmark) of the catchment-integrated coastal discharge takes a minimum;
ii) The best fit of simulations with the FHD-Model to the benchmark occurs for Indian Ocean and Pacific Ocean – for Atlantic Ocean and Arctic Ocean the agreement is slightly worse;
iii) The best fit is generated by assuming high flow-resistance (small *c*, approximately 10 $m^{4/3} \cdot s^{-1}$) in the catchments of Pacific Ocean and Indian Ocean; this pays regard to the relatively short distance between grid cells in the continental interior and the coast in these regions, creating relatively short river systems.
iv) In contrast, best agreement with the benchmark is found if assuming low flow resistance in the discharge simulation with the FHD-Model (large *c*, approximately 40 $m^{4/3}\ s^{-1}$) for the catchments of Arctic Ocean and Atlantic Ocean, where longer flow systems (the polar rivers Ob, Yenisey, and Lena, for example) are predominant.

Annual discharge climatology in the FHD-Model

One key parameter of a discharge simulation in a coupled atmosphere – ocean climate simulation, that necessitates verification during the development of a discharge transport scheme, is the annual cycle of the integrated discharge to a specific ocean basin. Here, the annual discharge climatology for present-day land surface conditions is shown at the example of the Indian Ocean catchment. Generally, timing of peaks and troughs in the discharge climatology is governed by the climatology of net-precipitation, which depends on physical conditions as computed by the atmosphere model and by the bucket model, the latter defining amplitude and timing of runoff-formation at grid cell scale. Yet, it must be verified that the time delay of the discharge volume along its path within a catchment is comparable to conditions in the respective natural flow system. Furthermore, the annually integrated amount of coastal discharge per catchment should be reasonable; that means it should agree with the benchmark. A respective discordance is likely caused by the misrepresentation of drainage divides in the discretized – and rather coarse-resolution – topography dataset utilised in the FHD-Model; differences in the water balance of the atmosphere model cannot explain such a deviation as the discharge curves derived from FHD-Model and benchmark are based on the same hydrological forcing from the atmosphere general circulation model.

Results of discharge simulations with various settings of the model parameter *c* show that the FHD-Model is able to reproduce the main characteristics of catchment-integrated discharge in the benchmark (i.e., the reference data set obtained from a comparable discharge simulation with the HD-Model, Fig. 3). In the FHD-Model, the annually integrated discharge to the Indian Ocean slightly overestimates the respective quantity of the benchmark. This indicates that the catchment

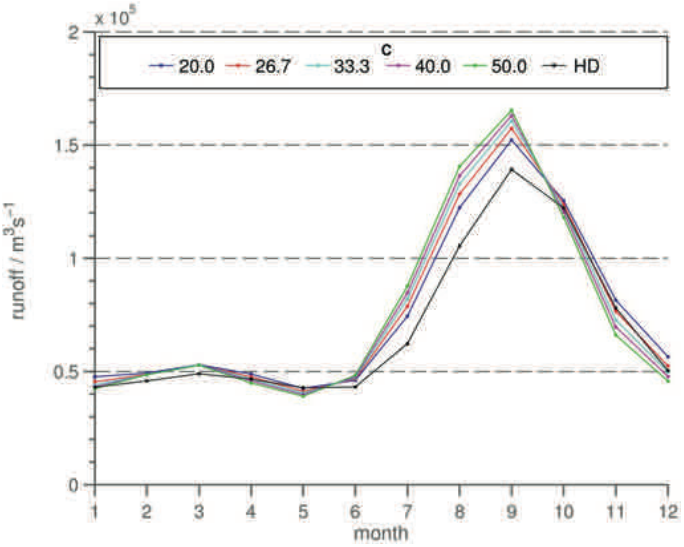

Fig. 3: Annual cycle of discharge to the Indian Ocean as simulated with the FHD-Model. Shown are results derived with various settings of the model parameter *c* ($m^{4/3}s^{-1}$). For reference, also the respective discharge climatology of the benchmark (a simulation based on the HD-Model, indicated by "HD" in the legend) is shown. The annually integrated discharge to the Indian Ocean in the given model setup with the FHD-Model is $2.37 \cdot 10^{12} m^3 yr^{-1}$, independently of the value of *c*. In the benchmark, the respective volume is slightly lower ($2.18 \cdot 10^{12} m^3 yr^{-1}$).

Abb. 3: Jahresgang des vom FHD-Modell simulierten kontinentalen Abfluss in den Indischen Ozean. Dargestellt sind Ergebnisse, die auf verschiedenen Werten des Modell-Parameters c beruhen. Zum Vergleich ist auch die entsprechende Datenreihe der Referenz (eine Simulation basierend auf dem HD-Modell, gekennzeichnet durch "HD" in der Legende) gezeigt. Der jährlich integrierte kontinentale Abfluss in den Indischen Ozean zu den vorgegebenen Randbedingungen ist im FHD-Modell $2.37 \cdot 10^{12} m^3 yr^{-1}$, unabhängig vom Wert des Parameters *c*. In der Referenzdatenreihe ist der Wert geringfügig kleiner ($2.18 \cdot 10^{12} m^3 yr^{-1}$).

area of the Indian Ocean inherent to the global coarse-resolution topography data set in the FHD-Model, which is taken over from ECHAM5, has a different size than and/or is shifted with respect to the catchment area in the higher resolution topography data set on which the benchmark is based. Indeed, area and location of the catchment of the Indian Ocean differ between the setups of FHD-Model and HD-Model (not shown here).

Application of the FHD-Model in a scenario of global sea level rise

In order to demonstrate the ability of the FHD-Model to flexibly adjust the flow direction of discharge transport in the climatologically interesting case of global sea-level rise, the FHD-Model is applied in a case study of continental flooding due to postglacial ice-sheet melt. In this case study, the FHD-Model is run offline (i.e., not coupled to an atmosphere – ocean model) and forced with a periodic time series of runoff and drainage at grid cell scale that has been derived from a climate simulation. The sea level time series, prescribed in this case study as a forcing, is based on a reconstruction of freshwater discharge (FAIRBANKS et al. 1992, Fig. 30.1B), and covers the time period from the Last Glacial Maximum (LGM) to about 7,000 years before present.

Figure 4 shows that the FHD-Model is able to correctly simulate the flooding of the initially exposed continental shelf of the LGM topography boundary condition (that is courtesy of ZHANG et al. 2013). The results imply that in coastal regions, and also in those regions of the low-lying continental interior where no topographic obstacles shield inflow from the ocean, the flow direction is indeed subject to change as indicated by the establishment of land-based volume reservoirs. Low-lying continental interior regions that are shielded by topographic obstacles from coastal inflow – for example the Amazon Basin and the Caspian Sea – on the other hand do not experience any change in regional water level.

CONCLUSIONS AND OUTLOOK

We have shown that the FHD-Model has characteristics that make it suitable for the computation of hydrological discharge transport at catchment scale of ocean basins in (palaeo)climatological applications of climate models. Due to the presence of only one model parameter, the FHD-Model is easily calibrated to a given discharge benchmark, which is currently done only for present-day conditions. Although this parameter calibration is not necessarily also valid for the application of the model for other land surface and climatic conditions, we believe that the derived value of c is generally a suitable first-order assumption in the framework of paleoclimatology, where the necessary auxiliary information for a model calibration is sparse or absent. Our rationale is based on the inference that for present-day land surface conditions, which are very different across the various continents, one globally uniform value can be found for which the FHD-Model provides a reasonable performance in the simulation of discharge to all the major ocean basins. Depending on the application, the value of c may be adjusted in the future, provided that the necessary benchmark data or sufficient information on land surface conditions are available.

The ability of the FHD-Model to automatically reroute the discharge and its ability to resolve the evolution of land-based water distribution in the presence of a changing sea level, enables sea-level height and ice-sheet variability to impact on

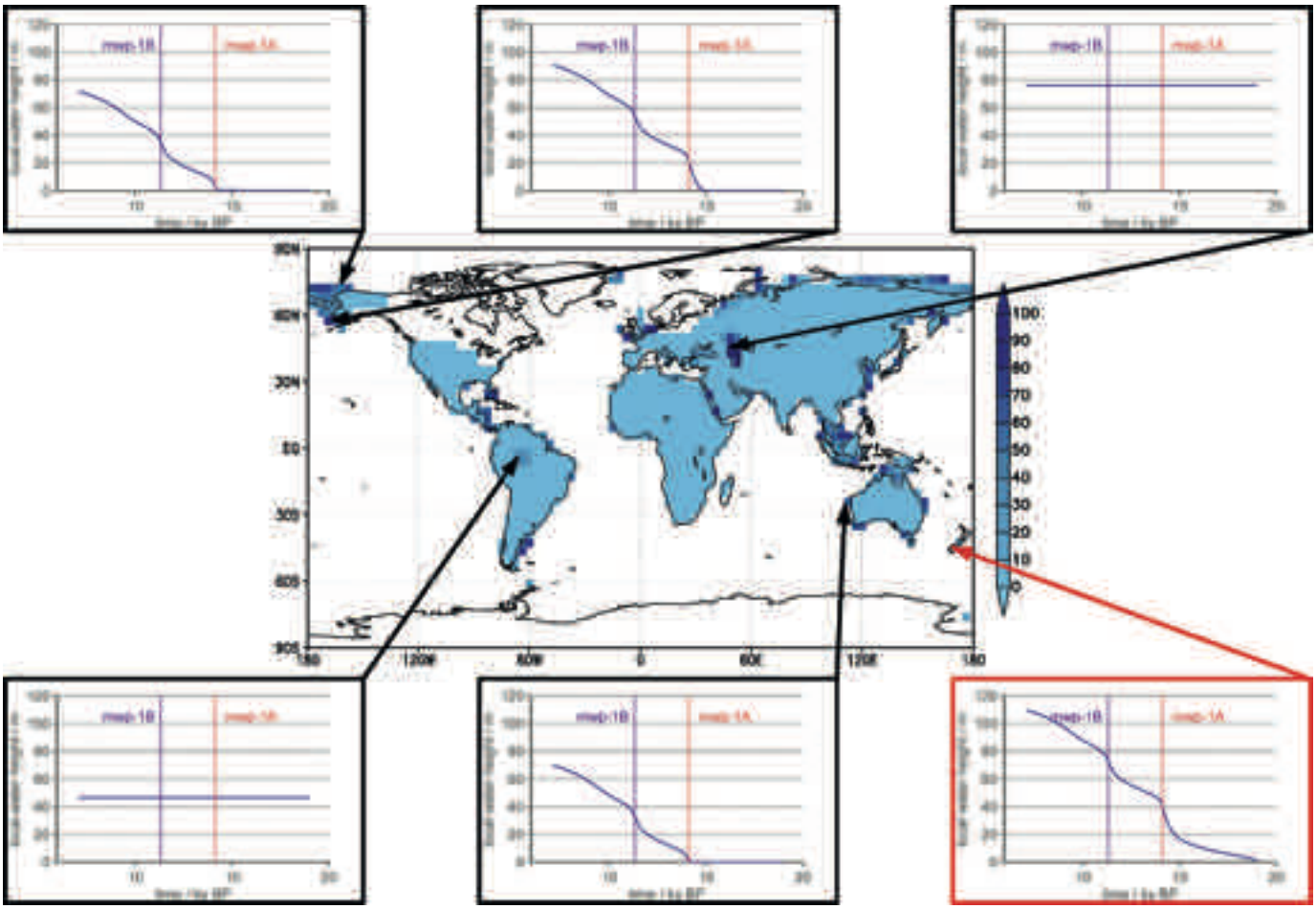

Fig. 4: Simulation of continental water surface height in the FHD-Model under the influence of postglacial sea-level rise, based on a topography boundary condition of the Last Glacial Maximum (courtesy of ZHANG et al. 2013). Shown is the height of the water column (m) at the end of the simulation (centre). Furthermore, the temporal evolution of regional water-surface height is illustrated for five locations of the continental interior (black) and one coastal location (red); the latter time series is identical to the applied sea-level forcing that considers major melt-water pulses (mwp).

Abb. 4: Simulation der Höhe des Wasserspiegels über den Kontinenten im FHD-Modell unter dem Einfluss von postglazialem Anstieg des globalen Meeresspiegels basierend auf einer topographischen Randbedingung für das letzte Hochglazial (bereitgestellt durch ZHANG et al. 2013). Gezeigt ist die Höhe der Wassersäule (m) am Ende der Simulation (Mitte). Daneben wird die zeitliche Entwicklung der regionalen Höhe der Wasseroberfläche an fünf verschiedenen Orten im Innern der kontinentalen Landmasse (schwarz), sowie an der Küste (rot) illustriert. Die letztgenannte Zeitserie ist identisch mit dem vorgeschriebenen Meeresspiegel, welcher ausgeprägte Schmelzwasser-Abflüsse (mwp) berücksichtigt.

the continental part of the hydrological cycle. These characteristics allow a more realistic simulation of the climate system with COSMOS, as routing of hydrological discharge is by design at all times consistent with topography, ice-sheet distribution, and sea level.

The FHD-Model improves the practical application of ECHAM5/MPIOM for use in combination with ice-sheet models. It is therefore of particular interest in applications that focus on the state of the Earth's Polar Regions. This also recommends the use of the FHD-Model for the application in future climate scenarios that include fully coupled ice-sheet models and consider the resultant variability in sea level. The FHD-Model improves the integration of the discharge scheme into climate models in that it accepts land surface conditions of arbitrary resolution. While the focus in the FHD-Model clearly is on global-scale climate modelling, the underlying physical formalism is also in use at smaller spatial scale, for example for the simulation of floods in river catchments (Dag Lohmann pers. com. 2013). Therefore, the FHD-Model may in principle be used also for climate modelling at spatial scales as small as river catchments. The necessity of only a small number of boundary conditions that may be easily derived from any common climate model setup, further simplifies the use of the FHD-Model in practical applications of climate modelling.

Currently, the FHD-Model only serves as a means of transporting land-bound water volume in a meaningful way back to the coast. Yet, it is intended to extend its capability in that the flow volume may be redistributed to the soil along the discharge route, wherever local climatic conditions suggest such a process. This additional mechanism will further enhance the completeness of climate simulations with COSMOS and its model components.

This publication is not intended to give a conclusive overview on all the properties, capabilities and the performance of the FHD-Model, which have been outlined only roughly here. Currently, a more detailed manuscript is in preparation that will present more results and a more detailed description and discussion of the FHD-Model.

ACKNOWLEDGMENTS

This work is based on a chapter of a dissertation thesis that has been submitted to the Fachbereich 1 (Physik / Elektrotechnik) of the University of Bremen. Support by and helpful discussions with Dag Lohmann are greatly appreciated. C. Stepanek acknowledges funding by the Helmholtz Climate Initiative Regional Climate Change (REKLIM), a joint research project of the Helmholtz Association of German Research Centres. G. Lohmann acknowledges funding by the research programme "Polar regions and Coasts in a changing Earth System" (PACES) of the Alfred Wegener Institute Helmholtz Centre for Polar and Marine Research. Ying Fan and one anonymous reviewer are acknowledged for providing constructive reviews and helpful comments. Klaus Grosfeld is acknowledged for kindly editing our manuscript.

References

Alkama, R., Decharme, B.R., Douville, H., Becker, M., Cazenave, A., Sheffield, J., Voldoire, A., Tyteca, S. & Le Moigne, P. (2010): Global evaluation of the ISBA-TRIP continental hydrological system. Part I: Comparison with GRACE terrestrial water storage estimates and in situ river discharges.- J. Hydrometeorol. 11: 583-600, doi: 10.1175/2010JHM1211.1.

Barbi, D., Lohmann, G., Grosfeld, K. & Thoma, M. (2014): Ice sheet dynamics within an Earth System Model: downscaling, coupling and first results.- Geosci. Model Dev. 7: 2003-2013, doi: 10.5194/gmd-7-2003-2014.

Brovkin, V., Raddatz, T., Reick, C.H., Claussen, M. & Gayler, V. (2009): Global biogeophysical interactions between forest and climate.- Geophys. Res. Lett. 36: L07405, doi: 10.1029/2009GL037543.

Chahine, M.T. (1992): The hydrological cycle and its influence on climate.- Nature 359: 373-380.

Chow, V.T. (1959): Open-Channel Hydraulics.- McGraw-Hill, New York, NY, 1-680.

Decharme, B., Douville, H., Prigent, C., Papa, F. & Aires, F. (2008): A new river flooding scheme for global climate applications: Off-line evaluation over South America.- J. Geophys. Res. 113: D11110, doi: 10.1029/2007JD009376.

Decharme, B., Alkama, R., Douville, H., Becker, M. & Cazenave, A. (2010): Global evaluation of the ISBA-TRIP continental hydrological system. Part II: Uncertainties in river routing simulation related to flow velocity and groundwater storage.- J. Hydrometeorol. 11: 601-617, doi: 10.1175/2010JHM1212.1

Dümenil, L. & Todini, E. (1992): A rainfall-runoff scheme for use in the Hamburg climate model.- In: J.P.O'KANE (ed): Advances in theoretical hydrology: a tribute to Jim Dooge, Elsevier, Amsterdam, European Geophysical Society Series on Hydrological Sciences (1): 129-157.

Fairbanks, R.G., Charles, C.D. & Wright, J.D. (1992): Origin of global meltwater pulses.- In: R.E. TAYLOR, A. LONG & R.S. KRA (eds): Radiocarbon after four decades, Springer, New York: 473-500.

Felis, T., Giry, C., Scholz, D., Lohmann, G., Pfeiffer, M., Pätzold, J., Kölling, M. & Scheffers, S.R. (2015): Tropical Atlantic temperature seasonality at the end of the last interglacial.- Nat. Commun. 6: 1-8, doi: 10.1038/ncomms7159.

Gong, X., Knorr, G., Lohmann, G. & Zhang, X. (2013): Dependence of abrupt Atlantic meridional ocean circulation changes on climate background states.- Geophys. Res. Lett. 40: 3698-3704, doi: 10.1002/grl.50701.

Gong, X., Zhang, X., Lohmann, G., Wei, W., Zhang, X. & Pfeiffer, M. (2015): Higher Laurentide and Greenland ice sheets strengthen the North Atlantic ocean circulation.- Clim. Dyn. 45: 139-150, doi: 10.1007/s00382-015-2502-8.

Hagemann, S. & Dümenil, L. (1998): A parametrization of the lateral waterflow for the global scale.- Clim. Dynam. 14: 17-31.

Haywood, A.M., Hill, D.J., Dolan, A.M., Otto-Bliesner, B., Bragg, F., Chan, W.-L., Chandler, M.A., Contoux, C., Jost, A., Kamae, Y., Lohmann, G., Lunt, D.J., Abe-Ouchi, A., Pickering, S.J., Ramstein, G., Rosenbloom, N.A., Sohl, L., Stepanek, C., Yan, Q., Ueda, H. & Zhang, Z. (2013): Large-scale features of Pliocene climate: Results from the Pliocene Model Intercomparison Project.- Clim. Past 9: 191-209, doi: 10.5194/cp-9-191-2013.

Jungclaus, J.H., Lorenz, S.J., Timmreck, C., Reick, C.H., Brovkin, V., Six, K., Segschneider, J., Giorgetta, M.A., Crowley, T.J., Pongratz, J., Krivova, N.A., Vieira, L.E., Solanki, S.K., Klocke, D., Botzet, M., Esch, M., Gayler, V., Haak, H., Raddatz, T.J., Roeckner, E., Schnur, R., Widmann, H., Claussen, M., Stevens, B. & Marotzke, J. (2010): Climate and carbon-cycle variability over the last millennium.- Clim. Past 6: 723-737, doi: 10.5194/cp-6-723-2010.

Kageyama, M., Merkel, U., Otto-Bliesner, B., Prange, M., Abe-Ouchi, A., Lohmann, G., Ohgaito, R., Roche, D.M., Singarayer, J., Swingedouw, D. & Zhang, X. (2013): Climatic impacts of fresh water hosing under Last Glacial Maximum conditions: a multi-model study.- Clim. Past 9: 935-953, doi: 10.5194/cp-9-935-2013.

Kite, G. (1998): Land surface parameterizations of GCMs and macroscale models.- J. Amer. Water Resour. Assoc. 34: 1247-1254.

Knorr, G., Butzin, M., Micheels, A. & Lohmann, G. (2011): A warm Miocene climate at low atmospheric CO2 levels.- Geophys. Res. Lett. 38: L20701, doi: 10.1029/2011GL048873.

Knorr, G. & Lohmann, G. (2014): Climate warming during Antarctic ice sheet expansion at the Middle Miocene transition.- Nat. Geosci. 7: 376-381, doi: 10.1038/NGEO2119.

Lohmann, G., Pfeiffer, M., Laepple, T., Leduc, G. & Kim, J.-H. (2013): A model-data comparison of the Holocene global sea surface temperature evolution.- Clim. Past 9: 1807-1839, doi: 10.5194/cp-9-1807-2013.

Lunt, D.J., Abe-Ouchi, A., Bakker, P., Berger, A., Braconnot, P., Charbit, S., Fischer, N., Herold, N., Jungclaus, J.H., Khon, V.C., Krebs-Kanzow, U., Langebroek, P.M., Lohmann, G., Nisancioglu, K.H., Otto-Bliesner, B.L., Park, W., Pfeiffer, M., Phipps, S.J., Prange, M., Rachmayani, R., Renssen, H., Rosenbloom, N., Schneider, B., Stone, E.J., Takahashi, K., Wei, W., Yin, Q. & Zhang, Z.S. (2013): A multi-model assessment of last interglacial temperatures.- Clim. Past 9: 699-717, doi: 10.5194/cp-9-699-2013.

Manabe, S. & Stouffer, R.J. (1993): Century-scale effects of increased atmospheric CO_2 on the ocean-atmosphere system.- Nature 364: 215-218.
Manabe, S. & Stouffer, R.J. (1999): The role of thermohaline circulation in climate.- Tellus B 51: 91-109.
Marsland, S.J., Haak, H., Jungclaus, J.H., Latif, M. & Roeske, F. (2003): The Max-Planck-Institute global ocean/sea ice model with orthogonal curvilinear coordinates.- Ocean Model. 5: 91-127.
Miguez-Macho, G. & Fan, Y. (2012): The role of groundwater in the Amazon water cycle: 1. Influence on seasonal streamflow, flooding and wetlands.- J. Geophys. Res. 117: D15113, doi: 10.1029/2012JD017539.
Pfeiffer, M. & Lohmann, G. (2016): Greenland Ice Sheet influence on Last Interglacial climate: global sensitivity studies performed with an atmosphere–ocean general circulation model.- Clim. Past 12: 1313-1338, doi:10.5194/cp-12-1313-2016.
Rennermalm, A.K., Wood, E.F., Weaver, A.J., Eby, M. & Déry, S.J. (2007): Relative sensitivity of the Atlantic meridional overturning circulation to river discharge into Hudson Bay and the Arctic Ocean.- J. Geophys. Res. 112: G04S48, doi: 10.1029/2006JG000330.
Roeckner, E., Brokopf, R., Esch, M., Giorgetta, M., Hagemann, S., Kirchner, I., Kornblueh, L., Manzini, E., Rhodin, A., Schlese, U., Schulzweida, U. & Tompkins, A. (2003): The atmospheric general circulation model ECHAM 5. PART I: Model description.- Max Planck Institute for Meteorology, MPI-Report 349: 1-127.
Stärz, M., Lohmann, G. & Knorr, G. (2013): Dynamic soil feedbacks on the climate of the mid-Holocene and the Last Glacial Maximum.- Clim. Past Discuss. 9: 2717-2770, doi: 10.5194/cpd-9-2717-2013.
Stepanek, C. & Lohmann, G. (2012): Modelling mid-Pliocene climate with COSMOS.- Geosci. Model Dev. 5: 1221-1243, doi: 10.5194/gmd-5-1221-2012.
Trenberth, K.E., Smith, L., Qian, T., Dai, A. & Fasullo, J. (2007): Estimates of the global water budget and its annual cycle using observational and model data.- J. Hydrometeorol. 8: 758-769, doi: 10.1175/JHM600.1.
Weber, M.E., Clark, P.U., Kuhn, G., Timmermann, A., Sprenk, D., Gladstone, R., Zhang, X., Lohmann, G., Menviel, L., Chikamoto, M.O., Friedrich, T. & Ohlwein, C. (2014): Millennial-scale variability in Antarctic ice-sheet discharge during the last deglaciation.- Nature 510: 134-138, doi: 10.1038/nature13397.
Wei, W. & Lohmann, G. (2012): Simulated Atlantic Multidecadal Oscillation during the Holocene.- J. Climate 25: 6989-7002, doi: 10.1175/JCLI-D-11-00667.1.
Wei, W., Lohmann, G. & Dima, M. (2012): Distinct modes of internal variability in the Global Meridional Overturning Circulation associated to the Southern Hemisphere westerly winds.- J. Phys. Oceanography 42: 785-801, doi: 10.1175/JPO-D-11-038.1.
Yamazaki, D., Kanae, S., Kim, H. & Oki, T. (2011): A physically based description of floodplain inundation dynamics in a global river routing model.- Water Resour. Res. 47: W04501, doi: 10.1029/2010WR009726.
Zhang, X., Lohmann, G., Knorr, G. & Xu, X. (2013): Different ocean states and transient characteristics in Last Glacial Maximum simulations and implications for deglaciation.- Clim. Past 9: 2319-2333, doi:10.5194/cp-9-2319-2013.
Zhang, X., Lohmann, G., Knorr, G. & Purcell, C. (2014): Abrupt glacial climate shifts controlled by ice sheet changes.- Nature 512: 290-294, doi: 10.1038/nature13592.

Polarforschung 85 (2), 179–181, 2015 (erschienen 2016)

Centennial Cycles Observed in Temperature Data from Antarctica to Central Europe

by Horst-J. Lüdecke[1], Carl-O. Weiss[2], Xinhua Zhao[3] and Xueshang Feng[3]

Abstract: Fourier analyses of worldwide temperature proxy data show a multitude of spectral lines, indicating multi-periodic dynamics of the climate system. The proxy data investigated in this study all show an approximately 200 year period, which has been related to the solar De Vries/Suess cycle. This cycle is consistent with temperature measurements from about 1750 to present, suggesting that the solar De Vries/Suess cycle is of importance for the recent and near future climate variations.

Zusammenfassung: Fourier Analysen von weltweiten Temperatur-Proxydaten für verschiedene Regionen der Erde weisen eine große Zahl von Spektrallinien auf, die die Dynamik des Klimasystems auf unterschiedlichen Zeitskalen (multiperiodisch) widerspiegeln. Die in dieser Studie untersuchten Proxydaten zeigen durchweg eine Periodizität von ungefähr 200 Jahren, wie sie mit dem solaren De Vries/Suess-Zyklus in Verbindung gebracht werden kann. Diese Periodizität lässt sich auch in instrumentellen Temperaturmessungen ab etwa 1750 bis heute erkennen, was einen Einfluss des De Vries/Suess-Zyklus' auf die vergangene und zukünftige Temperaturentwicklung wahrscheinlich macht.

INTRODUCTION

In recent years a sizeable number of studies have revealed periodic climate variations by analysing proxies of temperatures, rainfalls, droughts etc. (Kern et al. 2012, Cliver et al. 1998, Raspopov et al. 2008, Knudsen et al. 2011, Novello et al. 2012, Wagner et al. 2001). These studies concerned local proxies such as stalagmites, tree-rings, sediments, ice cores, biotic and instrumental temperatures. Because the most pronounced cycle of solar activity is the about 200 year De Vries/Suess cycle (Steinhilber & Beer 2013), we have looked for this about 200 year periodicity in the records of more globally distributed temperature proxies with a time resolution of one year and going back at least to the year 0 AD/BP. In particular we used the following datasets:

1) Christiansen & Ljundquist (2012): multiproxies, locally distributed over the Northern Hemisphere, covering the years 0 to 1973 AD, in the following "Chr/Lju".
2) Buentgen et al. (2011): tree-rings from the European Alps, covering the years -499 BP/AD to 2003 AD, in the following "Bue".
3) Cook et al. (2000): tree-rings from Tasmania, covering -1600 BP/AD to 1991, in the following "Cook".
4) Petit et al. (1999): ice-cores from the Antarctic Vostok station, covering the last 420,000 years, in the following "Petit".
5) Lüdecke et al. (2013): instrumental temperatures of six stations in central Europe, covering the years from approximately 1750 to 2011, in the following "M6".

RESULTS

Figure 1 (Zhao & Feng 2015) shows the Lomb-Scargle spectrum (Lomb 1976, Scargle 1982) for the last 11,000 years of "Petit", revealing a large number of spectral lines. Besides peaks at about 300, 480, 520 and 730 years, in particular spectral lines around the about 200 year period (188 and 204 years) sticks out, which exceed the 99 % confidence level.

The two upper and the lower left panel of Figure 2 show the spectra of "Chr/Lju", "Bue", and "Cook", where the about 200 year cycle is apparent, exceeding the 99 % and 95 % confidence level, respectively. The spectrum of "M6" in the lower right panel of Figure 2 has a much reduced frequency resolution due to the relatively shorter time span covered, compared to those of the proxy data, but prominently shows a about 200 year-period spectral line as well. However, there are reasons why this prominent line could be the result of artifacts, particularly, since the data span only one full period of a 200 year cycle. However, the appearances of the periodicity in the proxy data, on the one hand, and the correspondence of the recent temperatures with the solar activity with its dominant 200 year De Vries/Suess cycle (Steinhilber & Beer 2013), on the other hand, make it likely that the measured temperature variations of "M6" are essentially a section of a continuing about 200 year periodicity. We note that in general a certain distribution of the cycle frequencies is to be expected since the cycle period and phases vary over time as demonstrated for the solar De Vries/Suess cycle covering 8000 years (Steinhilber et al. 2012, Suess 1980).

Figure 3 shows the transformation from the frequency domain to the time domain for "M6", using only the six strongest cycles represented by the strongest peaks in the lower right panel of Figure 2, as given in Lüdecke et al. (2013, Tab. 1). It demonstrates a rather precise agreement with the measurements. It has often been suggested that the agreement between reconstruction and measurements is trivial and meaningless, since the reconstruction represents merely a low pass filtered version of the measurements. Although the chosen strongest cycles are in the low frequency range, the reconstruction means not merely a low pass filtering. The data may or may not contain secular components in addition to the cycles. The agreement of the reconstruction, which only uses cycle com–ponents with the measurement record, would indicate that the

doi:10.2312/polfor.2016.015

[1] HTW, University of Applied Sciences, Saarbrücken, Germany; Corresponding author: <moluedecke@t-online.de>, <carl.weiss@gmx.de>
[2] CINVESTAV, Queretaro, Mexico; visiting from PTB Braunschweig, Germany.
[3] SIGMA Weather Group, State Key Laboratory of Space Weather, Center for Space Sciences and Applied Research, Chinese Academy of Sciences, Beijing, China.
This extended abstract was presented as a poster presentation at the International Conference "Our Climate – Our Future: Regional perspectives on a global challenge", 6–9 October 2014 in Berlin, Germany.
Manuscript received 18 May 2015; revised version 7 October 2015; accepted 6 April 2016.

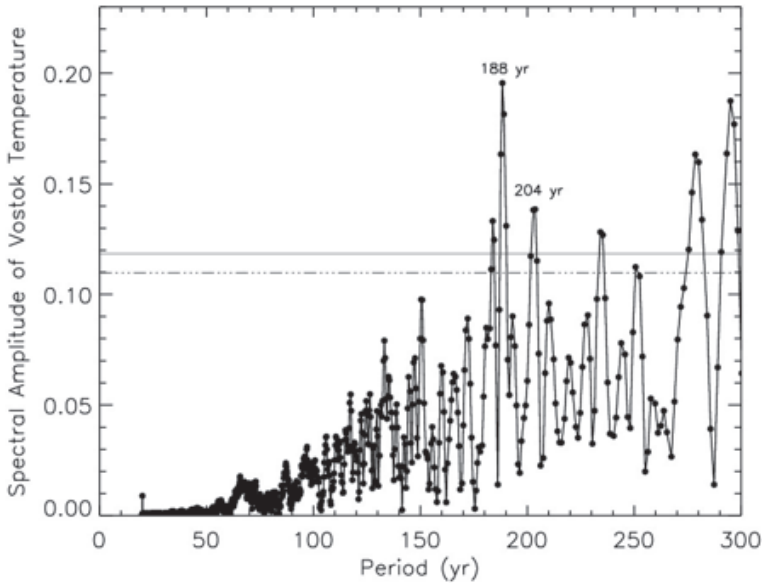

Fig. 1: Spectral power (in arbitrary units) of the Antarctic Vostok ice core temperature data over the last 11,000 years (PETIT et al. 1999). The gray and black (solid, chain-dotted) horizontal lines indicate the 95 % and 99 % confidence levels, exceeding random noise (Monte-Carlo simulations).

Abb. 1: Spektrale Stärke der Daten des antarktischen Vostok Eisbohrkerns über die letzten 11.000 Jahre (PETIT et al. 1999) in willkürlicher Einheit. Die graue durchgezogene und schwarze strichpunktierte horizontale Linien markieren die 99 % bzw. 95 % Konfidenzgrenzen gegenüber statistischem Rauschen (Monte-Carlo Simulation).

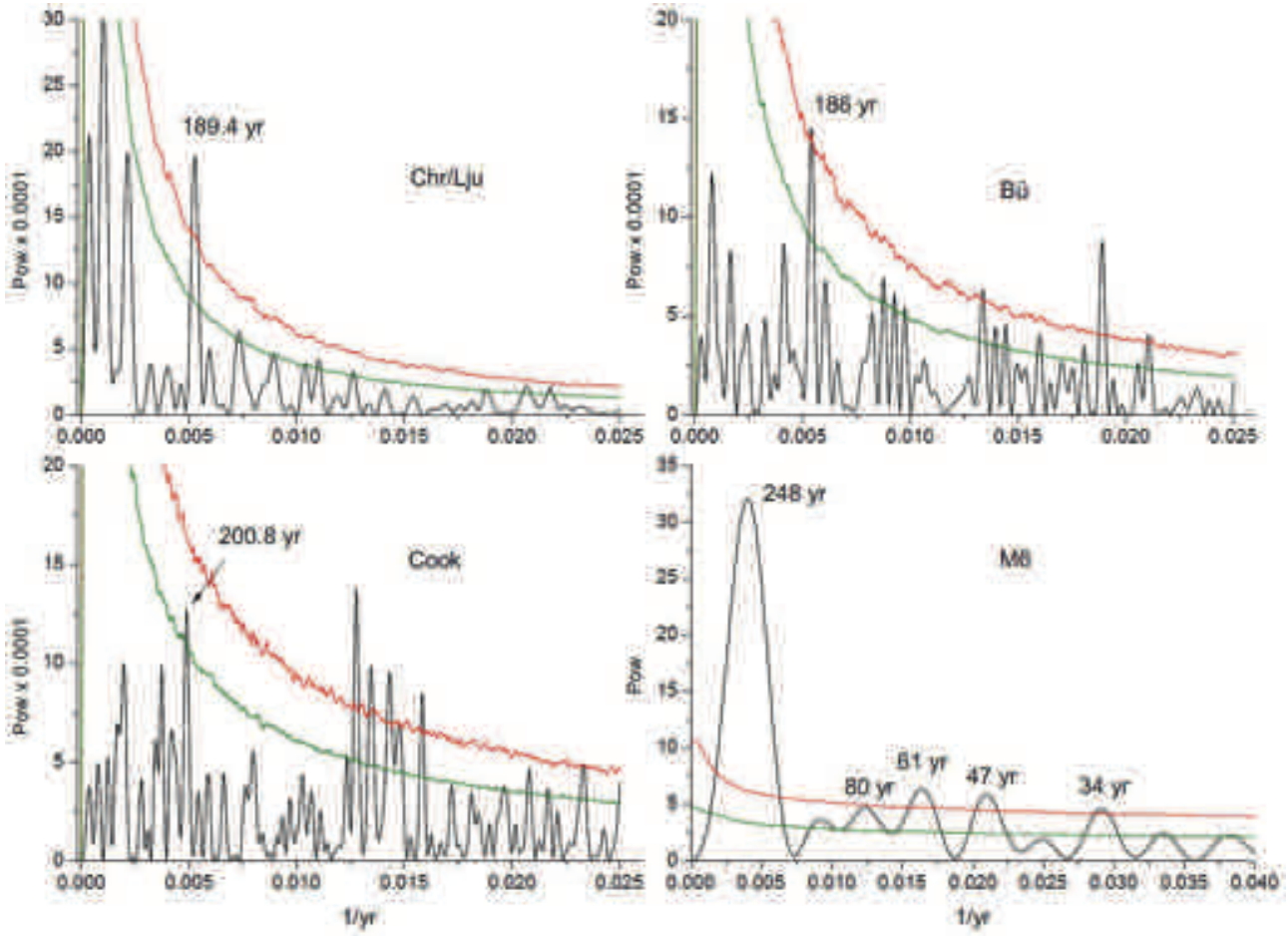

Fig. 2: Left upper panel: Spectral power of the temperature multiproxy data from 0 to 1973 AD ("Chr/Lju"), covering much of the Northern Hemisphere (CHRISTIANSEN & LJUNDQUIST 2012). Right upper panel: Spectral power of the temperature proxy data from -499 to 2003 BP/AD ("Bue") as tree-rings from the European Alps (BUENTGEN et al. 2011). Left lower panel: Spectral power of the temperature proxies from -1600 to 1991 BP/AD ("Cook") as tree-rings from Tasmania (COOK et al. 2000). Right lower panel: Spectral power of six instrumental temperature records from central Europe from ~1750 to 2011 ("M6"). All spectral powers are in arbitrary units. The green and red lines indicate the 99 % and 95 % confidence levels (LÜDECKE et al. 2013).

Abb. 2: Links oben: Spektrale Stärke der "Chr/Lju" Temperaturreihe von 0 to 1973 n. Chr., die weite Teile der Nordhemisphäre abdeckt (CHRISTIANSEN & LJUNDQUIST 2012). Rechts oben: Spektrale Stärke der "Bue" Temperaturreihe von 499 v.Chr. bis 2003 n.Chr. aus Baumringen der Europäischen Alpen (BUENTGEN et al. 2011). Links unten: Spektrale Stärke der "Cook" Temperaturreihe von 1600 v.Chr. bis 1991 n.Chr. aus Baumringen von Tasmanien (COOK et al. 2000). Rechts unten: Spektrale Stärke von sechs instrumentellen Temperaturreihen Zentraleuropas "M6" von ~1750 bis 2011 n.Chr. Alle spektralen Stärken in willkürlichen Einheiten. Die grünen und roten Linien markieren die 95 % und 99 % Konfidenzlinien gegenüber statistischem Rauschen (LÜDECKE et al. 2013).

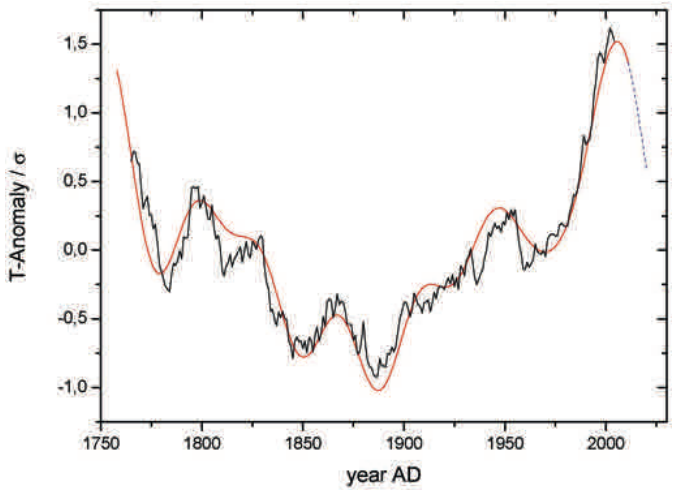

Fig. 3: 15-years running mean of the six instrumental temperature records ("M6", LÜDECKE et al. 2013) in black, and time domain reconstruction using the six strongest frequency components (in red) of the spectrum, shown in the right lower panel of Figure 2.

Abb. 3: Gleitendes Mittel (15 Jahr Fenster) der sechs mitteleuropäischen Temperaturmessreihen "M6" (LÜDECKE et al. 2013) in schwarz und Rekonstruktion unter ausschließlicher Benutzung der sechs stärksten Komponenten des Spektrums in Abbildung 2 in rot.

recent temperature variations are exclusively due to cycles and that secular components are absent. However, it has also been suggested that secular components could be hidden in the 200 year cycle.

CONCLUSION

We have analysed proxy data, extending over a large part of the globe, indicating multi-periodic climate dynamics. Based on least squares deviations between the data and a single sine we find that the dataset of "Chr/Lju" represents a 33 % fraction of a full sine, "Bue" a 27 % fraction and "Cook" a 17 % fraction (100 % as complete agreement with a sine and assuming that the deviations of the data from a sine function are real climate variations and not merely measurement noise). If the deviations were dominantly measurement noise, the 200 year cycle would represent a larger percentage. If the instrumental data in Figure 3 in fact represent a section of a continuing 200 year cycle, the contribution of this cycle to the recent temperature changes would be substantial. In addition, Figure 3 also implies an about 65 year cycle, indicative for the Atlantic Multidecadal Oscillation (AMO) or the Pacific Decadal Oscillation (PDO). The latter, together with the approximately 200 year cycle, appears to dominate the recent temperatures.

ACKNOWLEDGMENT

The authors wish to thank Michael Asten and one anonymous reviewer for helpful and constructive suggestions on the manuscript.

References

Buentgen, U., Tegel, W., Nicolussi, K., McCormic, M., Frank, D., Trouet, V., Kaplan, J. O., Herzig, F., Heussner, K.-U., Wanner, H.,Luterbacher, J. & Esper, J. (2011): 2500 years of European Climate variability and human susceptibility.- Science 331: 578-582.

Christiansen, B. & Ljundquist, F.C. (2012): The extra-tropical Northern Hemisphere temperature in the last two millennia, reconstruction of low-frequency variability.- Clim. Past 8: 765-786.

Cliver, E.W., Boriakov, V. & Feynman, J. (1998): Solar variability and climate change: geomagnetic as index and global surface temperature.- Geophys. Res. Lett. 25: 1035-1038.

Cook, E.R., Buckley, B.M., D'Arrigo, R.D. & Peterson, M.R. (2000): Warm season temperatures since 1600 BC reconstructed from Tasmanian tree rings and their relationship to large-scale sea surface temperature anomalies.- Clim. Dyn. 16: 79-91.

Kern, A.K., Harzhauser, M., Piller, W.E., Mandic, O. & Soliman, A. (2012): Strong evidence for the influence of solar cycles on a Late Miocene lake system revealed by biotic and abiotic proxies.- Paleogeogr. Paleoecol. 329-330: 124-136.

Knudsen, M.F., Jacobsen, B.H., Riisager, P., Olsen, J. & Seidenkrantz, M.-S. (2011): Evidence of Suess solar-cycle bursts in subtropical Holocene speleothem ^{18}O records.- Holocene 22: 597-602.

Lomb, N.R. (1976): Least squares frequency analysis of unequally spaced data.- Astrophys. Space Sci. 39: 447-462.

Lüdecke, H.-J., Hempelmann, A. & Weiss, C.O. (2013): Multiperiodic climate dynamics: spectral analysis of long-term instrumental and proxy temperature records.- Clim. Past 9: 447-452.

Novello,V.F., Karmann, I., Burns, S.J., Strikis, N.M., Vuille, M., Cheng, H., Edwards, R.L., Santos, R.V., Frigo, E. & Barreto, E.A.S. (2012): Multidecadal climate variability in Brazil's Nordeste during the last 3000 years based on speleothem isotope records.- Geophys. Res. Lett. 39: L23706.

Petit, J.R., Jouzel, J., Raynaud, D., Barkov, N.I., Barnola, J.M., Basile, I., Bender, M., Chappellas, J., Davis, J., Delaygue, G., Delmotte, M., Kotlyakov, V.M., Legrand, M., Lipenkov, V., Lorius, C., Pepin, L., Ritz, C., Saltzman, E. & Stievenard, M. (1999): Climate and atmospheric history of the past 420,000 years from the Vostok ice core, Antarctica.- Nature 399: 429-436.

Raspopov, O.M., Dergachev, V.R., Esper, J., Kozyreva, O.V., Frank, D., Ogurtsov, M., Kolström, T. & Shao, X. (2008): The influence of the de Vries ~200-year solar cycle on climate variations: results from the Central Asian Mountains and their global link.- Palaeogeogr. Palaeoecol. 259: 6-16.

Scargle, J.D. (1982): Studies in astronomical time series analysis. II. Statistical aspects of spectral analysis of unevenly spaced data.- Astrophys. J. 263: 835-853.

Steinhilber, F., Abreu. J.A., Beer, J., Brunner. I., Christl, M., Fischer, H., Heikkilä, U., Kubik, P.W., Mann, M., McCracken, K.G., Miller, H., Miyahara, H., Oerter, H. & Wilhelms, F. (2012): 9400 years of cosmic radiation and solar activity from ice cores and tree rings.- Proc. Nation. Acad. Sci. USA 109: 5967-5971.

Steinhilber, F. & Beer, J. (2013): Prediction of solar activity for the next 500 years.- J. Geophys. Res. Space 118: 1861-1867.

Suess, H.E. (1980): The radiocarbon record in tree rings of the last 8000 years.- Radiocarbon 22: 200-209.

Wagner, G., Beer, J., Masarik, J., Muscheler, R., Mende, W., Kubik, P.W., Laj, C., Raisbeck, G.M. & Yiou, F. (2001): Presence of the solar De Vries cycle (~205 years) during the last ice age.- Geophys. Res. Lett. 28: 303-306.

Zhao, X.H. & Feng, X.S. (2015): Correlation between solar activity and local temperature of Antarctica during the past 11,000 years.- J. Atmos. Sol.-Terr. Phys. 122: 26-33.

POLARFORSCHUNG
Organ der Deutschen Gesellschaft für Polarforschung e. V.
Journal of the German Society of Polar Research

Schriftleiter / *Editors*
Bernhard Diekmann, Alfred-Wegener-Institut Helmholtz-Zentrum für Polar- und Meeresforschung, Postfach 60 01 49, D-14401 Potsdam, E-Mail <Bernhard.Diekmann@awi.de>
Dieter K. Fütterer, Alfred-Wegener-Institut Helmholtz-Zentrum für Polar- und Meeresforschung, Postfach 12 01 61, D-27515 Bremerhaven, E-Mail <Dieter.Fuetterer@awi.de>

Redaktionsausschuss
Editorial Board
Manfred Bölter, Kiel
Reinhard Dietrich, Berlin
Monika Huch, Adelheidsdorf
Enn Kaup, Tallin
Hans-Ulrich Peter, Jena
Franz Tessensohn, Hannover
Horst Bornemann, Bremerhaven
Hajo Eicken, Fairbanks
Joachim Jacobs, Bergen
Cornelia Lüdecke, München
Rainer Sieger, Bremerhaven
Jörn Thiede, Kiel / St. Petersburg
Detlef Damaske, Hannover
Rolf Gradinger, Tromsö
Heidemarie Kassens, Kiel
Heinz Miller, Bremerhaven
Helmut Rott, Innsbruck

Mitteilungen für die Autoren: Die Zeitschrift POLARFORSCHUNG, herausgegeben von der Deutschen Gesellschaft für Polarforschung e.V. (DGP) und dem Alfred-Wegener-Institut Helmholtz-Zentrum für Polar- und Meeresforschung (AWI) dient der Publikation von Originalbeiträgen aus allen Bereichen der Polar- und Gletscherforschung in Arktis und Antarktis wie in alpinen Regionen mit polarem Klima. Manuskripte können in englischer (bevorzugt) und deutscher Sprache eingereicht werden und sind zu richten an: Deutsche Gesellschaft für Polarforschung, Schriftleitung, c/o Alfred-Wegener-Institut Helmholtz-Zentrum für Polar- und Meeresforschung, Postfach 60 0149, D-14401 Potsdam <Bernhard.Diekmann@awi.de> **oder** Postfach 12 0161, D-27515 Bremerhaven <Dieter.Fuetterer@awi.de>. Eingesandte Manuskripte werden Fachvertretern zur Begutachtung vorgelegt und gelten erst nach ausdrücklicher Bestätigung durch die Schriftleitung als zur Veröffentlichung angenommen. Für detaillierte Angaben zur Manuskripterstellung siehe die Web-Seite der DGP: <http://www.dgp-ev.de>.

Erscheinungsweise und Bezugsbedingungen: POLARFORSCHUNG erscheint ab Jahrgang 2011, Band 81 mit jährlich zwei Heften. Für Mitglieder der Deutschen Gesellschaft für Polarforschung e.V. (DGP) ist der Bezugspreis für die Zeitschrift im Mitgliedsbeitrag enthalten. Für Nichtmitglieder beträgt der Bezugspreis eines Heftes € 35,00; Bezug über die Geschäftsstelle.
Open access: Alle Artikel sind in elektronischer Form im Internet verfügbar <http://www.polarforschung.de>. Polarforschung wird im D*irectory of Open Access Journals* (DOAJ) <http://doaj.org> geführt.

Informations for contributors: *POLARFORSCHUNG – published by the Deutsche Gesellschaft für Polarforschung (DGP) and the Alfred Wegener Institute Helmholtz Centre for Polar and Marine Research (AWI) – is a peer-reviewed, multidisciplinary research journal that publishes the results of scientific research related to the Arctic and Antarctic realm, as well as to mountain regions associated with polar climate. The POLARFORSCHUNG editors welcome original papers and scientific review articles from all disciplines of natural as well as social and historical sciences dealing with polar and subpolar regions. Manuscripts may be submitted in English (preferred) or German. In addition, POLARFORSCHUNG publishes notes (mostly in German), which include book reviews, general commentaries and reports, as well as communications broadly associated with DGP issues. Manuscripts and all related correspondence should be sent to: Deutsche Gesellschaft für Polarforschung e.V., Editorial Office POLARFORSCHUNG, c/o Alfred Wegener Institute Helmholtz Centre for Polar and Marine Research, PO Box 60 0149, D-14401 Potsdam, E-Mail <Bernhard.Diekmann@awi.de>* ***or*** *PO Box 12 0161, D-27515 Bremerhaven, E-Mail <Dieter.Fuetterer@awi.de>. Manuscripts can be considered as definitly accepted only after written confirmation from the Editor. For a detailed guidance of authors please visit the DGP web page at: <http://www. dgp-ev.de>.*

Publication and Subscription rates: *Effective as of volume 81, 2011, POLARFORSCHUNG is being published twice a year. For members of the DGP, subscription to POLARFORSCHUNg is included in the membership dues. For non-members, the price for a single issue is € 35.00.*
Open access: *PDF versions of all Polarforschung articles are freely available from <http://www.polarforschung.de>. POLARFORSCHUNG is listed in the Directory of Open Access Journals (DOAJ) <http://www.doaj.org>.*